THEORY OF COMPUTING, Volume 11 (20), 2015, pp. 491–603
www.theoryofcomputing.org

The Bose-Hubbard Model is QMA-complete

Andrew M. Childs David Gosset Zak Webb

Received July 31, 2014; Revised June 25, 2015; Published December 31, 2015

Abstract: The Bose-Hubbard model is a system of interacting bosons that live on the vertices of a graph. The particles can move between adjacent vertices and experience a repulsive on-site interaction. The Hamiltonian is determined by a choice of graph that specifies the geometry in which the particles move and interact. We prove that approximating the ground energy of the Bose-Hubbard model on a graph at fixed particle number is QMA-complete. In our QMA-hardness proof, we encode the history of an n-qubit computation in the subspace with at most one particle per site (i. e., hard-core bosons). This feature, along with the well-known mapping between hard-core bosons and spin systems, lets us prove a related result for a class of 2-local Hamiltonians defined by graphs that generalizes the XY model. By avoiding the use of perturbation theory in our analysis, we circumvent the need to multiply terms in the Hamiltonian by large coefficients.

ACM Classification: F.1.3, F.2.2

AMS Classification: 68Q17, 81P68

Key words and phrases: complexity theory, QMA, quantum computing

1 Introduction

The problem of approximating the ground energy of a given Hamiltonian is a natural quantum analog of classical constraint satisfaction. Many authors have considered the computational complexity of such quantum ground state problems. For a variety of classes of Hamiltonians and a suitable notion of approximation, this task is complete for the complexity class QMA, the quantum version of NP with two-sided error (see reference [3] for a recent review). These results provide evidence that approximating the ground energy of such quantum systems is intractable.

The first such example is the Local Hamiltonian problem introduced by Kitaev [21]. A k-local Hamiltonian acts on a system of n qubits and can be written as a sum of terms, each acting nontrivially

© 2015 Andrew M. Childs, David Gosset, and Zak Webb
Licensed under a Creative Commons Attribution License (CC-BY)
DOI: 10.4086/toc.2015.v011a020

on at most k qubits. The k-Local Hamiltonian problem is a promise problem related to the task of approximating the ground energy of a k-local Hamiltonian. Given such a Hamiltonian and two thresholds a and b, one is asked to determine if the ground energy is below a or above b (promised that one of these conditions holds). Kitaev's original work showed that the 5-local Hamiltonian problem is QMA-complete [21]; subsequent works proved QMA-completeness of the 3-local Hamiltonian problem [20], the 2-local Hamiltonian problem [19], and the 2-local Hamiltonian problem with interactions between qubits restricted to a two-dimensional lattice [28].

The complexity of similar computational problems related to other classes of Hamiltonians has also been considered. These include Hamiltonians in one dimension [1, 14], frustration-free Hamiltonians [4, 13], and stoquastic Hamiltonians (Hamiltonians with no "sign problem") [5, 6], among others.

The QMA-hardness of ground energy problems for local Hamiltonians acting on qubits has implications for Hamiltonians acting on indistinguishable particles (bosons or fermions) due to formal mappings between these systems. By applying such mappings to the Local Hamiltonian problem, one can show that certain bosonic [30] and fermionic [23] Hamiltonian problems are QMA-hard. A more restrictive class of QMA-complete fermionic Hamiltonians was considered by Schuch and Verstraete, who showed that the Hubbard model with a site-dependent magnetic field is QMA-complete [29]. This is a specific model of interacting electrons (i. e., spin-1/2 fermions) on a two-dimensional lattice, with a magnetic field that may take different values and point in different directions (in three dimensions) at distinct sites of the lattice.

Many of the QMA-complete problems considered previously have the property that the form of the terms in the Hamiltonian is part of the specification of the instance. For example, a 2-local Hamiltonian is specified by a 2-local Hermitian operator for each pair of qubits. In the Hubbard model considered in reference [29], there is a similar freedom in the choice of magnetic field at each site. A recent classification of local Hamiltonian problems [10] likewise applies only to models with adjustable coefficients. In fact, these results typically require coefficients that grow with the problem size.

In contrast, here we consider a system of interacting bosons with fixed hopping and interaction terms. Specifically, we consider the Bose-Hubbard model, which has one of the simplest interactions between particles that conserves total particle number. Although the Bose-Hubbard model is traditionally defined on a lattice and with negative hopping strength [12], here we consider its extension to a general graph, with positive hopping strength.

We consider undirected graphs without multiple edges and with at most one self-loop per vertex. Any such graph G (with vertex set V) can be specified by its adjacency matrix, a symmetric 0-1 matrix denoted $A(G)$. The Bose-Hubbard model on G with hopping strength t_{hop} and interaction strength J_{int} has the Hamiltonian

$$H_G = t_{\mathrm{hop}} \sum_{i,j \in V} A(G)_{ij} a_i^\dagger a_j + J_{\mathrm{int}} \sum_{k \in V} n_k (n_k - 1) \tag{1.1}$$

where $a_i^\dagger$ creates a boson at vertex i and $n_i = a_i^\dagger a_i$ counts the number of bosons at vertex i. The precise definitions of these operators are given in Section 2.2, where we describe the model in more detail. Our results apply to the Bose-Hubbard model for any fixed positive hopping strength $t_{\mathrm{hop}} > 0$ and any fixed positive (i. e., repulsive) interaction strength $J_{\mathrm{int}} > 0$. Unlike in other QMA-completeness results, in our work the coefficients $t_{\mathrm{hop}}, J_{\mathrm{int}}$ are not inputs to the problem; rather, each fixed choice defines a computational problem and we prove QMA-completeness for each of them.

Observe that the Bose-Hubbard Hamiltonian (1.1) conserves the total number of particles $N = \sum_{k \in V} n_k$. We focus on the space of N-particle states, which can be identified with the symmetric subspace of $(\mathbb{C}^{|V|})^{\otimes N}$ (as we discuss in more detail in Section 2). The first term in (1.1) allows particles to move between vertices; the second term is an interaction between particles that assigns an energy penalty for each vertex occupied by more than one particle. The Bose-Hubbard model is an example of a multi-particle quantum walk, a generalization of quantum walk to systems with more than one walker.

Recently we showed that the Bose-Hubbard model on a graph can perform efficient universal quantum computation [8]. Sometimes universality goes hand-in-hand with QMA-completeness, e. g., for local Hamiltonians, whose dynamics are BQP-complete [11] and whose ground energy problem is QMA-complete [21]. However, not all classes of Hamiltonians with universal dynamics have QMA-complete ground energy problems. For example, the dynamics of stoquastic local Hamiltonians are BQP-complete (as follows from [16] and time reversal), whereas the corresponding ground energy problem is in AM [5] and hence unlikely to be QMA-hard. Similarly, the ground energy problem for a Bose-Hubbard model with $t_{\text{hop}} < 0$ is also in AM [5], whereas the dynamics of such Hamiltonians are universal [8]. The ferromagnetic Heisenberg model on a graph provides an even starker contrast: its dynamics are BQP-complete (as can be inferred from [8] using a correspondence between spins and hard-core bosons) but its ground energy problem is trivial since the ground space is the symmetric subspace.

1.1 Overview of results

In this paper we define the Bose-Hubbard Hamiltonian problem and characterize its complexity. In this problem one is given a graph G and a number of particles N and asked to approximate the ground energy of the Bose-Hubbard Hamiltonian (1.1) in the N-particle sector (in a precise sense described in Section 2). We prove that this problem is QMA-complete.

To prove QMA-hardness of the Bose-Hubbard Hamiltonian problem, we show that in fact a notable special case of this problem, called Frustration-Free Bose Hubbard Hamiltonian, is QMA-hard. In this problem one is asked (roughly) to determine if the ground energy of the Bose-Hubbard Hamiltonian (1.1) in the N-particle sector is close to N times its single-particle ground energy (i. e., N times the smallest eigenvalue of the adjacency matrix $A(G)$). This is always a lower bound on the N-particle energy, and when it is achieved we say the N-particle ground states are frustration free. A frustration-free state has the special property that it has minimal energy for both terms in (1.1), and in particular it is annihilated by the interaction term. Frustration-free states therefore live in the subspace of *hard-core* bosons, with at most one boson per vertex.

Furthermore, we prove a reduction from Frustration-Free Bose-Hubbard Hamiltonian to an eigenvalue problem for a class of 2-local Hamiltonians defined by graphs. The two problems are related by a well-known mapping between hard-core bosons and spin systems. Specifically, given a graph G (with vertex set V) we consider the Hamiltonian

$$\sum_{\substack{A(G)_{ij}=1 \\ i \neq j}} \left(|01\rangle\langle 10| + |10\rangle\langle 01| \right)_{ij} + \sum_{A(G)_{ii}=1} |1\rangle\langle 1|_i = \sum_{\substack{A(G)_{ij}=1 \\ i \neq j}} \frac{\sigma_x^i \sigma_x^j + \sigma_y^i \sigma_y^j}{2} + \sum_{A(G)_{ii}=1} \frac{1 - \sigma_z^i}{2}. \qquad (1.2)$$

Note that this Hamiltonian commutes with the magnetization operator

$$M_z = \sum_{i=1}^{|V|} \frac{1-\sigma_z^i}{2}$$

and has a sector for each of its eigenvalues $M_z \in \{0,1,\ldots,|V|\}$. We reduce Frustration-Free Bose-Hubbard Hamiltonian (with N particles on a graph G) to the problem of approximating the smallest eigenvalue of (1.2) within the sector with magnetization $M_z = N$. We call this the XY Hamiltonian problem because of its connection to the XY model from condensed matter physics. Since this problem is contained in QMA, our reduction shows it to be QMA-complete.

We also obtain a related result that may be of independent interest. In Section 3 we give a self-contained proof that computing the smallest eigenvalue of a sparse, efficiently row-computable [2] symmetric 0-1 matrix (the adjacency matrix of a graph) is QMA-complete. This can alternatively be viewed as a result about the QMA-completeness of a single-particle quantum walk on a graph with at most one self-loop per vertex. To prove this, we use a mapping from circuits to graphs that is also used in our main result. Note that Janzing and Wocjan used a similar construction to design a BQP-complete problem [16].

1.2 Proof techniques

We prove our main result by direct reduction from quantum circuit satisfiability. We introduce several new techniques in order to do this using the Bose-Hubbard model on an unweighted graph.

Kitaev's original proof of QMA-hardness of the Local Hamiltonian problem encodes a QMA verification circuit using ideas from a computationally universal Hamiltonian proposed by Feynman [11]. This Hamiltonian uses a "clock register" to record the progress of the computation; in an appropriate basis, the Hamiltonian can be seen as a quantum walk on a path whose vertices represent the steps of the computation. Other proofs of QMA-hardness have used alternative encodings of the temporal structure of a verification circuit into a quantum state. In our construction, we encode the history of an n-qubit verification circuit in the state of n interacting particles on a graph, where each particle encodes a single qubit.

Our construction uses a class of graphs we define called *gate graphs*. Gate graphs are built from a basic subgraph whose single-particle ground states encode the history of a simple single-qubit computation. By suitably combining copies of this basic unit, we define gadgets with other functionality. (Note that these gadgets realize some desired behavior exactly; they are not "perturbative gadgets" in the sense of [19, 17].) In particular, we design gadgets for two-qubit gates such that each ground state of the two-particle Bose-Hubbard model encodes a two-qubit computation. We now give a high-level description of how these gadgets work and how we use them to construct a graph for a QMA verification circuit.

For each two-qubit gate U from a fixed universal set, we design a graph G_U that can be divided into four overlapping regions as shown schematically in Figure 1.1(A). (The specific graphs we use for two-qubit gates each have 4096 vertices and are described using the gate graph formalism.) The two-particle Bose-Hubbard model on this graph has ground states that encode the two-qubit computation. To describe them it is helpful to first consider the single-particle ground states, i. e., the ground states of the adjacency matrix $A(G_U)$. This matrix has 16 orthonormal single-particle ground states $|\rho_{z,a}^{i,U}\rangle$.

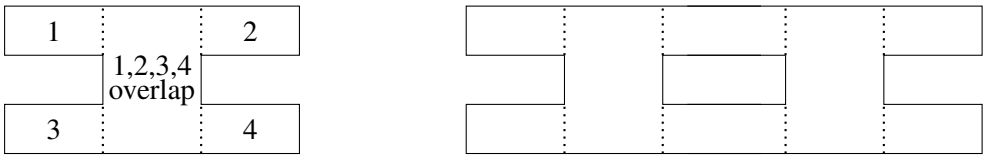

(A) (B)

Figure 1.1: We design graphs for two-qubit gates with overlapping regions as shown in (A). Regions 1 and 2 are associated with the first encoded qubit and regions 3 and 4 are associated with the second encoded qubit. One could imagine designing a graph for a circuit with two-qubit gates U_1 followed by U_2 by connecting the corresponding gadgets as in (B). In the text we describe a challenge with this approach.

Each index $i \in \{1,2,3,4\}$ is associated with the corresponding region in the graph, as $|\rho_{z,a}^{i,U}\rangle$ is supported entirely within region i. The index $z \in \{0,1\}$ corresponds to the computational basis states of a single encoded qubit. Note that, since $A(G_U)$ is a real matrix, the complex conjugate of any eigenstate is also an eigenstate with the same eigenvalue. The index $a \in \{0,1\}$ is associated with this freedom, i. e., $|\rho_{z,1}^{i,U}\rangle = |\rho_{z,0}^{i,U}\rangle^*$. The ground space of the two-particle Bose-Hubbard model on G_U is spanned by 16 states, indexed by two choices $z_1, z_2 \in \{0,1\}$ of computational basis states for the encoded qubits and two bits $a_1, a_2 \in \{0,1\}$ associated with complex conjugation. These states can be represented as symmetric states in the Hilbert space $\mathbb{C}^{4096} \otimes \mathbb{C}^{4096}$; they are

$$\frac{1}{2}(|\rho_{z_1,a_1}^{1,U}\rangle|\rho_{z_2,a_2}^{3,U}\rangle + |\rho_{z_2,a_2}^{3,U}\rangle|\rho_{z_1,a_1}^{1,U}\rangle) + \frac{1}{2}\sum_{x_1,x_2\in 0,1} U(a_1)_{x_1,x_2,z_1,z_2}(|\rho_{x_1,a_1}^{2,U}\rangle|\rho_{x_2,a_2}^{4,U}\rangle + |\rho_{x_2,a_2}^{4,U}\rangle|\rho_{x_1,a_1}^{2,U}\rangle)$$

where $U(0) = U$ is the two-qubit gate of interest and $U(1) = U^*$ is its elementwise complex conjugate. Observe that each of these states is a superposition of a term where both particles are on the left-hand side of the graph, encoding a two-qubit input state $|z_1\rangle|z_2\rangle$, and a term where both particles are on the right-hand side of the graph, encoding the two-qubit output state $U(a_1)|z_1\rangle|z_2\rangle$ where either U or its complex conjugate has been applied. In other words, the particles "move together" through the graph as the gate $U(a)$ is applied. While we might prefer the ground states to only encode the computation corresponding to U, we must include the possibility of U^* because the Hamiltonian is real. The same issue arises for n-qubit verification circuits. Fortunately, the complex conjugate of a circuit is equally useful for QMA verification.

It is natural to attempt to construct a graph for an n-qubit verification circuit by combining gadgets for each of the two-qubit gates. However, there is an obstacle to this approach, as illustrated by the example of a two-qubit circuit consisting of only two gates U_1 and U_2. One could construct a graph for such a circuit as shown schematically in Figure 1.1(B), where the two-qubit gadgets for U_1 and U_2 are connected in some unspecified way in the middle. However, not every ground state of the two-particle Bose-Hubbard model on such a graph encodes a computation. For example, there could be a ground state where one of the particles is in the single-particle state $|\rho_{z,a}^{1,U_1}\rangle$ localized on the left side of the graph and the other particle is in the state $|\rho_{z,a}^{2,U_2}\rangle$ with support on a disjoint region of the graph on the right-hand side. To eliminate such spurious ground states, we develop a method to enforce *occupancy constraints* on the locations of particles in gate graphs using the Bose-Hubbard interaction. Although this interaction

only directly penalizes simultaneous occupation of the same vertex, we show how to simulate terms that penalize simultaneous occupation of different regions of the graph. We formalize this method by proving an "Occupancy Constraints Lemma" for gate graphs.

In summary, our construction of the graph for an n-qubit verification circuit proceeds in two steps. We first construct a graph G by connecting two-qubit gadgets for each of the gates in the circuit. As discussed above, the ground space of the n-particle Bose-Hubbard model on G includes a subspace of states that encode computations and a subspace of states that do not. We construct a set of occupancy constraints that are only satisfied by states in the former subspace. We then apply the Occupancy Constraints Lemma to obtain a gate graph $G^{\square}$ where each n-particle ground state encodes a computation. (Note that the particles are somewhat dilute in this graph: the "filling fraction," or number of particles n divided by the size of the graph, approaches 0 as $n \to \infty$.)

Unlike many previous works, we do not use perturbation theory in our analysis. Instead, we use a "Nullspace Projection Lemma" that characterizes the smallest nonzero eigenvalue of a sum of two positive semidefinite matrices $H_A + H_B$ in terms of the smallest nonzero eigenvalue of H_A and the smallest nonzero eigenvalue of H_B restricted to the nullspace of H_A. This lemma allows us to establish an eigenvalue promise gap (i. e., to bound the ground energies of yes instances away from those of no instances) without having to multiply terms in the Hamiltonian by large coefficients, something that is not allowed in the setting of the Bose-Hubbard model on a graph. Whereas QMA-hardness proofs such as those of [20, 19, 28, 29] require multiplying terms in the Hamiltonian by unphysical, problem-size dependent coefficients, our approach avoids this. To the best of our knowledge, our proof would not be much simpler if we only demanded constant-size coefficients; the further restriction that the model is defined entirely by a graph is an extra benefit with little additional cost.

Note that the Nullspace Projection Lemma was used implicitly in [25], which claimed to give a simple proof of the computational universality of adiabatic evolution. That paper encoded a circuit into the multi-particle ground state of a fermionic Hamiltonian in a way that shares some features with our approach. Unfortunately, although the encoding from [25] is novel and interesting, the analysis of the resulting Hamiltonian appears to lack details that are crucial to proving the stated result. (For related approaches with more complete analysis, see [15, 7].)

1.3 Extensions and open questions

Our result shows that approximating the ground energy of the Bose-Hubbard model on a graph at fixed particle number is likely intractable. In showing this, we introduce techniques that we expect will be useful in other contexts. Here we briefly discuss some related questions for future work.

One might consider the complexity of variants of the Bose-Hubbard Hamiltonian problem. For example, one could consider the problem with negative hopping (i. e., $t_{\text{hop}} < 0$), with attractive interactions (i. e., $J_{\text{int}} < 0$), or both. For negative hopping, the results of [5] show that the problem is in AM; we do not know if it is AM-hard. Containment in AM suggests that the problem is easier with $t_{\text{hop}} < 0$ than with $t_{\text{hop}}, J_{\text{int}} > 0$. For attractive interactions, the problem is clearly in QMA (the verification procedure described in Section 4 applies independent of the signs of $t_{\text{hop}}, J_{\text{int}}$), but again we do not know the true complexity. Figure 1.2 summarizes our knowledge of the complexity of the Bose-Hubbard Hamiltonian problem with different choices of t_{hop} and J_{int}.

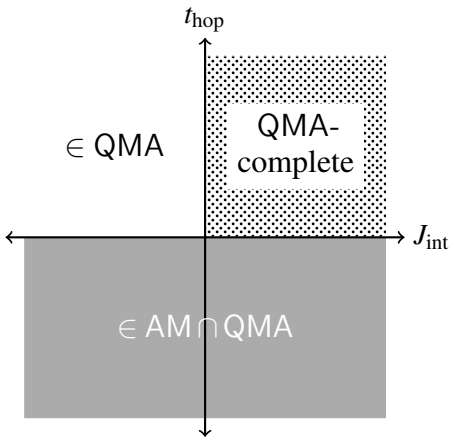

Figure 1.2: Each choice for the coefficients t_{hop} and J_{int} defines a computational problem. We prove the problem is QMA-complete for any positive hopping strength $t_{\text{hop}} > 0$ and repulsive interaction strength $J_{\text{int}} > 0$. For $t_{\text{hop}} < 0$ the problem is contained in AM [5]. For any values of J_{int} and t_{hop} the problem is contained in QMA (see Section 4).

One can define other variants of the Bose-Hubbard Hamiltonian problem by lifting the restriction to fixed particle number.

One could also consider other classes of graphs. The graphs we consider in this paper are described by symmetric 0-1 matrices and have at most one self-loop per vertex. We do not know if the model remains QMA-hard on simple graphs, i. e., without any self-loops. Our reduction from Frustration-Free Bose-Hubbard Hamiltonian to the ground energy problem for the spin model (1.2) gives a stronger result for simple graphs, in which case the second term in (1.2) vanishes. Thus, if the Frustration-Free Bose-Hubbard Hamiltonian problem for simple graphs is QMA-hard, then approximating the ground energy of the XY model on a (simple) graph at fixed magnetization is QMA-complete.

There are many open questions concerning the complexity of the ground energy problem for other quantum systems defined by graphs. For example, one could consider fermions or bosons on a graph with nearest-neighbor interactions. One could also consider quantum spin models such as the XY model or the antiferromagnetic Heisenberg model defined on graphs. Both of these examples correspond to Hamiltonians that conserve magnetization, so one could consider the ground energy problem with or without a restriction to a fixed-magnetization sector. This would complement existing results about the complexity of computing the lowest-energy configuration of classical spin models defined by graphs (for example, the antiferromagnetic Ising model on a graph is NP-complete, as it is equivalent to Max Cut).

As emphasized previously, the Hamiltonians we consider are determined entirely by a choice of graph, with the same type of hopping and interaction terms applied throughout the graph. It might be interesting to find other QMA-complete problems with similar features, such as a version of Local Hamiltonian with only one type of local term. Analogous classical constraint satisfaction problems with a fixed type of constraint are well known (e. g., Exact Cover and Not-All-Equal SAT) and have been widely studied. Along similar lines, it might be interesting to understand when local Hamiltonian problems remain QMA-hard with constant-size coefficients. Nagaj and Mozes have shown that the 3-local Hamiltonian

problem has this property [27], but whether the same holds for the 2-local Hamiltonian problem remains open.

1.4 Outline of the paper

The remainder of this paper is organized as follows. In Section 2 we define the class QMA, introduce the Bose-Hubbard model, and formally state our results. As a warm-up, in Section 3 we prove that computing the smallest eigenvalue of a (succinctly specified) graph is QMA-complete. In Section 4 we explain why the ground state problem for the Bose-Hubbard model is contained in QMA. In Section 5 we define the notion of gate graphs, analyze frustration-free ground states of gate graphs, and introduce the idea of occupancy constraints. In Section 6 we design and analyze gadgets for implementing gates. In Section 7 we construct the graph that we use to show QMA-hardness of the Bose-Hubbard model. In Section 8 we perform the spectral analysis needed to prove our main result. In Section 9 we reduce Frustration-Free Bose-Hubbard Hamiltonian to XY Hamiltonian. In Section 10 we prove the Occupancy Constraints Lemma. Finally, in Appendix A we provide various necessary technical results, including the Nullspace Projection Lemma.

Contents

1 Introduction **491**
1.1 Overview of results . . . 493
1.2 Proof techniques . . . 494
1.3 Extensions and open questions . . . 496
1.4 Outline of the paper . . . 498

2 Definitions and results **500**
2.1 Quantum Merlin-Arthur . . . 500
2.2 The Bose-Hubbard model on a graph . . . 501
2.3 Complexity of the Bose-Hubbard model . . . 504
2.4 Complexity of the XY Hamiltonian problem . . . 505
2.5 Complexity of approximating the smallest eigenvalue of a graph . . . 506

3 Minimum Graph Eigenvalue is QMA-complete **507**
3.1 Circuit-to-graph mapping . . . 508
3.2 Upper bound on the smallest eigenvalue for yes instances . . . 511
3.3 Lower bound on the smallest eigenvalue for no instances . . . 511

4 Bose-Hubbard Hamiltonian is contained in QMA **513**

5 Gate graphs **514**
5.1 The graph g_0 . . . 514
5.2 Gate graphs and gate diagrams . . . 515
5.3 Frustration-free states on e_1-gate graphs . . . 517

5.4 Occupancy constraints . . . 521

6 Gadgets **522**
6.1 The move-together gadget . . . 523
6.2 Gadgets for two-qubit gates . . . 526
6.3 The boundary gadget . . . 533

7 Bose-Hubbard Hamiltonian is QMA-hard **535**
7.1 The verification circuit . . . 536
7.2 The gate graph . . . 538
7.2.1 Notation for G_X . . . 540
7.3 The occupancy constraints graph . . . 541

8 Proof of Theorem 7.1 **542**
8.1 Strategy and outline of the proof . . . 542
8.1.1 Adjacency matrices of the gate graphs . . . 543
8.1.2 Building up the Hamiltonian . . . 544
8.2 Configurations . . . 546
8.3 Legal configurations . . . 549
8.4 Matrix elements between states with legal configurations . . . 551
8.5 From $H(G_2, G_X^{\mathrm{occ}}, n)$ to $H(G_4, G_X^{\mathrm{occ}}, n)$ . . . 556
8.6 Completeness and soundness . . . 562
8.6.1 Completeness . . . 562
8.6.2 Soundness . . . 563

9 XY Hamiltonian is QMA-complete **564**

10 Proof of the Occupancy Constraints Lemma **566**
10.1 Definitions and notation . . . 567
10.2 The gate graph $G^{\diamondsuit}$ . . . 570
10.3 The adjacency matrix of the gate graph $G^{\triangle}$ . . . 572
10.4 The Hamiltonian $H(G^{\triangle}, N)$ . . . 576
10.5 The gate graph $G^{\square}$ . . . 583

A Technical supporting material **586**
A.1 Proof of the Nullspace Projection Lemma . . . 586
A.2 Proof of Lemma 8.7 . . . 587
A.3 Computation of matrix elements between states with legal configurations . . . 593
A.3.1 Matrix elements of H_1 . . . 593
A.3.2 Matrix elements of H_2 . . . 596
A.3.3 Matrix elements of $H_{\mathrm{in},i}$ . . . 597
A.3.4 Matrix elements of H_{out} . . . 598

2 Definitions and results

In this section we define the complexity class QMA, introduce the Bose-Hubbard model and a related spin model, and formally state our results.

2.1 Quantum Merlin-Arthur

Quantum Merlin-Arthur, or QMA, is a class of promise problems. Informally, a promise problem is in QMA if, for any yes instance X, there exists a quantum state $|\psi_{\text{wit}}\rangle$ (with a number of qubits polynomial in the input size $|X|$) that "proves" X is a yes instance. We imagine that all-powerful Merlin prepares the quantum proof $|\psi_{\text{wit}}\rangle$ and hands it to polynomially-bounded Arthur, who checks it using his quantum computer.

Arthur checks Merlin's proof using a verification circuit $\mathcal{C}_X$ that is uniformly generated: $\mathcal{C}_X$ is computed from X using a deterministic polynomial-time (as a function of $|X|$) classical algorithm. The circuit $\mathcal{C}_X$ has an n_{in}-qubit input register, $n - n_{\text{in}}$ ancilla qubits initialized to $|0\rangle$, and one of the n qubits designated as an output qubit. The number of qubits n and the number of gates in the circuit are upper bounded by a polynomial function of $|X|$. We write $U_{\mathcal{C}_X}$ for the unitary operation that the verification circuit implements.

The acceptance probability of $\mathcal{C}_X$ given some n_{in}-qubit input state $|\phi\rangle$ is the probability of measuring the output qubit to be in the state $|1\rangle$ after the circuit is applied, namely

$$\text{AP}(\mathcal{C}_X, |\phi\rangle) = \left\| |1\rangle\langle 1|_{\text{out}} U_{\mathcal{C}_X} |\phi\rangle |0\rangle^{\otimes n - n_{\text{in}}} \right\|^2 .$$

Arthur applies the verification circuit to the input state $|\psi_{\text{wit}}\rangle$. If he measures the output qubit to be $|1\rangle$, he concludes X is a yes instance. QMA is the class of problems for which reliable verification circuits exist, so that Arthur can trust this conclusion with reasonable probability. In other words, if X is a yes instance then there exists a state $|\psi_{\text{wit}}\rangle$ that $\mathcal{C}_X$ accepts with high probability, whereas if X is a no instance then any state $|\phi\rangle$ has low probability of being accepted. To define the class we must specify which probabilities are considered "high" and which are "low." A standard choice uses thresholds of $2/3$ and $1/3$ (called completeness and soundness, respectively).

Definition 2.1 (QMA)**.** A promise problem $L_{\text{yes}} \cup L_{\text{no}} \subset \{0,1\}^*$ is contained in QMA if there exists a uniform polynomial-size circuit family $\mathcal{C}_X$ with the following two properties. If $X \in L_{\text{yes}}$, there exists an input state $|\psi_{\text{wit}}\rangle$ such that

$$\text{AP}(\mathcal{C}_X, |\psi_{\text{wit}}\rangle) \geq \frac{2}{3} \quad \text{(completeness)}.$$

If $X \in L_{\text{no}}$ then all input states $|\phi\rangle$ satisfy

$$\text{AP}(\mathcal{C}_X, |\phi\rangle) \leq \frac{1}{3} \quad \text{(soundness)}.$$

It is a nontrivial fact that many other choices for the completeness and soundness thresholds lead to equivalent definitions of QMA [21, 24]. In particular, we obtain the same class QMA if we change the completeness threshold $2/3$ in the above definition to $1 - (1/2^{|X|})$.

2.2 The Bose-Hubbard model on a graph

As discussed in Section 1, we consider the Bose-Hubbard model on a graph G, with Hamiltonian

$$H_G = t_{\text{hop}} \sum_{i,j \in V} A(G)_{ij} a_i^\dagger a_j + J_{\text{int}} \sum_{k \in V} n_k (n_k - 1) \tag{2.1}$$

where $a_i^\dagger$ creates a boson at vertex i and $n_i = a_i^\dagger a_i$ counts the number of particles at vertex i. In this second-quantized formulation of the Bose-Hubbard model, the Hamiltonian H_G acts on the Fock space with orthonormal basis vectors

$$|l_1, l_2, \ldots, l_{|V|}\rangle$$

where $l_j \in \{0, 1, 2, \ldots\}$ specifies the number of bosons at vertex $j \in V$. The operator a_i is defined by its action in this basis:

$$a_i |l_1, l_2, \ldots, l_i, \ldots, l_{|V|}\rangle = \sqrt{l_i} |l_1, l_2, \ldots, l_i - 1, \ldots, l_{|V|}\rangle . \tag{2.2}$$

The Hamiltonian (2.1) conserves the total particle number $N = n_1 + n_2 + \cdots + n_{|V|}$. In the N-particle sector, the Bose-Hubbard model acts on the finite-dimensional Hilbert space

$$\text{span}\{|l_1, \ldots, l_{|V|}\rangle : \sum_j l_j = N\} . \tag{2.3}$$

The dimension of this space is

$$D_N = \binom{N + |V| - 1}{|V| - 1} . \tag{2.4}$$

Our results apply to the Bose-Hubbard model for any strictly positive hopping and interaction strengths. Henceforth we set $t_{\text{hop}} = J_{\text{int}} = 1$ for convenience, but all our complexity-theoretic results hold for any fixed $t_{\text{hop}}, J_{\text{int}} > 0$.

An equivalent (first-quantized) formulation of the Bose-Hubbard model is as follows. Consider the Hilbert space

$$(\mathbb{C}^{|V|})^{\otimes N} = \text{span}\{|i_1, i_2, \ldots, i_N\rangle : i_1, i_2, \ldots, i_N \in V\} \tag{2.5}$$

where each basis state corresponds to an N-tuple of vertices in the graph. Define the linear operator Sym that symmetrizes over all $N!$ permutations of the N particles:

$$\text{Sym}(|i_1\rangle |i_2\rangle \ldots |i_N\rangle) = \frac{1}{\sqrt{N!}} \sum_{\pi \in S_N} |i_{\pi(1)}\rangle |i_{\pi(2)}\rangle \ldots |i_{\pi(N)}\rangle .$$

Note that Sym does not in general preserve the norm (for example, any antisymmetric state is mapped to zero). Every state in the Hilbert space (2.3) can be identified with a state in

$$\mathcal{Z}_N(G) = \text{span}\{\text{Sym}(|i_1, i_2, \ldots, i_N\rangle) : i_1, i_2, \ldots, i_N \in V\}$$

and vice versa since the two spaces have the same dimension. It is natural to identify states in the two Hilbert spaces by the following linear mapping, defined by its action on basis states. We identify each basis state $|l_1, \ldots, l_{|V|}\rangle$ with the normalized state

$$\frac{1}{\sqrt{l_1! l_2! \ldots l_{|V|}!}} \text{Sym}\left(\underbrace{|1\rangle |1\rangle \ldots |1\rangle}_{l_1} \underbrace{|2\rangle |2\rangle \ldots |2\rangle}_{l_2} \ldots \underbrace{||V|\rangle ||V|\rangle \ldots ||V|\rangle}_{l_{|V|}} \right) . \tag{2.6}$$

The Hamiltonian of the Bose-Hubbard model in the N-particle sector acts as an operator H_G^N on the space $\mathcal{Z}_N(G)$ (see for example [22, §64]):

$$H_G^N = \sum_{w=1}^{N} A(G)^{(w)} + \sum_{k \in V} \hat{n}_k (\hat{n}_k - 1) \tag{2.7}$$

(recall we set $t_{\text{hop}} = J_{\text{int}} = 1$) where the number operator is

$$\hat{n}_i = \sum_{w=1}^{N} |i\rangle\langle i|^{(w)}. \tag{2.8}$$

Here (and throughout the paper) we use the notation

$$M^{(w)} = 1^{\otimes w-1} \otimes M \otimes 1^{\otimes N-w}$$

to indicate that the operator M acts on subsystem w.

While H_G^N is defined as a $|V|^N \times |V|^N$ matrix in the space (2.5), we consider its restriction

$$\bar{H}_G^N = H_G^N \Big|_{\mathcal{Z}_N(G)}$$

to the bosonic N-particle subspace $\mathcal{Z}_N(G)$ (throughout the paper we write $H|_{\mathcal{W}}$ for the restriction of a Hermitian operator H to a subspace $\mathcal{W}$, which can be written as a $\dim \mathcal{W} \times \dim \mathcal{W}$ matrix). It is convenient to add a term proportional to the identity to obtain a positive semidefinite operator. Letting $\mu(G)$ denote the smallest eigenvalue of the adjacency matrix $A(G)$, we consider

$$H(G,N) = \bar{H}_G^N - N\mu(G).$$

Clearly $H(G,N) \geq 0$ since the interaction term is positive semidefinite. Also note that, given the graph G, the smallest eigenvalue $\mu(G)$ of its adjacency matrix can be efficiently approximated using a classical polynomial-time algorithm, so the complexity of approximating the ground energy of $H(G,N)$ is equivalent to the complexity of approximating $\bar{H}_G^N$. (Note that here the graph is specified explicitly by its adjacency matrix. In other contexts one might consider a graph specified compactly, e. g., by a circuit that computes rows of its adjacency matrix. Then the situation is more complex since the input size can be much smaller than the number of vertices in the graph. Indeed, we prove in Section 3 that approximating the smallest eigenvalue of such a graph is QMA-complete.)

We write

$$0 \leq \lambda_N^1(G) \leq \lambda_N^2(G) \leq \ldots \leq \lambda_N^{D_N}(G)$$

for the eigenvalues of $H(G,N)$ and $\{|\lambda_N^j(G)\rangle\}$ for the corresponding normalized eigenvectors.

When $\lambda_N^1(G) = 0$, the ground energy of the N-particle Bose-Hubbard model $\bar{H}_G^N$ is equal to N times the one-particle energy $\mu(G)$. In this case we say that the N-particle Bose-Hubbard model is frustration free. We also define frustration freeness for N-particle states.

Definition 2.2. If $|\psi\rangle \in \mathcal{Z}_N(G)$ satisfies $H(G,N)|\psi\rangle = 0$ then we say $|\psi\rangle$ is an N-particle frustration-free state for G.

We now present two basic properties of $H(G,N)$. The following lemma states that the ground energy is non-decreasing as a function of the number of particles N.

Lemma 2.3. *For all $N \geq 1$, $\lambda^1_{N+1}(G) \geq \lambda^1_N(G)$.*

Proof. Let $\widehat{n}_i^N$ be the number operator (2.8) defined in the N-particle space and let $\widehat{n}_i^{N+1}$ be the corresponding operator in the $(N+1)$-particle space. Note that

$$\widehat{n}_i^{N+1} = \widehat{n}_i^N \otimes 1 + |i\rangle\langle i|^{(N+1)} \geq \widehat{n}_i^N \otimes 1\,.$$

Using this and the fact that $A(G) \geq \mu(G)$, we get

$$H_G^{N+1} - (N+1)\,\mu(G) \geq \left(H_G^N - N\mu(G)\right) \otimes 1\,.$$

Hence

$$\begin{aligned}\lambda^1_{N+1}(G) &= \min_{|\psi\rangle \in \mathcal{Z}_{N+1}(G):\ \langle\psi|\psi\rangle = 1} \langle\psi| H_G^{N+1} - (N+1)\,\mu(G) |\psi\rangle \\ &\geq \min_{|\psi\rangle \in \mathcal{Z}_N(G)\otimes\mathbb{C}^{|V|}:\ \langle\psi|\psi\rangle = 1} \langle\psi| \left(H_G^N - N\mu(G)\right) \otimes 1 |\psi\rangle \\ &= \lambda^1_N(G)\end{aligned}$$

(using the fact that $\mathcal{Z}_{N+1}(G) \subset \mathcal{Z}_N(G) \otimes \mathbb{C}^{|V|}$). □

In this paper we will encounter disconnected graphs G. In the cases of interest, the smallest eigenvalue of the adjacency matrix for each component is the same. The following lemma shows that the eigenvalues of $H(G,N)$ on such a graph can be written as sums of eigenvalues for the components. In this lemma (and throughout the paper), we let $[k] = \{1,2,\ldots,k\}$.

Lemma 2.4. *Suppose $G = \bigcup_{i=1}^k G_i$ with $\mu(G_1) = \mu(G_2) = \cdots = \mu(G_k)$. The eigenvalues of $H(G,N)$ are*

$$\sum_{i\in[k]:\ N_i \neq 0} \lambda^{y_i}_{N_i}(G_i)$$

where $N_1,\ldots,N_k \in \{0,1,2,\ldots\}$ with $\sum_i N_i = N$ and $y_i \in [D_{N_i}]$. The corresponding eigenvectors are (up to normalization)

$$\mathrm{Sym}\left(\bigotimes_{i\in[k]:\ N_i\neq 0} |\lambda^{y_i}_{N_i}(G_i)\rangle\right). \tag{2.9}$$

Proof. Recall that the action of $H_G - N\mu(G)$ on the Hilbert space (2.3) is the same as the action of $H(G,N)$ on the Hilbert space $\mathcal{Z}_N(G)$. States in these Hilbert spaces are identified via the mapping described in equation (2.6). It is convenient to prove the lemma by working with the second-quantized Hamiltonian H_G. We then translate our results into the first-quantized picture to obtain the stated claims.

For a graph with k components, equation (2.1) gives

$$H_G = \sum_{i=1}^k H_{G_i} \tag{2.10}$$

where $[H_{G_i}, H_{G_j}] = 0$. Label each vertex of G by (a,b) where $b \in [k]$ and $a \in [|V_b|]$, where V_b is the vertex set of the component G_b. An occupation number basis state (2.3) can be written

$$|l_{1,1},\ldots,l_{|V_1|,1}\rangle|l_{1,2},\ldots,l_{|V_2|,2}\rangle\ldots|l_{1,k},\ldots,l_{|V_k|,k}\rangle. \tag{2.11}$$

The Hamiltonian $H_G - N\mu(G)$ conserves the number of particles N_b in each component b. Within the sector corresponding to a given set $N_1,\ldots,N_k$ with $\sum_{i\in[k]} N_i = N$, we have

$$\begin{aligned}
&(H_G - N\mu(G))\,|l_{1,1},\ldots,l_{|V_1|,1}\rangle|l_{1,2},\ldots,l_{|V_2|,2}\rangle\ldots|l_{1,k},\ldots,l_{|V_k|,k}\rangle \\
&\quad = \big(H_{G_1} - N_1\mu(G_1)|l_{1,1},\ldots,l_{|V_1|,1}\rangle\big)|l_{1,2},\ldots,l_{|V_2|,2}\rangle\ldots|l_{1,k},\ldots,l_{|V_k|,k}\rangle \\
&\qquad + |l_{1,1},\ldots,l_{|V_1|,1}\rangle\big(H_{G_2} - N_2\mu(G_2)|l_{1,2},\ldots,l_{|V_2|,2}\rangle\big)\ldots|l_{1,k},\ldots,l_{|V_k|,k}\rangle + \cdots \\
&\qquad + |l_{1,1},\ldots,l_{|V_1|,1}\rangle|l_{1,2},\ldots,l_{|V_2|,2}\rangle\ldots\big(H_{G_k} - N_k\mu(G_k)|l_{1,k},\ldots,l_{|V_k|,k}\rangle\big),
\end{aligned}$$

where we used the fact that $\mu(G_i) = \mu(G)$ for $i \in [k]$. From this equation we see that the eigenstates of H_G can be obtained as product states with k factors in the basis (2.11). In each such product state, the i-th factor is an eigenstate of $H_{G_i} - N_i\mu(G_i) = H_{G_i} - N_i\mu(G)$ in the N_i-particle sector, with eigenvalue $\lambda_{N_i}^{j_i}(G_i)$. Rewriting this result in the "first-quantized" language, we obtain the lemma. □

2.3 Complexity of the Bose-Hubbard model

Given a K-vertex graph G and a number of particles N, how hard is it to approximate the ground energy of the N-particle Bose-Hubbard model $\bar{H}_G^N$ on G? We consider the following decision version of this computational problem.

Problem 2.5 (Bose-Hubbard Hamiltonian). We are given a K-vertex graph G, a number of particles N, a real number c, and a precision parameter $\varepsilon = 1/T$. The positive integers N and T are provided in unary; the graph is specified by its adjacency matrix, which can be any $K \times K$ symmetric 0-1 matrix. We are promised that either the smallest eigenvalue of $\bar{H}_G^N$ is at most c (yes instance) or is at least $c+\varepsilon$ (no instance) and we are asked to decide which is the case.

Here and elsewhere in this paper, we require inputs such as ε and T to be provided in unary so that the input size is measured accordingly. The parameter c is provided in a straightforward manner, with enough precision to resolve ε, i. e., using $\mathcal{O}(\log|c| + \log T)$ bits. The input size is therefore $\Theta(K^2 + T + N + \log|c|)$ bits. We prove that this problem is QMA-complete, providing evidence that approximating the ground energy of the N-particle Bose-Hubbard model on a graph G is intractable.

Theorem 2.6. *Bose-Hubbard Hamiltonian is* QMA*-complete.*

The proof of this theorem has two parts.

The easy part is to show that Bose-Hubbard Hamiltonian is contained in QMA. The basic strategy of Arthur's verification protocol is to measure the energy of the Bose-Hubbard Hamiltonian in the state $|\phi\rangle$ given to him by Merlin, using phase estimation and Hamiltonian simulation. Arthur accepts if the energy is small enough and rejects otherwise. We give a more detailed description of the verification procedure in Section 4.

The more involved part is to show that Bose-Hubbard Hamiltonian is QMA-hard. For this we show that any instance of a QMA problem can be converted (in deterministic polynomial time on a classical computer) into an equivalent instance of Bose-Hubbard Hamiltonian. In fact, our reduction proves a slightly stronger result, namely that a notable extremal case of Bose-Hubbard Hamiltonian is already QMA-hard. We now discuss this special case.

Recall from the previous section that the ground energy of the N-particle Bose-Hubbard model is at least N times the single-particle ground energy $\mu(G)$, i. e., $\lambda_N^1(G) \geq 0$. We can ask if this inequality is close to equality, i. e., is the N-particle Bose-Hubbard model close to being frustration free?

Problem 2.7 (Frustration-Free Bose-Hubbard Hamiltonian). We are given a K-vertex graph G, a number of particles $N \leq K$, and a precision parameter $\varepsilon = 1/T$. The integer $T \geq 4K$ is provided in unary; the graph is specified by its adjacency matrix, which can be any $K \times K$ symmetric 0-1 matrix. We are promised that either $\lambda_N^1(G) \leq \varepsilon^3$ (yes instance) or $\lambda_N^1(G) \geq \varepsilon + \varepsilon^3$ (no instance) and we are asked to decide which is the case.

For concreteness, we have made some specific choices in defining this problem. Our proof that it is QMA-hard also applies, for example, to variants of the problem where ε^3 is replaced (in both places it appears) by ε^α for any constant $\alpha \in \{1,2,3,\ldots\}$. In Section 2.4, we use the version with $\alpha = 3$ as stated above to facilitate a reduction to the XY Hamiltonian problem.

The requirement $T \geq 4K$ ensures that ε is small so that, for a yes instance, the system is very close to being frustration free. We choose the specific threshold $4K$ for concreteness.

The restriction $N \leq K$ is without loss of generality since the problem is trivial otherwise. To see this, note that any state with more than K particles is orthogonal to the nullspace of the interaction term since there are always two or more particles located at one vertex; hence $\lambda_N^1(G) \geq 2$ whenever $N \geq K+1$.

Frustration-Free Bose-Hubbard Hamiltonian is a special case of Bose-Hubbard Hamiltonian with $c = N\mu(G) + \varepsilon^3$. To prove that Bose-Hubbard Hamiltonian is QMA-hard, it therefore suffices to prove that Frustration-Free Bose-Hubbard Hamiltonian is QMA-hard. The bulk of this paper is concerned with the proof of this fact.

2.4 Complexity of the XY Hamiltonian problem

We reduce Frustration-Free Bose-Hubbard Hamiltonian to an eigenvalue problem for a class of 2-local Hamiltonians defined by graphs. The reduction is based on a well-known mapping between hard-core bosons and spin systems, which we now review.

We define the subspace $\mathcal{W}_N(G) \subset \mathcal{Z}_N(G)$ of N hard-core bosons on a graph G to consist of the states where each vertex of G is occupied by either 0 or 1 particle, i. e.,

$$\mathcal{W}_N(G) = \operatorname{span}\{\operatorname{Sym}(|i_1, i_2, \ldots, i_N\rangle)\colon\ i_1, \ldots, i_N \in V,\ i_j \neq i_k \text{ for distinct } j,k \in [N]\}\,.$$

A basis for $\mathcal{W}_N(G)$ is the subset of occupation-number states (2.6) labeled by bit strings $l_1 \ldots l_{|V|} \in \{0,1\}^{|V|}$ with Hamming weight $\sum_{j\in V} l_j = N$. The space $\mathcal{W}_N(G)$ can thus be identified with the weight-N subspace

$$\mathrm{Wt}_N(G) = \operatorname{span}\{|z_1, \ldots, z_{|V|}\rangle :\ z_i \in \{0,1\},\ \sum_{i=1}^{|V|} z_i = N\}$$

of a $|V|$-qubit Hilbert space. We consider the restriction of H_G^N to the space $\mathcal{W}_N(G)$, which can equivalently be written as a $|V|$-qubit Hamiltonian O_G restricted to the space $\mathrm{Wt}_N(G)$. In particular,

$$H_G^N\big|_{\mathcal{W}_N(G)} = O_G\big|_{\mathrm{Wt}_N(G)} \tag{2.12}$$

where

$$\begin{aligned} O_G &= \sum_{\substack{A(G)_{ij}=1 \\ i\neq j}} \big(|01\rangle\langle 10| + |10\rangle\langle 01|\big)_{ij} + \sum_{A(G)_{ii}=1} |1\rangle\langle 1|_i \\ &= \sum_{\substack{A(G)_{ij}=1 \\ i\neq j}} \frac{\sigma_x^i\sigma_x^j + \sigma_y^i\sigma_y^j}{2} + \sum_{A(G)_{ii}=1} \frac{1-\sigma_z^i}{2}. \end{aligned}$$

Note that the Hamiltonian O_G conserves the total magnetization

$$M_z = \sum_{i=1}^{|V|} \frac{1-\sigma_z^i}{2}$$

along the z axis.

We define $\theta_N(G)$ to be the smallest eigenvalue of (2.12), i. e., the ground energy of O_G in the sector with magnetization N. We show that approximating this quantity is QMA-complete.

Problem 2.8 (XY Hamiltonian). We are given a K-vertex graph G, an integer $N \leq K$, a real number c, and a precision parameter $\varepsilon = 1/T$. The positive integer T is provided in unary; the graph is specified by its adjacency matrix, which can be any $K \times K$ symmetric 0-1 matrix. We are promised that either $\theta_N(G) \leq c$ (yes instance) or else $\theta_N(G) \geq c + \varepsilon$ (no instance) and we are asked to decide which is the case.

Theorem 2.9. *XY Hamiltonian is* QMA*-complete.*

We prove QMA-hardness of XY Hamiltonian by reduction from Frustration-Free Bose-Hubbard Hamiltonian. The proof of Theorem 2.9 appears in Section 9.

2.5 Complexity of approximating the smallest eigenvalue of a graph

How hard is it to compute the smallest eigenvalue of a symmetric 0-1 matrix (i. e., the adjacency matrix of a graph)? If the matrix is given explicitly then this can be done in time polynomial in the input size. Instead, we consider adjacency matrices A specified by a (classical) circuit that takes as input the index r of a row and outputs the indices $\{j\colon A_{rj} = 1\}$ of the nonzero entries in that row. Note that the circuit describing a $D \times D$ matrix A must have size $\Omega(\log(D))$ since it takes as input a row index $r \in [D]$. Efficiently row-computable matrices are those described by circuits of size polynomial in $\log D$ [2]. We consider the following promise problem.

Problem 2.10 (**Minimum Graph Eigenvalue**). We are given a $D \times D$ symmetric 0-1 matrix A, specified by a classical deterministic circuit that takes as input a row $r \in [D]$ and computes the locations of the nonzero entries in that row. We are also given a real number a and a precision parameter $\varepsilon = 1/N$, where $N \in \mathbb{N}$ is specified in unary. We are promised that either the smallest eigenvalue of A is at most a (yes instance), or else it is at least $a + \varepsilon$ (no instance), and asked to decide which is the case.

The input size of this problem is the size of the circuit that describes A, plus the description size of a, plus N bits. The interesting set of instances are those for which A is efficiently row-computable, so that the input size is $\mathrm{poly}(\log D, 1/\varepsilon)$.

Theorem 2.11. *Minimum Graph Eigenvalue is* QMA*-complete.*

In the next section we prove this theorem.

3 Minimum Graph Eigenvalue is QMA-complete

The fact that Minimum Graph Eigenvalue is contained in QMA follows from standard techniques (applying phase estimation to the adjacency matrix) since a Hamiltonian that is a symmetric 0-1 matrix can be simulated efficiently as a function of the size of the circuit computing its rows [2].

To prove that Minimum Graph Eigenvalue is QMA-hard, we show that an instance of any problem in QMA can be converted (in deterministic polynomial time on a classical computer) into an equivalent instance of Minimum Graph Eigenvalue.

Recall that an instance x of a problem in QMA has a verification circuit $\mathcal{C}_x$ with n qubits and M gates, both upper bounded by a polynomial function of $|x|$. Here we assume that the verification circuit $\mathcal{C}_x$ satisfies a modified version of Definition 2.1 where the completeness parameter $2/3$ is replaced by $1 - 1/2^{|x|}$ (modifying the definition in this way still gives the same class QMA [21, 24]). In Section 3.1 we map $\mathcal{C}_x$ to a row-sparse and efficiently row-computable symmetric 0-1 matrix A_x. The mapping we exhibit has the following two properties (shown in Section 3.2 and Section 3.3, respectively):

1. If x is a yes instance then the smallest eigenvalue of A_x is at most $-1 - 3\sqrt{2} + \frac{1}{2M}\frac{1}{2^{|x|}}$.
2. If x is a no instance then the smallest eigenvalue of A_x is at least $-1 - 3\sqrt{2} + \frac{1}{120M^4 n}$.

Note that if $|x|$ is larger than some constant, then

$$\frac{1}{2M}\frac{1}{2^{|x|}} \leq \frac{1}{240M^4 n},$$

since M and n are both upper bounded by a polynomial in $|x|$. We assume without loss of generality that this holds. For any such instance x, we associate an instance of Minimum Graph Eigenvalue defined by the matrix A_x along with the number

$$a = -1 - 3\sqrt{2} + \frac{1}{240M^4 n}$$

and precision parameter

$$\varepsilon = \frac{1}{240M^4 n}.$$

Using the two claimed properties of the circuit-to-graph mapping, we see that if x is a yes instance then the smallest eigenvalue of A_x is at most a, and if it is a no instance then this eigenvalue is at least $a+\varepsilon$. This shows that Minimum Graph Eigenvalue is QMA-hard.

3.1 Circuit-to-graph mapping

We suppose $\mathcal{C}_x$ implements a unitary

$$U_{\mathcal{C}_x} = U_M \dots U_2 U_1 \tag{3.1}$$

where each U_i is from the universal gate set

$$\mathcal{G} = \{H, HT, (HT)^\dagger, (H\otimes 1)\,\mathrm{CNOT}\}$$

with

$$H = \frac{1}{\sqrt{2}}\begin{pmatrix} 1 & 1 \\ 1 & -1 \end{pmatrix}, \quad T = \begin{pmatrix} 1 & 0 \\ 0 & e^{i\frac{\pi}{4}} \end{pmatrix}, \quad \mathrm{CNOT} = \begin{pmatrix} 1 & 0 & 0 & 0 \\ 0 & 1 & 0 & 0 \\ 0 & 0 & 0 & 1 \\ 0 & 0 & 1 & 0 \end{pmatrix}.$$

The verification circuit $\mathcal{C}_x$ has an n_{in}-qubit input register and $n - n_{\mathrm{in}}$ ancilla qubits initialized to $|0\rangle$ at the beginning of the computation. One of these n qubits serves as an output qubit.

It will be convenient to consider

$$U_{\mathcal{C}_x}^\dagger U_{\mathcal{C}_x} = W_{2M} \dots W_2 W_1$$

where

$$W_t = \begin{cases} U_t & 1 \le t \le M \\ U_{2M+1-t}^\dagger & M+1 \le t \le 2M. \end{cases}$$

As in Section 5.1 we start with a version of the Feynman-Kitaev Hamiltonian [11, 21]

$$H_x = -\sqrt{2}\sum_{t=1}^{2M}\left(W_t^\dagger \otimes |t\rangle\langle t+1| + W_t \otimes |t+1\rangle\langle t|\right) \tag{3.2}$$

acting on the Hilbert space $\mathcal{H}_{\mathrm{comp}} \otimes \mathcal{H}_{\mathrm{clock}}$ where $\mathcal{H}_{\mathrm{comp}} = \left(\mathbb{C}^2\right)^{\otimes n}$ is an n-qubit computational register and $\mathcal{H}_{\mathrm{clock}} = \mathbb{C}^{2M}$ is a $2M$-level register with periodic boundary conditions (i. e., we let $|2M+1\rangle = |1\rangle$). Note that

$$V^\dagger H_x V = -\sqrt{2}\sum_{t=1}^{2M}\left(1 \otimes |t\rangle\langle t+1| + 1 \otimes |t+1\rangle\langle t|\right) \tag{3.3}$$

where

$$V = \sum_{t=1}^{2M}\left(\prod_{j=t-1}^{1} W_j\right) \otimes |t\rangle\langle t|$$

and $W_0 = 1$. Since V is unitary, the eigenvalues of H_x are the same as the eigenvalues of (3.3), namely

$$-2\sqrt{2}\cos\left(\frac{\pi\ell}{M}\right)$$

for $\ell = 0,\ldots,2M-1$. The ground energy of (3.3) is $-2\sqrt{2}$ and its ground space is spanned by

$$|\phi\rangle\frac{1}{\sqrt{2M}}\sum_{j=1}^{2M}|t\rangle\,,\quad |\phi\rangle\in\Lambda\,,$$

where Λ is any orthonormal basis for $\mathcal{H}_{\text{comp}}$. A basis for the ground space of H_x is therefore

$$V\left(|\phi\rangle\frac{1}{\sqrt{2M}}\sum_{j=1}^{2M}|t\rangle\right)=\frac{1}{\sqrt{2M}}\sum_{t=1}^{2M}W_{t-1}W_{t-2}\ldots W_1|\phi\rangle|t\rangle$$

where $|\phi\rangle\in\Lambda$. The first excited energy of H_x is

$$\eta=-2\sqrt{2}\cos\left(\frac{\pi}{M}\right)$$

and the gap between ground and first excited energies is lower bounded as

$$\eta+2\sqrt{2}\geq\sqrt{2}\frac{\pi^2}{M^2} \tag{3.4}$$

(using the fact that $1-\cos(x)\leq x^2/2$).

Now we modify (3.2) to give a symmetric 0-1 matrix. The trick we use is a variant of one used in references [16, 18] for similar purposes.

The universal set $\mathcal{G}$ is chosen so that each gate has nonzero entries that are integer powers of $\omega = e^{i\frac{\pi}{4}}$. Correspondingly, the nonzero standard basis matrix elements of H_x are also integer powers of $\omega = e^{i\frac{\pi}{4}}$. We consider the 8×8 shift operator

$$S=\sum_{j=0}^{7}|j+1 \bmod 8\rangle\langle j| \tag{3.5}$$

and note that ω is an eigenvalue of S with eigenvector

$$|\omega\rangle=\frac{1}{\sqrt{8}}\sum_{j=0}^{7}\omega^{-j}|j\rangle\,. \tag{3.6}$$

We modify H_x as follows. For each operator $-\sqrt{2}H$, $-\sqrt{2}HT$, $-\sqrt{2}(HT)^\dagger$, or $-\sqrt{2}\,(H\otimes 1)\,\text{CNOT}$ appearing in equation (3.2), define another operator that acts on $\mathbb{C}^2\otimes\mathbb{C}^8$ or $\mathbb{C}^4\otimes\mathbb{C}^8$ (as appropriate) by replacing nonzero matrix elements with powers of the operator S:

$$\omega^k\mapsto S^k.$$

Matrix elements that are zero are mapped to the 8×8 all-zeroes matrix. Write $B(W)$ for the operators obtained by making this replacement, e. g.,

$$-\sqrt{2}HT = \begin{pmatrix} \omega^4 & \omega^5 \\ \omega^4 & \omega \end{pmatrix} \mapsto B(HT) = \begin{pmatrix} S^4 & S^5 \\ S^4 & S \end{pmatrix}.$$

Adjoining an 8-level ancilla as a third register and making this replacement in equation (3.2) gives

$$H_{\text{prop}} = \sum_{t=1}^{2M} \left(B(W_t)_{13}^{\dagger} \otimes |t\rangle\langle t+1|_2 + B(W_t)_{13} \otimes |t+1\rangle\langle t|_2 \right) \tag{3.7}$$

which is a symmetric 0-1 matrix (the subscripts indicate which registers the operators act on). Note that H_{prop} commutes with S (acting on the 8-level ancilla) and therefore is block diagonal with eight sectors. In the sector where S has eigenvalue ω, H_{prop} is identical to the Hamiltonian H_x that we started with (see equation (3.2)). There is also a sector (where S has eigenvalue ω^*) where the Hamiltonian is the complex conjugate of H_x. We will add a term to H_{prop} that introduces an energy penalty for states in any of the other six sectors, ensuring that none of these states lie in the ground space.

To see what kind of energy penalty is needed, we lower bound the eigenvalues of H_{prop}. Note that for each $W \in \mathcal{G}$, $B(W)$ contains at most 2 ones in each row or column. Looking at equation (3.7) and using this fact, we see that each row and each column of H_{prop} contains at most four ones (with the remaining entries all zero). Therefore $\|H_{\text{prop}}\| \leq 4$, so every eigenvalue of H_{prop} is at least -4.

The matrix A_x associated with the circuit $\mathcal{C}_x$ acts on the Hilbert space

$$\mathcal{H}_{\text{comp}} \otimes \mathcal{H}_{\text{clock}} \otimes \mathcal{H}_{\text{anc}}$$

where $\mathcal{H}_{\text{anc}} = \mathbb{C}^8$ holds the 8-level ancilla. We define

$$A_x = H_{\text{prop}} + H_{\text{penalty}} + H_{\text{input}} + H_{\text{output}} \tag{3.8}$$

where

$$H_{\text{penalty}} = 1 \otimes 1 \otimes \left(S^3 + S^4 + S^5 \right) \tag{3.9}$$

is the penalty ensuring that the ancilla register holds either $|\omega\rangle$ or $|\omega^*\rangle$ and the terms

$$H_{\text{input}} = \sum_{j=n_{\text{in}}+1}^{n} |1\rangle\langle 1|_j \otimes |1\rangle\langle 1| \otimes 1$$
$$H_{\text{output}} = |0\rangle\langle 0|_{\text{out}} \otimes |M+1\rangle\langle M+1| \otimes 1$$

ensure that the ancilla qubits are initialized in the state $|0\rangle$ when $t = 1$ and that the output qubit is in the state $|1\rangle\langle 1|$ when the circuit $\mathcal{C}_x$ has been applied (i. e., at time $t = M+1$). Observe that A_x is a symmetric 0-1 matrix.

Now consider the ground space of the first two terms $H_{\text{prop}} + H_{\text{penalty}}$ in (3.8). Note that

$$[H_{\text{prop}}, H_{\text{penalty}}] = 0\,,$$

so these operators can be simultaneously diagonalized. Furthermore, H_{penalty} has smallest eigenvalue $-1-\sqrt{2}$, with eigenspace spanned by $|\omega\rangle$ and $|\omega^*\rangle$. One can also easily confirm that the first excited energy of H_{penalty} is -1.

The ground space of $H_{\text{prop}}+H_{\text{penalty}}$ lives in the sector where H_{penalty} has minimal eigenvalue $-1-\sqrt{2}$. To see this, note that within this sector H_{prop} has the same eigenvalues as H_x, and therefore has lowest eigenvalue $-2\sqrt{2}$. The minimum eigenvalue e_1 of $H_{\text{prop}}+H_{\text{penalty}}$ in this sector is

$$e_1 = -2\sqrt{2}+\left(-1-\sqrt{2}\right) = -1-3\sqrt{2} = -5.24\ldots, \tag{3.10}$$

whereas in any other sector H_{penalty} has eigenvalue at least -1 and (using the fact that $H_{\text{prop}} \geq -4$) the minimum eigenvalue of $H_{\text{prop}}+H_{\text{penalty}}$ is at least -5. Thus, an orthonormal basis for the ground space of $H_{\text{prop}}+H_{\text{penalty}}$ is furnished by the states

$$\frac{1}{\sqrt{2M}}\sum_{t=1}^{2M} W_{t-1}W_{t-2}\ldots W_1|\phi\rangle|t\rangle|\omega\rangle \tag{3.11}$$

$$\frac{1}{\sqrt{2M}}\sum_{t=1}^{2M} (W_{t-1}W_{t-2}\ldots W_1)^*|\phi^*\rangle|t\rangle|\omega^*\rangle \tag{3.12}$$

where $|\phi\rangle$ ranges over the basis Λ for $\mathcal{H}_{\text{comp}}$ and $*$ denotes (elementwise) complex conjugation.

3.2 Upper bound on the smallest eigenvalue for yes instances

Suppose x is a yes instance; then there exists some n_{in}-qubit state $|\psi_{\text{in}}\rangle$ satisfying $\text{AP}(\mathcal{C}_x,|\psi_{\text{in}}\rangle) \geq 1-(1/2^{|x|})$. Let

$$|\text{wit}\rangle = \frac{1}{\sqrt{2M}}\sum_{t=1}^{2M} W_{t-1}W_{t-2}\ldots W_1\left(|\psi_{\text{in}}\rangle|0\rangle^{\otimes n-n_{\text{in}}}\right)|t\rangle|\omega\rangle$$

and note that this state is in the e_1-energy ground space of $H_{\text{prop}}+H_{\text{penalty}}$ (since it has the form (3.11)). One can also directly verify that $|\text{wit}\rangle$ has zero energy for H_{input}. Thus

$$\begin{aligned}
\langle\text{wit}|A_x|\text{wit}\rangle &= e_1 + \langle\text{wit}|H_{\text{output}}|\text{wit}\rangle \\
&= e_1 + \frac{1}{2M}\langle\psi_{\text{in}}|\langle 0|^{\otimes n-n_{\text{in}}}U_{\mathcal{C}_x}^\dagger|0\rangle\langle 0|_{\text{out}}U_{\mathcal{C}_x}|\psi_{\text{in}}\rangle|0\rangle^{\otimes n-n_{\text{in}}} \\
&= e_1 + \frac{1}{2M}\left(1-\text{AP}(\mathcal{C}_x,|\psi_{\text{in}}\rangle)\right) \\
&\leq e_1 + \frac{1}{2M}\frac{1}{2^{|x|}}.
\end{aligned}$$

3.3 Lower bound on the smallest eigenvalue for no instances

Now suppose x is a no instance. Then the verification circuit $\mathcal{C}_x$ has acceptance probability $\text{AP}(\mathcal{C}_x,|\psi\rangle) \leq 1/3$ for all n_{in}-qubit input states $|\psi\rangle$.

We backtrack slightly to obtain bounds on the eigenvalue gaps of the Hamiltonians $H_{\text{prop}}+H_{\text{penalty}}$ and $H_{\text{prop}}+H_{\text{penalty}}+H_{\text{input}}$. We begin by showing that the energy gap of $H_{\text{prop}}+H_{\text{penalty}}$ is at least an

inverse polynomial function of M. Subtracting a constant equal to the ground energy times the identity matrix sets the smallest eigenvalue to zero, and the smallest nonzero eigenvalue satisfies

$$\gamma(H_{\text{prop}} + H_{\text{penalty}} - e_1 \cdot 1) \geq \min\left\{\sqrt{2}\frac{\pi^2}{M^2}, -5 - e_1\right\} \geq \frac{1}{5M^2} \tag{3.13}$$

since $-5 - e_1 \approx 0.24\ldots > 1/5$. The first inequality above follows from the fact that every eigenvalue of H_{prop} in the range $[e_1, -5)$ is also an eigenvalue of H_x (as discussed above) and the bound (3.4) on the energy gap of H_x.

Now use the Nullspace Projection Lemma (Lemma 8.1) with

$$H_A = H_{\text{prop}} + H_{\text{penalty}} - e_1 \cdot 1\,, \qquad H_B = H_{\text{input}}\,.$$

Note that H_A and H_B are positive semidefinite. Let S_A be the ground space of H_A and consider the restriction $H_B|_{S_A}$. Here it is convenient to use the basis for S_A given by (3.11) and (3.12) with $|\phi\rangle$ ranging over the computational basis states of n qubits. In this basis, $H_B|_{S_A}$ is diagonal with all diagonal entries equal to $1/(2M)$ times an integer, so $\gamma(H_B|_{S_A}) \geq 1/(2M)$. We also have $\gamma(H_A) \geq 1/(5M^2)$ from equation (3.13), and clearly $\|H_B\| \leq n$. Thus Lemma 8.1 gives

$$\gamma(H_{\text{prop}} + H_{\text{penalty}} + H_{\text{input}} - e_1 \cdot 1) \geq \frac{\left(\frac{1}{5M^2}\right)\left(\frac{1}{2M}\right)}{\frac{1}{5M^2} + \frac{1}{2M} + n} \geq \frac{1}{10M^3\,(1+n)} \geq \frac{1}{20M^3 n}. \tag{3.14}$$

Now consider adding the final term H_{output}. We use Lemma 8.1 again, now setting

$$H_A = H_{\text{prop}} + H_{\text{penalty}} + H_{\text{input}} - e_1 \cdot 1\,, \qquad H_B = H_{\text{output}}\,.$$

Let S_A be the ground space of H_A. Note that it is spanned by states of the form (3.11) and (3.12) where $|\phi\rangle = |\psi\rangle|0\rangle^{\otimes n - n_{\text{in}}}$ and $|\psi\rangle$ ranges over any orthonormal basis of the n_{in}-qubit input register. The restriction $H_B|_{S_A}$ is block diagonal, with one block for states of the form

$$\frac{1}{\sqrt{2M}} \sum_{t=1}^{2M} W_{t-1} W_{t-2} \ldots W_1 \left(|\psi\rangle|0\rangle^{\otimes n - n_{\text{in}}}\right) |t\rangle|\omega\rangle \tag{3.15}$$

and another block for states of the form

$$\frac{1}{\sqrt{2M}} \sum_{t=1}^{2M} (W_{t-1} W_{t-2} \ldots W_1)^* \left(|\psi\rangle^*|0\rangle^{\otimes n - n_{\text{in}}}\right) |t\rangle|\omega^*\rangle\,. \tag{3.16}$$

We now show that the minimum eigenvalue of $H_B|_{S_A}$ is nonzero, and we lower bound it. We consider the two blocks separately. By linearity, every state in the first block can be written in the form (3.15) for some state $|\psi\rangle$. Thus the minimum eigenvalue within this block is the minimum expectation of H_{output} in a state (3.15), where the minimum is taken over all n_{in}-qubit states $|\psi\rangle$. This is equal to

$$\min_{|\psi\rangle} \frac{1}{2M}\left(1 - \text{AP}(\mathcal{C}_x, |\psi\rangle)\right) \geq \frac{1}{3M}$$

where we used the fact that $\mathrm{AP}(\mathcal{C}_x, |\psi\rangle) \leq 1/3$ for all $|\psi\rangle$. Likewise, every state in the second block can be written as (3.16) for some state $|\psi\rangle$, and the minimum eigenvalue within this block is

$$\min_{|\psi\rangle} \frac{1}{2M} \left(1 - \mathrm{AP}(\mathcal{C}_x, |\psi\rangle)^*\right) \geq \frac{1}{3M}$$

(since $\mathrm{AP}(\mathcal{C}_x, |\psi\rangle)^* = \mathrm{AP}(\mathcal{C}_x, |\psi\rangle) \leq 1/3$). Thus we see that $H_B|_{S_A}$ has an empty nullspace, so its smallest eigenvalue is equal to its smallest nonzero eigenvalue, namely

$$\gamma(H_B|_{S_A}) \geq \frac{1}{3M}.$$

Now applying Lemma 8.1 using this bound, the fact that $\|H_B\| = 1$, and the fact that

$$\gamma(H_A) \geq \frac{1}{20M^3 n}$$

(from equation (3.14)), we get

$$\gamma(A_x - e_1 \cdot 1) \geq \frac{\frac{1}{60M^4 n}}{\frac{1}{20M^3 n} + \frac{1}{3M} + 1} \geq \frac{1}{120M^4 n}.$$

Since $H_B|_{S_A}$ has an empty nullspace, $A_x - e_1 \cdot 1$ has an empty nullspace, and this is a lower bound on its smallest eigenvalue.

4 Bose-Hubbard Hamiltonian is contained in QMA

To prove that Bose-Hubbard Hamiltonian is contained in QMA, we provide a verification algorithm satisfying the requirements of Definition 2.1. In the definition this algorithm is specified by a circuit involving only one measurement of the output qubit at the end of the computation. The procedure we describe below, which contains intermediate measurements in the computational basis, can be converted into a verification circuit of the desired form by standard techniques.

We are given an instance specified by G, N, c, and ε. We are also given an input state $|\phi\rangle$ of n_{in} qubits, where $n_{\mathrm{in}} = \lceil \log_2 D_N \rceil$ and D_N is the dimension of $\mathcal{Z}_N(G)$ as given in equation (2.4). Note, using the inequality $\binom{a}{b} \leq a^b$ in equation (2.4), that $n_{\mathrm{in}} = \mathcal{O}(K \log(N+K))$, where $K = |V|$ is the number of vertices in the graph G. We embed $\mathcal{Z}_N(G)$ into the space of n_{in} qubits straightforwardly as the subspace spanned by the first D_N standard basis vectors (with lexicographic ordering, say). The first step of the verification procedure is to measure the projector onto this space $\mathcal{Z}_N(G)$. If the measurement outcome is 1 then the resulting state $|\phi'\rangle$ is in $\mathcal{Z}_N(G)$ and we continue; otherwise we reject.

In the second step of the verification procedure, the goal is to measure $\bar{H}_G^N$ in the state $|\phi'\rangle$. The Hamiltonian $\bar{H}_G^N$ is sparse and efficiently row-computable, with norm

$$\left\|\bar{H}_G^N\right\| \leq \left\|H_G^N\right\| \leq N \|A(G)\| + \left\| \sum_{k \in V} \hat{n}_k (\hat{n}_k - 1) \right\| \leq NK + N^2.$$

We use phase estimation (see for example [9]) to estimate the energy of $|\phi'\rangle$, using sparse Hamiltonian simulation [2] to approximate evolution according to $\bar{H}_G^N$. We choose the parameters of the phase estimation so that, with probability at least $2/3$, it produces an approximation E of the energy with error at most $\varepsilon/4$. This can be done in time $\mathrm{poly}(N,K,1/\varepsilon)$. If $E \leq c+\varepsilon/2$ then we accept; otherwise we reject.

We now show that this verification procedure satisfies the completeness and soundness requirements of Definition 2.1. For a yes instance, an eigenvector of $\bar{H}_G^N$ with eigenvalue $e \leq c$ is accepted by this procedure as long as the energy E computed in the phase estimation step has the desired precision. To see this, note that we measure $|E-e| \leq \varepsilon/4$, and hence $E \leq c+\varepsilon/4$, with probability at least $2/3$. For a no instance, write $|\phi'\rangle \in \mathcal{Z}_N(G)$ for a state obtained after passing the first step. The value E computed by the subsequent phase estimation step satisfies $E \geq c+(3\varepsilon/4)$ with probability at least $2/3$, in which case the state is rejected. From this we see that the probability of accepting a no instance is at most $1/3$.

5 Gate graphs

In Section 5 and Section 6, we develop machinery for proving that Bose-Hubbard Hamiltonian is QMA-hard (as shown in Section 7). In this section we define a class of graphs (*gate graphs*) and a diagrammatic notation for them (*gate diagrams*). We also discuss the Bose-Hubbard model on these graphs.

Every gate graph is constructed using a specific 128-vertex graph g_0 as a building block. This graph is shown in Figure 5.1 and discussed in Section 5.1. In Section 5.2 we define gate graphs and gate diagrams. A gate graph is obtained by adding edges and self-loops (in a prescribed way) to a collection of disjoint copies of g_0.

In Section 5.3 we discuss the ground states of the Bose-Hubbard model on gate graphs. For any gate graph G, the smallest eigenvalue $\mu(G)$ of the adjacency matrix $A(G)$ satisfies $\mu(G) \geq -1-3\sqrt{2}$. It is convenient to define the constant

$$e_1 = -1-3\sqrt{2}. \tag{5.1}$$

When $\mu(G) = e_1$ we say G is an e_1-gate graph. We focus on the frustration-free states of e_1-gate graphs (recall from Definition 2.2 that $|\phi\rangle \in \mathcal{Z}_N(G)$ is frustration free if and only if $H(G,N)|\phi\rangle = 0$). We show that all such states live in a convenient subspace (called $\mathcal{I}(G,N)$) of the N-particle Hilbert space. This subspace has the property that no two (or more) particles ever occupy vertices of the same copy of g_0. The restriction to this subspace makes it easier to analyze the ground space.

In Section 5.4 we consider a class of subspaces that, like $\mathcal{I}(G,N)$, are defined by a set of constraints on the locations of N particles in an e_1-gate graph G. We state an "Occupancy Constraints Lemma" (proven in Section 10) that relates a subspace of this form to the ground space of the Bose-Hubbard model on a graph derived from G.

5.1 The graph g_0

Consider the single-qubit circuit $\mathcal{C}_0$ with four gates

$$U_1 = U_2 = H\,, \qquad U_3 = HT\,, \qquad U_4 = (HT)^\dagger\,,$$

with

$$H = \frac{1}{\sqrt{2}}\begin{pmatrix}1 & 1\\ 1 & -1\end{pmatrix}, \qquad T = \begin{pmatrix}1 & 0\\ 0 & e^{i\frac{\pi}{4}}\end{pmatrix}.$$

We use the construction described in Section 3.1 to map this circuit to a graph g_0. The adjacency matrix of g_0 is $H_{\text{prop}} + H_{\text{penalty}}$ as defined in (3.7) and (3.9). The resulting graph is shown in Figure 5.1.

Each vertex of g_0 corresponds to a standard basis vector in the Hilbert space $\mathbb{C}^2 \otimes \mathbb{C}^8 \otimes \mathbb{C}^8$. We label the vertices (z,t,j) with $z \in \{0,1\}$ describing the state of the computational qubit, $t \in [8]$ giving the state of the clock, and $j \in \{0,\ldots,7\}$ describing the state of the ancilla.

As shown in Section 3.1, the smallest eigenvalue of $A(g_0)$ is $e_1 = -1-3\sqrt{2}$. According to equations (3.11) and (3.12), an orthonormal basis for the ground space of $A(g_0)$ consists of the states

$$|\psi_{z,0}\rangle = \frac{1}{\sqrt{8}}\big(|z\rangle(|1\rangle+|3\rangle+|5\rangle+|7\rangle) + H|z\rangle(|2\rangle+|8\rangle) + HT|z\rangle(|4\rangle+|6\rangle)\big)|\omega\rangle \tag{5.2}$$

$$|\psi_{z,1}\rangle = |\psi_{z,0}\rangle^* \tag{5.3}$$

where $z \in \{0,1\}$.

Note that the amplitudes of $|\psi_{z,0}\rangle$ in the above basis contain the result of computing either the identity, Hadamard, or HT gate acting on the "input" state $|z\rangle$.

5.2 Gate graphs and gate diagrams

We use three different schematic representations of the graph g_0 (defined in Section 5.1), as depicted in Figure 5.2. We call these figures *diagram elements*; they are also the simplest examples of *gate diagrams*, which we define shortly.

The black and grey circles in a diagram element are called "nodes." Each node has a label (z,t). The only difference between the three diagram elements is the labeling of their nodes. In particular, the nodes in the diagram element $U \in \{1,H,HT\}$ correspond to values of $t \in [8]$ where the first register in equation (5.2) is either $|z\rangle$ or $U|z\rangle$. For example, the nodes for the H diagram element have labels with $t \in \{1,3\}$ (where $|\psi_{z,0}\rangle$ contains the "input" $|z\rangle$) or $t = \{2,8\}$ (where $|\psi_{z,0}\rangle$ contains the "output" $H|z\rangle$). We draw the input nodes in black and the output nodes in grey.

The rules for constructing gate diagrams are simple. A gate diagram consists of some number $R \in \{1,2,\ldots\}$ of diagram elements, with self-loops attached to a subset $\mathcal{S}$ of the nodes and edges connecting a set $\mathcal{E}$ of pairs of nodes. A node may have a single edge or a single self-loop attached to it, but never more than one edge or self-loop and never both an edge and a self-loop. Each node in a gate diagram has a label (q,z,t) where $q \in [R]$ indicates the diagram element it belongs to. An example is shown in Figure 5.3. Sometimes it is convenient to draw the input nodes on the right-hand side of a diagram element; e. g., in Figure 6.1 the node closest to the top left corner is labeled $(q,z,t) = (3,0,2)$.

To every gate diagram we associate a *gate graph* G with vertex set

$$\{(q,z,t,j)\colon q \in [R], z \in \{0,1\}, t \in [8], j \in \{0,\ldots,7\}\}$$

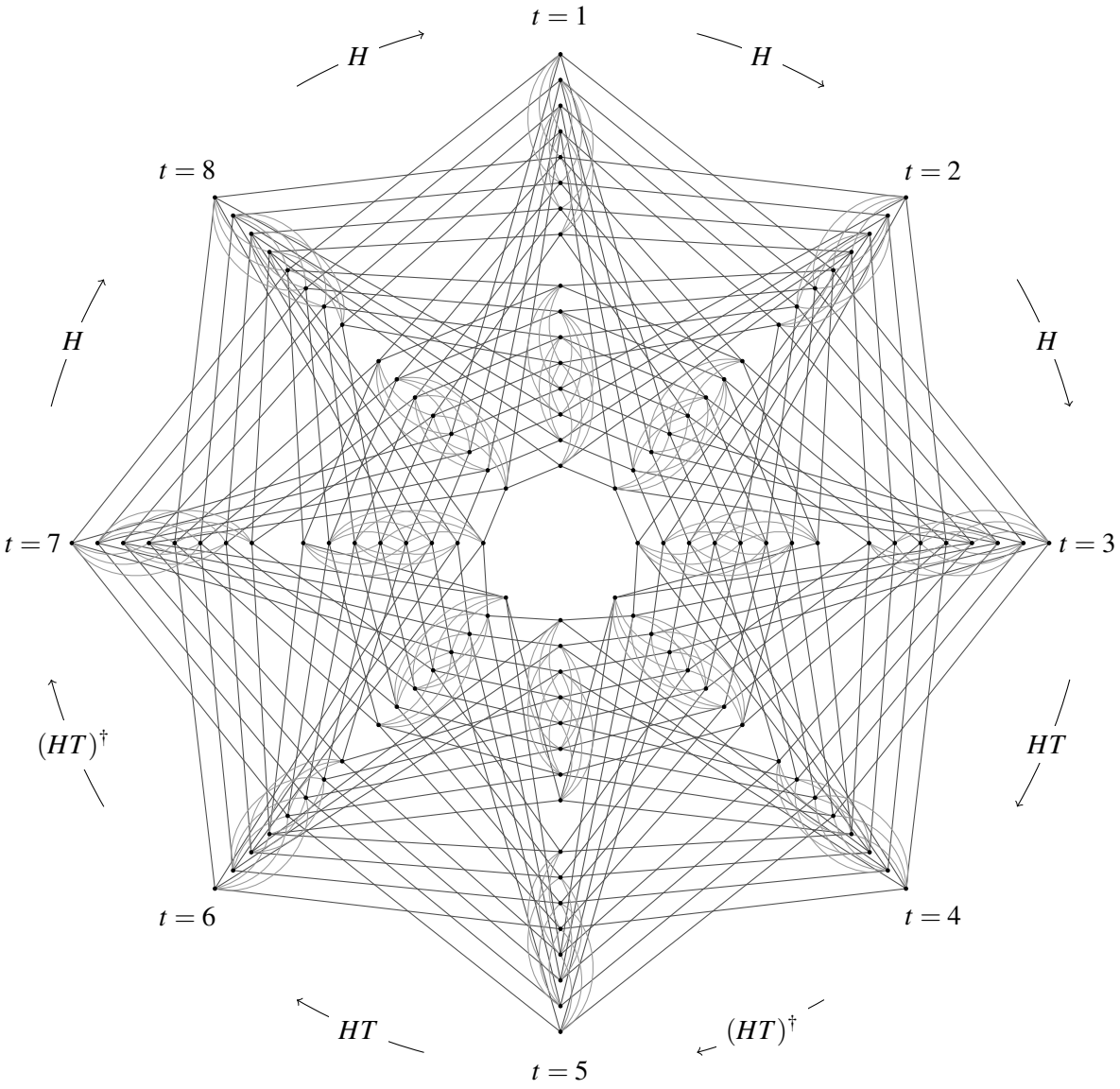

Figure 5.1: The graph g_0.

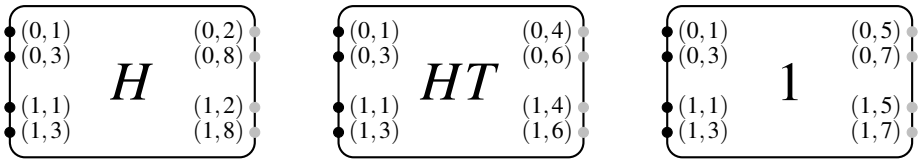

Figure 5.2: Diagram elements from which a gate diagram is constructed. Each diagram element is a schematic representation of the graph g_0 shown in Figure 5.1.

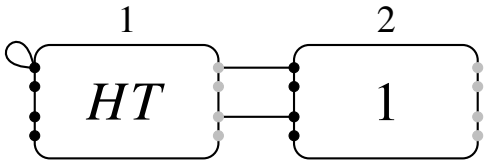

Figure 5.3: A gate diagram with two diagram elements labeled $q = 1$ (left) and $q = 2$ (right).

and adjacency matrix

$$A(G) = 1_q \otimes A(g_0) + h_{\mathcal{S}} + h_{\mathcal{E}} \tag{5.4}$$

$$h_{\mathcal{S}} = \sum_{\mathcal{S}} |q,z,t\rangle\langle q,z,t| \otimes 1_j \tag{5.5}$$

$$h_{\mathcal{E}} = \sum_{\mathcal{E}} \left(|q,z,t\rangle + |q',z',t'\rangle\right)\left(\langle q,z,t| + \langle q',z',t'|\right) \otimes 1_j. \tag{5.6}$$

The sums in equations (5.5) and (5.6) run over the set of nodes with self-loops $(q,z,t) \in \mathcal{S}$ and the set of pairs of nodes connected by edges $\{(q,z,t),(q',z',t')\} \in \mathcal{E}$, respectively. We write 1_q and 1_j for the identity operator on the registers with variables q and j, respectively. We see from the above expression that each self-loop in the gate diagram corresponds to 8 self-loops in the graph G, and an edge in the gate diagram corresponds to 8 edges and 16 self-loops in G.

Since a node in a gate graph never has more than one edge or self-loop attached to it, equations (5.5) and (5.6) are sums of orthogonal Hermitian operators. Therefore

$$\|h_{\mathcal{S}}\| = \max_{\mathcal{S}} \left\| |q,z,t\rangle\langle q,z,t| \otimes 1_j \right\| = 1 \quad \text{if } \mathcal{S} \neq \emptyset \tag{5.7}$$

$$\|h_{\mathcal{E}}\| = \max_{\mathcal{E}} \left\| \left(|q,z,t\rangle + |q',z',t'\rangle\right)\left(\langle q,z,t| + \langle q',z',t'|\right) \otimes 1_j \right\| = 2 \quad \text{if } \mathcal{E} \neq \emptyset \tag{5.8}$$

for any gate graph. (Of course, this also shows that $\|h_{\mathcal{S}'}\| = 1$ and $\|h_{\mathcal{E}'}\| = 2$ for any nonempty subsets $\mathcal{S}' \subseteq \mathcal{S}$ and $\mathcal{E}' \subseteq \mathcal{E}$.)

5.3 Frustration-free states on e_1-gate graphs

Consider the adjacency matrix $A(G)$ of a gate graph G, and note (from equation (5.4)) that its smallest eigenvalue $\mu(G)$ satisfies

$$\mu(G) \geq e_1$$

since $h_{\mathcal{S}}$ and $h_{\mathcal{E}}$ are positive semidefinite and $A(g_0)$ has smallest eigenvalue e_1. In the special case where $\mu(G) = e_1$, we say G is an e_1-gate graph.

Definition 5.1. An e_1-gate graph is a gate graph G such that the smallest eigenvalue of its adjacency matrix is $e_1 = -1 - 3\sqrt{2}$.

When G is an e_1-gate graph, a single-particle ground state $|\Gamma\rangle$ of $A(G)$ has minimal energy for each term in (5.4), i. e., it satisfies

$$(1 \otimes A(g_0))\,|\Gamma\rangle = e_1 |\Gamma\rangle \tag{5.9}$$

$$h_{\mathcal{S}}|\Gamma\rangle = 0 \tag{5.10}$$

$$h_{\mathcal{E}}|\Gamma\rangle = 0\,. \tag{5.11}$$

Indeed, to show that a given gate graph G is an e_1-gate graph, it suffices to find a state $|\Gamma\rangle$ satisfying these conditions. Note that equation (5.9) implies that $|\Gamma\rangle$ can be written as a superposition of the states

$$|\psi^q_{z,a}\rangle = |q\rangle|\psi_{z,a}\rangle, \quad z,a \in \{0,1\}, q \in [R]\,,$$

where $|\psi_{z,a}\rangle$ is given by equations (5.2) and (5.3). The coefficients in the superposition are then constrained by equations (5.10) and (5.11).

Example 5.2. As an example, we show the gate graph in Figure 5.3 is an e_1-gate graph. As noted above, equation (5.9) lets us restrict our attention to the space spanned by the eight states $|\psi^q_{z,a}\rangle$ with $z,a \in \{0,1\}$ and $q \in \{1,2\}$. In this basis, the operators $h_{\mathcal{S}}$ and $h_{\mathcal{E}}$ only have nonzero matrix elements between states with the same value of $a \in \{0,1\}$. We therefore solve for the e_1 energy ground states with $a = 0$ and those with $a = 1$ separately. Consider a ground state of the form

$$\left(\tau_1|\psi^1_{0,a}\rangle + \nu_1|\psi^1_{1,a}\rangle\right) + \left(\tau_2|\psi^2_{0,a}\rangle + \nu_2|\psi^2_{1,a}\rangle\right)$$

and note that in this case (5.10) implies $\tau_1 = 0$. Equation (5.11) gives

$$\begin{pmatrix}\tau_2\\ \nu_2\end{pmatrix} = \begin{cases} HT\begin{pmatrix}-\tau_1\\ -\nu_1\end{pmatrix} & a = 0 \\ (HT)^*\begin{pmatrix}-\tau_1\\ -\nu_1\end{pmatrix} & a = 1. \end{cases}$$

We find two orthogonal e_1-energy states, which are (up to normalization)

$$|\psi^1_{1,0}\rangle - \frac{e^{i\frac{\pi}{4}}}{\sqrt{2}}\left(|\psi^2_{0,0}\rangle - |\psi^2_{1,0}\rangle\right) \tag{5.12}$$

$$|\psi^1_{1,1}\rangle - \frac{e^{-i\frac{\pi}{4}}}{\sqrt{2}}\left(|\psi^2_{0,1}\rangle - |\psi^2_{1,1}\rangle\right). \tag{5.13}$$

We interpret each of these states as encoding a qubit that is transformed at each set of input/output nodes in the gate diagram in Figure 5.3. The encoded qubit begins on the input nodes of the first diagram element in the state

$$\begin{pmatrix} \tau_1 \\ \nu_1 \end{pmatrix} = \begin{pmatrix} 0 \\ 1 \end{pmatrix}$$

because the self-loop penalizes the basis vectors $|\psi^1_{0,a}\rangle$. On the output nodes of diagram element 1, the encoded qubit is in the state where either HT (if $a = 0$) or its complex conjugate (if $a = 1$) has been applied. The edges in the gate diagram ensure that the encoded qubit on the input nodes of diagram element 2 is minus the state on the output nodes of diagram element 1.

In this example, each single-particle ground state encodes a single-qubit computation. Later we show how N-particle frustration-free states on e_1-gate graphs can encode computations on N qubits. Recall from Definition 2.2 that an N-particle bosonic state $|\Gamma\rangle \in \mathcal{Z}_N(G)$ is said to be frustration free if and only if $H(G,N)|\Gamma\rangle = 0$. Note that $H(G,N) \geq 0$, so an N-particle frustration-free state is necessarily a ground state. Putting this together with Lemma 2.3, we see that the existence of an N-particle frustration-free state implies

$$\lambda^1_N(G) = \lambda^1_{N-1}(G) = \cdots = \lambda^1_1(G) = 0\,,$$

i. e., there are N'-particle frustration-free states for all $N' \leq N$.

We prove that the graph g_0 has no two-particle frustration-free states. By Lemma 2.3, it follows that g_0 has no N-particle frustration-free states for $N \geq 2$.

Lemma 5.3. $\lambda^1_2(g_0) > 0$.

Proof. Suppose (for a contradiction) that $|Q\rangle \in \mathcal{Z}_2(g_0)$ is a nonzero vector in the nullspace of $H(g_0,2)$, so

$$H^2_{g_0}|Q\rangle = \left(A(g_0)\otimes 1 + 1\otimes A(g_0) + 2\sum_{v\in g_0} |v\rangle\langle v|\otimes|v\rangle\langle v|\right)|Q\rangle = 2e_1|Q\rangle\,.$$

This implies

$$A(g_0)\otimes 1|Q\rangle = 1\otimes A(g_0)|Q\rangle = e_1|Q\rangle$$

since $A(g_0)$ has smallest eigenvalue e_1 and the interaction term is positive semidefinite. We can therefore write

$$|Q\rangle = \sum_{z,a,x,y\in\{0,1\}} Q_{za,xy}|\psi_{z,a}\rangle|\psi_{x,y}\rangle$$

with $Q_{za,xy} = Q_{xy,za}$ (since $|Q\rangle \in \mathcal{Z}_2(g_0)$) and

$$\left(|v\rangle\langle v|\otimes|v\rangle\langle v|\right)|Q\rangle = 0 \tag{5.14}$$

for all vertices $v = (z,t,j) \in g_0$. Using this equation with $|v\rangle = |0,1,j\rangle$ gives

$$\begin{aligned} &Q_{00,00}\langle 0,1,j|\psi_{0,0}\rangle^2 + 2Q_{01,00}\langle 0,1,j|\psi_{0,1}\rangle\langle 0,1,j|\psi_{0,0}\rangle + Q_{01,01}\langle 0,1,j|\psi_{0,1}\rangle^2 \\ &\quad = \frac{1}{64}\left(Q_{00,00}i^{-j} + 2Q_{01,00} + Q_{01,01}i^j\right) \\ &\quad = 0 \end{aligned}$$

for each $j \in \{0,\dots,7\}$. The only solution to this set of equations is $Q_{00,00} = Q_{01,00} = Q_{01,01} = 0$. The same analysis, now using $|v\rangle = |1,1,j\rangle$, gives $Q_{10,10} = Q_{11,10} = Q_{11,11} = 0$. Finally, using equation (5.14) with $|v\rangle = |0,2,j\rangle$ gives

$$\begin{aligned}&\frac{1}{64}\langle 0|H|1\rangle\langle 0|H|0\rangle\left(2Q_{10,00}i^{-j} + 2Q_{10,01} + 2Q_{11,00} + 2Q_{11,01}i^{j}\right)\\ &\quad = \frac{1}{64}\left(Q_{10,00}i^{-j} + Q_{10,01} + Q_{11,00} + Q_{11,01}i^{j}\right)\\ &\quad = 0\end{aligned}$$

for all $j \in \{0,\dots,7\}$, which implies that $Q_{10,00} = Q_{11,01} = 0$ and $Q_{11,00} = -Q_{10,01}$. Thus, up to normalization,

$$|Q\rangle = |\psi_{1,0}\rangle|\psi_{0,1}\rangle + |\psi_{0,1}\rangle|\psi_{1,0}\rangle - |\psi_{11}\rangle|\psi_{00}\rangle - |\psi_{00}\rangle|\psi_{11}\rangle\,.$$

Now applying equation (5.14) with $|v\rangle = |0,4,j\rangle$, we see that the quantity

$$\frac{1}{64}\left(2\langle 0|HT|1\rangle\langle 0|(HT)^*|0\rangle - 2\langle 0|(HT)^*|1\rangle\langle 0|HT|0\rangle\right) = \frac{1}{64}\left(e^{i\frac{\pi}{4}} - e^{-i\frac{\pi}{4}}\right)$$

must be zero, which is a contradiction. Hence we conclude that the nullspace of $H(g_0,2)$ is empty. □

We now characterize the space of N-particle frustration-free states on an e_1-gate graph G. Define the subspace $\mathcal{I}(G,N) \subset \mathcal{Z}_N(G)$ where each particle is in a ground state of $A(g_0)$ and no two particles are located within the same diagram element:

$$\mathcal{I}(G,N) = \operatorname{span}\{\operatorname{Sym}(|\psi^{q_1}_{z_1,a_1}\rangle\dots|\psi^{q_N}_{z_N,a_N}\rangle)\colon z_i,a_i \in \{0,1\},\ q_i \in [R],\ q_i \neq q_j \text{ whenever } i \neq j\}. \tag{5.15}$$

Lemma 5.4. *Let G be an e_1-gate graph. A state $|\Gamma\rangle \in \mathcal{Z}_N(G)$ is frustration free if and only if*

$$\left(A(G) - e_1\right)^{(w)}|\Gamma\rangle = 0 \text{ for all } w \in [N] \tag{5.16}$$

$$|\Gamma\rangle \in \mathcal{I}(G,N)\,. \tag{5.17}$$

Proof. First suppose that equations (5.16) and (5.17) hold. From (5.17) we see that $|\Gamma\rangle$ has no support on states where two or more particles are located at the same vertex. Hence

$$\sum_{k\in V} \hat{n}_k\left(\hat{n}_k - 1\right)|\Gamma\rangle = 0\,. \tag{5.18}$$

Putting together equations (5.16) and (5.18), we get

$$H(G,N)|\Gamma\rangle = \left(H_G^N - Ne_1\right)|\Gamma\rangle = 0\,,$$

so $|\Gamma\rangle$ is frustration free.

To complete the proof, we show that if $|\Gamma\rangle$ is frustration free, then conditions (5.16) and (5.17) hold. By definition, a frustration-free state $|\Gamma\rangle$ satisfies

$$H(G,N)|\Gamma\rangle = \left(\sum_{w=1}^{N}\left(A(G) - e_1\right)^{(w)} + \sum_{k\in V}\hat{n}_k\left(\hat{n}_k - 1\right)\right)|\Gamma\rangle = 0\,. \tag{5.19}$$

Since both terms in the large parentheses are positive semidefinite, they must both annihilate $|\Gamma\rangle$; similarly, each term in the first summation must be zero. Hence equation (5.16) holds. Let G_{rem} be the graph obtained from G by removing all of the edges and self-loops in the gate diagram of G. In other words,

$$A(G_{\mathrm{rem}}) = \sum_{q=1}^{R} |q\rangle\langle q| \otimes A(g_0) = 1 \otimes A(g_0)\,.$$

Noting that

$$H(G,N) \geq H(G_{\mathrm{rem}},N) \geq 0\,,$$

we see that equation (5.19) also implies

$$H(G_{\mathrm{rem}},N)|\Gamma\rangle = 0\,. \tag{5.20}$$

Since each of the R components of G_{rem} is an identical copy of g_0, the eigenvalues and eigenvectors of $H(G_{\mathrm{rem}},N)$ are characterized by Lemma 2.4 (along with knowledge of the eigenvalues and eigenvectors of g_0). By Lemma 5.3 and Lemma 2.3, no component has a two- (or more) particle frustration-free state. Combining these two facts, we see that in an N-particle frustration-free state, every component of G_{rem} must contain either 0 or 1 particles, and the nullspace of $H(G_{\mathrm{rem}},N)$ is the space $\mathcal{I}(G,N)$. From equation (5.20) we get $|\Gamma\rangle \in \mathcal{I}(G,N)$. □

Note that if $\mathcal{I}(G,N)$ is empty then Lemma 5.4 says that G has no N-particle frustration-free states. For example, this holds for any e_1-gate graph G whose gate diagram has $R < N$ diagram elements.

A useful consequence of Lemma 5.4 is the fact that every k-particle reduced density matrix of an N-particle frustration-free state $|\Gamma\rangle$ on an e_1-gate graph G (with $k \leq N$) has all of its support on k-particle frustration-free states. To see this, note that for any partition of the N registers into subsets A (of size k) and B (of size $N-k$), we have

$$\mathcal{I}(G,N) \subseteq \mathcal{I}(G,k)_A \otimes \mathcal{Z}_{N-k}(G)_B\,.$$

Thus, if condition (5.17) holds, then all k-particle reduced density matrices of $|\Gamma\rangle$ are contained in $\mathcal{I}(G,k)$. Furthermore, (5.16) is a statement about the single-particle reduced density matrices, so it also holds for each k-particle reduced density matrix. From this we see that each reduced density matrix of $|\Gamma\rangle$ is frustration free.

5.4 Occupancy constraints

Lemma 5.4 says in particular that a frustration-free state on an e_1-gate graph has no support on states where multiple particles occupy the same diagram element. Indeed, the lemma allows us to restrict our attention to the subspace $\mathcal{I}(G,N)$ when solving for N-particle frustration-free states. Here we consider restrictions to other subspaces corresponding to more general constraints on the locations of particles in a gate graph.

For any e_1-gate graph G with R diagram elements and any simple R-vertex graph G^{occ} with edge set $E(G^{\mathrm{occ}})$, we define a subspace

$$\mathcal{I}(G,G^{\mathrm{occ}},N) = \mathrm{span}\{\mathrm{Sym}(|\psi^{q_1}_{z_1,a_1}\rangle \ldots |\psi^{q_N}_{z_N,a_N}\rangle)\colon z_i,a_i \in \{0,1\},\ q_i \neq q_j \text{ for } i \neq j,\ \{q_i,q_j\} \notin E(G^{\mathrm{occ}})\}\,. \tag{5.21}$$

In this subspace, no two particles occupy the same diagram element and no two particles occupy diagram elements connected by an edge in G_{occ}. Note that

$$\mathcal{I}(G,G^{\mathrm{occ}},N) \subseteq \mathcal{I}(G,N) \subseteq \mathcal{Z}_N(G)\,.$$

We say that G^{occ} specifies a set of *occupancy constraints* on G. If $\mathcal{I}(G,G^{\mathrm{occ}},N)$ is not empty, we define the restriction

$$H(G,G^{\mathrm{occ}},N) = H(G,N)\big|_{\mathcal{I}(G,G^{\mathrm{occ}},N)}$$

and write $\lambda_N^1(G,G^{\mathrm{occ}})$ for its smallest eigenvalue.

We now explain how the subspace $\mathcal{I}(G,G^{\mathrm{occ}},N)$ relates to the Bose-Hubbard model on a graph derived from G and G^{occ}. Specifically, the following lemma states that we can construct another graph $G^{\square}$ (depending on G and G^{occ}) so that the ground state of the Bose-Hubbard model on $G^{\square}$ effectively "simulates" the restriction to $\mathcal{I}(G,G^{\mathrm{occ}},N)$. The ground energy $\lambda_N^1(G,G^{\mathrm{occ}})$ of $H(G,G^{\mathrm{occ}},N)$ is zero if and only if the ground energy $\lambda_N^1(G^{\square})$ of $H(G^{\square},N)$ is zero. The lemma also shows that the two energies are related even if they are nonzero.

Lemma 5.5 (**Occupancy Constraints Lemma**). *Let G be an e_1-gate graph specified as a gate diagram with $R \geq 2$ diagram elements. Let $N \in [R]$, let G^{occ} specify a set of occupancy constraints on G, and suppose the subspace $\mathcal{I}(G,G^{\mathrm{occ}},N)$ is nonempty. Then there exists an efficiently computable e_1-gate graph $G^{\square}$ with at most $7R^2$ diagram elements such that*

1. *If $\lambda_N^1(G,G^{\mathrm{occ}}) \leq a$ then $\lambda_N^1(G^{\square}) \leq \dfrac{a}{R}$.*
2. *If $\lambda_N^1(G,G^{\mathrm{occ}}) \geq b$ with $b \in [0,1]$, then $\lambda_N^1(G^{\square}) \geq \dfrac{b}{(13R)^9}$.*

Note that the lemma stipulates $N \leq R$ without loss of generality, since $\mathcal{I}(G,G^{\mathrm{occ}},N)$ is empty otherwise. The proof of this lemma appears in Section 10. In the proof we show how to construct the gate graph $G^{\square}$ from G and G^{occ}.

6 Gadgets

In Example 5.2 we saw how a single-particle ground state can encode a single-qubit computation. In this section we see how a two-particle frustration-free state on a suitably designed e_1-gate graph can encode a two-qubit computation. We design specific e_1-gate graphs (called *gadgets*) that we use in Section 7 to prove that Bose-Hubbard Hamiltonian is QMA-hard. For each gate graph we discuss, we show that the smallest eigenvalue of its adjacency matrix is e_1 and we solve for all of the frustration-free states.

We first design a gate graph where, in any two-particle frustration-free state, the locations of the particles are synchronized. This "move-together" gadget is presented in Section 6.1. In Section 6.2, we design gadgets for two-qubit gates using four move-together gadgets, one for each two-qubit computational basis state. Finally, in Section 6.3 we describe a small modification of a two-qubit gate gadget called the "boundary gadget."

The circuit-to-gate graph mapping described in Section 7 uses a two-qubit gate gadget for each gate in the circuit, together with boundary gadgets in parts of the graph corresponding to the beginning and end of the computation.

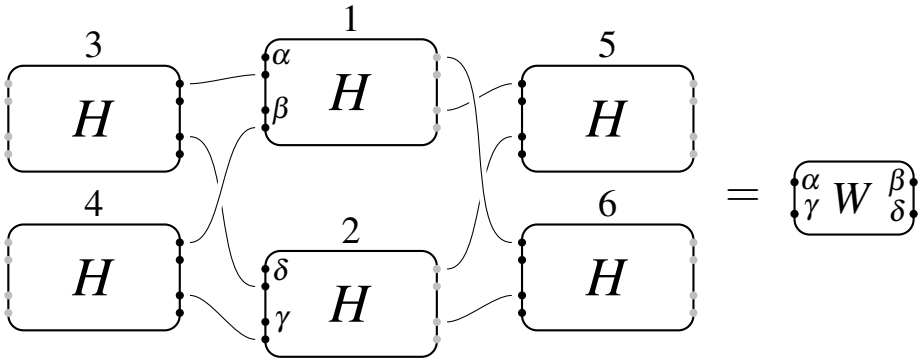

Figure 6.1: The gate diagram for the move-together gadget.

6.1 The move-together gadget

The gate diagram for the *move-together gadget* is shown in Figure 6.1. Using equation (5.4), we write the adjacency matrix of the corresponding gate graph G_W as

$$A(G_W) = \sum_{q=1}^{6} |q\rangle\langle q| \otimes A(g_0) + h_{\mathcal{E}} \tag{6.1}$$

where $h_{\mathcal{E}}$ is given by (5.6) and $\mathcal{E}$ is the set of edges in the gate diagram (in this case $h_S = 0$ as there are no self-loops).

We begin by solving for the single-particle ground states, i. e., the eigenvectors of (6.1) with eigenvalue $e_1 = -1 - 3\sqrt{2}$. As in Example 5.2, we can solve for the states with $a = 0$ and $a = 1$ separately, since

$$\langle \psi^j_{x,1} | h_{\mathcal{E}} | \psi^i_{z,0} \rangle = 0$$

for all $i, j \in \{1, \ldots, 6\}$ and $x, z \in \{0, 1\}$. We write a single-particle ground state as

$$\sum_{i=1}^{6} \left(\tau_i |\psi^i_{0,a}\rangle + \nu_i |\psi^i_{1,a}\rangle \right)$$

and solve for the coefficients τ_i and ν_i using equation (5.11) (in this case equation (5.10) is automatically satisfied since $h_S = 0$). Enforcing (5.11) gives eight equations, one for each edge in the gate diagram:

$$\begin{aligned}
\tau_3 &= -\tau_1 & \frac{1}{\sqrt{2}}(\tau_1 + \nu_1) &= -\tau_6 \\
\tau_4 &= -\nu_1 & \frac{1}{\sqrt{2}}(\tau_1 - \nu_1) &= -\tau_5 \\
\nu_3 &= -\tau_2 & \frac{1}{\sqrt{2}}(\tau_2 + \nu_2) &= -\nu_5 \\
\nu_4 &= -\nu_2 & \frac{1}{\sqrt{2}}(\tau_2 - \nu_2) &= -\nu_6 \,.
\end{aligned}$$

There are four linearly independent solutions to this set of equations, given by

$$\begin{array}{lllll}
\textit{Solution 1:} & \tau_1 = 1 & \tau_3 = -1 & \tau_5 = -\frac{1}{\sqrt{2}} & \tau_6 = -\frac{1}{\sqrt{2}} \quad \text{all other coefficients } 0 \\
\textit{Solution 2:} & \nu_1 = 1 & \tau_4 = -1 & \tau_5 = \frac{1}{\sqrt{2}} & \tau_6 = -\frac{1}{\sqrt{2}} \quad \text{all other coefficients } 0 \\
\textit{Solution 3:} & \nu_2 = 1 & \nu_4 = -1 & \nu_5 = -\frac{1}{\sqrt{2}} & \nu_6 = \frac{1}{\sqrt{2}} \quad \text{all other coefficients } 0 \\
\textit{Solution 4:} & \tau_2 = 1 & \nu_3 = -1 & \nu_5 = -\frac{1}{\sqrt{2}} & \nu_6 = -\frac{1}{\sqrt{2}} \quad \text{all other coefficients } 0.
\end{array}$$

For each of these solutions, and for each $a \in \{0,1\}$, we find a single-particle state with energy e_1. This result is summarized in the following lemma.

Lemma 6.1. *G_W is an e_1-gate graph. A basis for the eigenspace of $A(G_W)$ with eigenvalue e_1 is*

$$|\chi_{1,a}\rangle = \frac{1}{\sqrt{3}}|\psi^1_{0,a}\rangle - \frac{1}{\sqrt{3}}|\psi^3_{0,a}\rangle - \frac{1}{\sqrt{6}}|\psi^5_{0,a}\rangle - \frac{1}{\sqrt{6}}|\psi^6_{0,a}\rangle \tag{6.2}$$

$$|\chi_{2,a}\rangle = \frac{1}{\sqrt{3}}|\psi^1_{1,a}\rangle - \frac{1}{\sqrt{3}}|\psi^4_{0,a}\rangle + \frac{1}{\sqrt{6}}|\psi^5_{0,a}\rangle - \frac{1}{\sqrt{6}}|\psi^6_{0,a}\rangle \tag{6.3}$$

$$|\chi_{3,a}\rangle = \frac{1}{\sqrt{3}}|\psi^2_{1,a}\rangle - \frac{1}{\sqrt{3}}|\psi^4_{1,a}\rangle - \frac{1}{\sqrt{6}}|\psi^5_{1,a}\rangle + \frac{1}{\sqrt{6}}|\psi^6_{1,a}\rangle \tag{6.4}$$

$$|\chi_{4,a}\rangle = \frac{1}{\sqrt{3}}|\psi^2_{0,a}\rangle - \frac{1}{\sqrt{3}}|\psi^3_{1,a}\rangle - \frac{1}{\sqrt{6}}|\psi^5_{1,a}\rangle - \frac{1}{\sqrt{6}}|\psi^6_{1,a}\rangle \tag{6.5}$$

where $a \in \{0,1\}$.

In Figure 6.1 we have used a shorthand $\alpha, \beta, \gamma, \delta$ to identify four nodes of the move-together gadget; these are the nodes with labels $(q,z,t) = (1,0,1), (1,1,1), (2,1,1), (2,0,1)$, respectively. We view α and γ as "input" nodes and β and δ as "output" nodes for the move-together gadget. It is natural to associate each single-particle state $|\chi_{i,a}\rangle$ with one of these four nodes. Each node corresponds to 8 vertices of the underlying graph, e. g.,

$$S_\alpha = \{(1,0,1,j) \colon j \in \{0,\ldots,7\}\}.$$

Looking at equation (6.2) (and referring back to equation (5.2)) we see that $|\chi_{1,a}\rangle$ has support on vertices in S_α but not on vertices in S_β, S_γ, or S_δ. Looking at the picture on the right-hand side of the equality sign in Figure 6.1, we think of $|\chi_{1,a}\rangle$ as localized at the node α, with no support on the other three nodes. The states $|\chi_{2,a}\rangle, |\chi_{3,a}\rangle, |\chi_{4,a}\rangle$ are similarly localized at nodes β, γ, δ. We view $|\chi_{1,a}\rangle$ and $|\chi_{3,a}\rangle$ as input states and $|\chi_{2,a}\rangle$ and $|\chi_{4,a}\rangle$ as output states.

Now we turn our attention to the two-particle frustration-free states of the move-together gadget, i. e., the states $|\Phi\rangle \in \mathcal{Z}_2(G_W)$ in the nullspace of $H(G_W, 2)$. Using Lemma 5.4 we can write

$$|\Phi\rangle = \sum_{a,b \in \{0,1\}, I,J \in [4]} C_{(I,a),(J,b)} |\chi_{I,a}\rangle |\chi_{J,b}\rangle \tag{6.6}$$

where the coefficients are symmetric, i. e.,

$$C_{(I,a),(J,b)} = C_{(J,b),(I,a)}\,, \tag{6.7}$$

and where

$$\langle \psi^q_{z,a}| \langle \psi^q_{x,b}| \Phi\rangle = 0 \tag{6.8}$$

for all $z,a,x,b \in \{0,1\}$ and $q \in [6]$.

The move-together gadget is designed so that each solution $|\Phi\rangle$ to these equations is a superposition of a term where both particles are in input states and a term where both particles are in output states. The particles move from input nodes to output nodes together. We now solve equations (6.6)–(6.8) and prove the following.

Lemma 6.2. *A basis for the nullspace of $H(G_W,2)$ is*

$$|\Phi_{a,b}\rangle = \mathrm{Sym}\left(\frac{1}{\sqrt{2}}|\chi_{1,a}\rangle|\chi_{3,b}\rangle + \frac{1}{\sqrt{2}}|\chi_{2,a}\rangle|\chi_{4,b}\rangle\right), \quad a,b \in \{0,1\}\,. \tag{6.9}$$

There are no N-particle frustration-free states on G_W for $N \geq 3$, i. e.,

$$\lambda^1_N(G_W) > 0 \quad \textit{for } N \geq 3\,.$$

Proof. The states $|\Phi_{a,b}\rangle$ manifestly satisfy equations (6.6) and (6.7), and one can directly verify that they also satisfy (6.8) (the nontrivial cases to check are $q = 5$ and $q = 6$).

To complete the proof that (6.9) is a basis for the nullspace of $H(G_W,2)$, we verify that any state satisfying these conditions must be a linear combination of these four states. Applying equation (6.8) gives

$$\begin{aligned}
\langle \psi^1_{0,a}| \langle \psi^1_{0,b}| \Phi\rangle &= \frac{1}{3}C_{(1,a),(1,b)} = 0 & \qquad \langle \psi^1_{1,a}| \langle \psi^1_{1,b}| \Phi\rangle &= \frac{1}{3}C_{(2,a),(2,b)} = 0\\
\langle \psi^2_{1,a}| \langle \psi^2_{1,b}| \Phi\rangle &= \frac{1}{3}C_{(3,a),(3,b)} = 0 & \qquad \langle \psi^2_{0,a}| \langle \psi^2_{0,b}| \Phi\rangle &= \frac{1}{3}C_{(4,a),(4,b)} = 0\\
\langle \psi^1_{0,a}| \langle \psi^1_{1,b}| \Phi\rangle &= \frac{1}{3}C_{(1,a),(2,b)} = 0 & \qquad \langle \psi^2_{0,a}| \langle \psi^2_{1,b}| \Phi\rangle &= \frac{1}{3}C_{(4,a),(3,b)} = 0\\
\langle \psi^3_{0,a}| \langle \psi^3_{1,b}| \Phi\rangle &= \frac{1}{3}C_{(1,a),(4,b)} = 0 & \qquad \langle \psi^4_{0,a}| \langle \psi^4_{1,b}| \Phi\rangle &= \frac{1}{3}C_{(2,a),(3,b)} = 0
\end{aligned}$$

for all $a,b \in \{0,1\}$. Using the fact that all of these coefficients are zero, and using equation (6.7), we get

$$|\Phi\rangle = \sum_{a,b\in\{0,1\}} \left(C_{(1,a),(3,b)}\left(|\chi_{1,a}\rangle|\chi_{3,b}\rangle + |\chi_{3,b}\rangle|\chi_{1,a}\rangle\right) + C_{(2,a),(4,b)}\left(|\chi_{2,a}\rangle|\chi_{4,b}\rangle + |\chi_{4,b}\rangle|\chi_{2,a}\rangle\right)\right).$$

Finally, applying equation (6.8) again gives

$$\langle \psi^6_{0,a}| \langle \psi^6_{1,b}| \Phi\rangle = \frac{1}{6}C_{(2,a),(4,b)} - \frac{1}{6}C_{(1,a),(3,b)} = 0\,.$$

Hence

$$|\Phi\rangle = \sum_{a,b\in\{0,1\}} C_{(1,a),(3,b)}\left(|\chi_{1,a}\rangle|\chi_{3,b}\rangle + |\chi_{3,b}\rangle|\chi_{1,a}\rangle + |\chi_{2,a}\rangle|\chi_{4,b}\rangle + |\chi_{4,b}\rangle|\chi_{2,a}\rangle\right),$$

which is a superposition of the states $|\Phi_{a,b}\rangle$.

Finally, we prove that there are no frustration-free ground states of the Bose-Hubbard model on G_W with more than two particles. By Lemma 2.3, it suffices to prove that there are no frustration-free three-particle states.

Suppose (for a contradiction) that $|\Gamma\rangle \in \mathcal{Z}_3(G_W)$ is a normalized three-particle frustration-free state. Write

$$|\Gamma\rangle = \sum D_{(i,a),(j,b),(k,c)} |\chi_{i,a}\rangle|\chi_{j,b}\rangle|\chi_{k,c}\rangle\,.$$

Note that each reduced density matrix of $|\Gamma\rangle$ on two of the three subsystems must have all of its support on two-particle frustration-free states (see the remark following Lemma 5.4), i. e., on the states $|\Phi_{a,b}\rangle$. Using this fact for the subsystem consisting of the first two particles, we see in particular that

$$(i,j) \notin \{(1,3),(3,1),(2,4),(4,2)\} \quad \Longrightarrow \quad D_{(i,a),(j,b),(k,c)} = 0 \tag{6.10}$$

(since $|\Phi_{a_1,a_2}\rangle$ only has support on vectors $|\chi_{i,a}\rangle|\chi_{j,b}\rangle$ with $i,j \in \{(1,3),(3,1),(2,4),(4,2)\}$).

Using this fact for subsystems consisting of particles $2,3$ and $1,3$, respectively, gives

$$(j,k) \notin \{(1,3),(3,1),(2,4),(4,2)\} \quad \Longrightarrow \quad D_{(i,a),(j,b),(k,c)} = 0 \tag{6.11}$$

$$(i,k) \notin \{(1,3),(3,1),(2,4),(4,2)\} \quad \Longrightarrow \quad D_{(i,a),(j,b),(k,c)} = 0\,. \tag{6.12}$$

Putting together equations (6.10), (6.11), and (6.12), we see that $|\Gamma\rangle = 0$. This is a contradiction, so no three-particle frustration-free states exist. □

Next we show how the move-together gadget can be used to build gadgets that implement two-qubit gates.

6.2 Gadgets for two-qubit gates

In this section we define a gate graph for each of the two-qubit unitaries

$$\{\mathrm{CNOT}_{12}, \mathrm{CNOT}_{21}, \mathrm{CNOT}_{12}\,(H \otimes 1)\,, \mathrm{CNOT}_{12}\,(HT \otimes 1)\}.$$

Here CNOT_{12} is the standard controlled-not gate with the second qubit as a target, whereas CNOT_{21} has the first qubit as target.

We define the gate graphs by exhibiting their gate diagrams. For the three cases

$$U = \mathrm{CNOT}_{12}(\tilde{U} \otimes 1)$$

with $\tilde{U} \in \{1, H, HT\}$, we associate U with the gate diagram shown in Figure 6.2(A). In the figure we also indicate a shorthand used to represent this gate diagram. As one might expect, for the case $U = \mathrm{CNOT}_{21}$, we use the same gate diagram as for $U = \mathrm{CNOT}_{12}$; however, we use the slightly different shorthand shown in Figure 6.2(B).

Roughly speaking, the two-qubit gate gadgets work as follows. In Figure 6.2(A) there are four move-together gadgets, one for each two-qubit basis state $|00\rangle, |01\rangle, |10\rangle, |11\rangle$. These enforce the constraint that two particles must move through the graph together. The connections between the four diagram

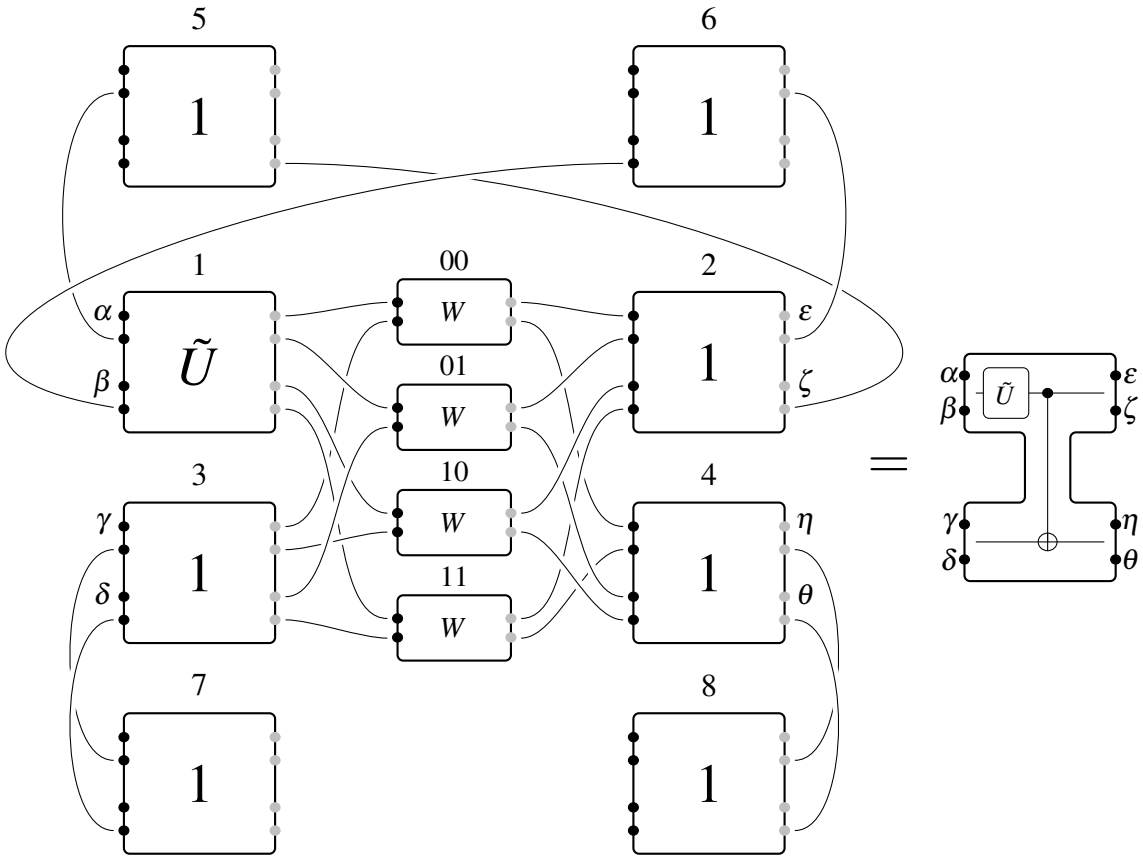

(A)

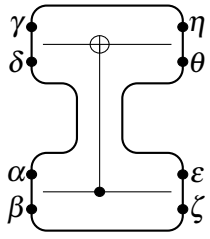

(B)

Figure 6.2: (A) Gadget for the two-qubit unitary $U = (\tilde{U} \otimes 1)\mathrm{CNOT}_{12}$ with $\tilde{U} \in \{1, H, HT\}$. (B) For the $U = \mathrm{CNOT}_{21}$ gate (first qubit is the target), we use the same gate graph as in (A) with $\tilde{U} = 1$; we represent it schematically as shown.

elements labeled $1,2,3,4$ and the move-together gadgets ensure that certain frustration-free two-particle states encode two-qubit computations, while the connections between diagram elements $1,2,3,4$ and $5,6,7,8$ ensure that there are no additional frustration-free two-particle states (i. e., states that do not encode computations).

To describe the frustration-free states of the gate graph depicted in Figure 6.2(A), first recall the definition of the states $|\chi_{1,a}\rangle, |\chi_{2,a}\rangle, |\chi_{3,a}\rangle, |\chi_{4,a}\rangle$ from equations (6.2)–(6.5). For each of the move-together gadgets $xy \in \{00,01,10,11\}$ in Figure 6.2(A), write

$$|\chi_{L,a}^{xy}\rangle$$

for the state $|\chi_{L,a}\rangle$ with support (only) on the gadget labeled xy. Write

$$U(a) = \begin{cases} U & \text{if } a = 0 \\ U^* & \text{if } a = 1 \end{cases}$$

and similarly for $\tilde{U}$ (we use this notation throughout the paper to indicate a unitary or its elementwise complex conjugate).

The following lemma shows that G_U is an e_1-gate graph and characterizes its frustration-free states.

Lemma 6.3. *Let $U = \mathrm{CNOT}_{12}(\tilde{U} \otimes 1)$ where $\tilde{U} \in \{1, H, HT\}$. The corresponding gate graph G_U is defined by its gate diagram shown in Figure 6.2(A). The adjacency matrix $A(G_U)$ has ground energy e_1; a basis for the corresponding eigenspace is*

$$|\rho_{z,a}^{1,U}\rangle = \frac{1}{\sqrt{8}}|\psi_{z,a}^{1}\rangle - \frac{1}{\sqrt{8}}|\psi_{z,a}^{5+z}\rangle - \sqrt{\frac{3}{8}}\sum_{x,y=0}^{1}\tilde{U}(a)_{yz}|\chi_{1,a}^{yx}\rangle \tag{6.13}$$

$$|\rho_{z,a}^{2,U}\rangle = \frac{1}{\sqrt{8}}|\psi_{z,a}^{2}\rangle - \frac{1}{\sqrt{8}}|\psi_{z,a}^{6-z}\rangle - \sqrt{\frac{3}{8}}\sum_{x=0}^{1}|\chi_{2,a}^{zx}\rangle \tag{6.14}$$

$$|\rho_{z,a}^{3,U}\rangle = \frac{1}{\sqrt{8}}|\psi_{z,a}^{3}\rangle - \frac{1}{\sqrt{8}}|\psi_{z,a}^{7}\rangle - \sqrt{\frac{3}{8}}\sum_{x=0}^{1}|\chi_{3,a}^{xz}\rangle \tag{6.15}$$

$$|\rho_{z,a}^{4,U}\rangle = \frac{1}{\sqrt{8}}|\psi_{z,a}^{4}\rangle - \frac{1}{\sqrt{8}}|\psi_{z,a}^{8}\rangle - \sqrt{\frac{3}{8}}\sum_{x=0}^{1}|\chi_{4,a}^{x(z\oplus x)}\rangle \tag{6.16}$$

where $z,a \in \{0,1\}$. A basis for the nullspace of $H(G_U,2)$ is

$$\mathrm{Sym}(|T_{z_1,a,z_2,b}^{U}\rangle), \quad z_1,z_2,a,b \in \{0,1\} \tag{6.17}$$

where

$$|T_{z_1,a,z_2,b}^{U}\rangle = \frac{1}{\sqrt{2}}|\rho_{z_1,a}^{1,U}\rangle|\rho_{z_2,b}^{3,U}\rangle + \frac{1}{\sqrt{2}}\sum_{x_1,x_2=0}^{1}U(a)_{x_1x_2,z_1z_2}|\rho_{x_1,a}^{2,U}\rangle|\rho_{x_2,b}^{4,U}\rangle \tag{6.18}$$

for $z_1,z_2,a,b \in \{0,1\}$. There are no N-particle frustration-free states on G_U for $N \geq 3$, i. e.,

$$\lambda_N^1(G_U) > 0 \quad \text{for } N \geq 3\,.$$

We view the nodes labeled $\alpha, \beta, \gamma, \delta$ in Figure 6.2(A) as "input" nodes and those labeled $\varepsilon, \zeta, \eta, \theta$ as "output nodes." Each of the states $|\rho_{x,y}^{i,U}\rangle$ is associated with one of the nodes, depending on the values of $i \in \{1,2,3,4\}$ and $x \in \{0,1\}$. For example, the states $|\rho_{0,0}^{1,U}\rangle$ and $|\rho_{0,1}^{1,U}\rangle$ are associated with input node α since they both have nonzero amplitude on vertices of the gate graph that are associated with α (and zero amplitude on vertices associated with other labeled nodes).

The two-particle state $\mathrm{Sym}(|T_{z_1,a,z_2,b}^{U}\rangle)$ is a superposition of a term

$$\mathrm{Sym}\left(\frac{1}{\sqrt{2}}|\rho_{z_1,a}^{1,U}\rangle|\rho_{z_2,b}^{3,U}\rangle\right)$$

with both particles located on vertices corresponding to input nodes and a term

$$\mathrm{Sym}\left(\frac{1}{\sqrt{2}}\sum_{x_1,x_2\in\{0,1\}} U(a)_{x_1x_2,z_1z_2}|\rho_{x_1,a}^{2,U}\rangle|\rho_{x_2,b}^{4,U}\rangle\right)$$

with both particles on vertices corresponding to output nodes. The two-qubit gate $U(a)$ is applied as the particles move from input nodes to output nodes.

Proof of Lemma 6.3. Recall that the gate graph G_U is specified by its gate diagram, shown in Figure 6.2(A). The adjacency matrix of the gate graph G_U is of the form in equation (5.4). There are 6 diagram elements for each of the move-together gadgets, so there are 32 diagram elements in total. We will need to refer to those diagram elements labeled $q \in [8]$ in Figure 6.2(A) (i. e., those not contained in the move-together gadgets).

Write

$$A(G_U) = A(G'_U) + h_{\mathcal{E}'}$$

where G'_U is the gate graph obtained from G_U by removing all 24 edges shown in Figure 6.2(A) (G'_U does include the edges within each of the move-together gadgets). Here $h_{\mathcal{E}'}$ is given by equation (5.6) with $\mathcal{E}'$ the set of 24 edges shown in Figure 6.2(A).

One basis for the e_1-energy ground space of $A(G'_U)$ is given by the 64 states

$$\begin{aligned}
&|\psi_{z,a}^{q}\rangle, \quad q \in [8], z, a \in \{0,1\}\\
&|\chi_{L,a}^{xy}\rangle, \quad x, y, a \in \{0,1\}, L \in [4]\,.
\end{aligned}$$

However, it is convenient to work with the following slightly different basis for this space:

$$\begin{aligned}
&|\psi_{z,a}^{q}\rangle, \quad q \in [8], z, a \in \{0,1\}\\
&\sum_{x\in\{0,1\}} \tilde{U}(a)_{xz}|\chi_{1,a}^{xy}\rangle, \quad y, z, a \in \{0,1\}\\
&|\chi_{L,a}^{xy}\rangle, \quad x, y, a \in \{0,1\}, L \in \{2,3,4\}\,.
\end{aligned}$$

Here some of the states are in a superposition corresponding to the output of the single-qubit unitary $\tilde{U}$.

We are interested in the intersection of the ground space of $A(G'_U)$ with the nullspace of $h_{\mathcal{E}'}$, so we compute the matrix elements of $h_{\mathcal{E}'}$ in the above basis. The resulting 64×64 matrix is block diagonal with sixteen 4×4 blocks. Each block is identical, with entries

$$\begin{pmatrix} \frac{3}{8} & \frac{1}{8} & \frac{1}{8\sqrt{3}} & \frac{1}{8\sqrt{3}} \\ \frac{1}{8} & \frac{1}{8} & 0 & 0 \\ \frac{1}{8\sqrt{3}} & 0 & \frac{1}{24} & 0 \\ \frac{1}{8\sqrt{3}} & 0 & 0 & \frac{1}{24} \end{pmatrix}. \tag{6.19}$$

The four states involved in each block are given by (in order from left to right as in the matrix above):

$$|\psi^1_{z,a}\rangle, |\psi^{5+z}_{z,a}\rangle, \sum_{x\in\{0,1\}} \tilde{U}(a)_{xz}|\chi^{x0}_{1,a}\rangle, \sum_{x\in\{0,1\}} \tilde{U}(a)_{xz}|\chi^{x1}_{1,a}\rangle$$
$$|\psi^2_{z,a}\rangle, |\psi^{6-z}_{z,a}\rangle, |\chi^{z0}_{2,a}\rangle, |\chi^{z1}_{2,a}\rangle$$
$$|\psi^3_{z,a}\rangle, |\psi^7_{z,a}\rangle, |\chi^{0z}_{3,a}\rangle, |\chi^{1z}_{3,a}\rangle$$
$$|\psi^4_{z,a}\rangle, |\psi^8_{z,a}\rangle, |\chi^{0z}_{4,a}\rangle, |\chi^{1(z\oplus 1)}_{4,a}\rangle.$$

The unique zero eigenvector of the matrix (6.19) is

$$\frac{1}{\sqrt{8}} \begin{pmatrix} 1 \\ -1 \\ -\sqrt{3} \\ -\sqrt{3} \end{pmatrix}.$$

Constructing this vector within each of the 16 blocks, we get the states $\{|\rho^{1,U}_{z,a}\rangle, |\rho^{2,U}_{z,a}\rangle, |\rho^{3,U}_{z,a}\rangle, |\rho^{4,U}_{z,a}\rangle\}$.

Now consider the two-particle sector. Using Lemma 5.4 we can write any two-particle frustration-free state as

$$|\Theta\rangle = \sum_{z,a,x,b\in\{0,1\}} \sum_{I,J\in[4]} B_{(z,a,I),(x,b,J)} |\rho^{I,U}_{z,a}\rangle |\rho^{J,U}_{x,b}\rangle \tag{6.20}$$

where

$$B_{(z,a,I),(x,b,J)} = B_{(x,b,J),(z,a,I)} \tag{6.21}$$

and

$$\langle\psi^q_{x,a}|\langle\psi^q_{z,b}|\Theta\rangle = 0 \tag{6.22}$$

for all $x,z,a,b \in \{0,1\}$ and $q \in [32]$. To enforce equation (6.22) we consider the diagram elements $q \in [8]$ (as labeled in Figure 6.2(A)) separately from the other 24 diagram elements (those inside the move-together gadgets).

Using equation (6.22) with $q \in \{1,2,3,4,7,8\}$ and $x,z,a,b \in \{0,1\}$ gives

$$B_{(x,a,I),(z,b,I)} = 0 \quad I \in [4],\ x,z,a,b \in \{0,1\}. \tag{6.23}$$

Using $q = 5$, $x = 0$, and $z = 1$ in equation (6.22) gives

$$\langle\psi^5_{0,a}|\langle\psi^5_{1,b}|\Theta\rangle = \frac{1}{8} B_{(0,a,1),(1,b,2)} = 0, \tag{6.24}$$

for $a,b \in \{0,1\}$, while $q=6$, $x=0$, and $z=1$ gives

$$\langle \psi^6_{0,a}|\langle \psi^6_{1,b}|\Theta\rangle = \frac{1}{8} B_{(0,a,2),(1,b,1)} = 0\,. \tag{6.25}$$

Applying equation (6.22) with $q=5$ or $q=6$ and other choices for x and z does not lead to any additional independent constraints on the state $|\Theta\rangle$.

Now consider the constraint (6.22) for diagram elements inside the move-together gadgets in Figure 6.2(A). Let Π_{xy} be the projector onto two-particle states where both particles are located at vertices contained within the move-together gadget labeled $xy \in \{00,01,10,11\}$. Using the results of Lemma 6.2, we see that for diagram elements inside the move-together gadgets, (6.22) is satisfied if and only if

$$\Pi_{xy}|\Theta\rangle \in \mathrm{span}\Big\{\mathrm{Sym}\left(|\chi^{xy}_{1,a}\rangle|\chi^{xy}_{3,b}\rangle + |\chi^{xy}_{2,a}\rangle|\chi^{xy}_{4,b}\rangle\right),\ a,b \in \{0,1\}\Big\}.$$

Since we already know

$$\Pi_{xy}|\Theta\rangle \in \mathrm{span}\Big\{\mathrm{Sym}\left(|\chi^{xy}_{i,a}\rangle|\chi^{xy}_{j,b}\rangle\right),\ i,j \in [4], a,b \in \{0,1\}\Big\}$$

we get

$$\langle \chi^{xy}_{K,a}|\langle \chi^{xy}_{K,b}|\Theta\rangle = 0 \quad K \in [4] \tag{6.26}$$

$$\langle \chi^{xy}_{K,a}|\langle \chi^{xy}_{L,b}|\Theta\rangle = 0 \quad (K,L) \in \{(1,2),(2,3),(3,4),(1,4)\} \tag{6.27}$$

$$\left(\langle \chi^{xy}_{1,a}|\langle \chi^{xy}_{3,b}| - \langle \chi^{xy}_{2,a}|\langle \chi^{xy}_{4,b}|\right)|\Theta\rangle = 0 \tag{6.28}$$

for all $a,b \in \{0,1\}$. Note that (6.26) is automatically satisfied whenever (6.23) holds.

Applying equation (6.27) with $(K,L)=(1,2)$ and $a,b,x,y \in \{0,1\}$, we get

$$\langle \chi^{xy}_{1,a}|\langle \chi^{xy}_{2,b}|\Theta\rangle = \frac{3}{8}\sum_{z\in\{0,1\}} \tilde{U}(a)_{xz} B_{(z,a,1),(x,b,2)} = \frac{3}{8}\tilde{U}(a)_{xx} B_{(x,a,1),(x,b,2)} = 0\,. \tag{6.29}$$

In the second equality we used the fact that $B_{(z,a,1),(x,b,2)}$ is zero whenever $z \neq x$ (from equations (6.21), (6.24), and (6.25)). Since $\tilde{U} \in \{1,H,HT\}$ we have $\tilde{U}(a)_{xx} \neq 0$, and it follows that

$$B_{(x,a,1),(x,b,2)} = 0 \tag{6.30}$$

for all $x,a,b \in \{0,1\}$.

Applying equation (6.27) with $(K,L)=(1,4)$ gives

$$\langle \chi^{xy}_{1,a}|\langle \chi^{xy}_{4,b}|\Theta\rangle = \frac{3}{8}\sum_{z\in\{0,1\}} \tilde{U}(a)_{xz} B_{(z,a,1),(x\oplus y,b,4)} = 0\,, \qquad x,y,a,b \in \{0,1\}. \tag{6.31}$$

By taking appropriate combinations of these equations, we have

$$\sum_{x\in\{0,1\}} \tilde{U}(a)^{\dagger}_{wx} \langle \chi^{x(y\oplus x)}_{1,a}|\langle \chi^{x(y\oplus x)}_{4,b}|\Theta\rangle = B_{(w,a,1),(y,b,4)} = 0\,, \qquad w,y,a,b \in \{0,1\}. \tag{6.32}$$

Applying equation (6.27) with $(K,L)=(2,3)$ and $(K,L)=(3,4)$ gives

$$\langle\chi^{xy}_{2,a}|\langle\chi^{xy}_{3,b}|\Theta\rangle = \frac{3}{8}B_{(x,a,2),(y,b,3)} = 0 \tag{6.33}$$

$$\langle\chi^{xy}_{3,a}|\langle\chi^{xy}_{4,b}|\Theta\rangle = \frac{3}{8}B_{(x,a,3),(x\oplus y,b,4)} = 0 \tag{6.34}$$

for all $x,y,a,b\in\{0,1\}$.

Now putting together equations (6.23), (6.24), (6.25), (6.30), (6.32), (6.33), and (6.34) (and using the symmetrization (6.21)), we get

$$B_{(x,a,I),(z,b,J)} = 0 \quad \text{for all } x,z,a,b\in\{0,1\}, \text{ where } I=J \text{ or } \{I,J\}\in\big\{\{1,2\},\{1,4\},\{2,3\},\{3,4\}\big\},$$

so $|\Theta\rangle$ can be written

$$\sum_{z,c,w,d\in\{0,1\}} B_{(z,c,1),(w,d,3)}\left(|\rho^{1,U}_{z,c}\rangle|\rho^{3,U}_{w,d}\rangle + |\rho^{3,U}_{w,d}\rangle|\rho^{1,U}_{z,c}\rangle\right) + B_{(z,c,2),(w,d,4)}\left(|\rho^{2,U}_{z,c}\rangle|\rho^{4,U}_{w,d}\rangle + |\rho^{4,U}_{w,d}\rangle|\rho^{2,U}_{z,c}\rangle\right). \tag{6.35}$$

Now

$$\langle\chi^{xy}_{1,a}|\langle\chi^{xy}_{3,b}|\rho^{1,U}_{z,c}\rangle|\rho^{3,U}_{w,d}\rangle = \frac{3}{8}\delta_{a,c}\delta_{b,d}\tilde{U}(a)_{xz}\delta_{y,w}$$

$$\langle\chi^{xy}_{2,a}|\langle\chi^{xy}_{4,b}|\rho^{2,U}_{z,c}\rangle|\rho^{4,U}_{w,d}\rangle = \frac{3}{8}\delta_{a,c}\delta_{b,d}\delta_{x,z}\delta_{y,w\oplus x},$$

so enforcing equation (6.28) gives

$$\sum_{z\in\{0,1\}}\tilde{U}(a)_{xz}B_{(z,a,1),(y,b,3)} = B_{(x,a,2),(x\oplus y,b,4)}$$

for each $x,y,a,b\in\{0,1\}$. In other words

$$B_{(z,c,2),(w,d,4)} = \sum_{x\in\{0,1\}}\tilde{U}(c)_{zx}B_{(x,c,1),(z\oplus w,d,3)} = \sum_{x,y\in\{0,1\}}U(c)_{zw,xy}B_{(x,c,1),(y,d,3)}$$

where we used $U(a)=\mathrm{CNOT}_{12}(\tilde{U}(a)\otimes 1)$. Plugging this into (6.35) gives

$$\begin{aligned}
|\Theta\rangle &= \sum_{z,c,w,d\in\{0,1\}}\Bigg(B_{(z,c,1),(w,d,3)}\left(|\rho^{1,U}_{z,c}\rangle|\rho^{3,U}_{w,d}\rangle + |\rho^{3,U}_{w,d}\rangle|\rho^{1,U}_{z,c}\rangle\right)\\
&\quad + \sum_{x,y\in\{0,1\}}U(c)_{zw,xy}B_{(x,c,1),(y,d,3)}\left(|\rho^{2,U}_{z,c}\rangle|\rho^{4,U}_{w,d}\rangle + |\rho^{4,U}_{w,d}\rangle|\rho^{2,U}_{z,c}\rangle\right)\Bigg)\\
&= \sum_{z,c,w,d\in\{0,1\}}B_{(z,c,1),(w,d,3)}\Bigg[|\rho^{1,U}_{z,c}\rangle|\rho^{3,U}_{w,d}\rangle + |\rho^{3,U}_{w,d}\rangle|\rho^{1,U}_{z,c}\rangle\\
&\quad + \sum_{x,y\in\{0,1\}}U(c)_{xy,zw}\left(|\rho^{2,U}_{x,c}\rangle|\rho^{4,U}_{y,d}\rangle + |\rho^{4,U}_{y,d}\rangle|\rho^{2,U}_{x,c}\rangle\right)\Bigg]\\
&= \sum_{z,c,w,d\in\{0,1\}}2B_{(z,c,1),(w,d,3)}\,\mathrm{Sym}(|T_{z,c,w,d}\rangle).
\end{aligned}$$

This is the general solution to equations (6.20)–(6.22), so the space of two-particle frustration-free states for G_U is spanned by the 16 orthonormal states (6.17).

Finally, we show that there are no three-particle frustration-free states. By Lemma 2.3, this implies that there are no frustration-free states for more than two particles. Suppose (to reach a contradiction) that $|\Gamma\rangle$ is a normalized three-particle frustration-free state. Write

$$|\Gamma\rangle = \sum E_{(x,a,q),(y,b,r),(z,c,s)} |\rho^q_{x,a}\rangle |\rho^r_{y,b}\rangle |\rho^s_{z,c}\rangle$$

and note that each reduced density matrix of $|\Gamma\rangle$ on two of the three subsystems must have all of its support on two-particle frustration-free states (see the remark following Lemma 5.4). Using this fact for each two-particle subsystem we get

$$\begin{aligned}
(q,r) \notin \{(1,3),(3,1),(2,4),(4,2)\} \quad &\Longrightarrow \quad E_{(x,a,q),(y,b,r),(z,c,s)} = 0 \\
(q,s) \notin \{(1,3),(3,1),(2,4),(4,2)\} \quad &\Longrightarrow \quad E_{(x,a,q),(y,b,r),(z,c,s)} = 0 \\
(r,s) \notin \{(1,3),(3,1),(2,4),(4,2)\} \quad &\Longrightarrow \quad E_{(x,a,q),(y,b,r),(z,c,s)} = 0
\end{aligned}$$

which together imply that $|\Gamma\rangle = 0$ (a contradiction). Hence no three-particle frustration-free state exists. □

6.3 The boundary gadget

The *boundary gadget* is shown in Figure 6.3. This gate diagram is obtained from Figure 6.2(A) (with $\tilde{U} = 1$) by adding self-loops. Although the boundary gadget will be used for a different purpose than the other gadgets, for technical reasons it is convenient to construct the boundary gadget similarly. The adjacency matrix is

$$A(G_{\text{bnd}}) = A(G_{\text{CNOT}_{12}}) + h_{\text{S}}$$

where

$$h_{\text{S}} = \sum_{z=0}^{1} (|1,z,1\rangle\langle 1,z,1| \otimes 1_j + |2,z,5\rangle\langle 2,z,5| \otimes 1_j + |3,z,1\rangle\langle 3,z,1| \otimes 1_j) .$$

The single-particle ground states (with energy e_1) are superpositions of the states $|\rho^{i,U}_{z,a}\rangle$ from Lemma 6.3 that are in the nullspace of h_{S}. Note that

$$\langle \rho^{j,U}_{x,b} | h_{\text{S}} | \rho^{i,U}_{z,a} \rangle = \delta_{a,b}\delta_{x,z}(\delta_{i,1}\delta_{j,1} + \delta_{i,2}\delta_{j,2} + \delta_{i,3}\delta_{j,3}) \frac{1}{8} \cdot \frac{1}{8}$$

(one factor of $1/8$ comes from the normalization in equations (6.13)–(6.16) and the other factor comes from the normalization in equation (5.2)), so the only single-particle ground states are

$$|\rho^{\text{bnd}}_{z,a}\rangle = |\rho^{4,U}_{z,a}\rangle$$

with $z,a \in \{0,1\}$. Thus there are no two- (or more) particle frustration-free states, because no superposition of the states (6.17) lies in the subspace

$$\text{span}\{\text{Sym}(|\rho^{4,U}_{z,a}\rangle |\rho^{4,U}_{x,b}\rangle) \colon z,a,x,b \in \{0,1\}\}$$

of states with single-particle reduced density matrices in the ground space of $A(G_{\text{bnd}})$. We summarize these results as follows.

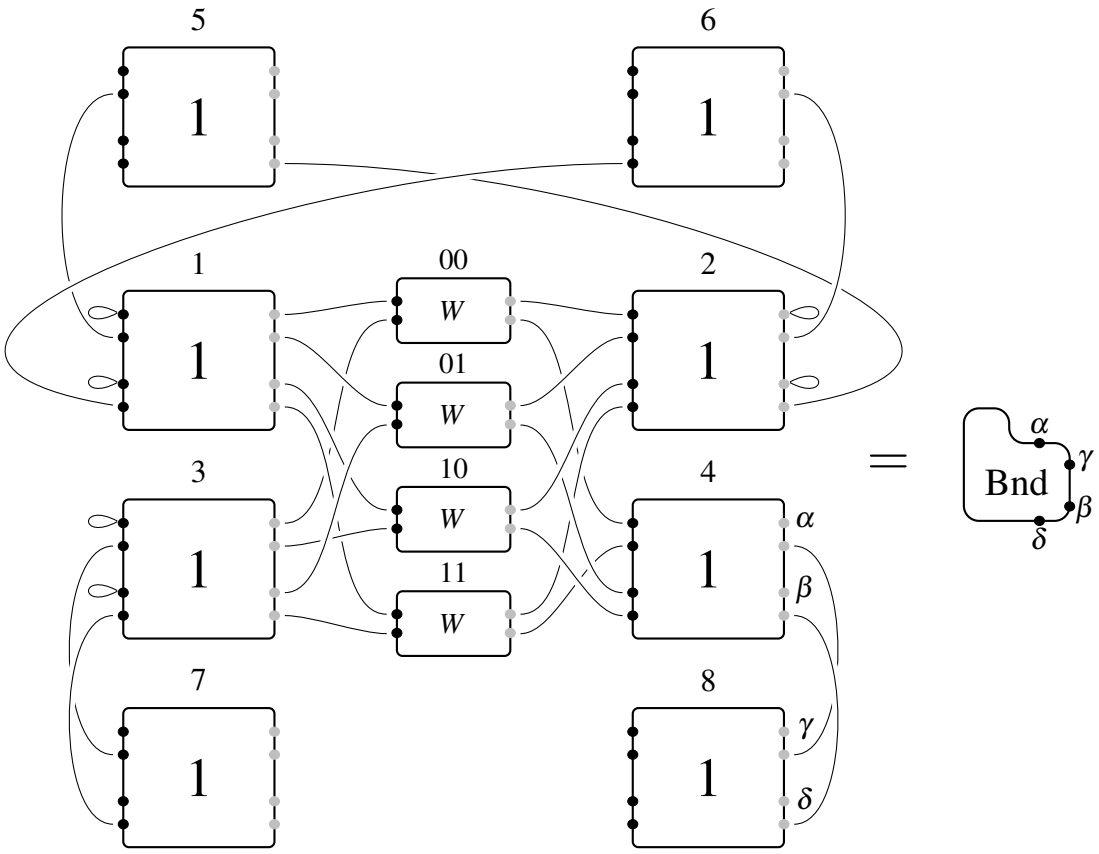

Figure 6.3: The gate diagram for the boundary gadget is obtained from Figure 6.2(A) by setting $\tilde{U} = 1$ and adding 6 self-loops.

Lemma 6.4. *The smallest eigenvalue of $A(G_{\mathrm{bnd}})$ is e_1, with corresponding eigenvectors*

$$|\rho^{\mathrm{bnd}}_{z,a}\rangle = \frac{1}{\sqrt{8}}|\psi^4_{z,a}\rangle - \frac{1}{\sqrt{8}}|\psi^8_{z,a}\rangle - \sqrt{\frac{3}{8}}\sum_{x=0,1}|\chi^{x(z\oplus x)}_{4,a}\rangle \tag{6.36}$$

for $z,a \in \{0,1\}$. There are no frustration-free states with two or more particles, i. e., $\lambda^1_N(G_{\mathrm{bnd}}) > 0$ for $N \geq 2$.

7 Bose-Hubbard Hamiltonian is QMA-hard

Since Frustration-Free Bose-Hubbard Hamiltonian is a special case of Bose-Hubbard Hamiltonian, to prove the latter is QMA-hard it suffices to prove the former is QMA-hard. To achieve this, we efficiently map any sufficiently large instance of any problem in QMA to an equivalent instance of Frustration-Free Bose-Hubbard Hamiltonian.

For any instance X of a problem in QMA there is a verification circuit $\mathcal{C}_X$. We require the verification circuit to be of a certain form described in Section 7.1. Since the class of circuits we consider is universal, this choice is without loss of generality. We also assume without loss of generality [21, 24] that $\mathcal{C}_X$ satisfies a stronger version of Definition 2.1 where the completeness threshold $2/3$ is replaced by $1-(1/2^{|X|})$, i. e.,

- If $X \in L_{\mathrm{yes}}$ then there exists a state $|\psi_{\mathrm{wit}}\rangle$ with $\mathrm{AP}(\mathcal{C}_X, |\psi_{\mathrm{wit}}\rangle) \geq 1 - \dfrac{1}{2^{|X|}}$.
- If $X \in L_{\mathrm{no}}$ then $\mathrm{AP}(\mathcal{C}_X, |\phi\rangle) \leq \dfrac{1}{3}$ for all $|\phi\rangle$.

In this section we exhibit an efficiently computable mapping from the n-qubit, M-gate verification circuit $\mathcal{C}_X$ to an e_1-gate graph G_X with $R = 32(M+2n-2)$ diagram elements and an occupancy constraints graph G^{occ}_X on R vertices. We consider the Hamiltonian $H(G_X, G^{\mathrm{occ}}_X, n)$ and its smallest eigenvalue $\lambda^1_n(G_X, G^{\mathrm{occ}}_X)$. In Section 8 we prove the following.

Theorem 7.1. *If there exists a state $|\psi_{\mathrm{wit}}\rangle$ with $\mathrm{AP}(\mathcal{C}_X, |\psi_{\mathrm{wit}}\rangle) \geq 1-(1/2^{|X|})$, then*

$$\lambda^1_n(G_X, G^{\mathrm{occ}}_X) \leq \frac{1}{2^{|X|}} \tag{7.1}$$

On the other hand, if $\mathrm{AP}(\mathcal{C}_X, |\phi\rangle) \leq 1/3$ for all $|\phi\rangle$, then

$$\lambda^1_n(G_X, G^{\mathrm{occ}}_X) \geq \frac{\mathcal{K}}{n^4 M^4} \tag{7.2}$$

where $\mathcal{K} \in (0,1]$ is an absolute constant.

The number $\mathcal{K}$ appearing in this theorem can in principle be computed (see Section 8) but we will not need to know its value.

Note that if X is a yes instance then (7.1) is satisfied and if X is a no instance then (7.2) is satisfied. By applying the Occupancy Constraints Lemma (Lemma 5.5), with gate graph G_X and occupancy constraints graph G^{occ}_X, and using the fact that $R = 32\,(M+2n-2) \leq 64(M+n)$, we get an efficiently computable e_1-gate graph $G^{\square}_X$ with at most $7 \cdot 64^2 (n+M)^2$ diagram elements such that the following holds.

Theorem 7.2. *If X is a yes instance, then*

$$\lambda_n^1(G_X^{\square}) \leq \frac{1}{2^{|X|}}.$$

On the other hand, if X is a no instance, then

$$\lambda_n^1(G_X^{\square}) \geq \frac{\mathcal{K}}{n^4 M^4 832^9 (M+n)^9}$$

where $\mathcal{K} \in (0,1]$ is the absolute constant from Theorem 7.1.

This theorem is sufficient to prove that Frustration-Free Bose-Hubbard Hamiltonian is QMA-hard. To see this, first let $Q = \lceil 1/\mathcal{K} \rceil$ and define the precision parameter

$$\varepsilon = \frac{1}{2Q} \frac{1}{n^4 M^4 832^9 (M+n)^9}.$$

Note that $1/\varepsilon$ is at least four times the number of vertices in the graph (i. e., at least $4 \cdot 128 \cdot 7 \cdot 64^2 (n+M)^2$, since each diagram element corresponds to 128 vertices); this condition is required in the definition of Frustration-Free Bose-Hubbard Hamiltonian. We now show that solving the instance of Frustration-Free Bose-Hubbard Hamiltonian with graph $G_X^{\square}$, number of particles n, and precision parameter ε is sufficient to solve the original instance X (for $|X|$ at least some constant).

If X is a no instance then the theorem states that $\lambda_n^1(G_X^{\square}) \geq 2\varepsilon \geq \varepsilon + \varepsilon^3$, so the corresponding instance of Frustration-Free Bose-Hubbard Hamiltonian is also a no instance. Furthermore, since M and n are upper bounded by a polynomial function of the instance size $|X|$, there exists a constant instance size above which

$$\frac{1}{2^{|X|}} \leq \varepsilon^3,$$

so when X is a sufficiently large yes instance, the theorem says $\lambda_n^1(G_X^{\square}) \leq \varepsilon^3$, i. e., the corresponding instance of Frustration-Free Bose-Hubbard Hamiltonian is also a yes instance. This proves that Frustration-Free Bose-Hubbard Hamiltonian is QMA-hard, which implies that Bose-Hubbard Hamiltonian is QMA-hard.

The remainder of this section describes the ingredients used to prove Theorem 7.1. In Section 7.1 we describe the verification circuit $\mathcal{C}_X$, in Section 7.2 we define the gate graph G_X, and in Section 7.3 we define the occupancy constraints graph G_X^{occ}. We prove Theorem 7.1 in Section 8.

7.1 The verification circuit

We take the verification circuit $\mathcal{C}_X$ to be from the following universal circuit family. Write n for the number of qubits and M for the number of gates in the circuit

$$U_{\mathcal{C}_X} = U_M U_{M-1} \dots U_1.$$

The qubits labeled $1, \dots, n_{\text{in}}$ hold the input state. The remaining $n - n_{\text{in}}$ ancilla qubits are each initialized to $|0\rangle$. We require each qubit to be involved in at least one gate. The qubit labeled 2 is the output qubit

that contains the result of the computation after the circuit is applied. The qubit labeled 1 mediates two-qubit gates: each gate U_j is a two-qubit gate acting nontrivially on the qubit labeled 1 and another qubit $s(j) \in \{2,\ldots,n\}$. Each unitary U_j is chosen from the set

$$\{\mathrm{CNOT}_{1s(j)},\ \mathrm{CNOT}_{s(j)1},\ \mathrm{CNOT}_{1s(j)}\,(H\otimes 1)\,,\ \mathrm{CNOT}_{1s(j)}\,(HT\otimes 1)\}\,, \tag{7.3}$$

but no two consecutive gates (U_j and U_{j+1}) act between the same two qubits, i. e.,

$$s(j) \neq s(j+1)\,, \qquad j \in [M-1]\,. \tag{7.4}$$

As discussed in Section 2, the acceptance probability for the circuit acting on input state $|\psi_{\mathrm{in}}\rangle \in (\mathbb{C}^2)^{\otimes n_{\mathrm{in}}}$ is the probability that a final measurement of the output qubit in the computational basis gives the value 1:

$$\mathrm{AP}\,(\mathcal{C}_X, |\psi_{\mathrm{in}}\rangle) = \left\| |1\rangle\langle 1|^{(2)} U_{\mathcal{C}_X} |\psi_{\mathrm{in}}\rangle |0\rangle^{\otimes n-n_{\mathrm{in}}} \right\|^2 .$$

We now establish that circuits of this form are universal. We show that any quantum circuit (with $n \geq 4$ qubits) expressed using the universal gate set

$$\{\mathrm{CNOT},\ H,\ HT\} \tag{7.5}$$

can be efficiently rewritten in the prescribed form without increasing the number of qubits and with at most a constant factor increase in the number of gates.

First we map a circuit from the gate set (7.5) to the gate set (7.3) (without necessarily satisfying condition (7.4)). A SWAP gate between qubits 1 and k can be performed using the identity

$$\mathrm{SWAP}_{1k} = \mathrm{CNOT}_{1k}\mathrm{CNOT}_{k1}\mathrm{CNOT}_{1k}\,.$$

To perform a CNOT_{ik} gate between two qubits i,k (neither of which is qubit 1), we swap qubits 1 and i, apply CNOT_{1k}, and then swap back. Similarly, we can apply a single-qubit gate $U \in \{H, HT\}$ to some qubit $k \neq 1$ using the sequence of gates

$$\mathrm{SWAP}_{1k}\mathrm{CNOT}_{12}\,(\mathrm{CNOT}_{12}U\otimes 1)\,\mathrm{SWAP}_{1k}\,.$$

Applying these replacement rules, we obtain a circuit over the gate set (7.3). However, the resulting circuit will not in general satisfy equation (7.4). To enforce this condition, we insert a sequence of four gates equal to the identity, namely

$$1 = \mathrm{CNOT}_{1a}\mathrm{CNOT}_{1b}\mathrm{CNOT}_{1a}\mathrm{CNOT}_{1b}\,,$$

between any two consecutive gates U_j and U_{j+1} with $s(j) = s(j+1)$, where $a \neq b \neq s(j)$. For example,

$$\mathrm{CNOT}_{15}\mathrm{CNOT}_{51} \quad\longrightarrow\quad \mathrm{CNOT}_{15}\mathrm{CNOT}_{12}\mathrm{CNOT}_{13}\mathrm{CNOT}_{12}\mathrm{CNOT}_{13}\mathrm{CNOT}_{51}\,.$$

Thus we map a circuit over the gate set (7.5) into the prescribed form. Note that $n \geq 4$ is needed to ensure that any quantum circuit can be efficiently rewritten so that $s(j) \neq s(j+1)$. (There do exist circuits of the desired of the form with $n = 3$, such as in the example shown in Figure 7.1.)

7.2 The gate graph

For any n-qubit, M-gate verification circuit $\mathcal{C}_X$ of the form described above, we associate a gate graph G_X. The gate diagram for G_X is built using the gadgets described in Section 6; specifically, we use M two-qubit gadgets and $2(n-1)$ boundary gadgets. Since each two-qubit gadget and each boundary gadget contains 32 diagram elements, the total number of diagram elements in G_X is $R = 32(M+2n-2)$.

We now present the construction of the gate diagram for G_X. We also describe some gate graphs obtained as intermediate steps that are used in our analysis in Section 8. The reader may find this description easier to follow by looking ahead to Figure 7.1, which illustrates the construction for a specific 3-qubit circuit.

1. **Draw a grid** with columns labeled $j = 0, 1, \ldots, M+1$ and rows labeled $i = 1, \ldots, n$ (this grid is only used to help describe the diagram).

2. **Place gadgets in the grid to mimic the quantum circuit.** For each $j = 1, \ldots, M$, place a gadget for the two-qubit gate U_j between rows 1 and $s(j)$ in the j-th column. Place boundary gadgets in rows $i = 2, \ldots, n$ of column 0 and in the same rows of column $M+1$. Write G_1 for the gate graph associated with the resulting diagram.

3. **Connect the nodes within each row.** First add edges connecting the nodes in rows $i = 2, \ldots, n$; call the resulting gate graph G_2. Then add edges connecting the nodes in row 1; call the resulting gate graph G_3.

4. **Add self-loops to the boundary gadgets.** In this step we add self-loops to enforce initialization of ancillas (at the beginning) and the proper output of the circuit (at the end). For each row $k = n_{\text{in}} + 1, \ldots, n$, add a self-loop to node δ (as shown in Figure 6.3) of the corresponding boundary gadget in column $r = 0$, giving the gate diagram for G_4. Finally, add a self-loop to node α of the boundary gadget (as in Figure 6.3) in row 2 and column $M+1$, giving the gate diagram for G_X (Recall from the previous section that qubit 2 is always taken to be the output qubit).

Figure 7.1 illustrates the step-by-step construction of G_X using a simple 3-qubit circuit with four gates

$$\text{CNOT}_{12}\,(\text{CNOT}_{13} HT \otimes 1)\,\text{CNOT}_{21}\text{CNOT}_{13}\,.$$

In this example, two of the qubits are input qubits (so $n_{\text{in}} = 2$), while the third qubit is an ancilla initialized to $|0\rangle$. Following the convention described in Section 7.1, we take qubit 2 to be the output qubit. (In this example the circuit is not meant to compute anything interesting; its only purpose is to illustrate our method of constructing a gate graph.)

We made some choices in designing this circuit-to-gate graph mapping that may seem arbitrary (e. g., we chose to place boundary gadgets in each row except the first). We have tried to achieve a balance between simplicity of description and ease of analysis, but we expect that other choices could be made to work.

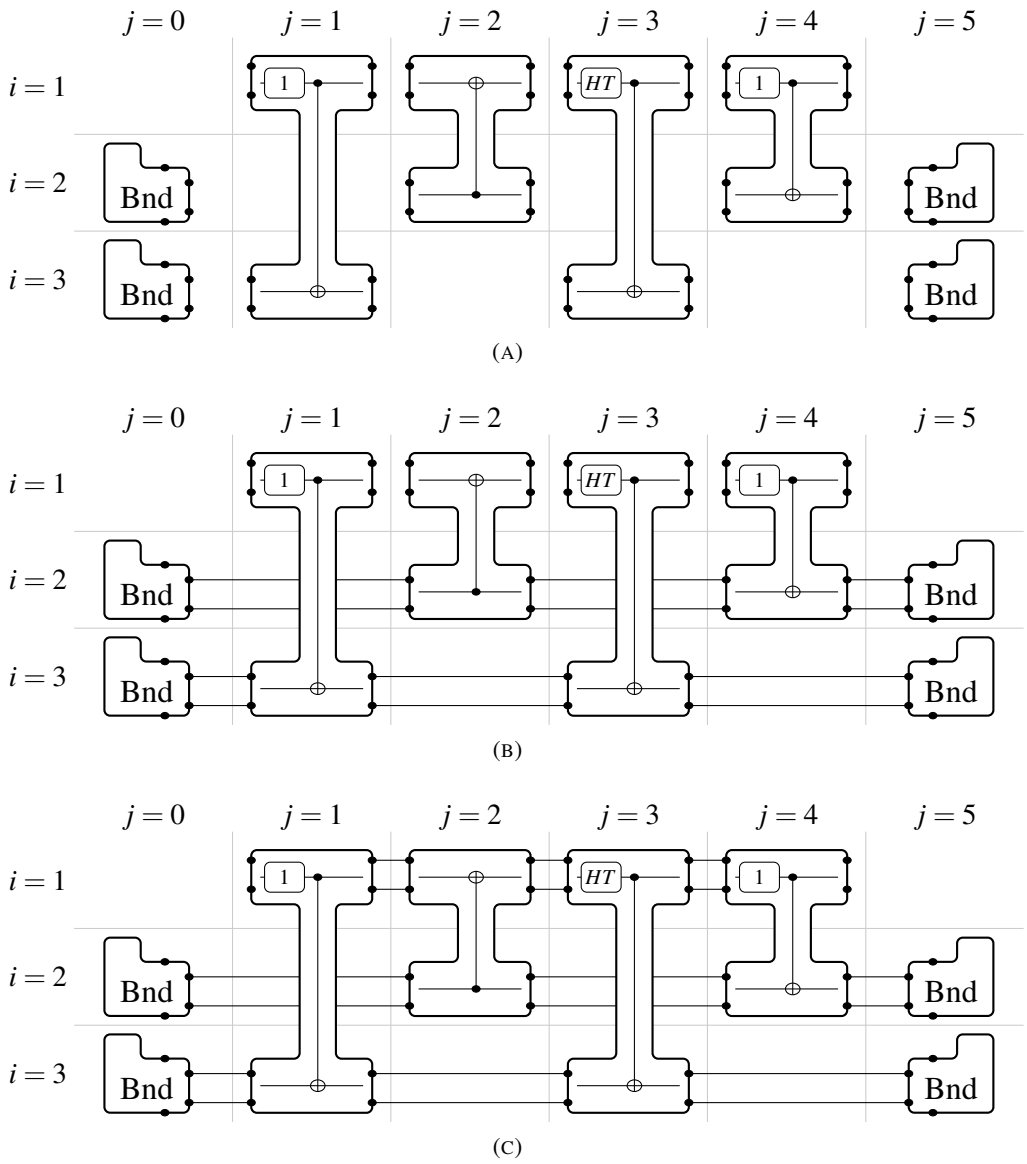

Figure 7.1: Step-by-step construction of the gate diagram for G_X for the three-qubit example circuit described in the text. (A) The gate diagram for G_1. (B) Add edges in all rows except the first to obtain the gate diagram for G_2. (C) Add edges in the first row to obtain the gate diagram for G_3. See the following figure for the remainder of the construction.

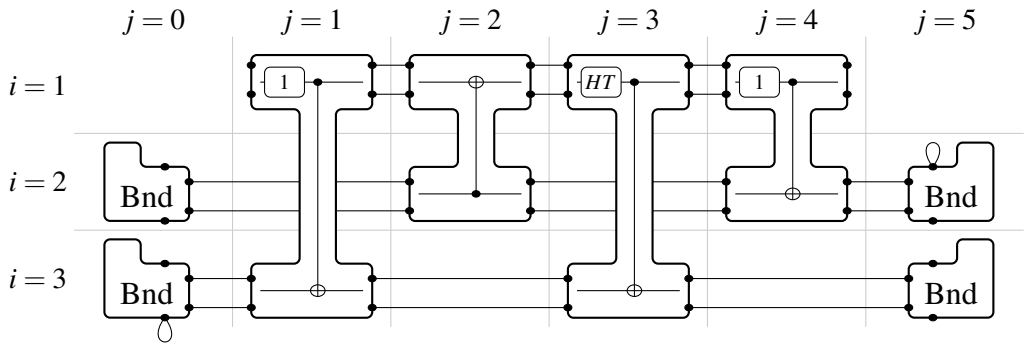

(D)

Figure 7.1: Continuation of step-by-step construction. (D) Add self-loops to the boundary gadgets to obtain the gate diagram for G_X (the diagram for G_4 in this case differs from (D) by removing the self-loop in column 5; this diagram is not shown).

7.2.1 Notation for G_X

We now introduce some notation that allows us to easily refer to a subset $\mathcal{L}$ of the diagram elements in the gate diagram for G_X.

Recall from Section 6 that each two-qubit gate gadget and each boundary gadget is composed of 32 diagram elements. This can be seen by looking at Figure 6.2(A) and Figure 6.3 and noting (from Figure 6.1) that each move-together gadget comprises 6 diagram elements.

For each of the two-qubit gate gadgets in the gate diagram for G_X, we focus our attention on the four diagram elements labeled 1–4 in Figure 6.2(A). In total there are $4M$ such diagram elements in the gate diagram for G_X: in each column $j \in \{1,\dots,M\}$ there are two in row 1 and two in row $s(j)$. When $U_j \in \{\mathrm{CNOT}_{1s(j)}, \mathrm{CNOT}_{1s(j)}\,(H\otimes 1)\,, \mathrm{CNOT}_{1s(j)}\,(HT\otimes 1)\}$ the diagram elements labeled $1,2$ are in row 1 and those labeled $3,4$ are in row $s(j)$; when $U_j = \mathrm{CNOT}_{s(j)1}$ those labeled $1,2$ are in row $s(j)$ and those labeled $3,4$ are in row 1. We denote these diagram elements by triples (i,j,d). Here i and j indicate (respectively) the row and column of the grid in which the diagram element is found, and d indicates whether it is the leftmost ($d=0$) or rightmost ($d=1$) diagram element in this row and column. We define

$$\mathcal{L}_{\text{gates}} = \{(i,j,d) : i \in \{1,s(j)\},\ j \in [M],\ d \in \{0,1\}\} \tag{7.6}$$

to be the set of all such diagram elements.

For example, in Figure 7.1 the first gate is

$$U_1 = \mathrm{CNOT}_{13}\,,$$

so the gadget from Figure 6.2(A) (with $\tilde{U} = 1$) appears between rows 1 and 3 in the first column. The diagram elements labeled $1,2,3,4$ from Figure 6.2(A) are denoted by $(1,1,0),(1,1,1),(3,1,0),(3,1,1)$, respectively. The second gate in Figure 7.1 is $U_2 = \mathrm{CNOT}_{21}$, so the gadget from Figure 6.2(B) (with $\tilde{U} = 1$) appears between rows 2 and 1; in this case the diagram elements labeled $1,2,3,4$ in Figure 6.2(A) are denoted by $(2,2,0),(2,2,1),(1,2,0),(1,2,1)$, respectively.

We also define notation for the boundary gadgets in G_X. For each boundary gadget. we focus on a single diagram element, labeled 4 in Figure 6.3. For the left hand-side and right-hand side boundary gadgets, respectively, we denote these diagram elements as

$$\mathcal{L}_{\text{in}} = \{(i,0,1) : i \in \{2,\ldots,n\}\} \tag{7.7}$$
$$\mathcal{L}_{\text{out}} = \{(i,M+1,0) : i \in \{2,\ldots,n\}\}. \tag{7.8}$$

Definition 7.3. Let $\mathcal{L}$ be the set of diagram elements

$$\mathcal{L} = \mathcal{L}_{\text{in}} \cup \mathcal{L}_{\text{gates}} \cup \mathcal{L}_{\text{out}}$$

where $\mathcal{L}_{\text{in}}$, $\mathcal{L}_{\text{gates}}$, and $\mathcal{L}_{\text{out}}$ are given by equations (7.7), (7.6), and (7.8), respectively.

Finally, it is convenient to define a function F that describes horizontal movement within the rows of the gate diagram for G_X. The function F takes as input a two-qubit gate $j \in [M]$, a qubit $i \in \{2,\ldots,n\}$, and a single bit and outputs a diagram element from the set $\mathcal{L}$. If the bit is 0 then F outputs the diagram element in row i that appears in a column $0 \leq k < j$ with k maximal (i. e., the closest diagram element in row i to the left of column j):

$$F(i,j,0) = \begin{cases} (i,k,1) & \text{where } 1 \leq k < j \text{ is the largest } k \text{ such that } s(k) = i, \text{ if it exists} \\ (i,0,1) & \text{otherwise.} \end{cases} \tag{7.9}$$

On the other hand, if the bit is 1, then F outputs the diagram element in row i that appears in a column $j < k \leq M+1$ with k minimal (i. e., the closest diagram element in row i to the right of column j).

$$F(i,j,1) = \begin{cases} (i,k,0) & \text{where } j < k \leq M \text{ is the smallest } k \text{ such that } s(k) = j, \text{ if it exists} \\ (i,M+1,0) & \text{otherwise.} \end{cases} \tag{7.10}$$

7.3 The occupancy constraints graph

In this section we define an occupancy constraints graph G_X^{occ}. Along with G_X and the number of particles n, this determines a subspace $\mathcal{I}(G_X, G_X^{\text{occ}}, n) \subset \mathcal{Z}_n(G_X)$ through equation (5.21). We will see in Section 8 how low-energy states of the Bose-Hubbard model that live entirely within this subspace encode computations corresponding to the quantum circuit $\mathcal{C}_X$. This fact is used in the proof of Theorem 7.1, which shows that the smallest eigenvalue $\lambda_n^1(G_X, G_X^{\text{occ}})$ of

$$H(G_X, G_X^{\text{occ}}, n) = H(G_X, n)\big|_{\mathcal{I}(G_X, G_X^{\text{occ}}, n)}$$

is related to the maximum acceptance probability of the circuit.

We encode quantum data in the locations of n particles in the graph G_X as follows. Each particle encodes one qubit and is located in one row of the graph G_X. Since all two-qubit gates in $\mathcal{C}_X$ involve the first qubit, the location of the particle in the first row determines how far along the computation has proceeded. We design the occupancy constraints graph to ensure that low-energy states of $H(G_X, G_X^{\text{occ}}, n)$ have exactly one particle in each row (since there are n particles and n rows), and so that the particles

in rows $2,\dots,n$ are not too far behind or ahead of the particle in the first row. To avoid confusion, we emphasize that not *all* states in the subspace $\mathcal{I}(G_X, G_X^{\mathrm{occ}}, n)$ have the desired properties—for example, there are states in this subspace with more than one particle in a given row. We see in the next section that states with low energy for $H(G_X, n)$ that also satisfy the occupancy constraints (i. e., low-energy states of $H(G_X, G_X^{\mathrm{occ}}, n)$) have the desired properties.

We now define G_X^{occ}, which is a simple graph with a vertex for each diagram element in G_X. Each edge in G_X^{occ} places a constraint on the locations of particles in G_X. The graph G_X^{occ} only has edges between diagram elements in the set $\mathcal{L}$ from Definition 7.3; we define the edge set $E(G_X^{\mathrm{occ}})$ by specifying pairs of diagram elements $L_1, L_2 \in \mathcal{L}$. We also indicate (in bold) the reason for choosing the constraints.

1. **No two particles in the same row.** For each $i \in [n]$ we add constraints between diagram elements $(i,j,c) \in \mathcal{L}$ and $(i,k,d) \in \mathcal{L}$ in row i but in different columns, i. e.,

$$\{(i,j,c),(i,k,d)\} \in E(G_X^{\mathrm{occ}}) \text{ whenever } j \neq k. \tag{7.11}$$

2. **Synchronization with the particle in the first row.** For each $j \in [M]$ we add constraints between row 1 and row $s(j)$:

$$\{(1,j,c),(s(j),k,d)\} \in E(G_X^{\mathrm{occ}}) \text{ whenever } k \neq j \text{ and } (s(j),k,d) \neq F(s(j),j,c).$$

For each $j \in [M]$ we also add constraints between row 1 and rows $i \in [n] \setminus \{1, s(j)\}$:

$$\{(1,j,c),(i,k,d)\} \in E(G_X^{\mathrm{occ}}) \text{ whenever } (i,k,d) \notin \{F(i,j,0), F(i,j,1)\}.$$

8 Proof of Theorem 7.1

We write $\gamma(H)$ for the smallest nonzero eigenvalue of a positive semidefinite matrix H.

8.1 Strategy and outline of the proof

Theorem 7.1 bounds the smallest eigenvalue $\lambda_n^1(G_X, G_X^{\mathrm{occ}})$ of $H(G_X, G_X^{\mathrm{occ}}, n)$. To prove the theorem, we investigate a sequence of Hamiltonians starting with $H(G_1, n)$ and $H(G_1, G_X^{\mathrm{occ}}, n)$ and then work our way up to the Hamiltonian $H(G_X, G_X^{\mathrm{occ}}, n)$ by adding positive semidefinite terms.

For each Hamiltonian we consider, we solve for the nullspace and the smallest nonzero eigenvalue. To go from one Hamiltonian to the next, we use the following "Nullspace Projection Lemma," which was used (implicitly) in reference [25]. The lemma bounds the smallest nonzero eigenvalue $\gamma(H_A + H_B)$ of a sum of positive semidefinite Hamiltonians H_A and H_B using knowledge of the smallest nonzero eigenvalue $\gamma(H_A)$ of H_A and the smallest nonzero eigenvalue $\gamma(H_B|_S)$ of the restriction of H_B to the nullspace S of H_A.

Lemma 8.1 (Nullspace Projection Lemma [25]). *Let $H_A, H_B \geq 0$. Suppose the nullspace S of H_A is non-empty and*

$$\gamma(H_B|_S) \geq c > 0 \qquad \text{and} \qquad \gamma(H_A) \geq d > 0.$$

Then

$$\gamma(H_A + H_B) \geq \frac{cd}{c + d + \|H_B\|}. \tag{8.1}$$

We prove the lemma in Section A.1. When we apply this lemma, we are usually interested in an asymptotic limit where $c, d \ll \|H_B\|$ and the right-hand side of (8.1) is $\Omega(cd/\|H_B\|)$.

Our proof strategy, using repeated applications of the Nullspace Projection Lemma, is analogous to that of reference [19], where the so-called Projection Lemma was used similarly. Our technique has the advantage of not requiring the terms we add to our Hamiltonian to have "unphysical" problem-size dependent coefficients (it also has this advantage over the method of perturbative gadgets [19, 17]). This allows us to prove results about the "physically realistic" Bose-Hubbard Hamiltonian. A similar technique based on Kitaev's Geometric Lemma was used in reference [13] (however, that method is slightly more computation intensive, requiring a lower bound on $\gamma(H_B)$ as well as bounds on $\gamma(H_A)$ and $\gamma(H_B|_S)$).

8.1.1 Adjacency matrices of the gate graphs

We begin by discussing the graphs

$$G_1,\ G_2,\ G_3,\ G_4,\ G_X$$

(as defined in Section 7; see Figure 7.1) in more detail and deriving some properties of their adjacency matrices.

The graph G_1 has a component for each of the two-qubit gates $j \in [M]$, for each of the boundary gadgets $i = 2, \ldots, n$ in column 0, and for each of the boundary gadgets $i = 2, \ldots, n$ in column $M+1$. In other words

$$G_1 = \underbrace{\left(\bigcup_{i=2}^{n} G_{\text{bnd}}\right)}_{\text{left boundary}} \cup \underbrace{\left(\bigcup_{j=1}^{M} G_{U_j}\right)}_{\text{two-qubit gates}} \cup \underbrace{\left(\bigcup_{i=2}^{n} G_{\text{bnd}}\right)}_{\text{right boundary}}. \tag{8.2}$$

We use our knowledge of the adjacency matrices of the components G_{bnd} and G_{U_j} to understand the ground space of $A(G_1)$. Recall (from Section 6) that the smallest eigenvalue of $A(G_{U_j})$ is

$$e_1 = -1 - 3\sqrt{2}$$

(with degeneracy 16) which is also the smallest eigenvalue of $A(G_{\text{bnd}})$ (with degeneracy 4). For each diagram element $L \in \mathcal{L}$ and pair of bits $z, a \in \{0,1\}$ there is an eigenstate $|\rho^L_{z,a}\rangle$ of $A(G_1)$ with this minimal eigenvalue e_1. In total we get sixteen eigenstates

$$|\rho^{(1,j,0)}_{z,a}\rangle,\ |\rho^{(1,j,1)}_{z,a}\rangle,\ |\rho^{(s(j),j,0)}_{z,a}\rangle,\ |\rho^{(s(j),j,1)}_{z,a}\rangle, \quad z, a \in \{0,1\},$$

for each two-qubit gate $j \in [M]$, four eigenstates

$$|\rho^{(i,0,1)}_{z,a}\rangle, \quad z, a \in \{0,1\},$$

for each boundary gadget $i \in \{2, \ldots, n\}$ in column 0, and four eigenstates

$$|\rho^{(i,M+1,0)}_{z,a}\rangle, \quad z, a \in \{0,1\},$$

for each boundary gadget $i \in \{2, \ldots, n\}$ in column $M+1$. The set

$$\left\{|\rho^L_{z,a}\rangle : z, a \in \{0,1\},\ L \in \mathcal{L}\right\}$$

is an orthonormal basis for the ground space of $A(G_1)$.

We write the adjacency matrices of G_2, G_3, G_4, and G_X as

$$A(G_2) = A(G_1) + h_1 \qquad A(G_4) = A(G_3) + \sum_{i=n_{\text{in}}+1}^{n} h_{\text{in},i}$$
$$A(G_3) = A(G_2) + h_2 \qquad A(G_X) = A(G_4) + h_{\text{out}}\,.$$

From step 3 of the construction of the gate diagram in Section 7.2, we see that h_1 and h_2 are both sums of terms of the form

$$\left(|q,z,t\rangle + |q',z,t'\rangle\right)\left(\langle q,z,t| + \langle q',z,t'|\right) \otimes 1_j\,,$$

where h_1 contains a term for each edge in rows $2,\ldots,n$ and h_2 contains a term for each of the $2(M-1)$ edges in the first row. The operators

$$h_{\text{in},i} = |(i,0,1),1,7\rangle\langle(i,0,1),1,7| \otimes 1 \qquad h_{\text{out}} = |(2,M+1,0),0,5\rangle\langle(2,M+1,0),0,5| \otimes 1 \tag{8.3}$$

correspond to the self-loops added in the gate diagram in step 4 of Section 7.2.

We prove that G_1, G_2, G_3, G_4, and G_X are e_1-gate graphs.

Lemma 8.2. *The smallest eigenvalues of G_1, G_2, G_3, G_4 and G_X are*

$$\mu(G_1) = \mu(G_2) = \mu(G_3) = \mu(G_4) = \mu(G_X) = e_1\,.$$

Proof. We showed in the above discussion that $\mu(G_1) = e_1$. The adjacency matrices of G_2, G_3, G_4, and G_X are obtained from that of G_1 by adding positive semidefinite terms (h_1, h_2, $h_{\text{in},i}$, and h_{out} are all positive semidefinite). It therefore suffices to exhibit an eigenstate $|\rho\rangle$ of $A(G_1)$ with

$$h_1|\rho\rangle = h_2|\rho\rangle = h_{\text{in},i}|\rho\rangle = h_{\text{out}}|\rho\rangle = 0$$

(for each $i \in \{n_{\text{in}}+1,\ldots,n\}$). There are many states $|\rho\rangle$ satisfying these conditions; one example is

$$|\rho\rangle = |\rho_{0,0}^{(1,1,0)}\rangle$$

which is supported on vertices where h_1, h_2, $h_{\text{in},i}$, and h_{out} have no support. □

8.1.2 Building up the Hamiltonian

We now outline the sequence of Hamiltonians considered in the following sections and describe the relationships between them. As a first step, in Section 8.2 we exhibit a basis $\mathcal{B}_n$ for the nullspace of $H(G_1,n)$ and we prove that its smallest nonzero eigenvalue is lower bounded by a positive constant. We then discuss the restriction

$$H(G_1, G_X^{\text{occ}}, n) = H(G_1,n)\big|_{\mathcal{J}(G_1,G_X^{\text{occ}},n)} \tag{8.4}$$

in Section 8.3, where we prove that a subset $\mathcal{B}_{\text{legal}} \subset \mathcal{B}_n$ is a basis for the nullspace of (8.4), and that its smallest nonzero eigenvalue is also lower bounded by a positive constant.

For the remainder of the proof we use the Nullspace Projection Lemma (Lemma 8.1) four times, using the decompositions

$$H(G_2, G_X^{\text{occ}}, n) = H(G_1, G_X^{\text{occ}}, n) + H_1\big|_{\mathcal{I}(G_2, G_X^{\text{occ}}, n)} \tag{8.5}$$

$$H(G_3, G_X^{\text{occ}}, n) = H(G_2, G_X^{\text{occ}}, n) + H_2\big|_{\mathcal{I}(G_3, G_X^{\text{occ}}, n)} \tag{8.6}$$

$$H(G_4, G_X^{\text{occ}}, n) = H(G_3, G_X^{\text{occ}}, n) + \sum_{i=n_{\text{in}}+1}^{n} H_{\text{in},i}\big|_{\mathcal{I}(G_4, G_X^{\text{occ}}, n)} \tag{8.7}$$

$$H(G_X, G_X^{\text{occ}}, n) = H(G_4, G_X^{\text{occ}}, n) + H_{\text{out}}\big|_{\mathcal{I}(G_X, G_X^{\text{occ}}, n)} \tag{8.8}$$

where

$$H_1 = \sum_{w=1}^{n} h_1^{(w)}, \qquad H_{\text{in},i} = \sum_{w=1}^{n} h_{\text{in},i}^{(w)}, \qquad H_2 = \sum_{w=1}^{n} h_2^{(w)}, \qquad H_{\text{out}} = \sum_{w=1}^{n} h_{\text{out}}^{(w)}$$

are all positive semidefinite, with $h_1, h_2, h_{\text{in},i}, h_{\text{out}}$ as defined in Section 8.1.1. Note that in writing equations (8.5), (8.6), (8.7), and (8.8), we have used the fact (from Lemma 8.2) that the adjacency matrices of the graphs we consider all have the same smallest eigenvalue e_1. Also note that

$$\mathcal{I}(G_i, G_X^{\text{occ}}, n) = \mathcal{I}(G_X, G_X^{\text{occ}}, n)$$

for $i \in [4]$ since the gate diagrams for each of the graphs G_1, G_2, G_3, G_4 and G_X have the same set of diagram elements.

Let S_k be the nullspace of $H(G_k, G_X^{\text{occ}}, n)$ for $k = 1, 2, 3, 4$. Since these positive semidefinite Hamiltonians are related by adding positive semidefinite terms, their nullspaces satisfy

$$S_4 \subseteq S_3 \subseteq S_2 \subseteq S_1 \subseteq \mathcal{I}(G_X, G_X^{\text{occ}}, n).$$

We solve for $S_1 = \text{span}(\mathcal{B}_{\text{legal}})$ in Section 8.3 and we characterize the spaces S_2, S_3, and S_4 in Section 8.5 in the course of applying our strategy.

For example, to use the Nullspace Projection Lemma to lower bound the smallest nonzero eigenvalue of $H(G_2, G_X^{\text{occ}}, n)$, we consider the restriction

$$\left(H_1\big|_{\mathcal{I}(G_2, G_X^{\text{occ}}, n)}\right)\Big|_{S_1} = H_1\big|_{S_1}. \tag{8.9}$$

We also solve for S_2, which is equal to the nullspace of (8.9). To obtain the corresponding lower bounds on the smallest nonzero eigenvalues of $H(G_k, G_X^{\text{occ}}, n)$ for $k = 2, 3, 4$ and $H(G_X, G_X^{\text{occ}}, n)$, we consider restrictions

$$H_2\big|_{S_2}, \quad \sum_{i=n_{\text{in}}+1}^{n} H_{\text{in},i}\big|_{S_3}, \quad \text{and} \quad H_{\text{out}}\big|_{S_4}.$$

Analyzing these restrictions involves extensive computation of matrix elements. To simplify and organize these computations, we first compute the restrictions of each of these operators to the space S_1. We present the results of this computation in Section 8.4; details of the calculation can be found in Section A.3. In Section 8.5 we proceed with the remaining computations and apply the Nullspace Projection Lemma three times using equations (8.5), (8.6), and (8.7). Finally, in Section 8.6 we apply the lemma again using equation (8.8) and we prove Theorem 7.1.

8.2 Configurations

In this section we use Lemma 2.4 to solve for the nullspace of $H(G_1, n)$, i. e., the n-particle frustration-free states on G_1. Lemma 2.4 describes how frustration-free states for G_1 are built out of frustration-free states for its components.

To see how this works, consider the example from Figure 7.1(A). In this example, with $n = 3$, we construct a basis for the nullspace of $H(G_1, 3)$ by considering two types of eigenstates. First, there are frustration-free states

$$\mathrm{Sym}(|\rho^{L_1}_{z_1,a_1}\rangle|\rho^{L_2}_{z_2,a_2}\rangle|\rho^{L_3}_{z_3,a_3}\rangle) \tag{8.10}$$

where $L_k = (i_k, j_k, d_k) \in \mathcal{L}$ belong to different components of G_1. That is to say, $j_w \neq j_t$ unless $j_w = j_t \in \{0, 5\}$, in which case $i_w \neq i_t$ (in this case the particles are located either at the left or right boundary, in different rows of G_1). There are also frustration-free states where two of the three particles are located in the same two-qubit gadget $J \in [M]$ and one of the particles is located in a diagram element L_1 from a different component of the graph. These states have the form

$$\mathrm{Sym}(|T^J_{z_1,a_1,z_2,a_2}\rangle|\rho^{L_1}_{z_3,a_3}\rangle) \tag{8.11}$$

where

$$|T^J_{z_1,a_1,z_2,a_2}\rangle = \frac{1}{\sqrt{2}}|\rho^{(1,J,0)}_{z_1,a_1}\rangle|\rho^{(s(J),J,0)}_{z_2,a_2}\rangle + \frac{1}{\sqrt{2}}\sum_{x_1,x_2\in\{0,1\}} U_J(a_1)_{x_1x_2,z_1z_2}|\rho^{(1,J,1)}_{x_1,a_1}\rangle|\rho^{(s(J),J,1)}_{x_2,a_2}\rangle \tag{8.12}$$

and $L_1 = (i, j, k) \in \mathcal{L}$ satisfies $j \neq J$ (using Lemma 6.3 and also the fact that the controlled-not gate is real for the case $U_J = \mathrm{CNOT}_{s(J)1}$).

Each of the states (8.10) and (8.11) is specified by 6 "data" bits $z_1, z_2, z_3, a_1, a_2, a_3 \in \{0, 1\}$ and a "configuration" indicating where the particles are located in the graph. The configuration is specified either by three diagram elements $L_1, L_2, L_3 \in \mathcal{L}$ from different components of G_1 or by a two-qubit gate $J \in [M]$ along with a diagram element $L_1 \in \mathcal{L}$ from a different component of the graph.

We now define the notion of a configuration for general n. Informally, we can think of an n-particle configuration as a way of placing n particles in the graph G_1 subject to the following restrictions. We first place each of the n particles in a component of the graph, with the restriction that no boundary gadget may contain more than one particle and no two-qubit gadget may contain more than two particles. For each particle on its own in a component (i. e., in a component with no other particles), we assign one of the diagram elements $L \in \mathcal{L}$ associated to that component. We therefore specify a configuration by a set of two-qubit gadgets $J_1, \ldots, J_Y$ that contain two particles, along with a set of diagram elements $L_k \in \mathcal{L}$ that give the locations of the remaining $n - 2Y$ particles. We choose to order the Js and the Ls so that each configuration is specified by a unique tuple $(J_1, \ldots, J_Y, L_1, \ldots, L_{n-2Y})$. For concreteness, we use the lexicographic order on diagram elements in the set $\mathcal{L}$: $L_A = (i_A, j_A, d_A)$ and $L_B = (i_B, j_B, d_B)$ satisfy $L_A < L_B$ iff either $i_A < i_B$, or $i_A = i_B$ and $j_A < j_B$, or $(i_A, j_A) = (i_B, j_B)$ and $d_A < d_B$.

Definition 8.3 (Configuration). An n-particle configuration on the gate graph G_1 is a tuple

$$(J_1, \ldots, J_Y, L_1, \ldots, L_{n-2Y})$$

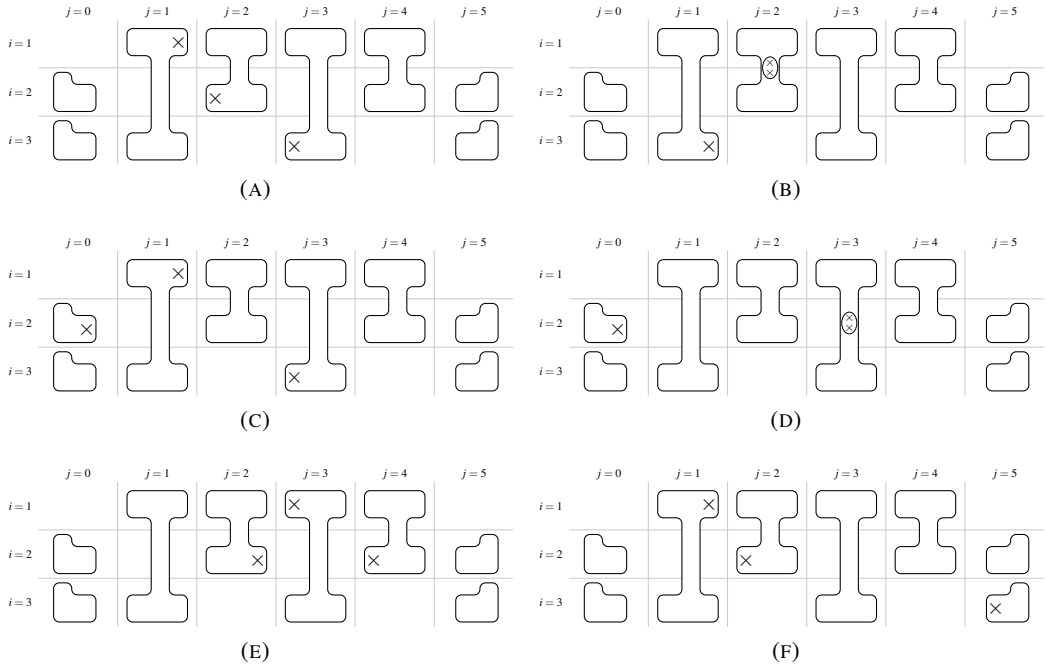

Figure 8.1: Diagrammatic depictions of configurations for the example where G_1 is the gate graph from Figure 7.1(A). The figures show the locations of each of the three particles in the gate graph. The symbol $\times$ indicates a single-particle state and the symbol $\otimes$ indicates a two-particle state. (A) $((1,1,1),(2,2,0),(3,3,0))$. (B) $(2,(3,1,1))$. (C) $((1,1,1),(2,0,1),(3,3,0)$. (D) $(3,(2,0,1))$. (E) $((1,3,0),(2,2,1),(2,4,0))$. (F) $((1,1,1),(2,2,0),(3,5,0))$. The examples in (A), (B), and (C) show legal configurations whereas the examples in (D), (E), and (F) are illegal, as defined in Section 8.3 .

with $Y \in \{0,\ldots,\lfloor n/2 \rfloor\}$, ordered integers

$$1 \leq J_1 < J_2 < \cdots < J_Y \leq M\,,$$

and lexicographically ordered diagram elements

$$L_1 < L_2 < \cdots < L_{n-2Y}\,, \qquad L_k = (i_k, j_k, d_k) \in \mathcal{L}\,.$$

We further require that each L_k is from a different component of G_1, i. e.,

$$j_w = j_t \quad \Longrightarrow \quad j_w \in \{0, M+1\} \text{ and } i_w \neq i_t\,,$$

and we require that $j_u \neq J_v$ for all $u \in [n-2Y]$ and $v \in [Y]$.

In Figure 8.1 we give some examples of configurations (for the example from Figure 7.1(A) with $n = 3$) and we introduce a diagrammatic notation for them.

For any configuration and n-bit strings $\vec{z}$ and $\vec{a}$, there is a state in the nullspace of $H(G_1, n)$, given by

$$\mathrm{Sym}(|T^{J_1}_{z_1,a_1,z_2,a_2}\rangle \ldots |T^{J_Y}_{z_{2Y-1},a_{2Y-1},z_{2Y},a_{2Y}}\rangle |\rho^{L_1}_{z_{2Y+1},a_{2Y+1}}\rangle \ldots |\rho^{L_{n-2Y}}_{z_n,a_n}\rangle)\,. \tag{8.13}$$

The ordering in the definition of a configuration ensures that each distinct choice of configuration and n-bit strings $\vec{z},\vec{a}$ gives a different state.

Definition 8.4. Let $\mathcal{B}_n$ be the set of all states of the form (8.13), where $(J_1,\ldots,J_Y,L_1,\ldots,L_{n-2Y})$ is a configuration and $\vec{z},\vec{a}\in\{0,1\}^n$.

Lemma 8.5. *The set $\mathcal{B}_n$ is an orthonormal basis for the nullspace of $H(G_1,n)$. Furthermore,*

$$\gamma(H(G_1,n))\geq\mathcal{K}_0 \tag{8.14}$$

where $\mathcal{K}_0\in(0,1]$ is an absolute constant.

Proof. Each component of G_1 is either a two-qubit gadget or a boundary gadget (see equation (8.2)). The single-particle states of $A(G_1)$ with energy e_1 are the states $|\rho^L_{z,a}\rangle$ for $L\in\mathcal{L}$ and $z,a\in\{0,1\}$, as discussed in Section 8.1.1. Each of these states has support on only one component of G_1. In addition, G_1 has a two-particle frustration-free state for each two-qubit gadget $J\in[M]$ and bits z,a,x,b, namely $\mathrm{Sym}(|T^J_{z,a,x,b}\rangle)$. Furthermore, no component of G_1 has any three- (or more) particle frustration-free states. Using these facts and applying Lemma 2.4, we see that $\mathcal{B}_n$ spans the nullspace of $H(G_1,n)$.

Lemma 2.4 also expresses each eigenvalue of $H(G_1,n)$ as a sum of eigenvalues for its components. We use this fact to obtain the desired lower bound on the smallest nonzero eigenvalue. Our analysis proceeds on a case-by-case basis, depending on the occupation numbers for each component of G_1 (the values $N_1,\ldots,N_k$ in Lemma 2.4).

First consider any set of occupation numbers where some two-qubit gate gadget $J\in[M]$ contains 3 or more particles. By Lemma 2.3 and Lemma 2.4, any such eigenvalue is at least $\lambda_3^1(G_{U_J})$, which is a positive constant by Lemma 6.3. Next consider a case where some boundary gadget contains more than one particle. The corresponding eigenvalues are similarly lower bounded by $\lambda_2^1(G_{\mathrm{bnd}})$, which is also a positive constant by Lemma 6.4. Finally, consider a set of occupation numbers where each two-qubit gadget contains at most two particles and each boundary gadget contains at most one particle. The smallest eigenvalue with such a set of occupation numbers is zero. The smallest nonzero eigenvalue is either

$$\gamma(H(G_{U_J},1)),\ \gamma(H(G_{U_J},2))\text{ for some }J\in[M],\text{ or }\gamma(H(G_{\mathrm{bnd}},1))\,.$$

However, these quantities are at least some positive constant since $H(G_{U_J},1)$, $H(G_{U_J},2)$, and $H(G_{\mathrm{bnd}},1)$ are nonzero constant-sized positive semidefinite matrices.

Now combining the lower bounds discussed above and using the fact that, for each $J\in[M]$, the two-qubit gate U_J is chosen from a fixed finite gate set (given in (7.3)), we see that $\gamma(H(G_1,n))$ is lower bounded by the positive constant

$$\min\{\lambda_3^1(G_U),\lambda_2^1(G_{\mathrm{bnd}}),\gamma(H(G_U,1)),\gamma(H(G_U,2)),\gamma(H(G_{\mathrm{bnd}},1)):U\text{ is from the gate set (7.3)}\}\,. \tag{8.15}$$

The condition $\mathcal{K}_0\leq 1$ can be ensured by setting $\mathcal{K}_0$ to be the minimum of 1 and (8.15). □

Note that the constant $\mathcal{K}_0$ can in principle be computed using (8.15): each quantity on the right-hand side can be evaluated by diagonalizing a specific finite-dimensional matrix.

8.3 Legal configurations

In this section we define a subset of the n-particle configurations that we call legal configurations, and we prove that the subset of the basis vectors in $\mathcal{B}_n$ that have legal configurations spans the nullspace of $H(G_1, G_X^{\text{occ}}, n)$.

We begin by specifying the set of legal configurations. Every legal configuration

$$(J_1, \ldots, J_Y, L_1, \ldots, L_{n-2Y})$$

has $Y \in \{0,1\}$. The legal configurations with $Y = 0$ are

$$((1, j, d_1), F(2, j, d_2), F(3, j, d_3), \ldots, F(n, j, d_n)) \tag{8.16}$$

where $j \in [M]$ and where $\vec{d} = (d_1, \ldots, d_n)$ satisfies $d_i \in \{0,1\}$ and $d_1 = d_{s(j)}$. (Recall that the function F, defined in equations (7.9) and (7.10), describes horizontal movement of particles.) The legal configurations with $Y = 1$ are

$$(j, F(2, j, d_2), \ldots, F(s(j)-1, j, d_{s(j)-1}), F(s(j)+1, j, d_{s(j)+1}), \ldots, F(n, j, d_n)) \tag{8.17}$$

where $j \in \{1, \ldots, M\}$ and $d_i \in \{0,1\}$ for $i \in [n] \setminus \{1, s(j)\}$. Although the values d_1 and $d_{s(j)}$ are not used in equation (8.17), we choose to set them to

$$d_1 = d_{s(j)} = 2$$

for any legal configuration with $Y = 1$. In this way we identify the set of legal configurations with the set of pairs $j, \vec{d}$ with $j \in [M]$ and

$$\vec{d} = (d_1, d_2, d_3, \ldots, d_n)$$

satisfying

$$d_1 = d_{s(j)} \in \{0,1,2\} \quad \text{and} \quad d_i \in \{0,1\} \text{ for } i \notin \{1, s(j)\}.$$

The legal configuration is given by equation (8.16) if $d_1 = d_{s(j)} \in \{0,1\}$ and equation (8.17) if $d_1 = d_{s(j)} = 2$.

The examples in Figures 8.1(A), (B), and (C) show legal configurations whereas the examples in Figures 8.1(D), (E), and (F) are illegal. The legal examples correspond to $j = 1$, $\vec{d} = (1,1,1)$; $j = 2$, $\vec{d} = (2,2,0)$; and $j = 1$, $\vec{d} = (1,0,1)$, respectively. We now explain why the other examples are illegal. Looking at (8.17), we see that the configuration $(3, (2,0,1))$ depicted in Figure 8.1(D) is illegal since $F(2,3,0) = (2,2,1) \neq (2,0,1)$ and $F(2,3,1) = (2,4,0) \neq (2,0,1)$. The configuration in Figure 8.1(E) is illegal since there are two particles in the same row. Looking at equation (8.16), we see that the configuration $((1,1,1),(2,2,0),(3,5,0))$ in Figure 8.1(F) is illegal since $(3,5,0) \notin \{F(3,1,0), F(3,1,1)\} = \{(3,0,1),(3,3,0)\}$.

We now identify the subset of basis vectors $\mathcal{B}_{\text{legal}} \subset \mathcal{B}_n$ that have legal configurations. We write each such basis vector as

$$|j, \vec{d}, \vec{z}, \vec{a}\rangle = \begin{cases} \text{Sym}\left(|\rho^{(1,j,d_1)}_{z_1,a_1}\rangle \bigotimes_{i=2}^{n} |\rho^{F(i,j,d_i)}_{z_i,a_i}\rangle \right) & d_1 = d_{s(j)} \in \{0,1\} \\ \text{Sym}\left(|T^{j}_{z_1,a_1,z_{s(j)},a_{s(j)}}\rangle \bigotimes_{\substack{i=2 \\ i \neq s(j)}}^{n} |\rho^{F(i,j,d_i)}_{z_i,a_i}\rangle \right) & d_1 = d_{s(j)} = 2 \end{cases} \tag{8.18}$$

where $j,\vec{d}$ specifies the legal configuration and $\vec{z},\vec{a} \in \{0,1\}^n$. (Note that the bits in $\vec{z}$ and $\vec{a}$ are ordered slightly differently than in equation (8.13); here the labeling reflects the indices of the encoded qubits.)

Definition 8.6. Let

$$\mathcal{B}_{\text{legal}} = \left\{ |j,\vec{d},\vec{z},\vec{a}\rangle : \; j \in [M],\; d_1 = d_{s(j)} \in \{0,1,2\} \text{ and } \; d_i \in \{0,1\} \text{ for } i \notin \{1,s(j)\},\; \vec{z},\vec{a} \in \{0,1\}^n \right\}$$

and $\mathcal{B}_{\text{illegal}} = \mathcal{B}_n \setminus \mathcal{B}_{\text{illegal}}$.

The basis $\mathcal{B}_n = \mathcal{B}_{\text{legal}} \cup \mathcal{B}_{\text{illegal}}$ is convenient when considering the restriction to the subspace $\mathcal{I}(G_1, G_X^{\text{occ}}, n)$. Letting Π_0 be the projector onto $\mathcal{I}(G_1, G_X^{\text{occ}}, n)$, the following lemma (proven in Section A.2) shows that the restriction

$$\Pi_0\big|_{\text{span}(\mathcal{B}_n)} \tag{8.19}$$

is diagonal in the basis $\mathcal{B}_n$. The lemma also bounds the diagonal entries.

Lemma 8.7. *Let Π_0 be the projector onto $\mathcal{I}(G_1, G_X^{\text{occ}}, n)$. For any $|j,\vec{d},\vec{z},\vec{a}\rangle \in \mathcal{B}_{\text{legal}}$, we have*

$$\Pi_0 |j,\vec{d},\vec{z},\vec{a}\rangle = |j,\vec{d},\vec{z},\vec{a}\rangle. \tag{8.20}$$

Furthermore, for any two distinct basis vectors $|\phi\rangle, |\psi\rangle \in \mathcal{B}_{\text{illegal}}$, we have

$$\langle\phi|\Pi_0|\phi\rangle \leq \frac{255}{256} \tag{8.21}$$

$$\langle\phi|\Pi_0|\psi\rangle = 0\,. \tag{8.22}$$

We use this lemma to characterize the nullspace of $H(G_1, G_X^{\text{occ}}, n)$ and bound its smallest nonzero eigenvalue.

Lemma 8.8. *The nullspace S_1 of $H(G_1, G_X^{\text{occ}}, n)$ is spanned by the orthonormal basis $\mathcal{B}_{\text{legal}}$. Its smallest nonzero eigenvalue is*

$$\gamma(H(G_1, G_X^{\text{occ}}, n)) \geq \frac{\mathcal{K}_0}{256} \tag{8.23}$$

where $\mathcal{K}_0 \in (0,1]$ is the absolute constant from Lemma 8.5.

Proof. Recall from Section 7.3 that

$$H(G_1, G_X^{\text{occ}}, n) = H(G_1, n)|_{\mathcal{I}(G_1, G_X^{\text{occ}}, n)}\,.$$

Its nullspace is the space of states $|\kappa\rangle$ satisfying

$$\Pi_0|\kappa\rangle = |\kappa\rangle \quad \text{and} \quad H(G_1,n)|\kappa\rangle = 0$$

(recall that Π_0 is the projector onto $\mathcal{I}(G_1, G_X^{\text{occ}}, n)$, the states satisfying the occupancy constraints). Since $\mathcal{B}_n$ is a basis for the nullspace of $H(G_1,n)$, to solve for the nullspace of $H(G_1, G_X^{\text{occ}}, n)$ we consider the restriction (8.19) and solve for the eigenspace with eigenvalue 1. This calculation is simple because (8.19) is diagonal in the basis $\mathcal{B}_n$, according to Lemma 8.7. We see immediately from the lemma that $\mathcal{B}_{\text{legal}}$

spans the nullspace of $H(G_1, G_X^{\text{occ}}, n)$; we now show that Lemma 8.7 also implies the lower bound (8.23). Note that

$$\gamma(H(G_1, G_X^{\text{occ}}, n)) = \gamma(\Pi_0 H(G_1, n)\Pi_0)\,.$$

Let Π_{legal} and Π_{illegal} project onto the spaces spanned by $\mathcal{B}_{\text{legal}}$ and $\mathcal{B}_{\text{illegal}}$ respectively, so $\Pi_{\text{legal}} + \Pi_{\text{illegal}}$ projects onto the nullspace of $H(G_1, n)$. The operator inequality

$$H(G_1, n) \geq \gamma(H(G_1, n)) \cdot \left(1 - \Pi_{\text{legal}} - \Pi_{\text{illegal}}\right)$$

implies

$$\Pi_0 H(G_1, n)\Pi_0 \geq \gamma(H(G_1, n)) \cdot \Pi_0(1 - \Pi_{\text{legal}} - \Pi_{\text{illegal}})\Pi_0\,.$$

Since the operators on both sides of this inequality are positive semidefinite and have the same nullspace, their smallest nonzero eigenvalues are bounded as

$$\gamma(\Pi_0 H(G_1, n)\Pi_0) \geq \gamma(H(G_1, n)) \cdot \gamma(\Pi_0(1 - \Pi_{\text{legal}} - \Pi_{\text{illegal}})\Pi_0)\,.$$

Hence

$$\gamma(H(G_1, G_X^{\text{occ}}, n)) = \gamma(\Pi_0 H(G_1, n)\Pi_0) \geq \mathcal{K}_0 \cdot \gamma(\Pi_0(1 - \Pi_{\text{legal}} - \Pi_{\text{illegal}})\Pi_0) \tag{8.24}$$

where we used Lemma 8.5. From equations (8.21) and (8.22) we see that

$$\Pi_0|g\rangle = |g\rangle \quad \text{and} \quad \Pi_{\text{illegal}}|f\rangle = |f\rangle \qquad \Longrightarrow \qquad \langle f|g\rangle\langle g|f\rangle \leq \frac{255}{256}\,. \tag{8.25}$$

The nullspace of

$$\Pi_0 \left(1 - \Pi_{\text{legal}} - \Pi_{\text{illegal}}\right) \Pi_0 \tag{8.26}$$

is spanned by

$$\mathcal{B}_{\text{legal}} \cup \{|\tau\rangle : \Pi_0|\tau\rangle = 0\}\,.$$

To see this, note that (8.26) commutes with Π_0, and the space of $+1$ eigenvectors of Π_0 that are annihilated by (8.26) is spanned by $\mathcal{B}_{\text{legal}}$ (by Lemma 8.7). Any eigenvector $|g_1\rangle$ corresponding to the smallest nonzero eigenvalue of this operator therefore satisfies $\Pi_0|g_1\rangle = |g_1\rangle$ and $\Pi_{\text{legal}}|g_1\rangle = 0$, so

$$\gamma(\Pi_0(1 - \Pi_{\text{legal}} - \Pi_{\text{illegal}})\Pi_0) = 1 - \langle g_1|\Pi_{\text{illegal}}|g_1\rangle \geq \frac{1}{256}$$

using equation (8.25). Plugging this into equation (8.24) gives the lower bound (8.23). □

8.4 Matrix elements between states with legal configurations

We now consider

$$H_1|_{S_1}, H_2|_{S_1}, H_{\text{in},i}|_{S_1}, H_{\text{out}}|_{S_1} \tag{8.27}$$

where these operators are defined in Section 8.1.2 and

$$S_1 = \text{span}(\mathcal{B}_{\text{legal}})$$

is the nullspace of $H(G_1, G_X^{\mathrm{occ}}, n)$.

We specify the operators (8.27) by their matrix elements in an orthonormal basis for S_1. Although the basis $\mathcal{B}_{\mathrm{legal}}$ was convenient in Section 8.3, here we use a different basis in which the matrix elements of H_1 and H_2 are simpler. We define

$$|j,\vec{d},\mathrm{In}(\vec{z}),\vec{a}\rangle = \sum_{\vec{x}\in\{0,1\}^n} \left(\langle\vec{x}|\bar{U}_{j,d_1}(a_1)|\vec{z}\rangle\right)|j,\vec{d},\vec{x},\vec{a}\rangle \tag{8.28}$$

where

$$\bar{U}_{j,d_1}(a_1) = \begin{cases} U_{j-1}(a_1)U_{j-2}(a_1)\dots U_1(a_1) & \text{if } d_1 \in \{0,2\} \\ U_j(a_1)U_{j-1}(a_1)\dots U_1(a_1) & \text{if } d_1 = 1. \end{cases} \tag{8.29}$$

In each of these states the quantum data (represented by the $\vec{x}$ register on the right-hand side) encodes the computation in which the unitary $\bar{U}_{j,d_1}(a_1)$ is applied to the initial n-qubit state $|\vec{z}\rangle$ (the notation $\mathrm{In}(\vec{z})$ indicates that $\vec{z}$ is the input). The vector $\vec{a}$ is only relevant insofar as its first bit a_1 determines whether or not each two-qubit unitary is complex conjugated; the other bits of $\vec{a}$ go along for the ride. Letting $\vec{z},\vec{a} \in \{0,1\}^n$, $j \in [M]$, and

$$\vec{d} = (d_1,\dots,d_n) \quad \text{with} \quad d_1 = d_{s(j)} \in \{0,1,2\} \quad \text{and} \quad d_i \in \{0,1\},\ i \notin \{1,s(j)\},$$

we see that the states (8.28) form an orthonormal basis for S_1. In Section A.3 we compute the matrix elements of the operators (8.27) in this basis, which are reproduced below.

Roughly speaking, the nonzero off-diagonal matrix elements of the operator H_1 in the basis (8.28) occur between states $|j,\vec{d},\mathrm{In}(\vec{z}),\vec{a}\rangle$ and $|j,\vec{c},\mathrm{In}(\vec{z}),\vec{a}\rangle$ where the legal configurations $j,\vec{d}$ and $j,\vec{c}$ are related by horizontal motion of a particle in one of the rows $i \in \{2,\dots,n\}$.

Matrix elements of H_1

$$\langle k,\vec{c},\mathrm{In}(\vec{x}),\vec{b}|H_1|j,\vec{d},\mathrm{In}(\vec{z}),\vec{a}\rangle = \delta_{k,j}\delta_{\vec{a},\vec{b}}\delta_{\vec{z},\vec{x}}\cdot \begin{cases} \frac{n-1}{64} & \vec{c} = \vec{d} \\ \frac{1}{64}\prod_{\substack{r=1 \\ r\neq i}}^{n} \delta_{d_r,c_r} & d_i \neq c_i \text{ for some } i \in [n]\setminus\{1,s(j)\} \\ \frac{1}{64\sqrt{2}}\prod_{\substack{r=2 \\ r\neq s(j)}}^{n} \delta_{d_r,c_r} & (c_1,d_1) \in \{(2,0),(0,2),(1,2),(2,1)\} \\ 0 & \text{otherwise.} \end{cases} \tag{8.30}$$

From this expression we see that $H_1|_{S_1}$ is block diagonal in the basis (8.28), with a block for each $\vec{z},\vec{a} \in \{0,1\}^n$ and $j \in [M]$. Moreover, the submatrix for each block is the same. In Figure 8.2 we illustrate some of the off-diagonal matrix elements of $H_1|_{S_1}$ for the example from Figure 7.1.

Next, we present the matrix elements of H_2.

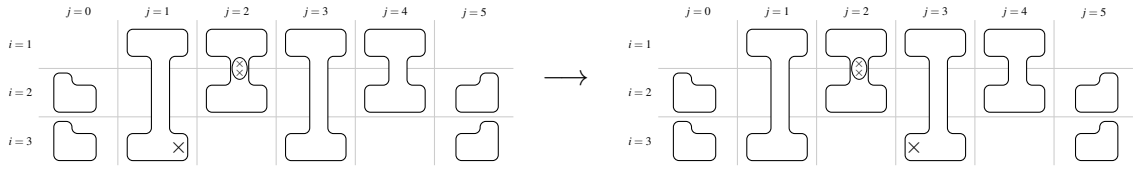

(A) $\langle j,\vec{c},\mathrm{In}(\vec{z}),\vec{a}|H_1|j,\vec{d},\mathrm{In}(\vec{z}),\vec{a}\rangle = \frac{1}{64}$; here $j=2$ and $\vec{d}=(2,2,0) \to \vec{c}=(2,2,1)$.

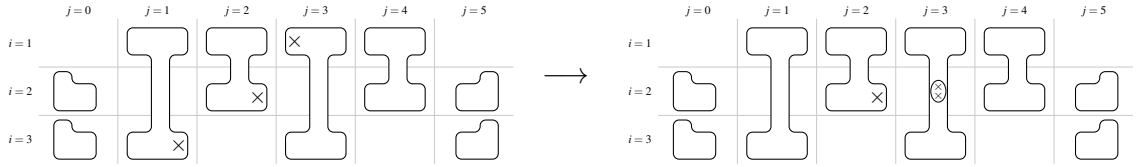

(B) $\langle j,\vec{c},\mathrm{In}(\vec{z}),\vec{a}|H_1|j,\vec{d},\mathrm{In}(\vec{z}),\vec{a}\rangle = \frac{1}{64\sqrt{2}}$; here $j=3$ and $\vec{d}=(0,0,0) \to \vec{c}=(2,0,2)$.

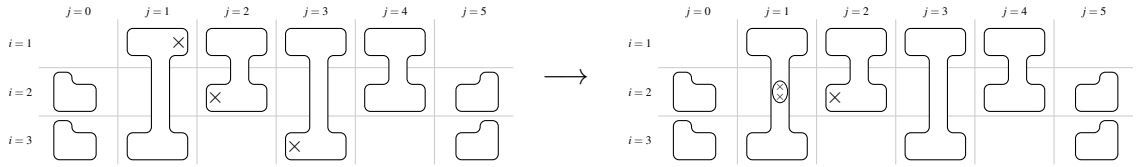

(C) $\langle j,\vec{c},\mathrm{In}(\vec{z}),\vec{a}|H_1|j,\vec{d},\mathrm{In}(\vec{z}),\vec{a}\rangle = \frac{1}{64\sqrt{2}}$; here $j=1$ and $\vec{d}=(1,1,1) \to \vec{c}=(2,1,2)$.

Figure 8.2: Examples of matrix elements of H_1 in the basis (8.28) of S_1. The relevant matrix elements (as indicated above) are computed using (A) the second case and (B), (C) the third case in equation (8.30).

Matrix elements of H_2

$$\langle k,\vec{c},\mathrm{In}(\vec{x}),\vec{b}|H_2|j,\vec{d},\mathrm{In}(\vec{z}),\vec{a}\rangle = f_{\mathrm{diag}(\vec{d},j)\cdot\delta_{j,k}\delta_{\vec{a},\vec{b}}\delta_{\vec{z},\vec{x}}\delta_{\vec{c},\vec{d}}} + \left(f_{\text{off-diag}}(\vec{c},\vec{d},j)\cdot\delta_{k,j-1} + f_{\text{off-diag}}(\vec{d},\vec{c},k)\cdot\delta_{k-1,j}\right)\delta_{\vec{a},\vec{b}}\delta_{\vec{z},\vec{x}} \tag{8.31}$$

where

$$f_{\mathrm{diag}}(\vec{d},j) = \begin{cases} 0 & d_1 = 0 \text{ and } j = 1, \text{ or } d_1 = 1 \text{ and } j = M \\ \frac{1}{128} & d_1 = 2 \text{ and } j \in \{1,M\} \\ \frac{1}{64} & \text{otherwise} \end{cases} \tag{8.32}$$

and

$$f_{\text{off-diag}}(\vec{c},\vec{d},j) = \left(\prod_{\substack{r=2 \\ r\notin\{s(j-1),s(j)\}}}^{n}\delta_{d_r,c_r}\right)\cdot\begin{cases} \frac{1}{64\sqrt{2}} & (c_1,c_{s(j)},d_1,d_{s(j-1)}) \in \{(2,0,0,0),(1,1,2,1)\} \\ \frac{1}{64} & (c_1,c_{s(j)},d_1,d_{s(j-1)}) = (1,0,0,1) \\ \frac{1}{128} & (c_1,c_{s(j)},d_1,d_{s(j-1)}) = (2,1,2,0) \\ 0 & \text{otherwise.} \end{cases} \tag{8.33}$$

This shows that $H_2|_{S_1}$ is block diagonal in the basis (8.28), with a block for each $\vec{z},\vec{a} \in \{0,1\}^n$. Also note that (in contrast with H_1) H_2 connects states with different values of j. In Figure 8.3 we illustrate some of the off-diagonal matrix elements of $H_2|_{S_1}$, for the example from Figure 7.1.

Finally, we present the matrix elements of $H_{\mathrm{in},i}$ (for $i \in \{n_{\mathrm{in}}+1,\ldots,n\}$) and H_{out}:

Matrix elements of $H_{\mathrm{in},i}$ For each ancilla qubit $i \in \{n_{\mathrm{in}}+1,\ldots,n\}$, define

$$j_{\mathrm{min},i} = \min\{j \in [M] \colon s(j) = i\}$$

to be the index of the first gate in the circuit that involves this qubit (recall from Section 7 that we consider circuits where each ancilla qubit is involved in at least one gate). The operator $H_{\mathrm{in},i}$ is diagonal in the basis (8.28), with entries

$$\langle j,\vec{d},\mathrm{In}(\vec{z}),\vec{a}|H_{\mathrm{in},i}|j,\vec{d},\mathrm{In}(\vec{z}),\vec{a}\rangle = \begin{cases} \frac{1}{64} & j \le j_{\mathrm{min},i},\ z_i = 1, \text{ and } d_i = 0 \\ 0 & \text{otherwise.} \end{cases} \tag{8.34}$$

Matrix elements of H_{out} Let $j_{\max} = \max\{j \in [M] \colon s(j) = 2\}$ be the index of the last gate $U_{j_{\max}}$ in the circuit that acts between qubits 1 and 2 (the output qubit). Then

$$\langle k,\vec{c},\mathrm{In}(\vec{x}),\vec{b}|H_{\mathrm{out}}|j,\vec{d},\mathrm{In}(\vec{z}),\vec{a}\rangle = \delta_{j,k}\delta_{\vec{c},\vec{d}}\delta_{\vec{a},\vec{b}}\begin{cases} \langle\vec{x}|U^{\dagger}_{\mathcal{C}_X}(a_1)|0\rangle\langle 0|_2 U_{\mathcal{C}_X}(a_1)|\vec{z}\rangle\frac{1}{64} & j \ge j_{\max} \text{ and } d_2 = 1 \\ 0 & \text{otherwise.} \end{cases} \tag{8.35}$$

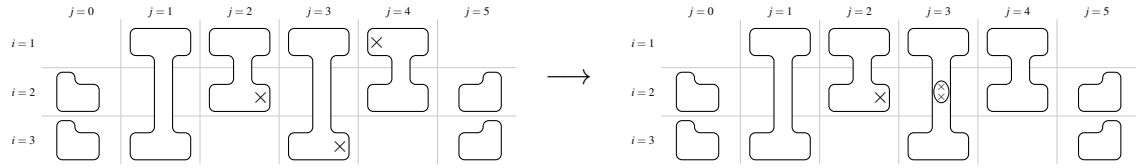

(A) $\langle j-1,\vec{c},\mathrm{In}(\vec{z}),\vec{a}|H_2|j,\vec{d},\mathrm{In}(\vec{z}),\vec{a}\rangle = \frac{1}{64\sqrt{2}}$; here $j=4$ and $\vec{d}=(0,0,0)\to\vec{c}=(2,0,2)$

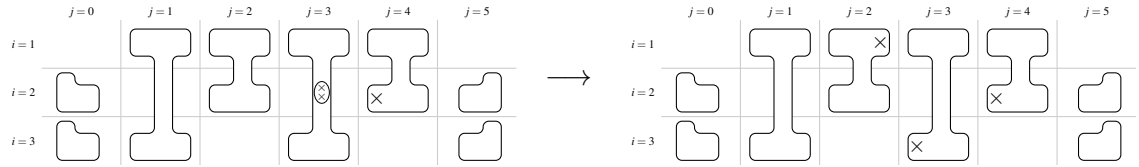

(B) $\langle j-1,\vec{c},\mathrm{In}(\vec{z}),\vec{a}|H_2|j,\vec{d},\mathrm{In}(\vec{z}),\vec{a}\rangle = \frac{1}{64\sqrt{2}}$; here $j=3$ and $\vec{d}=(2,1,2)\to\vec{c}=(1,1,1)$

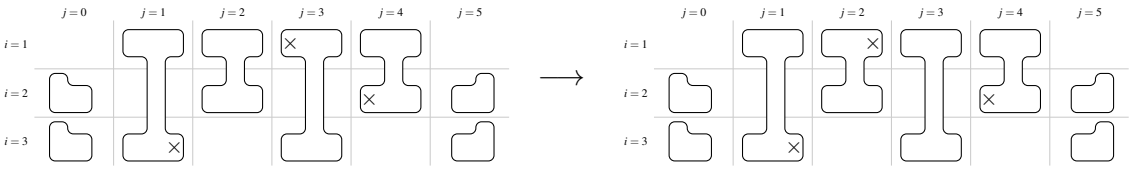

(C) $\langle j-1,\vec{c},\mathrm{In}(\vec{z}),\vec{a}|H_2|j,\vec{d},\mathrm{In}(\vec{z}),\vec{a}\rangle = \frac{1}{64}$; here $j=3$ and $\vec{d}=(0,1,0)\to\vec{c}=(1,1,0)$

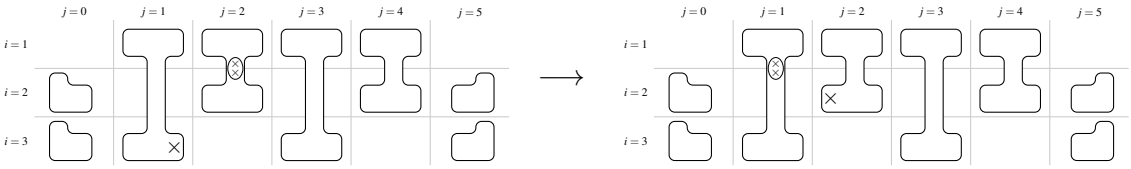

(D) $\langle j-1,\vec{c},\mathrm{In}(\vec{z}),\vec{a}|H_2|j,\vec{d},\mathrm{In}(\vec{z}),\vec{a}\rangle = \frac{1}{128}$; here $j=2$ and $\vec{d}=(2,2,0)\to\vec{c}=(2,1,2)$

Figure 8.3: Examples of matrix elements of H_2 in the basis (8.28) of S_1. The relevant matrix elements (as indicated above) are computed using the (A), (B) first, (C) second, and (D) third cases in equation (8.33).

8.5 From $H(G_2, G_X^{\text{occ}}, n)$ to $H(G_4, G_X^{\text{occ}}, n)$

Define the $(n-2)$-dimensional hypercubes

$$\mathcal{D}_k^j = \left\{(d_1, \ldots, d_n) \colon d_1 = d_{s(j)} = k,\, d_i \in \{0,1\} \text{ for } i \in [n] \setminus \{1, s(j)\}\right\}$$

for $j \in \{1, \ldots, M\}$ and $k \in \{0,1,2\}$, and the superpositions

$$|\text{Cube}_k(j, \vec{z}, \vec{a})\rangle = \frac{1}{\sqrt{2^{n-2}}} \sum_{\vec{d} \in \mathcal{D}_k^j} (-1)^{\sum_{i=1}^n d_i} |j, \vec{d}, \text{In}(\vec{z}), \vec{a}\rangle$$

for $k \in \{0,1,2\}$, $j \in [M]$, and $\vec{z}, \vec{a} \in \{0,1\}^n$. For each $j \in [M]$ and $\vec{z}, \vec{a} \in \{0,1\}^n$, let

$$|C(j, \vec{z}, \vec{a})\rangle = \frac{1}{2}|\text{Cube}_0(j, \vec{z}, \vec{a})\rangle + \frac{1}{2}|\text{Cube}_1(j, \vec{z}, \vec{a})\rangle - \frac{1}{\sqrt{2}}|\text{Cube}_2(j, \vec{z}, \vec{a})\rangle. \tag{8.36}$$

We prove

Lemma 8.9. *The Hamiltonian $H(G_2, G_X^{\text{occ}}, n)$ has nullspace S_2 spanned by the states*

$$|C(j, \vec{z}, \vec{a})\rangle$$

for $j \in [M]$ and $\vec{z}, \vec{a} \in \{0,1\}^n$. Its smallest nonzero eigenvalue is

$$\gamma(H(G_2, G_X^{\text{occ}}, n)) \geq \frac{\mathcal{K}_0}{35000n}$$

where $\mathcal{K}_0 \in (0,1]$ is the absolute constant from Lemma 8.5.

Proof. Recall from the previous section that $H_1|_{S_1}$ is block diagonal in the basis (8.28), with a block for each $j \in [M]$ and $\vec{z}, \vec{a} \in \{0,1\}^n$. That is to say, $\langle k, \vec{c}, \text{In}(\vec{x}), \vec{b}|H_1|j, \vec{d}, \text{In}(\vec{z}), \vec{a}\rangle$ is zero unless $\vec{a} = \vec{b}$, $k = j$, and $\vec{z} = \vec{x}$. Equation (8.30) gives the nonzero matrix elements within a given block, which we use to compute the frustration-free ground states of $H_1|_{S_1}$.

Looking at equation (8.30), we see that the matrix for each block can be written as a sum of n commuting matrices: $\frac{(n-1)}{/}64$ times the identity matrix (case 1 in equation (8.30)), $n-2$ terms that each flip a single bit $i \notin \{1, s(j)\}$ of $\vec{d}$ (case 2), and a term that changes the value of the "special" components $d_1 = d_{s(j)} \in \{0,1,2\}$ (case 3). Thus

$$\langle j, \vec{c}, \text{In}(\vec{z}), \vec{a}|H_1|j, \vec{d}, \text{In}(\vec{z}), \vec{a}\rangle = \left\langle j, \vec{c}, \text{In}(\vec{z}), \vec{a} \,\middle|\, \frac{1}{64}\left[(n-1) + \sum_{i \in [n]\setminus\{1, s(j)\}} H_{\text{flip},i} + H_{\text{special},j}\right] \,\middle|\, j, \vec{d}, \text{In}(\vec{z}), \vec{a}\right\rangle$$

where

$$\langle j, \vec{c}, \text{In}(\vec{z}), \vec{a}|H_{\text{flip},i}|j, \vec{d}, \text{In}(\vec{z}), \vec{a}\rangle = \delta_{c_i, d_i \oplus 1} \prod_{r \in [n]\setminus\{i\}} \delta_{c_r, d_r}$$

and

$$\langle j,\vec{c},\mathrm{In}(\vec{z}),\vec{a}|H_{\mathrm{special},j}|j,\vec{d},\mathrm{In}(\vec{z}),\vec{a}\rangle = \begin{cases} \frac{1}{\sqrt{2}} & (c_1,d_1)\in\{(2,0),(0,2),(1,2),(2,1)\} \\ & \text{and } d_r = c_r \text{ for } r\in[n]\setminus\{1,s(j)\} \\ 0 & \text{otherwise.} \end{cases}$$

Note that these n matrices are mutually commuting, each eigenvalue of $H_{\mathrm{flip},i}$ is ± 1, and each eigenvalue of $H_{\mathrm{special},j}$ is equal to one of the eigenvalues of the matrix

$$\frac{1}{\sqrt{2}}\begin{pmatrix} 0 & 0 & 1 \\ 0 & 0 & 1 \\ 1 & 1 & 0 \end{pmatrix},$$

which are $\{-1,0,1\}$. Thus we see that the eigenvalues of $H_1|_{S_1}$ within a block for some $j\in[M]$ and $\vec{z},\vec{a}\in\{0,1\}^n$ are

$$\frac{1}{64}\left(n-1+\sum_{i\notin\{1,s(j)\}} y_i + w\right) \tag{8.37}$$

where $y_i\in\pm 1$ for each $i\in[n]\setminus\{1,s(j)\}$ and $w\in\{-1,0,1\}$. In particular, the smallest eigenvalue within the block is zero (corresponding to $y_i = w = -1$). The corresponding eigenspace is spanned by the simultaneous -1 eigenvectors of each $H_{\mathrm{flip},i}$ for $i\in[n]\setminus\{1,s(j)\}$ and $H_{\mathrm{special},j}$. The space of simultaneous -1 eigenvectors of $H_{\mathrm{flip},i}$ for $i\in[n]\setminus\{1,s(j)\}$ within the block is spanned by $\{|\mathrm{Cube}_0(j,\vec{z},\vec{a})\rangle, |\mathrm{Cube}_1(j,\vec{z},\vec{a})\rangle, |\mathrm{Cube}_2(j,\vec{z},\vec{a})\rangle\}$. The state $|C(j,\vec{z},\vec{a})\rangle$ is the unique superposition of these states that is a -1 eigenvector of $H_{\mathrm{special},j}$. Hence, for each block we obtain a unique state $|C(j,\vec{z},\vec{a})\rangle$ in the space S_2. Ranging over all blocks $j\in[M]$ and $\vec{z},\vec{a}\in\{0,1\}^n$, we get the basis described in the lemma.

The smallest nonzero eigenvalue within each block is $1/64$ (corresponding to $y_i = -1$ and $w = 0$ in equation (8.37)), so

$$\gamma(H_1|_{S_1}) = \frac{1}{64}. \tag{8.38}$$

To get the stated lower bound, we use Lemma 8.1 with $H(G_2,G_X^{\mathrm{occ}},n) = H_A + H_B$ where

$$H_A = H(G_1,G_X^{\mathrm{occ}},n), \qquad H_B = H_1|_{\mathcal{I}(G_2,G_X^{\mathrm{occ}},n)}$$

(as in equation (8.5)), along with the bounds

$$\gamma(H_A)\geq\frac{\mathcal{K}_0}{256}, \qquad \gamma(H_B|_{S_1}) = \gamma(H_1|_{S_1}) = \frac{1}{64}, \qquad \|H_B\|\leq\|H_1\|\leq n\|h_1\| = 2n,$$

from Lemma 8.8, equations (8.9) and (8.38), and the fact that $\|h_1\| = 2$ from (5.8). This gives

$$\gamma(H(G_2,G_X^{\mathrm{occ}},n))\geq\frac{\mathcal{K}_0}{64\mathcal{K}_0+256+2n\cdot 64\cdot 256}\geq\frac{\mathcal{K}_0}{35000n}$$

where we used the facts that $\mathcal{K}_0\leq 1$ and $n\geq 1$. □

For each $\vec{z},\vec{a} \in \{0,1\}^n$ define the uniform superposition

$$|\mathcal{H}(\vec{z},\vec{a})\rangle = \frac{1}{\sqrt{M}} \sum_{j=1}^{M} |C(j,\vec{z},\vec{a})\rangle$$

that encodes (somewhat elaborately) the history of the computation that consists of applying either $U_{\mathcal{C}_X}$ or $U^*_{\mathcal{C}_X}$ to the state $|\vec{z}\rangle$. The first bit of $\vec{a}$ determines whether the circuit $\mathcal{C}_X$ or its complex conjugate is applied.

Lemma 8.10. *The Hamiltonian $H(G_3, G_X^{\mathrm{occ}}, n)$ has nullspace S_3 spanned by the states*

$$|\mathcal{H}(\vec{z},\vec{a})\rangle$$

for $\vec{z},\vec{a} \in \{0,1\}^n$. Its smallest nonzero eigenvalue is

$$\gamma(H(G_3, G_X^{\mathrm{occ}}, n)) \geq \frac{\mathcal{K}_0}{10^7 n^2 M^2}$$

where $\mathcal{K}_0 \in (0,1]$ is the absolute constant from Lemma 8.5.

Proof. Recall that

$$H(G_3, G_X^{\mathrm{occ}}, n) = H(G_2, G_X^{\mathrm{occ}}, n) + H_2|_{\mathcal{I}(G_3, G_X^{\mathrm{occ}}, n)}$$

with both terms on the right-hand side positive semidefinite. To solve for the nullspace of $H(G_3, G_X^{\mathrm{occ}}, n)$, it suffices to restrict our attention to the space

$$S_2 = \mathrm{span}\{|C(j,\vec{z},\vec{a})\rangle : \ j \in [M],\ \vec{z},\vec{a} \in \{0,1\}^n\} \tag{8.39}$$

of states in the nullspace of $H(G_2, G_X^{\mathrm{occ}}, n)$. We begin by computing the matrix elements of H_2 in the basis for S_2 given above. We use equations (8.31) and (8.36) to compute the diagonal matrix elements:

$$\begin{aligned}
\langle C(j,\vec{z},\vec{a})|H_2|C(j,\vec{z},\vec{a})\rangle =& \frac{1}{4}\langle \mathrm{Cube}_0(j,\vec{z},\vec{a})|H_2|\mathrm{Cube}_0(j,\vec{z},\vec{a})\rangle + \frac{1}{4}\langle \mathrm{Cube}_1(j,\vec{z},\vec{a})\rangle|H_2|\mathrm{Cube}_1(j,\vec{z},\vec{a})\rangle \\
&+ \frac{1}{2}\langle \mathrm{Cube}_2(j,\vec{z},\vec{a})|H_2|\mathrm{Cube}_2(j,\vec{z},\vec{a})\rangle \qquad (8.40)\\
=& \begin{cases} 0+\frac{1}{256}+\frac{1}{256} & j=1 \\ \frac{1}{256}+\frac{1}{256}+\frac{1}{128} & j\in\{2,\ldots,M-1\} \\ \frac{1}{256}+0+\frac{1}{256} & j=M \end{cases} \qquad (8.41)\\
=& \begin{cases} \frac{1}{128} & j\in\{1,M\} \\ \frac{1}{64} & j\in\{2,\ldots,M-1\}. \end{cases} \qquad (8.42)
\end{aligned}$$

In the second line we used equation (8.32). Looking at equation (8.31), we see that the only nonzero off-diagonal matrix elements of H_2 in this basis are of the form

$$\langle C(j-1,\vec{z},\vec{a})|H_2|C(j,\vec{z},\vec{a})\rangle \quad \text{or} \quad \langle C(j,\vec{z},\vec{a})|H_2|C(j-1,\vec{z},\vec{a})\rangle = \langle C(j-1,\vec{z},\vec{a})|H_2|C(j,\vec{z},\vec{a})\rangle^*$$

for $j \in \{2,\ldots,M\}$, $\vec{z},\vec{a} \in \{0,1\}^n$. To compute these matrix elements we first use equation (8.33) to evaluate

$$\langle \mathrm{Cube}_w(j-1,\vec{z},\vec{a})|H_2|\mathrm{Cube}_v(j,\vec{z},\vec{a})\rangle$$

for $v,w \in \{0,1,2\}$ and $j \in \{2,\ldots,M\}$. For example, using the second case of equation (8.33), we get

$$\begin{aligned}
&\langle \mathrm{Cube}_1(j-1,\vec{z},\vec{a})|H_2|\mathrm{Cube}_0(j,\vec{z},\vec{a})\rangle \\
&\qquad = \frac{1}{2^{n-2}} \sum_{\vec{d}\in\mathcal{D}_0^j} \sum_{\vec{c}\in\mathcal{D}_1^{j-1}} (-1)^{\sum_{i\in[n]}(c_i+d_i)} \langle j-1,\vec{c},\mathrm{In}(\vec{z}),\vec{a}|H_2|j,\vec{d},\mathrm{In}(\vec{z}),\vec{a}\rangle \\
&\qquad = \frac{1}{2^{n-2}} \sum_{\vec{d}\in\mathcal{D}_0^j : d_{s(j-1)}=1} (-1)\cdot\frac{1}{64} = -\frac{1}{128}\,.
\end{aligned}$$

To go from the first to the second line we used the fact that, for each $\vec{d}\in\mathcal{D}_0^j$ with $d_{s(j-1)}=1$, there is one $\vec{c}\in\mathcal{D}_1^{j-1}$ for which $\langle j-1,\vec{c},\mathrm{In}(\vec{z}),\vec{a}|H_2|j,\vec{d},\mathrm{In}(\vec{z}),\vec{a}\rangle = 1/64$ (with all other such matrix elements equal to zero). This $\vec{c}$ satisfies $c_1 = c_{s(j-1)} = 1$ and $c_{s(j)} = 0$, with all other bits equal to those of $\vec{d}$, so

$$(-1)^{\sum_{i=1}^n (c_i+d_i)} = (-1)^{c_1+c_{s(j)}+c_{s(j-1)}+d_1+d_{s(j)}+d_{s(j-1)}} = -1$$

for each nonzero term in the sum.

We perform a similar calculation using cases 1, 3, and 4 in equation (8.33) to obtain

$$\langle \mathrm{Cube}_w(j-1,\vec{z},\vec{a})|H_2|\mathrm{Cube}_v(j,\vec{z},\vec{a})\rangle = \begin{cases} -\frac{1}{128} & (w,v)=(1,0) \\ \frac{1}{128\sqrt{2}} & (w,v)\in\{(2,0),(1,2)\} \\ -\frac{1}{256} & (w,v)=(2,2) \\ 0 & \text{otherwise.} \end{cases}$$

Hence

$$\begin{aligned}
&\langle C(j-1,\vec{z},\vec{a})|H_2|C(j,\vec{z},\vec{a})\rangle \\
&\quad = \frac{1}{4}\langle \mathrm{Cube}_1(j-1,\vec{z},\vec{a})|H_2|\mathrm{Cube}_0(j,\vec{z},\vec{a})\rangle - \frac{1}{2\sqrt{2}}\langle \mathrm{Cube}_2(j-1,\vec{z},\vec{a})|H_2|\mathrm{Cube}_0(j,\vec{z},\vec{a})\rangle \\
&\qquad + \frac{1}{2}\langle \mathrm{Cube}_2(j-1,\vec{z},\vec{a})|H_2|\mathrm{Cube}_2(j,\vec{z},\vec{a})\rangle - \frac{1}{2\sqrt{2}}\langle \mathrm{Cube}_1(j-1,\vec{z},\vec{a})|H_2|\mathrm{Cube}_2(j,\vec{z},\vec{a})\rangle \\
&\quad = -\frac{1}{128}\,.
\end{aligned}$$

Combining this with equation (8.42), we see that $H_2|_{S_2}$ is block diagonal in the basis (8.39), with a block

for each pair of n-bit strings $\vec{z},\vec{a} \in \{0,1\}^n$. Each of the 2^{2n} blocks is equal to the $M \times M$ matrix

$$\frac{1}{128}\begin{pmatrix} 1 & -1 & 0 & 0 & \cdots & 0 \\ -1 & 2 & -1 & 0 & \cdots & 0 \\ 0 & -1 & 2 & -1 & \ddots & \vdots \\ 0 & 0 & -1 & \ddots & \ddots & 0 \\ \vdots & \vdots & \ddots & \ddots & 2 & -1 \\ 0 & 0 & \cdots & 0 & -1 & 1 \end{pmatrix}.$$

This matrix is just $1/128$ times the Laplacian of a path of length M, whose spectrum is well known. In particular, it has a unique eigenvector with eigenvalue zero (the all-ones vector) and its eigenvalue gap is $2(1-\cos(\pi/M)) \geq 4/M^2$. Thus for each of the 2^{2n} blocks there is an eigenvector of $H_2|_{S_2}$ with eigenvalue 0, equal to the uniform superposition $|\mathcal{H}(\vec{z},\vec{a})\rangle$ over the M states in the block. Furthermore, the smallest nonzero eigenvalue within each block is at least $1/(32M^2)$. Hence

$$\gamma(H_2|_{S_2}) \geq \frac{1}{32M^2}. \tag{8.43}$$

To get the stated lower bound on $\gamma(H(G_3,G_X^{\mathrm{occ}},n))$, we apply Lemma 8.1 with

$$H_A = H(G_2,G_X^{\mathrm{occ}},n), \qquad H_B = H_2|_{\mathcal{I}(G_3,G_X^{\mathrm{occ}},n)},$$

and

$$\gamma(H_A) \geq \frac{\mathcal{K}_0}{35000n}, \qquad \gamma(H_B|_{S_2}) = \gamma(H_2|_{S_2}) \geq \frac{1}{32M^2}, \qquad \|H_B\| \leq \|H_2\| \leq n\|h_2\| = 2n, \tag{8.44}$$

from Lemma 8.9, equation (8.43), and the fact that $\|h_2\| = 2$ from (5.8). This gives

$$\begin{aligned}\gamma(H(G_3,G_X^{\mathrm{occ}},n)) &\geq \frac{\mathcal{K}_0}{32M^2\mathcal{K}_0 + 35000n + 2n(35000n)(32M^2)} \\ &\geq \frac{\mathcal{K}_0}{M^2n^2(32+35000+70000\cdot 32)} \geq \frac{\mathcal{K}_0}{10^7M^2n^2}.\end{aligned}$$

□

Lemma 8.11. *The nullspace S_4 of $H(G_4,G_X^{\mathrm{occ}},n)$ is spanned by the states*

$$|\mathcal{H}(\vec{z},\vec{a})\rangle \quad \textit{where} \quad \vec{z} = z_1z_2\ldots z_{n_{\mathrm{in}}}\underbrace{00\ldots0}_{n-n_{\mathrm{in}}} \tag{8.45}$$

for $\vec{a} \in \{0,1\}^n$ and $z_1,\ldots,z_{n_{\mathrm{in}}} \in \{0,1\}$. Its smallest nonzero eigenvalue satisfies

$$\gamma(H(G_4,G_X^{\mathrm{occ}},n)) \geq \frac{\mathcal{K}_0}{10^{10}M^3n^3}$$

where $\mathcal{K}_0 \in (0,1]$ is the absolute constant from Lemma 8.5.

Proof. Using equation (8.34), we find

$$\begin{aligned}\langle C(k,\vec{x},\vec{b})|H_{\mathrm{in},i}|C(j,\vec{z},\vec{a})\rangle &= \delta_{k,j}\delta_{\vec{x},\vec{z}}\delta_{\vec{a},\vec{b}}\Big(\frac{1}{4}\langle \mathrm{Cube}_0(j,\vec{z},\vec{a})|H_{\mathrm{in},i}|\mathrm{Cube}_0(j,\vec{z},\vec{a})\rangle \\ &\quad + \frac{1}{4}\langle \mathrm{Cube}_1(j,\vec{z},\vec{a})|H_{\mathrm{in},i}|\mathrm{Cube}_1(j,\vec{z},\vec{a})\rangle \\ &\quad + \frac{1}{2}\langle \mathrm{Cube}_2(j,\vec{z},\vec{a})|H_{\mathrm{in},i}|\mathrm{Cube}_2(j,\vec{z},\vec{a})\rangle\Big) \\ &= \delta_{k,j}\delta_{\vec{x},\vec{z}}\delta_{\vec{a},\vec{b}}\left(\frac{1}{64}\delta_{z_i,1}\right)\begin{cases}\frac{1}{4}\cdot\frac{1}{2}+\frac{1}{4}\cdot\frac{1}{2}+\frac{1}{2}\cdot\frac{1}{2} & j<j_{\min,i}\\ \frac{1}{4}+0+0 & j=j_{\min,i}\\ 0+0+0 & j>j_{\min,i}\end{cases}\end{aligned}$$

for each $i \in \{n_{\mathrm{in}}+1,\ldots,n\}$. Hence

$$\langle \mathcal{H}(\vec{x},\vec{b})|\sum_{i=n_{\mathrm{in}}+1}^{n} H_{\mathrm{in},i}|\mathcal{H}(\vec{z},\vec{a})\rangle = \frac{1}{M}\delta_{\vec{x},\vec{z}}\delta_{\vec{a},\vec{b}}\sum_{i=n_{\mathrm{in}}+1}^{n}\frac{1}{64}\left(\frac{j_{\min,i}-1}{2}+\frac{1}{4}\right)\delta_{z_i,1}\,.$$

Therefore

$$\sum_{i=n_{\mathrm{in}}+1}^{n} H_{\mathrm{in},i}\big|_{S_3}$$

is diagonal in the basis $\{|\mathcal{H}(\vec{z},\vec{a})\rangle : \vec{z},\vec{a}\in\{0,1\}^n\}$. The zero eigenvectors are given by equation (8.45), and the smallest nonzero eigenvalue is

$$\gamma\left(\sum_{i=n_{\mathrm{in}}+1}^{n} H_{\mathrm{in},i}\big|_{S_3}\right) \geq \frac{1}{256M} \tag{8.46}$$

since $j_{\min,i}\geq 1$. To get the stated lower bound we now apply Lemma 8.1 with

$$H_A = H(G_3, G_X^{\mathrm{occ}}, n)\,, \qquad H_B = \sum_{i=n_{\mathrm{in}}+1}^{n} H_{\mathrm{in},i}\big|_{\mathcal{J}(G_4,G_X^{\mathrm{occ}},n)}$$

and

$$\gamma(H_A)\geq\frac{\mathcal{K}_0}{10^7M^2n^2}\,, \qquad \gamma(H_B|_{S_3})\geq\frac{1}{256M}\,, \qquad \|H_B\|\leq n\left\|\sum_{i=n_{\mathrm{in}}+1}^{n} h_{\mathrm{in},i}\right\| = n\,,$$

where we used Lemma 8.10, equation (8.46), and the fact that $\left\|\sum_{i=n_{\mathrm{in}}+1}^{n} h_{\mathrm{in},i}\right\| = 1$ (from equation (5.7)). This gives

$$\begin{aligned}\gamma(H(G_4,G_X^{\mathrm{occ}},n)) &\geq \frac{\mathcal{K}_0}{256M\mathcal{K}_0+10^7n^2M^2+n(256M)(10^7n^2M^2)} \\ &\geq \frac{\mathcal{K}_0}{(M^3n^3)(256+10^7+256\cdot 10^7)} \geq \frac{\mathcal{K}_0}{10^{10}M^3n^3}\,.\end{aligned}$$

□

8.6 Completeness and soundness

We now finish the proof of Theorem 7.1. Using equation (8.35) we get

$$\begin{aligned}\langle C(k,\vec{x},\vec{b})|H_{\text{out}}|C(j,\vec{z},\vec{a})\rangle &= \delta_{k,j}\delta_{\vec{a},\vec{b}}\Big(\frac{1}{4}\langle \text{Cube}_0(j,\vec{x},\vec{a})|H_{\text{out}}|\,\text{Cube}_0(j,\vec{z},\vec{a})\rangle \\ &\quad + \frac{1}{4}\langle \text{Cube}_1(j,\vec{x},\vec{a})|H_{\text{out}}|\,\text{Cube}_1(j,\vec{z},\vec{a})\rangle \\ &\quad + \frac{1}{2}\langle \text{Cube}_2(j,\vec{x},\vec{a})|H_{\text{out}}|\,\text{Cube}_2(j,\vec{z},\vec{a})\rangle\Big) \\ &= \frac{\delta_{k,j}\delta_{\vec{a},\vec{b}}}{64}\langle\vec{x}|U^\dagger_{\mathcal{C}_X}(a_1)\,(|0\rangle\langle 0|_2)\,U_{\mathcal{C}_X}(a_1)|\vec{z}\rangle \begin{cases} \frac{1}{4}\cdot\frac{1}{2}+\frac{1}{4}\cdot\frac{1}{2}+\frac{1}{2}\cdot\frac{1}{2} & j > j_{\max} \\ 0+\frac{1}{4}+0 & j = j_{\max} \\ 0+0+0 & j < j_{\max}\end{cases}\end{aligned}$$

and

$$\langle \mathcal{H}(\vec{x},\vec{b})|H_{\text{out}}|\mathcal{H}(\vec{z},\vec{a})\rangle = \delta_{\vec{a},\vec{b}}\frac{1}{128M}(M-j_{\max}+\tfrac{1}{2})\langle\vec{x}|U^\dagger_{\mathcal{C}}(a_1)\,(|0\rangle\langle 0|_2)\,U_{\mathcal{C}}(a_1)|\vec{z}\rangle. \tag{8.47}$$

For any n_{in}-qubit state $|\phi\rangle$, define

$$|\widehat{\mathcal{H}}(\phi,\vec{a})\rangle = \sum_{\vec{z}\in\{0,1\}^n}\left(\langle\vec{z}|\phi\rangle|0\rangle^{\otimes n-n_{\text{in}}}\right)|\mathcal{H}(\vec{z},\vec{a})\rangle. \tag{8.48}$$

Note (from Lemma 8.11) that $|\widehat{\mathcal{H}}(\phi,\vec{a})\rangle$ is in the nullspace of $H(G_4,G_X^{\text{occ}},n)$.

8.6.1 Completeness

Suppose there exists an n_{in}-qubit state $|\psi_{\text{wit}}\rangle$ such that $\text{AP}(\mathcal{C}_X,|\psi_{\text{wit}}\rangle)\geq 1-(1/2^{|X|})$, i. e.,

$$\langle\psi_{\text{wit}}|\langle 0|^{n-n_{\text{in}}}U^\dagger_{\mathcal{C}_X}|0\rangle\langle 0|_2U_{\mathcal{C}_X}|\psi_{\text{wit}}\rangle|0\rangle^{n-n_{\text{in}}} \leq \frac{1}{2^{|X|}}. \tag{8.49}$$

Then (letting $\vec{0}$ denote the all-zeros vector)

$$\begin{aligned}&\langle\widehat{\mathcal{H}}(\psi_{\text{wit}},\vec{0})|H(G_X,G_X^{\text{occ}},n)|\widehat{\mathcal{H}}(\psi_{\text{wit}},\vec{0})\rangle \\ &\quad= \langle\widehat{\mathcal{H}}(\psi_{\text{wit}},\vec{0})|H(G_4,G_X^{\text{occ}},n)+H_{\text{out}}|\widehat{\mathcal{H}}(\psi_{\text{wit}},\vec{0})\rangle \\ &\quad= \langle\widehat{\mathcal{H}}(\psi_{\text{wit}},\vec{0})|H_{\text{out}}|\widehat{\mathcal{H}}(\psi_{\text{wit}},\vec{0})\rangle \\ &\quad= \frac{1}{128M}(M-j_{\max}+\tfrac{1}{2})\langle\psi_{\text{wit}}|\langle 0|^{n-n_{\text{in}}}U^\dagger_{\mathcal{C}_X}|0\rangle\langle 0|_2U_{\mathcal{C}_X}|\psi_{\text{wit}}\rangle|0\rangle^{n-n_{\text{in}}} \\ &\quad\leq \frac{1}{2^{|X|}}\end{aligned}$$

(using equations (8.47) and (8.48) to go from the second to the third line, and equation (8.49) in the last line). Hence $\lambda_n^1(G_X,G_X^{\text{occ}})\leq 1/2^{|X|}$, establishing equation (7.1).

8.6.2 Soundness

Now suppose $\mathrm{AP}(\mathcal{C}_X, |\phi\rangle) \leq \frac{1}{3}$ for all normalized n_{in}-qubit states $|\phi\rangle$, i. e.,

$$\langle\phi|\langle 0|^{n-n_{\mathrm{in}}} U_{\mathcal{C}_X}^{\dagger} |0\rangle\langle 0|_2 U_{\mathcal{C}_X} |\phi\rangle|0\rangle^{n-n_{\mathrm{in}}} \geq \frac{2}{3} \quad \text{for all normalized } |\phi\rangle \in (\mathbb{C}^2)^{\otimes n_{\mathrm{in}}}. \tag{8.50}$$

Complex-conjugating this equation gives

$$\langle\phi|^*\langle 0|^{n-n_{\mathrm{in}}} U_{\mathcal{C}_X}^{\dagger *} |0\rangle\langle 0|_2 U_{\mathcal{C}_X}^{*} |\phi\rangle^*|0\rangle^{n-n_{\mathrm{in}}} \geq \frac{2}{3} \quad \text{for all normalized } |\phi\rangle \in (\mathbb{C}^2)^{\otimes n_{\mathrm{in}}},$$

or equivalently (replacing $|\phi\rangle$ with its complex conjugate),

$$\langle\phi|\langle 0|^{n-n_{\mathrm{in}}} U_{\mathcal{C}_X}^{\dagger *} |0\rangle\langle 0|_2 U_{\mathcal{C}_X}^{*} |\phi\rangle|0\rangle^{n-n_{\mathrm{in}}} \geq \frac{2}{3} \quad \text{for all normalized } |\phi\rangle \in (\mathbb{C}^2)^{\otimes n_{\mathrm{in}}}. \tag{8.51}$$

Recall that S_4 is the nullspace of $H(G_4, G_X^{\mathrm{occ}}, n)$ and consider the restriction

$$H_{\mathrm{out}}\big|_{S_4}. \tag{8.52}$$

We now show that the smallest eigenvalue of (8.52) is strictly positive. This implies that the nullspace of $H(G_X, G_X^{\mathrm{occ}}, n)$ is empty, which can be seen from (8.8) since both terms in this equation are positive semidefinite and S_4 is the nullspace of the first term. We then use Nullspace Projection Lemma to lower bound the smallest eigenvalue $\lambda_n^1(G_X, G_X^{\mathrm{occ}})$ of $H(G_X, G_X^{\mathrm{occ}}, n)$.

By Lemma 8.11, the states

$$|\widehat{\mathcal{H}}(\vec{z},\vec{a})\rangle = |\mathcal{H}(z_1 z_2 \ldots z_{n_{\mathrm{in}}} \underbrace{00\ldots0}_{n-n_{\mathrm{in}}}, \vec{a})\rangle, \quad \vec{a} \in \{0,1\}^n, \vec{z} \in \{0,1\}^{n_{\mathrm{in}}},$$

are a basis for S_4 and in this basis H_{out} is block diagonal with a block for each $\vec{a} \in \{0,1\}^n$, as can be seen using equation (8.47):

$$\langle\widehat{\mathcal{H}}(\vec{x},\vec{b})|H_{\mathrm{out}}|\widehat{\mathcal{H}}(\vec{z},\vec{a})\rangle = \delta_{\vec{a},\vec{b}} \frac{1}{128M}(M - j_{\max} + \tfrac{1}{2})\langle\vec{x}|\langle 0|^{n-n_{\mathrm{in}}} U_{\mathcal{C}_X}^{\dagger}(a_1)|0\rangle\langle 0|_2 U_{\mathcal{C}_X}(a_1)|\vec{z}\rangle|0\rangle^{n-n_{\mathrm{in}}}.$$

From equation (8.48) we can see that any normalized state that lives in the block corresponding to some fixed $\vec{a} \in \{0,1\}^n$ can be written as $|\widehat{\mathcal{H}}(\phi,\vec{a})\rangle$ for some normalized n_{in}-qubit state $|\phi\rangle$. The smallest eigenvalue of $H_{\mathrm{out}}|_{S_4}$ is therefore

$$\langle\widehat{\mathcal{H}}(\theta,\vec{\alpha})|H_{\mathrm{out}}|\widehat{\mathcal{H}}(\theta,\vec{\alpha})\rangle$$

for some normalized n_{in}-qubit state $|\theta\rangle$ and some $\vec{\alpha} \in \{0,1\}^n$. Now

$$\begin{aligned}\langle\widehat{\mathcal{H}}(\theta,\vec{\alpha})|H_{\mathrm{out}}|\widehat{\mathcal{H}}(\theta,\vec{\alpha})\rangle &= \frac{1}{128M}(M - j_{\max} + \tfrac{1}{2})\langle\theta|\langle 0|^{n-n_{\mathrm{in}}} U_{\mathcal{C}_X}^{\dagger}(\alpha_1)|0\rangle\langle 0|_2 U_{\mathcal{C}_X}(\alpha_1)|\theta\rangle|0\rangle^{n-n_{\mathrm{in}}} \\ &\geq \frac{1}{256M}\cdot\frac{2}{3}\end{aligned} \tag{8.53}$$

using equation (8.50) if $\alpha_1 = 0$ and equation (8.51) if $\alpha_1 = 1$. Since (8.53) is a lower bound on the smallest eigenvalue within each block, the nullspace of $H_{\text{out}}|_{S_4}$ is empty and

$$\gamma(H_{\text{out}}|_{S_4}) \geq \frac{1}{384M}. \tag{8.54}$$

As noted above, the fact that this matrix has strictly positive eigenvalues implies the same property of $H(G_X, G_X^{\text{occ}}, n)$, i. e.,

$$\lambda_n^1(G_X, G_X^{\text{occ}}) = \gamma(H(G_X, G_X^{\text{occ}}, n)).$$

To lower bound this quantity we apply Lemma 8.1 with

$$H_A = H(G_4, G_X^{\text{occ}}, n), \qquad H_B = H_{\text{out}}\big|_{\mathcal{I}(G_X, G_X^{\text{occ}}, n)},$$

and we use the bound (8.54) as well as

$$\gamma(H_A) \geq \frac{\mathcal{K}_0}{10^{10} n^3 M^3}$$

(from Lemma 8.11) and $\|H_B\| \leq \|H_{\text{out}}\| \leq n\|h_{\text{out}}\| = n$ (using equation (8.3)). Applying the lemma gives

$$\begin{aligned}
\lambda_n^1(G_X, G_X^{\text{occ}}) &= \gamma(H(G_X, G_X^{\text{occ}}, n)) \\
&\geq \frac{\mathcal{K}_0}{10^{10} n^3 M^3 + 384 M \mathcal{K}_0 + n(10^{10} n^3 M^3)(384M)} \\
&\geq \frac{\mathcal{K}_0}{n^4 M^4 (10^{10} + 384 + 10^{10} \cdot 384)} \\
&\geq \frac{\mathcal{K}_0}{10^{13} n^4 M^4}.
\end{aligned}$$

Now choosing $\mathcal{K}$ (the constant in the statement of Theorem 7.1) to be equal to $\mathcal{K}_0/10^{13}$ (recall $\mathcal{K}_0 \in (0,1]$ is the absolute constant from Lemma 8.5) proves equation (7.2). This completes the proof of Theorem 7.1.

9 XY Hamiltonian is QMA-complete

In this section we prove Theorem 2.9, showing that XY Hamiltonian is QMA-complete.

Proof. An instance of XY Hamiltonian can be verified by the standard QMA verification protocol for the Local Hamiltonian problem [21] with one slight modification: before running the protocol Arthur measures the magnetization of the witness and rejects unless it is equal to N. Thus the problem is contained in QMA.

To prove QMA-Hardness, we show that the solution (yes or no) of an instance of Frustration-Free Bose-Hubbard Hamiltonian with input G, N, ε is equal to the solution of the instance of XY Hamiltonian with the same graph G and integer N, with precision parameter $\varepsilon/4$ and $c = N\mu(G) + \varepsilon/4$.

We separately consider yes instances and no instances of Frustration-Free Bose-Hubbard Hamiltonian and show that the corresponding instance of XY Hamiltonian has the same solution in both cases.

Case 1: no instances

First consider a no instance of Frustration-Free Bose-Hubbard Hamiltonian, for which $\lambda_N^1(G) \geq \varepsilon + \varepsilon^3$. We have

$$\lambda_N^1(G) = \min_{\substack{|\phi\rangle \in \mathcal{Z}_N(G) \\ \langle\phi|\phi\rangle = 1}} \langle\phi| H_G^N - N\mu(G) |\phi\rangle \tag{9.1}$$

$$\leq \min_{\substack{|\phi\rangle \in \mathcal{W}_N(G) \\ \langle\phi|\phi\rangle = 1}} \langle\phi| H_G^N - N\mu(G) |\phi\rangle \tag{9.2}$$

$$= \min_{\substack{|\phi\rangle \in \mathrm{Wt}_N(G) \\ \langle\phi|\phi\rangle = 1}} \langle\phi| O_G - N\mu(G) |\phi\rangle \tag{9.3}$$

$$= \theta_N(G) - N\mu(G) \tag{9.4}$$

where in the inequality we used the fact that $\mathcal{W}_N(G) \subset \mathcal{Z}_N(G)$. Hence

$$\theta_N(G) \geq N\mu(G) + \lambda_N^1(G) \geq N\mu(G) + \varepsilon + \varepsilon^3 \geq N\mu(G) + \frac{\varepsilon}{2},$$

so the corresponding instance of XY Hamiltonian is a no instance.

Case 2: yes instances

Now consider a yes instance of Frustration-Free Bose-Hubbard Hamiltonian, so $0 \leq \lambda_N^1(G) \leq \varepsilon^3$.

We consider the case $\lambda_N^1(G) = 0$ separately from the case where it is strictly positive. If $\lambda_N^1(G) = 0$ then any state $|\psi\rangle$ in the ground space of H_G^N satisfies

$$\langle\phi| \sum_{w=1}^{N} \left(A(G) - \mu(G)\right)^{(w)} + \sum_{k \in V} \widehat{n}_k(\widehat{n}_k - 1) |\phi\rangle = 0.$$

Since both terms are positive semidefinite, the state $|\phi\rangle$ has zero energy for each of them. In particular, it has zero energy for the second term, or equivalently, $|\phi\rangle \in \mathcal{W}_N(G)$. Therefore

$$\lambda_N^1(G) = \min_{\substack{|\phi\rangle \in \mathcal{W}_N(G) \\ \langle\phi|\phi\rangle = 1}} \langle\phi| H_G^N - N\mu(G) |\phi\rangle = \min_{\substack{|\phi\rangle \in \mathrm{Wt}_N(G) \\ \langle\phi|\phi\rangle = 1}} \langle\phi| O_G - N\mu(G) |\phi\rangle = \theta_N(G) - N\mu(G),$$

so $\theta_N(G) = N\mu(G)$, and the corresponding instance of XY Hamiltonian is a yes instance.

Finally, suppose $0 < \lambda_N^1(G) \leq \varepsilon^3$. Then $\lambda_N^1(G)$ is also the smallest *nonzero* eigenvalue of $H(G,N)$, which we denote by $\gamma(H(G,N))$. (Here and throughout this paper we write $\gamma(M)$ for the smallest nonzero eigenvalue of a positive semidefinite matrix M.) Note that $\lambda_N^1(G) > 0$ also implies (by the inequalities (9.1)–(9.4)) that $\theta_N(G) - N\mu(G) > 0$, so

$$\theta_N(G) - N\mu(G) = \gamma\Big(\left(O_G - N\mu(G)\right)\big|_{\mathrm{Wt}_N(G)} \Big).$$

To upper bound $\theta_N(G)$ we use the Nullspace Projection Lemma (Lemma 8.1). We apply this lemma using the decomposition $H(G,N) = H_A + H_B$ where

$$H_A = \sum_{k\in V} \widehat{n}_k(\widehat{n}_k - 1)\big|_{\mathcal{Z}_N(G)}\,, \qquad H_B = \sum_{w=1}^{N} \left(A(G) - \mu(G)\right)^{(w)}\big|_{\mathcal{Z}_N(G)}\,.$$

Note that H_A and H_B are both positive semidefinite, and that the nullspace S of H_A is equal the space $\mathcal{W}_N(G)$ of hard-core bosons. To apply the lemma we compute bounds on $\gamma(H_A)$, $\|H_B\|$, and $\gamma(H_B|_S)$. We use the bounds $\gamma(H_A) = 2$ (since the operators $\{\widehat{n}_k : k \in V\}$ commute and have nonnegative integer eigenvalues),

$$\|H_B\| \leq N\|A(G) - \mu(G)\| \leq N(\|A(G)\| + \mu(G)) \leq 2N\|A(G)\| \leq 2KN \leq 2K^2$$

(where we used the fact that $\|A(G)\|$ is at most the maximum degree of G, which is at most the number of vertices K), and

$$\begin{aligned}\gamma(H_B|_S) &= \gamma\left(\sum_{w=1}^{N} \left(A(G) - \mu(G)\right)^{(w)}\big|_{\mathcal{W}_N(G)}\right)\\ &= \gamma\Big(\left(O_G - N\mu(G)\right)\big|_{\mathrm{Wt}_N(G)}\Big)\\ &= \theta_N(G) - N\mu(G)\,.\end{aligned}$$

Now applying the lemma, we get

$$\lambda_N^1(G) = \gamma(H(G,N)) \geq \frac{2(\theta_N(G) - N\mu(G))}{2 + (\theta_N(G) - N\mu(G)) + 2K^2}\,.$$

Rearranging this inequality gives

$$\theta_N(G) - N\mu(G) \leq \lambda_N^1(G)\frac{2(K^2+1)}{2 - \lambda_N^1(G)} \leq 4K^2\lambda_N^1(G) \leq 4K^2\varepsilon^3$$

where in going from the second to the third inequality we used the fact that $1 \leq K^2$ in the numerator and $\lambda_N^1(G) \leq \varepsilon^3 < 1$ in the denominator. Now using the fact (from the definition of Frustration-Free Bose-Hubbard Hamiltonian) that $\varepsilon \leq 1/(4K)$, we get

$$\theta_N(G) \leq N\mu(G) + \frac{\varepsilon}{4}\,,$$

i. e., the corresponding instance of XY Hamiltonian is a yes instance. □

10 Proof of the Occupancy Constraints Lemma

In this section we prove the Occupancy Constraints Lemma.

Lemma 10.1 (**Occupancy Constraints Lemma**). *Let G be an e_1-gate graph specified as a gate diagram with $R \geq 2$ diagram elements. Let $N \in [R]$, let G^{occ} specify a set of occupancy constraints on G, and suppose the subspace $\mathcal{I}(G, G^{\mathrm{occ}}, N)$ is nonempty. Then there exists an efficiently computable e_1-gate graph $G^{\square}$ with at most $7R^2$ diagram elements such that*

1. *If $\lambda_N^1(G, G^{\mathrm{occ}}) \leq a$ then $\lambda_N^1(G^{\square}) \leq \dfrac{a}{R}$.*
2. *If $\lambda_N^1(G, G^{\mathrm{occ}}) \geq b$ with $b \in [0,1]$, then $\lambda_N^1(G^{\square}) \geq \dfrac{b}{(13R)^9}$.*

10.1 Definitions and notation

In this section we establish notation and we describe how the gate graph $G^{\square}$ is constructed from G and G^{occ}. We also define two related gate graphs $G^{\triangle}$ and $G^{\diamondsuit}$ that we use in our analysis.

Let us first fix notation for the gate graph G and the occupancy constraints graph G^{occ}. Write the adjacency matrix of G as (see equation (5.4))

$$A(G) = \sum_{q=1}^{R} |q\rangle\langle q| \otimes A(g_0) + h_{\mathcal{E}^G} + h_{\mathcal{S}^G}$$

where $h_{\mathcal{E}^G}$ and $h_{\mathcal{S}^G}$ are determined (through equations (5.6) and (5.5)) by the sets $\mathcal{E}^G$ and $\mathcal{S}^G$ of edges and self-loops in the gate diagram for G, and where g_0 is the 128-vertex graph from Figure 5.1. Recall that the occupancy constraints graph G^{occ} is a simple graph with vertices labeled $q \in [R]$, one for each diagram element in G. We write

$$E(G^{\mathrm{occ}}) \subseteq \binom{[R]}{2} = \{\{x,y\} : x,y \in [R], x \neq y\}$$

for the edge set of G^{occ}.

Definition of $G^{\square}$

To ensure that the ground space has the appropriate form, the construction of $G^{\square}$ is slightly different depending on whether R is even or odd. The following description handles both cases.

1. Replace each diagram element $q \in [R]$ in the gate diagram for G as shown in Figure 10.1, with diagram elements labeled $q_{\mathrm{in}}, q_{\mathrm{out}}$ and $d(q,s)$ where $q,s \in [R]$ and $q \neq s$ if R is even. Each node (q,z,t) in the gate diagram for G is mapped to a new node $\mathrm{new}(q,z,t)$ as shown by the black and grey arrows, i. e.,

$$\mathrm{new}(q,z,t) = \begin{cases} (q_{\mathrm{in}}, z, t) & \text{if } (q,z,t) \text{ is an input node} \\ (q_{\mathrm{out}}, z, t) & \text{if } (q,z,t) \text{ is an output node.} \end{cases} \tag{10.1}$$

   Edges and self-loops in the gate diagram for G are replaced by edges and self-loops between the corresponding nodes in the modified diagram.

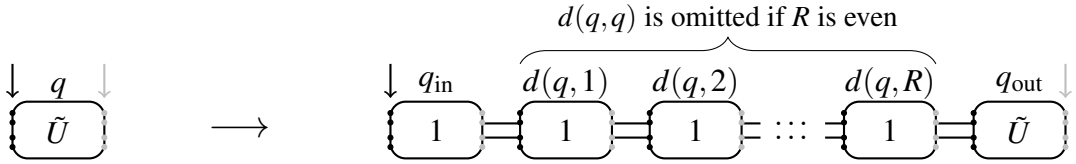

Figure 10.1: The first step in constructing the gate diagram of $G^{\square}$ from that of G is to replace each diagram element as shown. The four input nodes (black arrow) and four output nodes (grey arrow) on the left-hand side are identified with nodes on the right-hand side as shown.

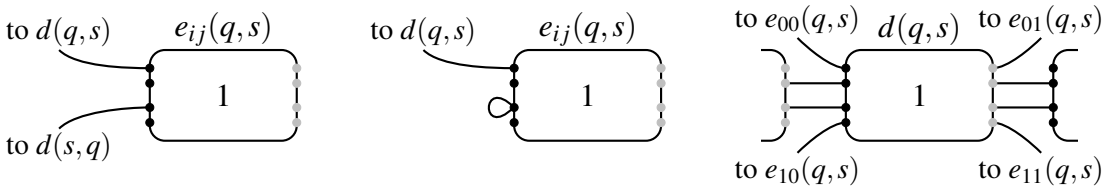

(A) $\{q,s\} \in E(G^{\mathrm{occ}})$, $q < s$ (B) $\{q,s\} \notin E(G^{\mathrm{occ}})$ (C)

Figure 10.2: Edges and self-loops added in step 4 of the construction of the gate diagram of $G^{\square}$. When $\{q,s\} \in E(G^{\mathrm{occ}})$ with $q < s$, we add two outgoing edges to $e_{ij}(q,s)$ as shown in (A). Note that if $q > s$ and $\{q,s\} \in E(G^{\mathrm{occ}})$ then $e_{ij}(q,s) = e_{ji}(s,q)$. When $\{q,s\} \notin E(G^{\mathrm{occ}})$ we add a self-loop and a single outgoing edge from $e_{ij}(q,s)$ as shown in (B). Each diagram element $d(q,s)$ has eight outgoing edges (four of which are added in step 4), as shown in (C).

2. For each edge $\{q_1,q_2\} \in E(G^{\mathrm{occ}})$ in the occupancy constraints graph we add four diagram elements of the type shown in Figure 5.2(C) (i. e., diagram elements corresponding to the identity). We refer to these diagram elements by labels $e_{ij}(q_1,q_2)$ with $i,j \in \{0,1\}$. For these diagram elements the labeling function is symmetric, i. e., $e_{ij}(q_1,q_2) = e_{ji}(q_2,q_1)$ whenever $\{q_1,q_2\} \in E(G^{\mathrm{occ}})$.

3. For each non-edge $\{q_1,q_2\} \notin E(G^{\mathrm{occ}})$ with $q_1,q_2 \in [R]$ and $q_1 \neq q_2$ we add 8 diagram elements of the type shown in Figure 5.2(C). We refer to these diagram elements as $e_{ij}(q_1,q_2)$ and $e_{ij}(q_2,q_1)$ with $i,j \in \{0,1\}$; when $\{q_1,q_2\} \notin E(G^{\mathrm{occ}})$ the labeling function is not symmetric, i. e., $e_{ij}(q_1,q_2) \neq e_{ji}(q_2,q_1)$. If R is odd we also add $4R$ diagram elements labeled $e_{ij}(q,q)$ with $i,j \in \{0,1\}$ and $q \in [R]$.

4. Finally, we add edges and self-loops to the gate diagram as shown in Figure 10.2. This gives the gate diagram for $G^{\square}$.

The set of diagram elements in the gate graph for $G^{\square}$ is indexed by

$$L^{\square} = Q_{\mathrm{in}} \cup D \cup E_{\mathrm{edges}} \cup E_{\text{non-edges}} \cup Q_{\mathrm{out}} \tag{10.2}$$

where

$$Q_{\text{in}} = \{q_{\text{in}} : q \in [R]\} \tag{10.3}$$

$$D = \{d(q,s) : q,s \in [R] \text{ and } q \neq s \text{ if } R \text{ is even}\} \tag{10.4}$$

$$E_{\text{edges}} = \left\{e_{ij}(q,s) : i,j \in \{0,1\}, \{q,s\} \in E(G^{\text{occ}}) \text{ and } q < s\right\}$$

$$E_{\text{non-edges}} = \left\{e_{ij}(q,s) : i,j \in \{0,1\}, \{q,s\} \notin E(G^{\text{occ}}) \text{ and } q \neq s \text{ if } R \text{ is even}\right\}$$

$$Q_{\text{out}} = \{q_{\text{out}} : q \in [R]\}. \tag{10.5}$$

The total number of diagram elements in $G^{\square}$ is

$$\begin{aligned}
|L^{\square}| &= |Q_{\text{in}}| + |D| + |E_{\text{edges}}| + |E_{\text{non-edges}}| + |Q_{\text{out}}| \\
&= \begin{cases} R + R^2 + 4|E(G^{\text{occ}})| + 4\left(R^2 - 2|E(G^{\text{occ}})|\right) + R & R \text{ odd} \\ R + R(R-1) + 4|E(G^{\text{occ}})| + 4\left(R(R-1) - 2|E(G^{\text{occ}})|\right) + R & R \text{ even} \end{cases} \\
&= \begin{cases} 5R^2 + 2R - 4|E(G^{\text{occ}})| & R \text{ odd} \\ 5R^2 - 3R - 4|E(G^{\text{occ}})| & R \text{ even.} \end{cases}
\end{aligned}$$

In both cases this is upper bounded by $7R^2$ as claimed in the statement of the lemma. Write

$$A(G^{\square}) = \sum_{l \in L^{\square}} |l\rangle\langle l| \otimes A(g_0) + h_{\mathcal{S}^{\square}} + h_{\mathcal{E}^{\square}} \tag{10.6}$$

where $\mathcal{S}^{\square}$ and $\mathcal{E}^{\square}$ are the sets of self-loops and edges in the gate diagram for $G^{\square}$.

We now focus on the input nodes of diagram elements in Q_{in} and the output nodes of the diagram elements in Q_{out}. These are the nodes indicated by the black and grey arrows in Figure 10.1. Write $\mathcal{E}^0 \subset \mathcal{E}^{\square}$ and $\mathcal{S}^0 \subset \mathcal{S}^{\square}$ for the sets of edges and self-loops that are incident on these nodes in the gate diagram for $G^{\square}$. Note that the sets $\mathcal{E}^0$ and $\mathcal{S}^0$ are in one-to-one correspondence with (respectively) the sets $\mathcal{E}^G$ and $\mathcal{S}^G$ of edges and self-loops in the gate diagram for G. The other edges and self-loops in $G^{\square}$ do not depend on the sets of edges and self-loops in G. Writing

$$\mathcal{S}^{\triangle} = \mathcal{S}^{\square} \setminus \mathcal{S}^0, \qquad \mathcal{E}^{\triangle} = \mathcal{E}^{\square} \setminus \mathcal{E}^0,$$

we have

$$h_{\mathcal{S}^{\square}} = h_{\mathcal{S}^0} + h_{\mathcal{S}^{\triangle}}, \qquad h_{\mathcal{E}^{\square}} = h_{\mathcal{E}^0} + h_{\mathcal{E}^{\triangle}}. \tag{10.7}$$

Definition of $G^{\triangle}$

The gate diagram for $G^{\triangle}$ is obtained from that of $G^{\square}$ by removing all edges and self-loops attached to the input nodes of the diagram elements in Q_{in} and the output nodes of the diagram elements in Q_{out}. Its adjacency matrix is

$$A(G^{\triangle}) = \sum_{l \in L^{\square}} |l\rangle\langle l| \otimes A(g_0) + h_{\mathcal{S}^{\triangle}} + h_{\mathcal{E}^{\triangle}}. \tag{10.8}$$

Note that $G^{\triangle} = G^{\square}$ whenever the gate diagram for G contains no edges or self-loops.

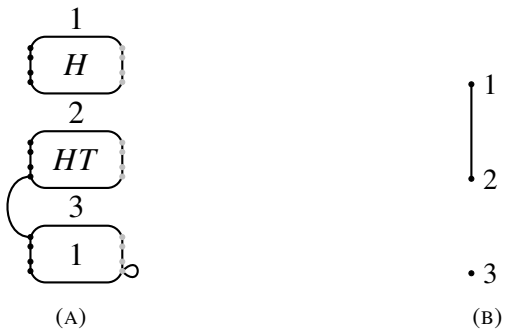

(A) (B)

Figure 10.3: An example (A) Gate diagram for a gate graph G and (B) Occupancy constraints graph G^{occ}. In the text we describe how these two ingredients are mapped to a gate graph $G^{\square}$; the gate diagram for $G^{\square}$ is shown in Figure 10.4.

Definition of $G^{\diamondsuit}$

We also define a gate graph $G^{\diamondsuit}$ with gate diagram obtained from that of $G^{\triangle}$ by removing all edges (but leaving the self-loops). Note that $G^{\diamondsuit}$ has a component for each diagram element $l \in L^{\square}$. The components corresponding to diagram elements without a self-loop (those with $l \in L^{\square} \setminus E_{\text{non-edges}}$) have adjacency matrix $A(g_0)$; those with a self-loop ($l \in E_{\text{non-edges}}$) have adjacency matrix $A(g_0) + |1,1\rangle\langle 1,1| \otimes 1$, so

$$A(G^{\diamondsuit}) = \sum_{l \in L^{\square}} |l\rangle\langle l| \otimes A(g_0) + h_{S^{\triangle}} \tag{10.9}$$

$$= \sum_{l \in L^{\square} \setminus E_{\text{non-edges}}} |l\rangle\langle l| \otimes A(g_0) + \sum_{l \in E_{\text{non-edges}}} |l\rangle\langle l| \otimes (A(g_0) + |1,1\rangle\langle 1,1| \otimes 1)\,. \tag{10.10}$$

Example

We provide an example of this construction in Figure 10.3 (which shows a gate graph and an occupancy constraints graph) and Figure 10.4 (which describes the derived gate graphs $G^{\square}$, $G^{\triangle}$, and $G^{\diamondsuit}$).

10.2 The gate graph $G^{\diamondsuit}$

We now solve for the e_1-energy ground states of the adjacency matrix $A(G^{\diamondsuit})$. Write g_1 for the graph with adjacency matrix

$$A(g_1) = A(g_0) + |1,1\rangle\langle 1,1| \otimes 1$$

(i. e., g_0 with 8 self-loops added), so (recalling equation (10.10)) each component of $G^{\diamondsuit}$ is either g_0 or g_1. Recall from Section 5.1 that $A(g_0)$ has four orthonormal e_1-energy ground states $|\psi_{z,a}\rangle$ with $z,a \in \{0,1\}$. It is also not hard to verify that the e_1-energy ground space of $A(g_1)$ is spanned by two of these states $|\psi_{0,a}\rangle$ for $a \in \{0,1\}$. Now letting $|\psi^l_{z,a}\rangle = |l\rangle|\psi_{z,a}\rangle$, we choose a basis $\mathcal{W}$ for the e_1-energy ground space of $A(G^{\diamondsuit})$ where each basis vector is supported on one of the components:

$$\mathcal{W} = \left\{|\psi^l_{z,a}\rangle : z,a \in \{0,1\}, l \in L^{\square} \setminus E_{\text{non-edges}}\right\} \cup \left\{|\psi^l_{0,a}\rangle : a \in \{0,1\}, l \in E_{\text{non-edges}}\right\}. \tag{10.11}$$

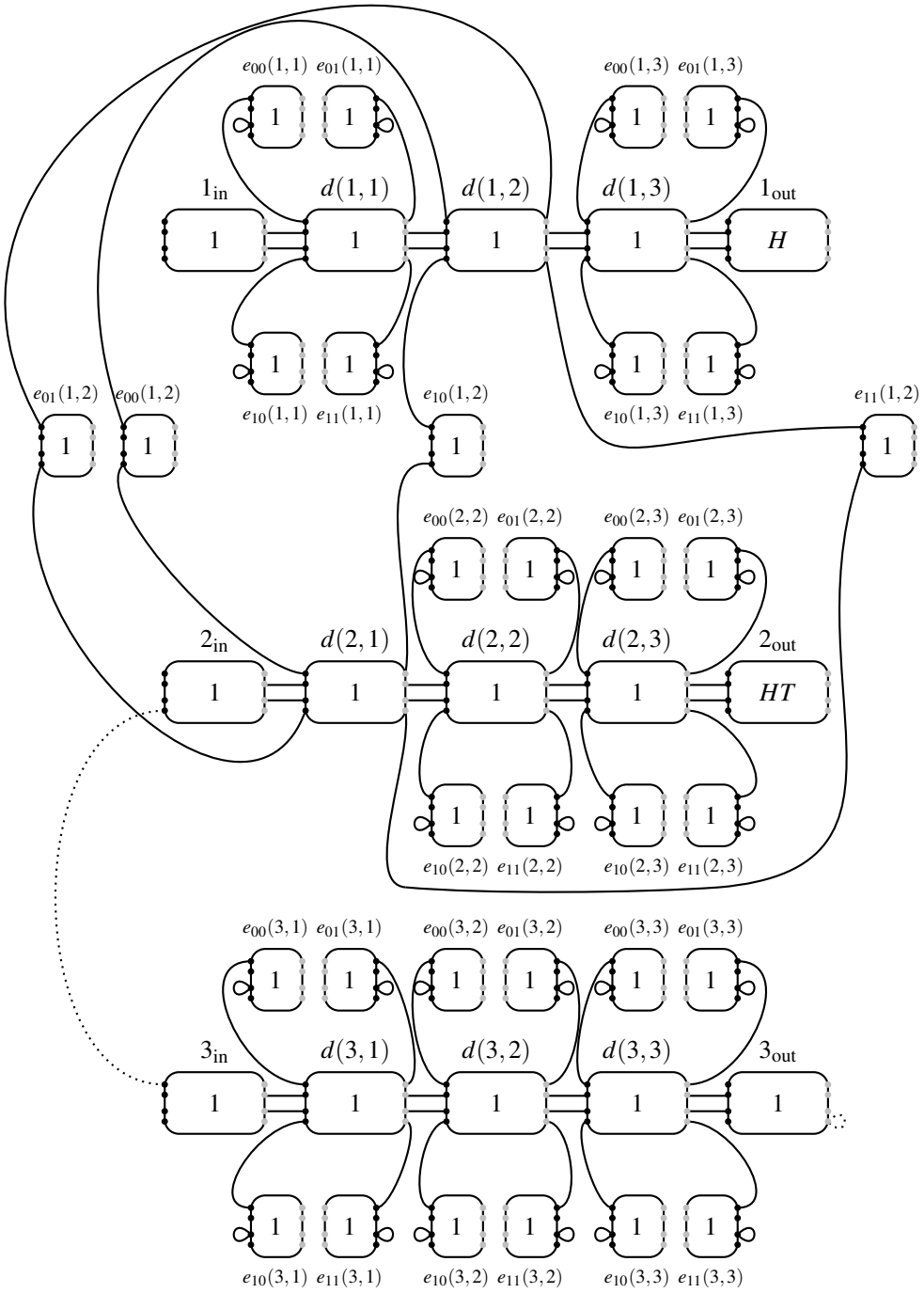

Figure 10.4: The gate diagram for $G^{\triangle}$ (only solid lines) and $G^{\square}$ (including dotted lines) derived from the example gate graph G and occupancy constraints graph G^{occ} from Figure 10.3. The gate diagram for $G^{\diamondsuit}$ is obtained from that of $G^{\triangle}$ by removing all edges (but leaving the self-loops).

The eigenvalue gap of $A(G^{\diamondsuit})$ is equal to that of either $A(g_0)$ or $A(g_1)$. Since g_0 and g_1 are specific 128-vertex graphs we can calculate their eigenvalue gaps using a computer; we get $\gamma(A(g_0)-e_1) = 0.7785\ldots$ and $\gamma(A(g_1)-e_1) = 0.0832\ldots$. Hence

$$\gamma(A(G^{\diamondsuit})-e_1) \geq 0.0832\ldots > \frac{1}{13}. \tag{10.12}$$

The ground space of $A(G^{\diamondsuit})$ has dimension

$$|\mathcal{W}| = 4\left|L^{\square}\right| - 2\left|E_{\text{non-edges}}\right| = \begin{cases} 4\left(5R^2+2R-4|E(G^{\text{occ}})|\right) - 2\left(4R^2-8|E(G^{\text{occ}})|\right) & R \text{ odd} \\ 4\left(5R^2-3R-4|E(G^{\text{occ}})|\right) - 2\left(4R(R-1)-8|E(G^{\text{occ}})|\right) & R \text{ even} \end{cases}$$
$$= \begin{cases} 12R^2+8R & R \text{ odd} \\ 12R^2-4R & R \text{ even.} \end{cases} \tag{10.13}$$

We now consider the N-particle Hamiltonian $H(G^{\diamondsuit},N)$ and characterize its nullspace.

Lemma 10.2. *The nullspace of $H(G^{\diamondsuit},N)$ is*

$$\mathcal{I}_{\diamondsuit} = \text{span}\{\text{Sym}(|\psi^{q_1}_{z_1,a_1}\rangle|\psi^{q_2}_{z_2,a_2}\rangle\ldots|\psi^{q_N}_{z_N,a_N}\rangle) : |\psi^{q_i}_{z_i,a_i}\rangle \in \mathcal{W} \text{ and } q_i \neq q_j \text{ for all distinct } i,j \in [N]\}$$

where $\mathcal{W}$ is given in equation (10.11). The smallest nonzero eigenvalue satisfies $\gamma(H(G^{\diamondsuit},N)) > 1/300$.

Proof. For the first part of the proof we use the fact that the basis vectors $|\psi^{l}_{z,a}\rangle \in \mathcal{W}$ span the e_1-eigenspace of the component $G^{\diamondsuit}_l$ of $G^{\diamondsuit}$ corresponding to the diagram element $l \in L^{\square}$, i. e., the nullspace of $H(G^{\diamondsuit}_l,1)$. Furthermore, no component of $G^{\diamondsuit}$ supports a two-particle frustration-free state, i. e., $\lambda^1_2(g_0) > 0$ and $\lambda^1_2(g_1) > 0$ (by Lemma 5.3). Now applying Lemma 2.4 we see that $\mathcal{I}_{\diamondsuit}$ is the nullspace of $H(G^{\diamondsuit},N)$. We also see that the smallest nonzero eigenvalue $\gamma(H(G^{\diamondsuit},N))$ is either $\lambda^1_2(g_0)$, $\lambda^1_2(g_1)$, $\gamma(H(g_0,1))$, or $\gamma(H(g_1,1))$. These constants can be calculated numerically using a computer; they are

$$\lambda^1_2(g_0) = 0.0035\ldots, \quad \lambda^1_2(g_1) = 0.0185\ldots, \quad \gamma(H(g_0,1)) = 0.7785\ldots,$$
$$\text{and} \quad \gamma(H(g_1,1)) = 0.0832\ldots.$$

Hence

$$\gamma(H(G^{\diamondsuit},N)) \geq \min\{\lambda^1_2(g_0),\lambda^1_2(g_1),\gamma(H(g_0,1)),\gamma(H(g_1,1))\} > \frac{1}{300}. \qquad \square$$

10.3 The adjacency matrix of the gate graph $G^{\triangle}$

We begin by solving for the e_1-energy ground space of the adjacency matrix $A(G^{\triangle})$. From equations (10.8) and (10.9) we have

$$A(G^{\triangle}) = A(G^{\diamondsuit}) + h_{\mathcal{E}^{\triangle}}. \tag{10.14}$$

Recall the e_1-energy ground space of $A(G^{\diamondsuit})$ is spanned by $\mathcal{W}$ from equation (10.11). Since $h_{\mathcal{E}^{\triangle}} \geq 0$ it follows that $A(G^{\triangle}) \geq e_1$. To solve for the e_1-energy ground space of $A(G^{\triangle})$ we construct superpositions of vectors from $\mathcal{W}$ that are in the nullspace of $h_{\mathcal{E}^{\triangle}}$. To this end we consider the restriction

$$h_{\mathcal{E}^{\triangle}}\big|_{\text{span}(\mathcal{W})}. \tag{10.15}$$

We now show that it is block diagonal in the basis $\mathcal{W}$ and we compute its matrix elements.

First recall from equation (5.6) that

$$h_{\mathcal{E}^\triangle} = \sum_{\{(l,z,t),(l',z',t')\}\in\mathcal{E}^\triangle} \big(|l,z,t\rangle + |l',z',t'\rangle\big)\big(\langle l,z,t| + \langle l',z',t'|\big) \otimes 1\,. \tag{10.16}$$

The edges $\{(l,z,t),(l',z',t')\} \in \mathcal{E}^\triangle$ can be read off from Figure 10.1 and Figure 10.2, respectively (referring back to Figure 5.2 for our convention regarding the labeling of nodes on a diagram element). The edges from Figure 10.1 are

$$\big\{(q_{\text{in}},z,t),\ (d(q,1),z,t')\big\},\ \big\{(d(q,2),z,t),(d(q,3),z,t')\big\},\ \ldots,\ \big\{(d(q,R),z,t),(q_{\text{out}},z,t')\big\} \tag{10.17}$$

with $q \in [R]$ and $(z,t,t') = (0,7,3)$ or $(1,5,1)$, and where $d(q,q)$ does not appear if R is even (i. e., $d(q,q-1)$ is followed by $d(q,q+1)$). The edges from Figure 10.2 are

$$\begin{aligned}&\{(d(q,s),0,1),(e_{00}(q,s),\alpha(q,s),1)\},\{(d(q,s),1,3),(e_{10}(q,s),\alpha(q,s),1)\},\\ &\{(d(q,s),0,5),(e_{01}(q,s),\alpha(q,s),1)\},\{(d(q,s),1,7),(e_{11}(q,s),\alpha(q,s),1)\}\end{aligned} \tag{10.18}$$

with $q,s \in [R]$ and $q \neq s$ if R is even, and where

$$\alpha(q,s) = \begin{cases} 1 & q > s \text{ and } \{q,s\} \in E(G^{\text{occ}}) \\ 0 & \text{otherwise.}\end{cases}$$

The set $\mathcal{E}^\triangle$ consists of all edges (10.17) and (10.18).

We claim that (10.15) is block diagonal with a block $\mathcal{W}_{(z,a,q)} \subseteq \mathcal{W}$ of size

$$\big|\mathcal{W}_{(z,a,q)}\big| = \begin{cases} 3R+2 & R \text{ odd} \\ 3R-1 & R \text{ even}\end{cases}$$

for each for each triple (z,a,q) with $z,a \in \{0,1\}$ and $q \in [R]$. Using equation (10.13) we confirm that $|\mathcal{W}| = 4R\big|\mathcal{W}_{(z,a,q)}\big|$, so this accounts for all basis vectors in $\mathcal{W}$. The subset of basis vectors for a given block is

$$\begin{aligned}\mathcal{W}_{(z,a,q)} = &\big\{|\psi_{z,a}^{q_{\text{in}}}\rangle, |\psi_{z,a}^{q_{\text{out}}}\rangle\big\} \cup \big\{|\psi_{z,a}^{d(q,s)}\rangle : s \in [R],\, s \neq q \text{ if } R \text{ even}\big\} \\ &\cup \big\{|\psi_{\alpha(q,s),a}^{e_{zx}(q,s)}\rangle : x \in \{0,1\},\, s \in [R],\, s \neq q \text{ if } R \text{ even}\big\}.\end{aligned} \tag{10.19}$$

Using equation (10.16) and the description of $\mathcal{E}^\triangle$ from (10.17) and (10.18), one can check by direct inspection that (10.15) only has nonzero matrix elements between basis vectors in $\mathcal{W}$ from the same block. We also compute the matrix elements between vectors from the same block. For example, if R is odd or if R is even and $q \neq 1$, there are edges $\{(q_{\text{in}},0,7),(d(q,1),0,3)\},\{(q_{\text{in}},1,5),(d(q,1),1,1)\} \in \mathcal{E}^\triangle$. Using the fact that $|\psi_{z,a}^l\rangle = |l\rangle|\psi_{z,a}\rangle$ where $|\psi_{z,a}\rangle$ is given by (5.2) and (5.3), we compute the relevant

matrix elements:

$$\begin{aligned}
&\langle \psi_{z,a}^{q_{\mathrm{in}}} | h_{\mathcal{E}^{\triangle}} | \psi_{z,a}^{d(q,1)} \rangle \\
&\quad = \langle \psi_{z,a}^{q_{\mathrm{in}}} | \left(\sum_{(z',t,t') \in \{(0,7,3),(1,5,1)\}} \left(|q_{\mathrm{in}}, z', t\rangle + |d(q,1), z', t'\rangle \right) \left(\langle q_{\mathrm{in}}, z', t| + \langle d(q,1), z', t'| \right) \otimes 1 \right) | \psi_{z,a}^{d(q,1)} \rangle \\
&\quad = \sum_{(z',t,t') \in \{(0,7,3),(1,5,1)\}} \langle \psi_{z,a} | \left(|z', t\rangle\langle z', t'| \otimes 1 \right) | \psi_{z,a} \rangle = \frac{1}{8} .
\end{aligned}$$

Continuing in this manner, we compute the principal submatrix of (10.15) corresponding to the set $\mathcal{W}_{(z,a,q)}$. This matrix is shown in Figure 10.5(A). In the figure each vertex is associated with a state in the block and the weight on a given edge is the matrix element between the two states associated with vertices joined by that edge. The diagonal matrix elements are described by the weights on the self-loops. The matrix described by Figure 10.5(A) is the same for each block.

For each triple (z,a,q) with $z,a \in \{0,1\}$ and $q \in [R]$, define $|\phi_{z,a}^{q}\rangle$ to be

$$\begin{cases} \frac{1}{\sqrt{3R+2}} \left(|\psi_{z,a}^{q_{\mathrm{in}}}\rangle + \sum_{j \in [R]} (-1)^j \left(|\psi_{z,a}^{d(q,j)}\rangle - |\psi_{\alpha(q,j),a}^{e_{z0}(q,j)}\rangle - |\psi_{\alpha(q,j),a}^{e_{z1}(q,j)}\rangle \right) + |\psi_{z,a}^{q_{\mathrm{out}}}\rangle \right) & \text{if } R \text{ odd}, \\ \frac{1}{\sqrt{3R-1}} \left(|\psi_{z,a}^{q_{\mathrm{in}}}\rangle + \left(\sum_{j<q} - \sum_{j>q} \right) (-1)^j \left(|\psi_{z,a}^{d(q,j)}\rangle - |\psi_{\alpha(q,j),a}^{e_{z0}(q,j)}\rangle - |\psi_{\alpha(q,j),a}^{e_{z1}(q,j)}\rangle \right) + |\psi_{z,a}^{q_{\mathrm{out}}}\rangle \right) & \text{if } R \text{ even}. \end{cases} \tag{10.20}$$

Next we show that these states span the ground space of $A(G^{\triangle})$. The choice to omit $d(q,q)$ for R even ensures that $|\psi_{z,a}^{q_{\mathrm{in}}}\rangle$ and $|\psi_{z,a}^{q_{\mathrm{out}}}\rangle$ have the same sign in these ground states.

Lemma 10.3. *An orthonormal basis for the e_1-energy ground space of $A(G^{\triangle})$ is given by the states*

$$\left\{ |\phi_{z,a}^{q}\rangle : z,a \in \{0,1\}, q \in [R] \right\}$$

defined by equation (10.20). The eigenvalue gap is bounded as

$$\gamma(A(G^{\triangle}) - e_1) > \frac{1}{(30R)^2} . \tag{10.21}$$

Proof. The e_1-energy ground space of $A(G^{\triangle})$ is equal to the nullspace of (10.15). Since this operator is block diagonal in the basis $\mathcal{W}$, we can solve for the eigenvectors in the nullspace of each block. Thus, to prove the first part of the lemma, we analyze the $|\mathcal{W}_{(z,a,q)}| \times |\mathcal{W}_{(z,a,q)}|$ matrix described by Figure 10.5(A) and show that (10.20) is the unique vector in its nullspace. We first rewrite it in a slightly different basis obtained by multiplying some of the basis vectors by a phase of -1. Specifically, we use the basis

$$\left\{ |\psi_{z,a}^{q_{\mathrm{in}}}\rangle, -|\psi_{z,a}^{d(q,1)}\rangle, |\psi_{\alpha(q,1),a}^{e_{z0}(q,1)}\rangle, |\psi_{\alpha(q,1),a}^{e_{z1}(q,1)}\rangle, |\psi_{z,a}^{d(q,2)}\rangle, -|\psi_{\alpha(q,2),a}^{e_{z0}(q,2)}\rangle, -|\psi_{\alpha(q,2),a}^{e_{z1}(q,2)}\rangle, \ldots, |\psi_{z,a}^{q_{\mathrm{out}}}\rangle \right\}$$

where the state associated with each vertex on one side of a bipartition of the graph is multiplied by -1; these are the phases appearing in equation (10.20). Changing to this basis replaces the weight $1/8$ on each edge in Figure 10.5(A) by $-1/8$ and does not change the weights on the self-loops. The resulting matrix is $(1/8)L_0$, where L_0 is the Laplacian matrix of the graph shown in Figure 10.5(B). Now we use the fact that the Laplacian of any connected graph has smallest eigenvalue zero, with a unique eigenvector

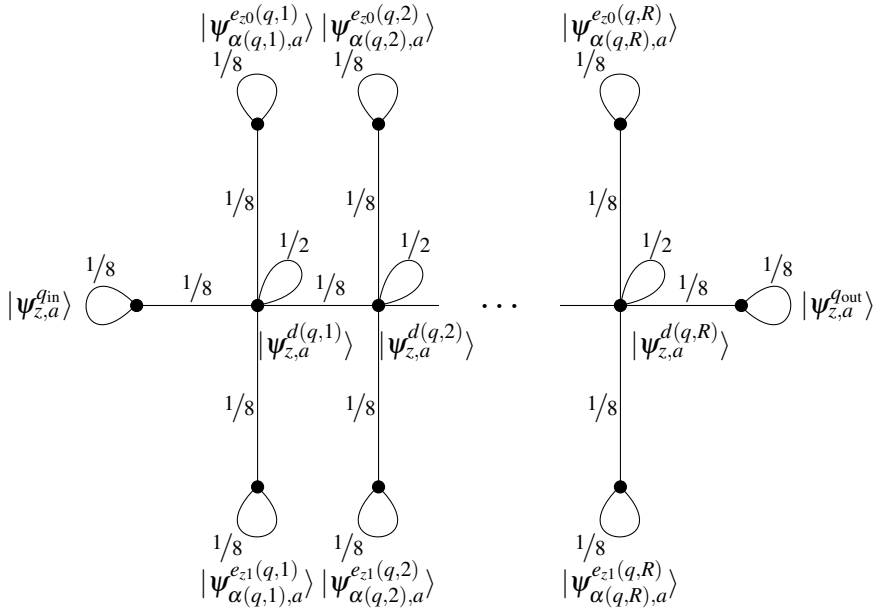

(A) The matrix $h^{\triangle}_{\mathcal{L}}|_{\text{span}(\mathcal{W})}$ is block diagonal in the basis $\mathcal{W}$, with a block $\mathcal{W}_{(z,a,q)}$ for each $z,a \in \{0,1\}$ and $q \in \{1,\ldots,R\}$. The states involved in a given block and the matrix elements between them are depicted.

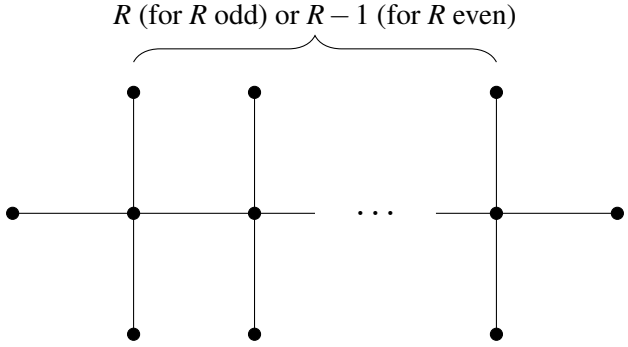

(B) After multiplying some of the basis vectors by -1, the matrix depicted in (A) is transformed into $1/8$ times the Laplacian matrix of this graph.

Figure 10.5

equal to the all-ones vector. Hence for each block we get an eigenvector in the nullspace of (10.15)) given by (10.20). Ranging over all $z,a \in \{0,1\}$ and $q \in [R]$ gives the claimed basis for the e_1-energy ground space of $A(G^{\triangle})$.

To prove the lower bound, we use the Nullspace Projection Lemma (Lemma 8.1) with

$$H_A = A(G^{\diamondsuit}) - e_1\,, \qquad H_B = h_{\mathcal{E}^{\triangle}}\,,$$

and where $S = \mathrm{span}(\mathcal{W})$ is the nullspace of H_A as shown in Section 10.2. Since it is block diagonal in the basis $\mathcal{W}$, the smallest nonzero eigenvalue of (10.15) is equal to the smallest nonzero eigenvalue of one of its blocks. The matrix for each block is $\frac{1}{8}L_0$. Thus we can lower bound the smallest nonzero eigenvalue of $H_B|_S$ using standard bounds on the smallest nonzero eigenvalue of the Laplacian L of a graph G. In particular, Theorem 4.2 of reference [26] shows that

$$\gamma(L) \geq \frac{4}{|V(G)|\,\mathrm{diam}(G)} \geq \frac{4}{|V(G)|^2}$$

(where $\mathrm{diam}(G)$ is the diameter of G). Since the size of the graph in Figure 10.5(B) is either $3R-1$ or $3R+2$, we have

$$\gamma(H_B|_S) = \frac{1}{8}\gamma(L_0) \geq \frac{1}{8}\frac{4}{(3R+2)^2} \geq \frac{1}{32R^2}$$

since $R \geq 2$. Using this bound and the fact that $\gamma(H_A) > 1/13$ (from equation (10.12)) and $\|H_B\| = 2$ (from equation (5.8)) and plugging into Lemma 8.1 gives

$$\gamma(A(G^{\triangle}) - e_1) \geq \frac{\frac{1}{13}\cdot\frac{1}{32R^2}}{\frac{1}{13}+\frac{1}{32R^2}+2} \geq \frac{1}{(32+13+832)R^2} > \frac{1}{(30R)^2}\,. \qquad \square$$

10.4 The Hamiltonian $H(G^{\triangle}, N)$

We now consider the N-particle Hamiltonian $H(G^{\triangle}, N)$ and solve for its nullspace. We use the following fact about the subsets $\mathcal{W}_{(z,a,q)} \subset \mathcal{W}$ defined in equation (10.19).

Definition 10.4. We say $\mathcal{W}_{(z_1,a_1,q_1)}$ and $\mathcal{W}_{(z_2,a_2,q_2)}$ *overlap on a diagram element* if there exists $l \in L^{\square}$ such that

$$|\psi^l_{x_1,b_1}\rangle \in \mathcal{W}_{(z_1,a_1,q_1)} \qquad \text{and} \qquad |\psi^l_{x_2,b_2}\rangle \in \mathcal{W}_{(z_2,a_2,q_2)}$$

for some $x_1, x_2, b_1, b_2 \in \{0,1\}$.

Fact 10.5 (Key property of $\mathcal{W}_{(z,a,q)}$)**.** *Sets $\mathcal{W}_{(z_1,a_1,q_1)}$ and $\mathcal{W}_{(z_2,a_2,q_2)}$ overlap on a diagram element if and only if $q_1 = q_2$ or $\{q_1,q_2\} \in E(G^{\mathrm{occ}})$.*

This fact can be confirmed by direct inspection of the sets $\mathcal{W}_{(z,a,q)}$. If $q_1 = q_2 = q$ the diagram element l on which they overlap can be chosen to be $l = q_{\mathrm{in}}$; if $q_1 \neq q_2$ and $\{q_1,q_2\} \in E(G^{\mathrm{occ}})$ then $l = e_{z_1 z_2}(q_1,q_2) = e_{z_2 z_1}(q_2,q_1)$.

Conversely, if $\{q_1,q_2\} \notin E(G^{\mathrm{occ}})$ with $q_1 \neq q_2$, then there is no overlap.

We show that the nullspace $\mathcal{I}_\triangle$ of $H(G^\triangle, N)$ is

$$\mathcal{I}_\triangle = \mathrm{span}\{\mathrm{Sym}(|\phi^{q_1}_{z_1,a_1}\rangle|\phi^{q_2}_{z_2,a_2}\rangle \ldots |\phi^{q_N}_{z_N,a_N}\rangle) \colon z_i, a_i \in \{0,1\},\, q_i \in [R],\, q_i \neq q_j, \text{ and } \{q_i, q_j\} \notin E(G^{\mathrm{occ}})\}. \tag{10.22}$$

Note that $\mathcal{I}_\triangle \subset \mathcal{Z}_N(G^\triangle)$ is very similar to $\mathcal{I}(G, G^{\mathrm{occ}}, N) \subset \mathcal{Z}_N(G)$ (from equation (5.21)) but with each single-particle state $|\psi^q_{z,a}\rangle \in \mathcal{Z}_N(G)$ replaced by $|\phi^q_{z,a}\rangle \in \mathcal{Z}_N(G^\triangle)$.

Lemma 10.6. *The nullspace of $H(G^\triangle, N)$ is $\mathcal{I}_\triangle$ as defined in equation (10.22). Its smallest nonzero eigenvalue is*

$$\gamma(H(G^\triangle, N)) > \frac{1}{(17R)^7}. \tag{10.23}$$

In addition to Fact 10.5, we use the following simple fact in the proof of the lemma.

Fact 10.7. *Let $|p\rangle = c|\alpha_0\rangle + \sqrt{1-c^2}|\alpha_1\rangle$ with $\langle\alpha_i|\alpha_j\rangle = \delta_{ij}$ and $c \in [0,1]$. Then*

$$|p\rangle\langle p| = c^2|\alpha_0\rangle\langle\alpha_0| + M$$

where $\|M\| \leq 1 - (3/4)c^4$.

To prove this fact, one can calculate

$$\|M\| = \frac{1}{2}(1-c^2) + \frac{1}{2}\sqrt{1 + 2c^2 - 3c^4}$$

and use the inequality $\sqrt{1+x} \leq 1 + x/2$ for $x \geq -1$.

Proof of Lemma 10.6. Using equation (10.14) and the fact that the smallest eigenvalues of $A(G^\diamondsuit)$ and $A(G^\triangle)$ are the same (equal to e_1, from Section 10.2 and Lemma 10.3), we have

$$H(G^\triangle, N) = H(G^\diamondsuit, N) + \sum_{w=1}^{N} h^{(w)}_{\mathcal{E}^\triangle}\Big|_{\mathcal{Z}_N(G^\triangle)}. \tag{10.24}$$

Recall from Lemma 10.2 that the nullspace of $H(G^\diamondsuit, N)$ is $\mathcal{I}_\diamondsuit$. We consider

$$\sum_{w=1}^{N} h^{(w)}_{\mathcal{E}^\triangle}\Big|_{\mathcal{I}_\diamondsuit}. \tag{10.25}$$

We show that its nullspace is equal to $\mathcal{I}_\triangle$ (establishing the first part of the lemma), and we lower bound its smallest nonzero eigenvalue. Specifically, we prove

$$\gamma\left(\sum_{w=1}^{N} h^{(w)}_{\mathcal{E}^\triangle}\Big|_{\mathcal{I}_\diamondsuit}\right) > \frac{1}{(9R)^6}. \tag{10.26}$$

Now we prove equation (10.23) using this bound. We apply the Nullspace Projection Lemma (Lemma 8.1) with H_A and H_B given by the first and second terms in equation (10.24); in this case the nullspace of H_A is $S = \mathcal{I}_\diamondsuit$ (from Lemma 10.2). Now applying Lemma 8.1 and using the bounds

$\gamma(H_A) > 1/300$ (from Lemma 10.2), $\|H_B\| \leq N\|h_{\mathcal{E}^\triangle}\| = 2N \leq 2R$ (from equation (5.8) and the fact that $N \leq R$), and the bound (10.26) on $\gamma(H_B|_S)$, we find

$$\gamma(H(G^\triangle, N)) \geq \frac{\frac{1}{300(9R)^6}}{\frac{1}{300} + \frac{1}{(9R)^6} + 2R} \geq \left(\frac{1}{9^6 + 300 + 600 \cdot 9^6}\right) \frac{1}{R^7} > \frac{1}{(17R)^7}.$$

To complete the proof we must establish that the nullspace of (10.25) is $\mathcal{I}_\triangle$ and prove the lower bound (10.26). To analyze (10.25) we use the fact (established in Section 10.3) that (10.15) is block diagonal with a block $\mathcal{W}_{(z,a,q)} \subset \mathcal{W}$ for each triple (z,a,q) with $z,a \in \{0,1\}$ and $q \in [R]$. The operator (10.25) inherits a block structure from this fact. For any basis vector

$$\mathrm{Sym}(|\psi^{q_1}_{z_1,a_1}\rangle |\psi^{q_2}_{z_2,a_2}\rangle \ldots |\psi^{q_N}_{z_N,a_N}\rangle) \in \mathcal{I}_\diamondsuit, \tag{10.27}$$

we define a set of occupation numbers

$$\mathcal{N} = \left\{N_{(x,b,r)} : x,b \in \{0,1\}, r \in [R]\right\}$$

where

$$N_{(x,b,r)} = |\{j : |\psi^{q_j}_{z_j,a_j}\rangle \in \mathcal{W}_{(x,b,r)}\}|.$$

Now observe that (10.25) conserves the set of occupation numbers and is therefore block diagonal with a block for each possible set $\mathcal{N}$.

For a given block corresponding to a set of occupation numbers $\mathcal{N}$, we write $\mathcal{I}_\diamondsuit(\mathcal{N}) \subset \mathcal{I}_\diamondsuit$ for the subspace spanned by basis vectors (10.27) in the block. We classify the blocks into three categories depending on $\mathcal{N}$.

Classification of the blocks of (10.25) according to $\mathcal{N}$ Consider the following two conditions on a set $\mathcal{N} = \{N_{(x,b,r)} : x,b \in \{0,1\}, r \in [R]\}$ of occupation numbers:

(a) $N_{(x,b,r)} \in \{0,1\}$ for all $x,b \in \{0,1\}$ and $r \in [R]$. If this holds, write (y_i, c_i, s_i) for the nonzero occupation numbers (with some arbitrary ordering), i. e., $N_{(y_i,c_i,s_i)} = 1$ for $i \in [N]$.

(b) The sets $\mathcal{W}_{(y_i,c_i,s_i)}$ and $\mathcal{W}_{(y_j,c_j,s_j)}$ do not overlap on a diagram element for all distinct $i,j \in [N]$.

We say a block is of type 1 if $\mathcal{N}$ satisfies (a) and (b). We say it is of type 2 if $\mathcal{N}$ does not satisfy (a). We say it is of type 3 if $\mathcal{N}$ satisfies (a) but does not satisfy (b).

Note that every block is either of type 1, 2, or 3. We consider each type separately. Specifically, we show that each block of type 1 contains one state in the nullspace of (10.25) and, ranging over all blocks of this type, we obtain a basis for $\mathcal{I}_\triangle$. We also show that the smallest nonzero eigenvalue within a block of type 1 is at least $1/(32R^2)$. Finally, we show that blocks of type 2 and 3 do not contain any states in the nullspace of (10.25) and that the smallest eigenvalue within any block of type 2 or 3 is greater than $1/(9R)^6$. Hence, the nullspace of (10.25) is $\mathcal{I}_\triangle$ and its smallest nonzero eigenvalue is lower bounded as in equation (10.26).

Type 1 Note (from Definition 10.4) that (b) implies $q \neq r$ whenever

$$|\psi^q_{x,b}\rangle \in \mathcal{W}_{(y_i,c_i,s_i)} \text{ and } |\psi^r_{z,a}\rangle \in \mathcal{W}_{(y_j,c_j,s_j)}$$

for distinct $i, j \in [N]$. Hence

$$\begin{aligned}\mathcal{I}_\diamondsuit(\mathcal{N}) &= \operatorname{span}\{\operatorname{Sym}(|\psi^{q_1}_{z_1,a_1}\rangle|\psi^{q_2}_{z_2,a_2}\rangle\ldots|\psi^{q_N}_{z_N,a_N}\rangle)\colon q_i \neq q_j \text{ and } |\psi^{q_j}_{z_j,a_j}\rangle \in \mathcal{W}_{(y_j,c_j,s_j)}\}\\ &= \operatorname{span}\{\operatorname{Sym}(|\psi^{q_1}_{z_1,a_1}\rangle|\psi^{q_2}_{z_2,a_2}\rangle\ldots|\psi^{q_N}_{z_N,a_N}\rangle)\colon |\psi^{q_j}_{z_j,a_j}\rangle \in \mathcal{W}_{(y_j,c_j,s_j)}\}\,.\end{aligned}$$

From this we see that

$$\dim(\mathcal{I}_\diamondsuit(\mathcal{N})) = \prod_{j=1}^N \left|\mathcal{W}_{(y_j,c_j,s_j)}\right| = \begin{cases}(3R+2)^N & R \text{ odd}\\ (3R-1)^N & R \text{ even.}\end{cases}$$

We now solve for all the eigenstates of (10.25) within the block.

It is convenient to write an orthonormal basis of eigenvectors of the $|\mathcal{W}_{(z,a,q)}| \times |\mathcal{W}_{(z,a,q)}|$ matrix described by Figure 10.5(A) as

$$|\phi^q_{z,a}(u)\rangle\,, \quad u \in [|\mathcal{W}_{(z,a,q)}|]\,, \tag{10.28}$$

and their ordered eigenvalues as

$$\theta_1 \leq \theta_2 \leq \ldots \leq \theta_{|\mathcal{W}_{(z,a,q)}|}\,.$$

From the proof of Lemma 10.3, the eigenvector with smallest eigenvalue $\theta_1 = 0$ is $|\phi^q_{z,a}\rangle = |\phi^q_{z,a}(1)\rangle$ and $\theta_2 \geq 1/(32R^2)$. For any $u_1, u_2, \ldots, u_N \in [|\mathcal{W}_{(z,a,q)}|]$, the state

$$\operatorname{Sym}(|\phi^{s_1}_{y_1,c_1}(u_1)\rangle|\phi^{s_2}_{y_2,c_2}(u_2)\rangle\ldots|\phi^{s_N}_{y_N,c_N}(u_N)\rangle)$$

is an eigenvector of (10.25) with eigenvalue $\sum_{j=1}^N \theta_j$. Furthermore, states corresponding to different choices of $u_1, \ldots, u_N$ are orthogonal, and ranging over all $\dim(\mathcal{I}_\diamondsuit(\mathcal{N}))$ choices we get every eigenvector in the block. The smallest eigenvalue within the block is $N\theta_1 = 0$ and there is a unique vector in the nullspace, given by

$$\operatorname{Sym}(|\phi^{s_1}_{y_1,c_1}\rangle|\phi^{s_2}_{y_2,c_2}\rangle\ldots|\phi^{s_N}_{y_N,c_N}\rangle) \tag{10.29}$$

(recall $|\phi^q_{z,a}\rangle = |\phi^q_{z,a}(1)\rangle$). The smallest nonzero eigenvalue of (10.25) within the block is

$$(N-1)\theta_1 + \theta_2 = \theta_2 \geq \frac{1}{32R^2}\,.$$

Finally, we show that the collection of states (10.29) obtained from all blocks of type 1 spans the space $\mathcal{I}_\triangle$. Each block of type 1 corresponds to a set of occupation numbers

$$N_{(y_1,c_1,s_1)} = N_{(y_2,c_2,s_2)} = \cdots = N_{(y_N,c_N,s_N)} = 1 \quad \text{(with all other occupation numbers zero)}$$

and gives a unique vector (10.29) in the nullspace of $H(G^\triangle, N)$. The sets $\mathcal{W}_{(y_i,c_i,s_i)}$ and $\mathcal{W}_{(y_j,c_j,s_j)}$ do not overlap on a diagram element for all distinct $i, j \in [N]$. Using Fact 10.5 we see this is equivalent to $s_i \neq s_j$ and $\{s_i, s_j\} \notin E(G^{\text{occ}})$ for distinct $i, j \in [N]$. Hence the set of states (10.29) obtained from of all blocks of type 1 is

$$\left\{\operatorname{Sym}(|\phi^{s_1}_{y_1,c_1}\rangle|\phi^{s_2}_{y_2,c_2}\rangle\ldots|\phi^{s_N}_{y_N,c_N}\rangle)\colon y_i, c_i \in \{0,1\},\, s_i \in [R],\, s_i \neq s_j,\, \{s_i,s_j\} \notin E(G^{\text{occ}})\right\}$$

which spans $\mathcal{I}_\triangle$.

Type 2 If $\mathcal{N}$ is of type 2 then there exist $x,b \in \{0,1\}$ and $r \in [R]$ such that $N_{(x,b,r)} \geq 2$. We show there are no eigenvectors in the nullspace of (10.25) within a block of this type and we lower bound the smallest eigenvalue within the block. Specifically, we show

$$\min_{|\kappa\rangle \in \mathcal{I}_\diamondsuit(\mathcal{N})} \langle \kappa | \sum_{w=1}^{N} h^{(w)}_{\mathcal{E}^\triangle} | \kappa \rangle > \frac{1}{(9R)^6}. \tag{10.30}$$

First note that all $|\kappa\rangle \in \mathcal{I}_\diamondsuit$ satisfy $(A(G^\diamondsuit) - e_1)^{(w)} |\kappa\rangle = 0$ for each $w \in [N]$, which can be seen using the definition of $\mathcal{I}_\diamondsuit$ and the fact that $\mathcal{W}$ spans the nullspace of $A(G^\diamondsuit) - e_1$. Using this fact and equation (10.14), we get

$$\min_{|\kappa\rangle \in \mathcal{I}_\diamondsuit(\mathcal{N})} \langle \kappa | \sum_{w=1}^{N} h^{(w)}_{\mathcal{E}^\triangle} | \kappa \rangle = \min_{|\kappa\rangle \in \mathcal{I}_\diamondsuit(\mathcal{N})} \langle \kappa | \sum_{w=1}^{N} \left(A(G^\triangle) - e_1 \right)^{(w)} | \kappa \rangle. \tag{10.31}$$

Now we use the operator inequality

$$\begin{aligned} \sum_{w=1}^{N} \left(A(G^\triangle) - e_1 \right)^{(w)} &\geq \gamma \left(\sum_{w=1}^{N} \left(A(G^\triangle) - e_1 \right)^{(w)} \right) \cdot \left(1 - \Pi^\triangle \right) \\ &= \gamma (A(G^\triangle) - e_1) \cdot \left(1 - \Pi^\triangle \right) > \frac{1}{(30R)^2} \left(1 - \Pi^\triangle \right), \end{aligned} \tag{10.32}$$

where $\Pi^\triangle$ is the projector onto the nullspace of $\sum_{w=1}^{N} \left(A(G^\triangle) - e_1 \right)^{(w)}$, and where in the last step we used Lemma 10.3. Plugging equation (10.32) into equation (10.31) gives

$$\min_{|\kappa\rangle \in \mathcal{I}_\diamondsuit(\mathcal{N})} \langle \kappa | \sum_{w=1}^{N} h^{(w)}_{\mathcal{E}^\triangle} | \kappa \rangle > \frac{1}{(30R)^2} \left(1 - \max_{|\kappa\rangle \in \mathcal{I}_\diamondsuit(\mathcal{N})} \langle \kappa | \Pi^\triangle | \kappa \rangle \right). \tag{10.33}$$

In the following we show that $\langle \kappa | \Pi^\triangle | \kappa \rangle = \langle \kappa | \Pi^\triangle_{\mathcal{N}} | \kappa \rangle$ for all $|\kappa\rangle \in \mathcal{I}_\diamondsuit(\mathcal{N})$, where $\Pi^\triangle_{\mathcal{N}}$ is a Hermitian operator with

$$1 - \left\| \Pi^\triangle_{\mathcal{N}} \right\| \geq \frac{3}{4} \left(\frac{1}{4R} \right)^4 = \frac{3}{1024 R^4}. \tag{10.34}$$

Plugging this into (10.33) gives

$$\min_{|\kappa\rangle \in \mathcal{I}_\diamondsuit(\mathcal{N})} \langle \kappa | \sum_{w=1}^{N} h^{(w)}_{\mathcal{E}^\triangle} | \kappa \rangle > \frac{3}{(30R)^2 \cdot 1024 R^4} > \frac{1}{(9R)^6}.$$

To complete the proof, we exhibit the operator $\Pi^\triangle_{\mathcal{N}}$ and show that its norm is bounded as (10.34). Using Lemma 10.3 we can write $\Pi^\triangle$ explicitly as

$$\Pi^\triangle = \sum_{(\vec{z},\vec{a},\vec{q}) \in \Omega} \mathcal{P}_{(\vec{z},\vec{a},\vec{q})} \tag{10.35}$$

where

$$\begin{aligned} \mathcal{P}_{(\vec{z},\vec{a},\vec{q})} &= |\phi^{q_1}_{z_1,a_1}\rangle\langle\phi^{q_1}_{z_1,a_1}| \otimes |\phi^{q_2}_{z_2,a_2}\rangle\langle\phi^{q_2}_{z_2,a_2}| \otimes \cdots \otimes |\phi^{q_N}_{z_N,a_N}\rangle\langle\phi^{q_N}_{z_N,a_N}| \\ \Omega &= \{(z_1,\ldots z_N, a_1,\ldots,a_N,q_1,\ldots,q_N) : z_i,a_i \in \{0,1\} \text{ and } q_i \in [R]\}. \end{aligned}$$

For each $(\vec{z},\vec{a},\vec{q}) \in \mathcal{Q}$ we also define a space

$$S_{(\vec{z},\vec{a},\vec{q})} = \operatorname{span}(\mathcal{W}_{(z_1,a_1,q_1)}) \otimes \operatorname{span}(\mathcal{W}_{(z_2,a_2,q_2)}) \otimes \cdots \otimes \operatorname{span}(\mathcal{W}_{(z_N,a_N,q_N)}).$$

Note that $\mathcal{P}_{(\vec{z},\vec{a},\vec{q})}$ has all of its support in $S_{(\vec{z},\vec{a},\vec{q})}$, and that

$$S_{(\vec{z},\vec{a},\vec{q})} \perp S_{(\vec{z}',\vec{a}',\vec{q}')} \text{ for distinct } (\vec{z},\vec{a},\vec{q}),(\vec{z}',\vec{a}',\vec{q}') \in \mathcal{Q}. \tag{10.36}$$

Therefore $\mathcal{P}_{(\vec{z},\vec{a},\vec{q})}\mathcal{P}_{(\vec{z}',\vec{a}',\vec{q}')} = 0$ for distinct $(\vec{z},\vec{a},\vec{q}),(\vec{z}',\vec{a}',\vec{q}') \in \mathcal{Q}$. (Below we use similar reasoning to obtain a less obvious result.) Note that $\mathcal{P}_{(\vec{z},\vec{a},\vec{q})}$ is orthogonal to $\mathcal{I}_{\diamondsuit}(\mathcal{N})$ unless

$$\left|\left\{j : (z_j,a_j,q_j) = (w,u,v)\right\}\right| = N_{(w,u,v)} \quad \text{for all } w,u \in \{0,1\},\, v \in [R]. \tag{10.37}$$

We restrict our attention to the projectors that are not orthogonal to $\mathcal{I}_{\diamondsuit}(\mathcal{N})$. Letting $\mathcal{Q}(\mathcal{N}) \subset \mathcal{Q}$ be the set of $(\vec{z},\vec{a},\vec{q})$ satisfying equation (10.37), we have

$$\langle\kappa| \sum_{(\vec{z},\vec{a},\vec{q})\in\mathcal{Q}} \mathcal{P}_{(\vec{z},\vec{a},\vec{q})} |\kappa\rangle = \langle\kappa| \sum_{(\vec{z},\vec{a},\vec{q})\in\mathcal{Q}(\mathcal{N})} \mathcal{P}_{(\vec{z},\vec{a},\vec{q})} |\kappa\rangle \quad \text{for all } |\kappa\rangle \in \mathcal{I}_{\diamondsuit}(\mathcal{N}). \tag{10.38}$$

Since $N_{(x,b,r)} \geq 2$, note that in each term $\mathcal{P}_{(\vec{z},\vec{a},\vec{q})}$ with $(\vec{z},\vec{a},\vec{q}) \in \mathcal{Q}(\mathcal{N})$, the operator

$$|\phi^r_{x,b}\rangle\langle\phi^r_{x,b}| \otimes |\phi^r_{x,b}\rangle\langle\phi^r_{x,b}|$$

appears between two of the N registers (tensored with rank-1 projectors on the other $N-2$ registers). Using equation (10.20) we may expand $|\phi^r_{x,b}\rangle$ as a sum of states from $\mathcal{W}_{(x,b,r)}$. This gives

$$|\phi^r_{x,b}\rangle|\phi^r_{x,b}\rangle = c_0|\psi^{r_{\text{in}}}_{x,b}\rangle|\psi^{r_{\text{in}}}_{x,b}\rangle + \left(1-c_0^2\right)^{\frac{1}{2}}|\Phi^r_{x,b}\rangle$$

where c_0 is either $1/(3R+2)$ (if R is odd) or $1/(3R-1)$ (if R is even), and where $|\psi^{r_{\text{in}}}_{x,b}\rangle|\psi^{r_{\text{in}}}_{x,b}\rangle$ is orthogonal to $|\Phi^r_{x,b}\rangle$. Note that each of the states $|\phi^r_{x,b}\rangle|\phi^r_{x,b}\rangle$, $|\psi^{r_{\text{in}}}_{x,b}\rangle|\psi^{r_{\text{in}}}_{x,b}\rangle$, and $|\Phi^r_{x,b}\rangle$ lie in the space

$$\operatorname{span}(\mathcal{W}_{(x,b,r)}) \otimes \operatorname{span}(\mathcal{W}_{(x,b,r)}). \tag{10.39}$$

Now applying Fact 10.7 gives

$$|\phi^r_{x,b}\rangle\langle\phi^r_{x,b}| \otimes |\phi^r_{x,b}\rangle\langle\phi^r_{x,b}| = c_0^2|\psi^{r_{\text{in}}}_{x,b}\rangle\langle\psi^{r_{\text{in}}}_{x,b}| \otimes |\psi^{r_{\text{in}}}_{x,b}\rangle\langle\psi^{r_{\text{in}}}_{x,b}| + M^r_{x,b} \tag{10.40}$$

where $M^r_{x,b}$ is a Hermitian operator with all of its support on the space (10.39) and

$$\left\|M^r_{x,b}\right\| \leq 1 - \frac{3}{4}c_0^4 \leq 1 - \frac{3}{4}\left(\frac{1}{3R+2}\right)^4 \leq 1 - \frac{3}{4}\frac{1}{(4R)^4} \tag{10.41}$$

since $R \geq 2$. For each $(\vec{z},\vec{a},\vec{q}) \in \mathcal{Q}(\mathcal{N})$ we define $\mathcal{P}^M_{(\vec{z},\vec{a},\vec{q})}$ to be the operator obtained from $\mathcal{P}_{(\vec{z},\vec{a},\vec{q})}$ by replacing

$$|\phi^r_{x,b}\rangle\langle\phi^r_{x,b}| \otimes |\phi^r_{x,b}\rangle\langle\phi^r_{x,b}| \mapsto M^r_{x,b}$$

on two of the registers (if $N_{(x,b,r)} > 2$ there is more than one way to do this; we fix one choice for each $(\vec{z},\vec{a},\vec{q}) \in \mathcal{Q}(\mathcal{N})$). Note that $\mathcal{P}^M_{(\vec{z},\vec{a},\vec{q})}$ has all of its support in the space $S_{(\vec{z},\vec{a},\vec{q})}$. Using (10.36) gives

$$\mathcal{P}^M_{(\vec{z},\vec{a},\vec{q})}\mathcal{P}^M_{(\vec{z}',\vec{a}',\vec{q}')} = 0 \text{ for distinct } (\vec{z},\vec{a},\vec{q}),(\vec{z}',\vec{a}',\vec{q}') \in \mathcal{Q}(\mathcal{N}).$$

Using equation (10.40) and the fact that

$$\langle\kappa|\left(|\psi^{r_{\text{in}}}_{x,b}\rangle\langle\psi^{r_{\text{in}}}_{x,b}|^{(w_1)}\right)\left(|\psi^{r_{\text{in}}}_{x,b}\rangle\langle\psi^{r_{\text{in}}}_{x,b}|^{(w_2)}\right)|\kappa\rangle = 0 \quad \text{for all } |\kappa\rangle \in \mathcal{I}_\diamond(\mathcal{N}) \text{ and distinct } w_1,w_2 \in [N]$$

(which can be seen from the definition of $\mathcal{I}_\diamond$), we have

$$\langle\kappa|\mathcal{P}_{(\vec{z},\vec{a},\vec{q})}|\kappa\rangle = \langle\kappa|\mathcal{P}^M_{(\vec{z},\vec{a},\vec{q})}|\kappa\rangle \quad \text{for all } |\kappa\rangle \in \mathcal{I}_\diamond(\mathcal{N}).$$

Hence, letting

$$\Pi^{\triangle}_{\mathcal{N}} = \sum_{(\vec{z},\vec{a},\vec{q})\in\mathcal{Q}(\mathcal{N})} \mathcal{P}^M_{(\vec{z},\vec{a},\vec{q})}, \tag{10.42}$$

we have $\langle\kappa|\Pi^{\triangle}|\kappa\rangle = \langle\kappa|\Pi^{\triangle}_{\mathcal{N}}|\kappa\rangle$ for all $|\kappa\rangle \in \mathcal{I}_\diamond(\mathcal{N})$. To obtain the desired bound (10.34) on the norm of $\Pi^{\triangle}_{\mathcal{N}}$, we use the fact that the norm of a sum of pairwise orthogonal Hermitian operators is upper bounded by the maximum norm of an operator in the sum, so

$$\left\|\Pi^{\triangle}_{\mathcal{N}}\right\| = \left\|\sum_{(\vec{z},\vec{a},\vec{q})\in\mathcal{Q}(\mathcal{N})} \mathcal{P}^M_{(\vec{z},\vec{a},\vec{q})}\right\| = \max_{(\vec{z},\vec{a},\vec{q})\in\mathcal{Q}(\mathcal{N})} \left\|\mathcal{P}^M_{(\vec{z},\vec{a},\vec{q})}\right\| = \left\|M^r_{x,b}\right\| \leq 1 - \frac{3}{4}\frac{1}{(4R)^4}. \tag{10.43}$$

Type 3 If $\mathcal{N}$ is of type 3 then $N_{(x,b,r)} \in \{0,1\}$ for all $x,b \in \{0,1\}$ and $r \in [R]$, and

$$N_{(y,c,s)} = N_{(t,d,u)} = 1$$

for some $(y,c,s) \neq (t,d,u)$ with either $u = s$ or $\{u,s\} \in E(G^{\text{occ}})$ (using property (b) and Fact 10.5). We show there are no eigenvectors in the nullspace of (10.25) within a block of this type and we lower bound the smallest eigenvalue within the block. We establish the same bound (10.30) as for blocks of Type 2.

The proof is very similar to that given above for blocks of Type 2. In fact, the first part of proof is identical, from equation (10.31) up to and including equation (10.38). That is to say, as in the previous case we have

$$\langle\kappa|\sum_{(\vec{z},\vec{a},\vec{q})\in\mathcal{Q}} \mathcal{P}_{(\vec{z},\vec{a},\vec{q})}|\kappa\rangle = \langle\kappa|\sum_{(\vec{z},\vec{a},\vec{q})\in\mathcal{Q}(\mathcal{N})} \mathcal{P}_{(\vec{z},\vec{a},\vec{q})}|\kappa\rangle \quad \text{for all } |\kappa\rangle \in \mathcal{I}_\diamond(\mathcal{N}). \tag{10.44}$$

In this case, since $N_{(y,c,s)} = N_{(t,d,u)} = 1$, in each term $\mathcal{P}_{(\vec{z},\vec{a},\vec{q})}$ with $(\vec{z},\vec{a},\vec{q}) \in \mathcal{Q}(\mathcal{N})$, the operator

$$|\phi^s_{y,c}\rangle\langle\phi^s_{y,c}| \otimes |\phi^u_{t,d}\rangle\langle\phi^u_{t,d}|$$

appears between two of the N registers (tensored with rank 1 projectors on the other $N-2$ registers). Using equation (10.20) we may expand $|\phi^s_{y,c}\rangle$ and $|\phi^u_{t,d}\rangle$ as superpositions (with amplitudes $\pm 1/\sqrt{3R+2}$ if R is odd or $\pm 1/\sqrt{3R-1}$ if R is even) of the basis states from $\mathcal{W}_{(y,c,s)}$ and $\mathcal{W}_{(t,d,u)}$ respectively. Since

$\mathcal{W}_{(y,c,s)}$ and $\mathcal{W}_{(t,d,u)}$ overlap on some diagram element, there exists $l \in L^{\square}$ such that $|\psi^l_{x_1,b_1}\rangle \in \mathcal{W}_{(y,c,s)}$ and $|\psi^l_{x_2,b_2}\rangle \in \mathcal{W}_{(t,d,u)}$ for some $x_1,x_2,b_1,b_2 \in \{0,1\}$. Hence

$$|\phi^s_{y,c}\rangle|\phi^u_{t,d}\rangle = c_0\left(\pm|\psi^l_{x_1,b_1}\rangle|\psi^l_{x_2,b_2}\rangle\right) + \left(1-c_0^2\right)^{\frac{1}{2}}|\Phi^{s,u}_{y,c,t,d}\rangle$$

where c_0 is either $1/(3R+2)$ (if R is odd) or $1/(3R-1)$ (if R is even). Now applying Fact 10.7 we get

$$|\phi^s_{y,c}\rangle\langle\phi^s_{y,c}| \otimes |\phi^u_{t,d}\rangle\langle\phi^u_{t,d}| = c_0^2|\psi^l_{x_1,b_1}\rangle\langle\psi^l_{x_1,b_1}| \otimes |\psi^l_{x_2,b_2}\rangle\langle\psi^l_{x_2,b_2}| + M^{s,u}_{y,c,t,d} \tag{10.45}$$

where

$$\|M^{s,u}_{y,c,t,d}\| \leq 1 - \frac{3}{4}\left(\frac{1}{4R}\right)^4.$$

For each $(\vec{z},\vec{a},\vec{q}) \in \mathcal{Q}(\mathcal{N})$ we define $\mathcal{P}^{M}_{(\vec{z},\vec{a},\vec{q})}$ to be the operator obtained from $\mathcal{P}_{(\vec{z},\vec{a},\vec{q})}$ by replacing

$$|\phi^s_{y,c}\rangle\langle\phi^s_{y,c}| \otimes |\phi^u_{t,d}\rangle\langle\phi^u_{t,d}| \mapsto M^{s,u}_{y,c,t,d}$$

on two of the registers and we let $\Pi^{\triangle}_{\mathcal{N}}$ be given by (10.42). Then, as in the previous case, $\langle\kappa|\Pi^{\triangle}|\kappa\rangle = \langle\kappa|\Pi^{\triangle}_{\mathcal{N}}|\kappa\rangle$ for all $|\kappa\rangle \in \mathcal{I}_{\diamondsuit}(\mathcal{N})$ and using the same reasoning as before, we get the bound (10.34) on $\|\Pi^{\triangle}_{\mathcal{N}}\|$. Using these two facts we get the same bound on the smallest eigenvalue within a block of type 3 as the bound we obtained for blocks of type 2:

$$\min_{|\kappa\rangle\in\mathcal{I}_{\diamondsuit}(\mathcal{N})} \langle\kappa|\sum_{w=1}^{N} h^{(w)}_{\mathcal{E}^{\triangle}}|\kappa\rangle > \frac{1}{(30R)^2}\left(1-\left\|\Pi^{\triangle}_{\mathcal{N}}\right\|\right) > \frac{1}{(9R)^6}. \qquad \square$$

10.5 The gate graph $G^{\square}$

We now consider the gate graph $G^{\square}$ and prove Lemma 5.5. We first show that $G^{\square}$ is an e_1-gate graph. From equations (10.6), (10.7), and (10.8) we have

$$A(G^{\square}) = A(G^{\triangle}) + h_{\mathcal{E}^0} + h_{\mathcal{S}^0}. \tag{10.46}$$

Lemma 10.3 characterizes the e_1-energy ground space of $G^{\triangle}$ and gives an orthonormal basis $\{|\phi^q_{z,a}\rangle : z,a \in \{0,1\}, q \in [R]\}$ for it. To solve for the e_1-energy ground space of $A(G^{\square})$, we solve for superpositions of the states $\{|\phi^q_{z,a}\rangle\}$ in the nullspace of $h_{\mathcal{E}^0} + h_{\mathcal{S}^0}$.

Recall the definition of the sets $\mathcal{E}^0$ and $\mathcal{S}^0$. From Section 10.1, each node (q,z,t) in the gate diagram for G is associated with a node $\mathrm{new}(q,z,t)$ in the gate diagram for $G^{\square}$ as described by (10.1). This mapping is depicted in Figure 10.1 by the black and grey arrows. Applying this mapping to each pair of nodes in the edge set $\mathcal{E}^G$ and each node in the self-loop set $\mathcal{S}^G$ of the gate diagram for G, we get the sets $\mathcal{E}^0$ and $\mathcal{S}^0$. Hence, using equations (5.5) and (5.6),

$$h_{\mathcal{S}^0} = \sum_{(q,z,t)\in\mathcal{S}^G} |\mathrm{new}(q,z,t)\rangle\langle\mathrm{new}(q,z,t)| \otimes 1 \tag{10.47}$$

$$h_{\mathcal{E}^0} = \sum_{\{(q,z,t),(q',z',t')\}\in\mathcal{E}^G} \left(|\mathrm{new}(q,z,t)\rangle + |\mathrm{new}(q',z',t')\rangle\right)\left(\langle\mathrm{new}(q,z,t)| + \langle\mathrm{new}(q',z',t')|\right) \otimes 1. \tag{10.48}$$

Using equation (10.20), we see that for all nodes (q,z,t) in the gate diagram for G and for all $j \in \{0,\dots,7\}$, $x,b \in \{0,1\}$, and $r \in [R]$,

$$\begin{aligned}\langle \mathrm{new}(q,z,t), j | \phi^r_{x,b} \rangle &= \sqrt{c_0} \begin{cases} \langle q_{\mathrm{in}}, z, t, j | \psi^{r_{\mathrm{in}}}_{x,b} \rangle & \text{if } (q,z,t) \text{ is an input node} \\ \langle q_{\mathrm{out}}, z, t, j | \psi^{r_{\mathrm{out}}}_{x,b} \rangle & \text{if } (q,z,t) \text{ is an output node} \end{cases} \\ &= \sqrt{c_0}\, \delta_{r,q} \langle z, t, j | \psi_{x,b} \rangle \end{aligned} \tag{10.49}$$

where c_0 is $1/(3R+2)$ if R is odd or $1/(3R-1)$ if R is even, and where $|\psi_{x,b}\rangle$ is defined by equations (5.2) and (5.3). The matrix element on the left-hand side of this equation is evaluated in the Hilbert space $\mathcal{Z}_1(G^{\square})$ where each basis vector corresponds to a vertex of the graph $G^{\square}$; these vertices are labeled (l,z,t,j) with $l \in L^{\square}$, $z \in \{0,1\}$, $t \in [8]$, and $j \in \{0,\dots,7\}$. However, from (10.49) we see that

$$\underbrace{\langle \mathrm{new}(q,z,t), j | \phi^r_{x,b} \rangle}_{\text{in } \mathcal{Z}_1(G^{\square})} = \sqrt{c_0}\, \underbrace{\langle q,z,t,j | \psi^r_{x,b} \rangle}_{\text{in } \mathcal{Z}_1(G)} \tag{10.50}$$

where the right-hand side is evaluated in the Hilbert space $\mathcal{Z}_1(G)$.

Putting together equations (10.47), (10.48), and (10.50) gives

$$\langle \phi^q_{z,a} | h_{\mathcal{E}^0} + h_{\mathcal{S}^0} | \phi^r_{x,b} \rangle = \langle \psi^q_{z,a} | h_{\mathcal{E}^G} + h_{\mathcal{S}^G} | \psi^r_{x,b} \rangle \cdot \begin{cases} \frac{1}{3R+2} & R \text{ odd} \\ \frac{1}{3R-1} & R \text{ even} \end{cases} \tag{10.51}$$

for all $z,a,x,b \in \{0,1\}$ and $q,r \in [R]$. On the left-hand side of this equation, the Hilbert space is $\mathcal{Z}_1(G^{\square})$; on the right-hand side it is $\mathcal{Z}_1(G)$.

We use equation (10.51) to relate the e_1-energy ground states of $A(G)$ to those of $A(G^{\square})$. Since G is an e_1-gate graph, there is a state

$$|\Gamma\rangle = \sum_{z,a,q} \alpha_{z,a,q} |\psi^q_{z,a}\rangle \in \mathcal{Z}_1(G)$$

that satisfies $A(G)|\Gamma\rangle = e_1|\Gamma\rangle$ and hence $h_{\mathcal{E}^G}|\Gamma\rangle = h_{\mathcal{S}^G}|\Gamma\rangle = 0$. Letting

$$|\Gamma'\rangle = \sum_{z,a,q} \alpha_{z,a,q} |\phi^q_{z,a}\rangle \in \mathcal{Z}_1(G^{\square})$$

and using equation (10.51), we see that $\langle \Gamma' | h_{\mathcal{E}^0} + h_{\mathcal{S}^0} | \Gamma' \rangle = 0$ and therefore $\langle \Gamma' | A(G^{\square}) | \Gamma' \rangle = e_1$. Hence $G^{\square}$ is an e_1-gate graph. Moreover, the linear mapping from $\mathcal{Z}_1(G)$ to $\mathcal{Z}_1(G^{\square})$ defined by

$$|\psi^q_{z,a}\rangle \mapsto |\phi^q_{z,a}\rangle \tag{10.52}$$

maps each e_1-energy eigenstate of $A(G)$ to an e_1-energy eigenstate of $A(G^{\square})$.

Now consider the N-particle Hamiltonian $H(G^{\square},N)$. Using equation (10.46) and the fact that both $A(G^{\square})$ and $A(G^{\triangle})$ have smallest eigenvalue e_1, we have

$$H(G^{\square},N) = H(G^{\triangle},N) + \sum_{w=1}^{N} (h_{\mathcal{E}^0} + h_{\mathcal{S}^0})^{(w)} \Big|_{\mathcal{Z}_N(G^{\square})}.$$

Recall from Lemma 10.3 that the nullspace of the first term is $\mathcal{I}_\triangle$. The N-fold tensor product of the mapping (10.52) acts on basis vectors of $\mathcal{I}(G,G^{\mathrm{occ}},N)$ as

$$\mathrm{Sym}(|\psi^{q_1}_{z_1,a_1}\rangle|\psi^{q_2}_{z_2,a_2}\rangle\ldots|\psi^{q_N}_{z_N,a_N}\rangle)\mapsto\mathrm{Sym}(|\phi^{q_1}_{z_1,a_1}\rangle|\phi^{q_2}_{z_2,a_2}\rangle\ldots|\phi^{q_N}_{z_N,a_N}\rangle)\,, \tag{10.53}$$

where $z_i,a_i\in\{0,1\}$, $q_i\neq q_j$, and $\{q_i,q_j\}\notin E(G^{\mathrm{occ}})$. Clearly this defines an invertible linear map between the two spaces $\mathcal{I}(G,G^{\mathrm{occ}},N)$ and $\mathcal{I}_\triangle$. Let $|\Theta\rangle\in\mathcal{I}(G,G^{\mathrm{occ}},N)$ and write $|\Theta'\rangle\in\mathcal{I}_\triangle$ for its image under the map (10.53). Then

$$\langle\Theta'|H(G^{\square},N)|\Theta'\rangle=\langle\Theta'|\sum_{w=1}^{N}\left(h_{\mathcal{E}^0}+h_{\mathcal{S}^0}\right)^{(w)}|\Theta'\rangle=\langle\Theta|\sum_{w=1}^{N}\left(h_{\mathcal{E}^G}+h_{\mathcal{S}^G}\right)^{(w)}|\Theta\rangle\cdot\begin{cases}\frac{1}{3R+2} & R\text{ odd}\\ \frac{1}{3R-1} & R\text{ even}\end{cases} \tag{10.54}$$

where in the first equality we used the fact that $|\Theta'\rangle$ is in the nullspace $\mathcal{I}_\triangle$ of $H(G^{\triangle},N)$ and in the second equality we used equation (10.51) and the fact that $\langle\phi^q_{z,a}|\phi^r_{x,b}\rangle=\langle\psi^q_{z,a}|\psi^r_{x,b}\rangle$. We now complete the proof of Lemma 5.5 using equation (10.54).

Case 1: $\lambda_N(G,G^{\mathrm{occ}})\leq a$**.**

In this case there exists a state $|\Theta\rangle\in\mathcal{I}(G,G^{\mathrm{occ}},N)$ satisfying

$$\langle\Theta|\sum_{w=1}^{N}\left(h_{\mathcal{E}^G}+h_{\mathcal{S}^G}\right)^{(w)}|\Theta\rangle\leq a\,.$$

From equation (10.54) we see that the state $|\Theta'\rangle\in\mathcal{I}_\triangle$ satisfies

$$\langle\Theta'|H(G^{\square},N)|\Theta'\rangle\leq\frac{a}{3R-1}\leq\frac{a}{R}\,.$$

Case 2: $\lambda_N(G,G^{\mathrm{occ}})\geq b$**.**

In this case

$$\lambda_N(G,G^{\mathrm{occ}})=\min_{|\Theta\rangle\in\mathcal{I}(G,G^{\mathrm{occ}},N)}\langle\Theta|H(G,G^{\mathrm{occ}},N)|\Theta\rangle=\min_{|\Theta\rangle\in\mathcal{I}(G,G^{\mathrm{occ}},N)}\langle\Theta|\sum_{w=1}^{N}\left(h_{\mathcal{E}^G}+h_{\mathcal{S}^G}\right)^{(w)}|\Theta\rangle\geq b\,.$$

Now applying equation (10.54) gives

$$\min_{|\Theta'\rangle\in\mathcal{I}_\triangle}\langle\Theta'|H(G^{\square},N)|\Theta'\rangle=\min_{|\Theta'\rangle\in\mathcal{I}_\triangle}\langle\Theta'|\sum_{w=1}^{N}\left(h_{\mathcal{E}^0}+h_{\mathcal{S}^0}\right)^{(w)}|\Theta'\rangle\geq\frac{1}{3R+2}b\,. \tag{10.55}$$

This establishes that the nullspace of $H(G^{\square},N)$ is empty, i. e., $\lambda_N^1(G^{\square})>0$, so $\lambda_N^1(G^{\square})=\gamma(H(G^{\square},N))$. We lower bound $\lambda_N^1(G^{\square})$ using the Nullspace Projection Lemma (Lemma 8.1) with

$$H_A=H(G^{\triangle},N)\,,\qquad H_B=\sum_{w=1}^{N}\left(h_{\mathcal{E}^0}+h_{\mathcal{S}^0}\right)^{(w)}\Big|_{\mathcal{Z}_N(G^{\square})}\,,$$

and where the nullspace of H_A is $S = \mathcal{I}_\triangle$. We apply Lemma 8.1 and use the bounds $\gamma(H_A) > 1/(17R)^7$ (from Lemma 10.6), $\gamma(H_B|_S) \geq b/(3R+2)$ (from equation (10.55)), and $\|H_B\| \leq N\|h_{\mathcal{E}^0} + h_{\mathcal{S}^0}\| \leq 3N \leq 3R$ (using equations (5.8) and (5.7) and the fact that $N \leq R$) to find

$$\begin{aligned}\lambda_N^1(G^\square) &= \gamma(H(G^\square, N)) \\ &\geq \frac{b}{(3R+2)(17R)^7(\frac{1}{(17R)^7} + \frac{b}{3R+2} + 3R)} \\ &\geq \frac{b}{R^9} \cdot \frac{1}{3+2+b\cdot(17)^7 + 3\cdot(3+2)\,(17)^7} \\ &> \frac{b}{(13R)^9}\end{aligned}$$

where in the denominator we used the fact that $b \leq 1$.

Acknowledgments

This work was supported in part by NSERC; the Ontario Ministry of Research and Innovation; the Ontario Ministry of Training, Colleges, and Universities; and the US ARO.

A Technical supporting material

A.1 Proof of the Nullspace Projection Lemma

The following proof fills in the details of the argument given in reference [25]. Recall that we write $\gamma(M)$ for the smallest nonzero eigenvalue of a positive semidefinite matrix M.

Lemma A.1 (Nullspace Projection Lemma [25]). *Let $H_A, H_B \geq 0$. Suppose the nullspace S of H_A is non-empty and*

$$\gamma(H_B|_S) \geq c > 0 \qquad \text{and} \qquad \gamma(H_A) \geq d > 0\,.$$

Then

$$\gamma(H_A + H_B) \geq \frac{cd}{c + d + \|H_B\|}\,. \tag{8.1}$$

Proof. Let $|\psi\rangle$ be a normalized state satisfying

$$\langle\psi|H_A + H_B|\psi\rangle = \gamma(H_A + H_B)\,.$$

Let Π_S be the projector onto the nullspace of H_A. First suppose that $\Pi_S|\psi\rangle = 0$, in which case

$$\langle\psi|H_A + H_B|\psi\rangle \geq \langle\psi|H_A|\psi\rangle \geq \gamma(H_A)$$

and the result follows. On the other hand, if $\Pi_S|\psi\rangle \neq 0$ then we can write

$$|\psi\rangle = \alpha|a\rangle + \beta|a^\perp\rangle$$

with $|\alpha|^2+|\beta|^2=1$, $\alpha\neq 0$, and two normalized states $|a\rangle$ and $|a^\perp\rangle$ such that $|a\rangle\in S$ and $|a^\perp\rangle\in S^\perp$. (If $\beta=0$ then we may choose $|a^\perp\rangle$ to be an arbitrary state in $S^\perp$ but in the following we fix one specific choice for concreteness.) Note that any state $|\phi\rangle$ in the nullspace of H_A+H_B satisfies $H_A|\phi\rangle=0$ and hence $\langle\phi|a^\perp\rangle=0$. Since $\langle\phi|\psi\rangle=0$ and $\alpha\neq 0$ we also see that $\langle\phi|a\rangle=0$. Hence any state

$$|f(q,r)\rangle = q|a\rangle + r|a^\perp\rangle$$

is orthogonal to the nullspace of H_A+H_B, and

$$\gamma(H_A+H_B) = \min_{|q|^2+|r|^2=1} \langle f(q,r)|H_A+H_B|f(q,r)\rangle\,.$$

The operator H_A+H_B acts on the two-dimensional space spanned by $|a\rangle$ and $|a^\perp\rangle$ as the matrix

$$\begin{pmatrix} w & v^* \\ v & y+z \end{pmatrix}$$

where $w=\langle a|H_B|a\rangle$, $v=\langle a^\perp|H_B|a\rangle$, $y=\langle a^\perp|H_A|a^\perp\rangle$, and $z=\langle a^\perp|H_B|a^\perp\rangle$. The smallest eigenvalue of this matrix is

$$\gamma(H_A+H_B) = \frac{w+y+z-\sqrt{(w+y+z)^2+4\,(|v|^2-wy-wz)}}{2}\,.$$

Since H_B is positive semidefinite, its principal minors are nonnegative, and in particular $wz-|v|^2\geq 0$. Using this inequality in the above gives

$$\gamma(H_A+H_B) \geq \frac{w+y+z}{2}\left(1-\sqrt{1-\frac{4wy}{(w+y+z)^2}}\right) \geq \frac{wy}{w+y+z} = \frac{1}{\frac{1}{w}+\frac{1}{y}+\frac{z}{wy}} \tag{A.1}$$

where in the second step we used the fact that $\sqrt{1-x}\leq 1-x/2$ for $x\in[0,1]$. Since $|a\rangle$ is orthogonal to the nullspace of H_A+H_B, we have

$$w\geq \gamma(H_B|_S)\geq c\,.$$

We also have $y\geq\gamma(H_A)\geq d$ and $z\leq\|H_B\|$. Since the right-hand side of (A.1) increases monotonically with w and y and decreases monotonically with z, we find

$$\gamma(H_A+H_B)\geq\frac{cd}{c+d+\|H_B\|}$$

as claimed. □

A.2 Proof of Lemma 8.7

Here we prove Lemma 8.7. We begin with the following lemma relating the occupancy constraints graph G_X^{occ} to the illegal configurations. The proof of this lemma uses the definitions of a configuration (Definition 8.3), the sets of legal and illegal configurations (from Section 8.3), and the occupancy constraints graph G_X^{occ} (from Section 7.3).

Lemma A.2. *For any illegal configuration*

$$(J_1,\dots,J_Y,L_1,\dots,L_{n-2Y}) \tag{A.2}$$

there exist diagram elements $\{Q_1,Q_2\}\in E(G_X^{\mathrm{occ}})$ *satisfying at least one of the following conditions:*

(i) $Q_1=(1,J_k,0)$ *and* $Q_2=(1,J_l,0)$ *for some* $k,l\in[Y]$.

(ii) $Y\in\{0,1\}$, $Q_1=L_s$, *and* $Q_2=L_t$ *for some* $s,t\in[n-2Y]$.

(iii) $Y=1$ *and* $Q_1=(i,J_1,d)$ *and* $Q_2=L_t$ *for some* $i\in\{1,s(J_1)\}$, $t\in[n-2]$ *and* $d\in\{0,1\}$.

Proof. We prove the contrapositive: we suppose the configuration (A.2) violates each of the conditions (i), (ii), and (iii) for all $\{Q_1,Q_2\}\in E(G_X^{\mathrm{occ}})$ and show it is a legal configuration.

From part (1) of the definition of the occupancy constraints graph in Section 7.3, we see that

$$\{(1,j,0),(1,k,0)\}\in E(G_X^{\mathrm{occ}})$$

for all $j,k\in[M]$ with $j\neq k$. If the configuration (A.2) has $Y\geq 2$, then we may choose $Q_1=(1,J_1,0)$ and $Q_2=(1,J_2,0)$ so that $\{Q_1,Q_2\}\in E(G_X^{\mathrm{occ}})$ and condition (i) is satisfied (note $J_1\neq J_2$ follows from the definition of a configuration). Since by assumption, (A.2) violates condition (i) for all $\{Q_1,Q_2\}\in E(G_X^{\mathrm{occ}})$, this implies that $Y\in\{0,1\}$. We consider the cases $Y=0$ and $Y=1$ separately.

First suppose $Y=0$, so (A.2) is equal to

$$(L_1,\dots,L_n).$$

Since (ii) is violated, $\{L_s,L_t\}\notin E(G_X^{\mathrm{occ}})$ for all $s,t\in[n]$. Using part (1) of the definition of G_X^{occ} and the definition of a configuration, this implies that each diagram element is in a different row, i. e., $L_i=(i,j_i,c_i)$ for each $i\in[n]$. From part (2) of the definition of G_X^{occ}, we see in particular that $\{L_1,L_t\}\notin E(G_X^{\mathrm{occ}})$ for each $t\in\{2,\dots,n\}$ implies

$$L_{s(j_1)}=(s(j_1),j_1,c_1)\quad\text{and}\quad L_i=F(i,j_1,d_i)$$

for $i\in[n]\setminus\{1,s(j_1)\}$ and bits $d_2,\dots,d_n\in\{0,1\}$, i. e., the configuration is legal.

Now suppose $Y=1$, so (A.2) is

$$(J_1,L_1,\dots,L_{n-2}).$$

Since (ii) is violated, each L_i for $i\in[n-2]$ is from a different row. Since (iii) is violated, none of these diagram elements are in rows 1 or $s(J_1)$. Now applying part (2) of the definition of G_X^{occ}, we see that the configuration is legal:

$$\begin{aligned}&(J_1,L_1,\dots,L_{n-2})\\&\quad=(J_1,F(2,J_1,d_2),\dots,F(s(J_1)-1,J_1,d_{s(J_1)-1}),F(s(J_1)+1,J_1,d_{s(J_1)+1}),\dots,F(n,J_1,d_n))\end{aligned}$$

where $d_i\in\{0,1\}$ for $i\in[n]\setminus\{1,s(J_1)\}$. □

Lemma A.3. *Let Π_0 be the projector onto $\mathcal{I}(G_1, G_X^{\mathrm{occ}}, n)$. For any $|j,\vec{d},\vec{z},\vec{a}\rangle \in \mathcal{B}_{\mathrm{legal}}$, we have*

$$\Pi_0 |j,\vec{d},\vec{z},\vec{a}\rangle = |j,\vec{d},\vec{z},\vec{a}\rangle. \tag{8.20}$$

Furthermore, for any two distinct basis vectors $|\phi\rangle, |\psi\rangle \in \mathcal{B}_{\mathrm{illegal}}$, we have

$$\langle\phi|\Pi_0|\phi\rangle \leq \frac{255}{256} \tag{8.21}$$

$$\langle\phi|\Pi_0|\psi\rangle = 0\,. \tag{8.22}$$

Proof. We begin with equation (8.20). Recall from (5.21) that

$$\mathcal{I}(G_1, G_X^{\mathrm{occ}}, n) = \mathrm{span}\{\mathrm{Sym}(|\psi^{q_1}_{z_1,a_1}\rangle|\psi^{q_2}_{z_2,a_2}\rangle \ldots |\psi^{q_n}_{z_n,a_n}\rangle)\colon z_i, a_i \in \{0,1\},\ q_i \neq q_j, \text{ and } \{q_i,q_j\} \notin E(G_X^{\mathrm{occ}})\}$$

which can alternatively be characterized as the subspace of

$$\mathcal{I}(G_1, n) = \mathrm{span}\{\mathrm{Sym}(|\psi^{q_1}_{z_1,a_1}\rangle|\psi^{q_2}_{z_2,a_2}\rangle \ldots |\psi^{q_n}_{z_n,a_n}\rangle)\colon z_i, a_i \in \{0,1\},\ q_i \neq q_j\}$$

consisting of zero eigenvectors of each of the operators

$$|\psi^q_{s,t}\rangle\langle\psi^q_{s,t}| \otimes |\psi^r_{u,v}\rangle\langle\psi^r_{u,v}| \otimes 1^{\otimes n-2}, \qquad \{q,r\} \in E(G_X^{\mathrm{occ}}), \quad s,t,u,v \in \{0,1\}\,. \tag{A.3}$$

Now using equation (8.18) and the fact that

$$\langle\psi^{\tilde{L}}_{x,b}|\rho^L_{z,a}\rangle = \frac{1}{\sqrt{8}}\delta_{\tilde{L},L}\delta_{x,z}\delta_{a,b} = \frac{1}{\sqrt{8}}\langle\rho^{\tilde{L}}_{x,b}|\rho^L_{z,a}\rangle \tag{A.4}$$

for all $x,z,a,b \in \{0,1\}$ and $\tilde{L}, L \in \mathcal{L}$ (from equations (6.13)–(6.16), and (6.36)), we get

$$\begin{aligned}
&\langle j,\vec{d},\vec{z},\vec{a}| \left(|\psi^q_{s,t}\rangle\langle\psi^q_{s,t}| \otimes |\psi^r_{u,v}\rangle\langle\psi^r_{u,v}| \otimes 1^{\otimes n-2}\right) |j,\vec{d},\vec{z},\vec{a}\rangle \\
&\quad = \frac{1}{64}\langle j,\vec{d},\vec{z},\vec{a}| \left(|\rho^q_{s,t}\rangle\langle\rho^q_{s,t}| \otimes |\rho^r_{u,v}\rangle\langle\rho^r_{u,v}| \otimes 1^{\otimes n-2}\right) |j,\vec{d},\vec{z},\vec{a}\rangle \\
&\quad = 0 \quad \text{if } \{q,r\} \in E(G_X^{\mathrm{occ}})\,.
\end{aligned}$$

In the last line we used equations (8.12) and (8.18) and the definition of the occupancy constraints graph G_X^{occ} from Section 7.3. Hence each legal state $|j,\vec{d},\vec{z},\vec{a}\rangle \in \mathcal{I}(G_1,n)$ is a zero eigenvector of each of the operators (A.3), so $|j,\vec{d},\vec{z},\vec{a}\rangle \in \mathcal{I}(G_1, G_X^{\mathrm{occ}}, n)$. This gives equation (8.20).

Now we prove equation (8.21). For each illegal configuration we associate two diagram elements Q_1 and Q_2 with $(Q_1,Q_2) \in E(G_X^{\mathrm{occ}})$ as in Lemma A.2 (if there is more than one such pair we fix a specific choice). Likewise for each basis vector $|\phi\rangle \in \mathcal{B}_{\mathrm{illegal}}$ we associate the two diagram elements Q_1 and Q_2 corresponding to its (illegal) configuration. Let P_ϕ be the projector onto the space

$$\mathrm{span}\{\mathrm{Sym}(|\psi^{Q_1}_{z_1,a_1}\rangle|\psi^{Q_2}_{z_2,a_2}\rangle|\psi^{q_3}_{z_3,a_3}\rangle \ldots |\psi^{q_n}_{z_n,a_n}\rangle)\colon z_i, a_i \in \{0,1\},\ q_i \notin \{Q_1,Q_2\}\}$$

where (exactly) one particle is located at Q_1 and (exactly) one particle is located at Q_2. We show that

$$\langle\phi|P_\phi|\phi\rangle \geq \frac{1}{256}\,. \tag{A.5}$$

Note that $\Pi_0 P_\phi = 0$ since Π_0 projects onto a subspace for which no two (or more) particles are simultaneously located at Q_1 and Q_2. Therefore

$$\langle\phi|\Pi_0|\phi\rangle + \langle\phi|P_\phi|\phi\rangle \leq 1\,,$$

and applying (A.5) gives (8.20). Equation (A.5) can be shown by considering cases (i), (ii), and (iii) from Lemma A.2. It is convenient to define

$$\Pi_{Q_1} = \sum_{x,y\in\{0,1\}} |\psi^{Q_1}_{x,y}\rangle\langle\psi^{Q_1}_{x,y}|\,, \qquad\qquad \Pi_{Q_2} = \sum_{x,y\in\{0,1\}} |\psi^{Q_2}_{x,y}\rangle\langle\psi^{Q_2}_{x,y}|\,.$$

In case (i) we have $Q_1 = (1, J_k, 0)$ and $Q_2 = (1, J_l, 0)$ for some $k, l \in [Y]$. Here we consider the case $k = 1, l = 2$ without loss of generality. Then

$$\begin{aligned} P_\phi|\phi\rangle &= \mathrm{Sym}\left(P_\phi(|T^{J_1}_{z_1,a_1,z_2,a_2}\rangle|T^{J_2}_{z_3,a_3,z_4,a_4}\rangle\ldots|T^{J_Y}_{z_{2Y-1},a_{2Y-1},z_{2Y},a_{2Y}}\rangle|\rho^{L_1}_{z_{2Y+1},a_{2Y+1}}\rangle\ldots|\rho^{L_{n-2Y}}_{z_n,a_n}\rangle)\right) \\ &= \mathrm{Sym}\left((\Pi_{Q_1}\otimes 1)|T^{J_1}_{z_1,a_1,z_2,a_2}\rangle(\Pi_{Q_2}\otimes 1)|T^{J_2}_{z_3,a_3,z_4,a_4}\rangle\ldots|T^{J_Y}_{z_{2Y-1},a_{2Y-1},z_{2Y},a_{2Y}}\rangle|\rho^{L_1}_{z_{2Y+1},a_{2Y+1}}\rangle\ldots|\rho^{L_{n-2Y}}_{z_n,a_n}\rangle\right) \end{aligned} \tag{A.6}$$

for some configuration and some $\vec{z}, \vec{a}$, where in the first line we used the fact that P_ϕ commutes with any permutation of the n registers and in the second line we used the fact that

$$\begin{aligned} \Pi^{(w)}_{Q_1}|T^{J_1}_{z_1,a_1,z_2,a_2}\rangle|T^{J_2}_{z_3,a_3,z_4,a_4}\rangle\ldots|T^{J_Y}_{z_{2Y-1},a_{2Y-1},z_{2Y},a_{2Y}}\rangle|\rho^{L_1}_{z_{2Y+1},a_{2Y+1}}\rangle\ldots|\rho^{L_{n-2Y}}_{z_n,a_n}\rangle &= 0 \text{ unless } w = 1 \\ \Pi^{(w)}_{Q_2}|T^{J_1}_{z_1,a_1,z_2,a_2}\rangle|T^{J_2}_{z_3,a_3,z_4,a_4}\rangle\ldots|T^{J_Y}_{z_{2Y-1},a_{2Y-1},z_{2Y},a_{2Y}}\rangle|\rho^{L_1}_{z_{2Y+1},a_{2Y+1}}\rangle\ldots|\rho^{L_{n-2Y}}_{z_n,a_n}\rangle &= 0 \text{ unless } w = 3. \end{aligned}$$

We find

$$\begin{aligned} \langle\phi|P_\phi|\phi\rangle &= \langle T^{J_1}_{z_1,a_1,z_2,a_2}|\,(\Pi_{Q_1}\otimes 1)\,|T^{J_1}_{z_1,a_1,z_2,a_2}\rangle\cdot\langle T^{J_2}_{z_3,a_3,z_4,a_4}|\,(\Pi_{Q_2}\otimes 1)\,|T^{J_2}_{z_3,a_3,z_4,a_4}\rangle \\ &= \left(\frac{1}{2}\langle\rho^{(1,J_1,0)}_{z_1,a_1}|\langle\rho^{(s(J_1),J_1,0)}_{z_2,a_2}|\Pi_{Q_1}\otimes 1|\rho^{(1,J_1,0)}_{z_1,a_1}\rangle|\rho^{(s(J_1),J_1,0)}_{z_2,a_2}\rangle\right)^2 \\ &= \left(\frac{1}{16}\right)^2 = \frac{1}{256}\,, \end{aligned} \tag{A.7}$$

where in the second line we used the fact that both terms in the product are equal and in the third line we used equation (A.4).

In case (ii) we have $Y \in \{0,1\}$ and $Q_1 = L_s$, $Q_2 = L_t$ for some $s, t \in [n-2Y]$. By a similar argument as in (A.6),

$$\langle\phi|P_\phi|\phi\rangle = \langle\rho^{L_s}_{z_s a_s}|\Pi_{Q_1}|\rho^{L_s}_{z_s,a_s}\rangle\cdot\langle\rho^{L_t}_{z_t a_t}|\Pi_{Q_2}|\rho^{L_t}_{z_t,a_t}\rangle = \frac{1}{8}\cdot\frac{1}{8} = \frac{1}{64}\,. \tag{A.8}$$

In case (iii) we have $Y = 1$, $Q_1 = (i, J_1, d)$, and $Q_2 = L_t$ for some $i \in \{1, s(J_1)\}$, $t \in [n-2]$, and $d \in \{0,1\}$. If $i = 1$ then, again by a similar reasoning as in (A.6),

$$\langle\phi|P_\phi|\phi\rangle = \langle T^{J_1}_{z_1,a_1,z_2,a_2}|\Pi_{Q_1}\otimes 1|T^{J_1}_{z_1,a_1,z_2,a_2}\rangle\cdot\langle\rho^{L_t}_{z_{2Y+t}a_{2Y+t}}|\Pi_{Q_2}|\rho^{L_t}_{z_{2Y+t}a_{2Y+t}}\rangle \tag{A.9}$$

$$= \frac{1}{16}\cdot\frac{1}{8} = \frac{1}{128}\,. \tag{A.10}$$

If $i = s(J_1)$ then $\Pi_{Q_1} \otimes 1$ should be replaced with $1 \otimes \Pi_{Q_1}$ in (A.9) but the lower bound in (A.10) is the same.

From equations (A.7), (A.8), and (A.10), we see that equation (A.5) holds in cases (i), (ii), and (iii), respectively, thereby establishing (8.21).

Finally, we prove equation (8.22), showing that $\Pi_0|_{\mathrm{span}(\mathcal{B}_n)}$ is diagonal in the basis $\mathcal{B}_n$. Let

$$|\phi\rangle = \mathrm{Sym}(|T^{J_1}_{z_1,a_1,z_2,a_2}\rangle \dots |T^{J_Y}_{z_{2Y-1},a_{2Y}-1,z_{2Y},a_{2Y}}\rangle |\rho^{L_1}_{z_{2Y+1},a_{2Y+1}}\rangle \dots |\rho^{L_{n-2Y}}_{z_n,a_n}\rangle) \tag{A.11}$$

$$|\psi\rangle = \mathrm{Sym}(|T^{\tilde{J}_1}_{x_1,b_1,x_2,b_2}\rangle \dots |T^{\tilde{J}_K}_{x_{2K-1},b_{2K}-1,x_{2K},b_{2K}}\rangle |\rho^{\tilde{L}_1}_{x_{2K+1},b_{2K+1}}\rangle \dots |\rho^{\tilde{L}_{n-2K}}_{x_n,b_n}\rangle) \tag{A.12}$$

be distinct vectors from $\mathcal{B}_n$ (note it is possible that $K = 0$ or $Y = 0$ or both). Expand each of the $|T\rangle$ states using equation (8.12), which we can also write as

$$|T^J_{z,a,y,b}\rangle = \frac{1}{\sqrt{2}} \sum_{c=0}^{1} U_J(a)^c |\rho^{(1,J,c)}_{z,a}\rangle |\rho^{(s(J),J,c)}_{y,b}\rangle$$

where we use the shorthand

$$U_J(a)|\rho^{(1,J,1)}_{z,a}\rangle |\rho^{(s(J),J,1)}_{y,b}\rangle = \sum_{x_1,x_2\in\{0,1\}} U_J(a)_{x_1x_2,zy} |\rho^{(1,J,1)}_{x_1,a}\rangle |\rho^{(s(J),J,1)}_{x_2,b}\rangle . \tag{A.13}$$

For the state $|\phi\rangle$, this gives the expansion

$$|\phi\rangle = \left(\frac{1}{\sqrt{2}}\right)^Y \sum_{c_1,\dots,c_Y\in\{0,1\}} \mathrm{Sym}(|O^{(J_1,\dots,J_Y,L_1,\dots,L_{n-2Y}),(c_1,\dots,c_Y)}_{\vec{z},\vec{a}}\rangle)$$

where

$$|O^{(J_1,\dots,J_Y,L_1,\dots,L_{n-2Y}),(c_1,\dots,c_Y)}_{\vec{z},\vec{a}}\rangle = \left(\bigotimes_{i=1}^{Y} U_{J_i}(a_{2i-1})^{c_i} |\rho^{(1,J_i,c_i)}_{z_{2i-1},a_{2i-1}}\rangle |\rho^{(s(J_i),J_i,c_i)}_{z_{2i},a_{2i}}\rangle\right) |\rho^{L_1}_{z_{2Y+1},a_{2Y+1}}\rangle \dots |\rho^{L_{n-2Y}}_{z_n,a_n}\rangle . \tag{A.14}$$

Define the projector

$$P^1_{\mathcal{L}} = \sum_{z,a\in\{0,1\}} \sum_{L\in\mathcal{L}} |\psi^L_{z,a}\rangle\langle\psi^L_{z,a}|$$

which has support only on diagram elements contained in $\mathcal{L}$, and let $P^0_{\mathcal{L}} = 1 - P^1_{\mathcal{L}}$. Note that for each $L \in \mathcal{L}$ and $z, a \in \{0,1\}$, we can write

$$|\rho^L_{z,a}\rangle = P^1_{\mathcal{L}}|\rho^L_{z,a}\rangle + P^0_{\mathcal{L}}|\rho^L_{z,a}\rangle \tag{A.15}$$

where (from equation (A.4))

$$P^1_{\mathcal{L}}|\rho^L_{z,a}\rangle = \frac{1}{\sqrt{8}}|\psi^L_{z,a}\rangle .$$

Since the states $|\rho^L_{z,a}\rangle$ are orthonormal, and similarly for the states $|\psi^L_{z,a}\rangle$, we get

$$\langle\rho^{\tilde{L}}_{x,b}|P^\alpha_{\mathcal{L}}|\rho^L_{z,a}\rangle = \begin{cases} \frac{1}{8}\delta_{z,x}\delta_{a,b}\delta_{L,\tilde{L}} & \alpha = 1 \\ \frac{7}{8}\delta_{z,x}\delta_{a,b}\delta_{L,\tilde{L}} & \alpha = 0. \end{cases} \tag{A.16}$$

Inserting n copies of the identity $P_{\mathcal{L}}^1 + P_{\mathcal{L}}^0 = 1$ gives

$$|\phi\rangle = \left(\frac{1}{\sqrt{2}}\right)^Y \sum_{c_1,\ldots,c_Y \in \{0,1\}} \sum_{\alpha_1,\ldots,\alpha_n \in \{0,1\}} \mathrm{Sym}(P_{\mathcal{L}}^{\alpha_1} \otimes \cdots \otimes P_{\mathcal{L}}^{\alpha_n} |O_{\vec{z},\vec{a}}^{(J_1,\ldots,J_Y,L_1,\ldots,L_{n-2Y}),(c_1,\ldots,c_Y)}\rangle). \tag{A.17}$$

Likewise for $|\psi\rangle$ we get

$$|\psi\rangle = \left(\frac{1}{\sqrt{2}}\right)^K \sum_{e_1,\ldots,e_K \in \{0,1\}} \sum_{\beta_1,\ldots,\beta_n \in \{0,1\}} \mathrm{Sym}(P_{\mathcal{L}}^{\beta_1} \otimes \cdots \otimes P_{\mathcal{L}}^{\beta_n} |O_{\vec{x},\vec{b}}^{(\tilde{J}_1,\ldots,\tilde{J}_K,\tilde{L}_1,\ldots,\tilde{L}_{n-2K}),(e_1,\ldots,e_K)}\rangle). \tag{A.18}$$

Using equations (A.4), (A.14), and (A.13), we see that the states

$$|O_{\vec{z},\vec{a}}^{(J_1,\ldots,J_Y,L_1,\ldots,L_{n-2Y}),(c_1,\ldots,c_Y)}\rangle \qquad \text{and} \qquad |O_{\vec{x},\vec{b}}^{(\tilde{J}_1,\ldots,\tilde{J}_K,\tilde{L}_1,\ldots,\tilde{L}_{n-2K}),(e_1,\ldots,e_K)}\rangle$$

are orthogonal for any choice of bit strings $c_1,\ldots,c_Y$ and $e_1,\ldots,e_K$, since $|\phi\rangle \neq |\psi\rangle$ implies that

$$((J_1,\ldots,J_Y,L_1,\ldots,L_{n-2Y}),\vec{z},\vec{a}) \neq ((\tilde{J}_1,\ldots,\tilde{J}_K,\tilde{L}_1,\ldots,\tilde{L}_{n-2K}),\vec{x},\vec{b}).$$

Using equation (A.16), we have

$$\begin{aligned}
&\langle O_{\vec{x},\vec{b}}^{(\tilde{J}_1,\ldots,\tilde{J}_K,\tilde{L}_1,\ldots,\tilde{L}_{n-2K}),(e_1,\ldots,e_K)} | P_{\mathcal{L}}^{\alpha_1} \otimes \cdots \otimes P_{\mathcal{L}}^{\alpha_n} | O_{\vec{z},\vec{a}}^{(J_1,\ldots,J_Y,L_1,\ldots,L_{n-2Y}),(c_1,\ldots,c_Y)} \rangle \\
&\quad = \left(\frac{1}{8}\right)^{\sum_{i=1}^n \alpha_i} \left(\frac{7}{8}\right)^{n-\sum_{i=1}^n \alpha_i} \langle O_{\vec{x},\vec{b}}^{(\tilde{J}_1,\ldots,\tilde{J}_K,\tilde{L}_1,\ldots,\tilde{L}_{n-2K}),(e_1,\ldots,e_K)} | O_{\vec{z},\vec{a}}^{(J_1,\ldots,J_Y,L_1,\ldots,L_{n-2Y}),(c_1,\ldots,c_Y)} \rangle,
\end{aligned}$$

so the states

$$P_{\mathcal{L}}^{\alpha_1} \otimes \cdots \otimes P_{\mathcal{L}}^{\alpha_n} |O_{\vec{z},\vec{a}}^{(J_1,\ldots,J_Y,L_1,\ldots,L_{n-2Y}),(c_1,\ldots,c_Y)}\rangle \tag{A.19}$$

and

$$P_{\mathcal{L}}^{\beta_1} \otimes \cdots \otimes P_{\mathcal{L}}^{\beta_n} |O_{\vec{x},\vec{b}}^{(\tilde{J}_1,\ldots,\tilde{J}_K,\tilde{L}_1,\ldots,\tilde{L}_{n-2K}),(e_1,\ldots,e_K)}\rangle \tag{A.20}$$

are orthogonal for each choice of bit strings $\alpha_1,\ldots,\alpha_n$, $\beta_1,\ldots,\beta_n$, $c_1,\ldots,c_Y$, and $e_1,\ldots,e_K$. Furthermore, observe that

$$\begin{aligned}
&\mathrm{Sym}(\langle O_{\vec{x},\vec{b}}^{(\tilde{J}_1,\ldots,\tilde{J}_K,\tilde{L}_1,\ldots,\tilde{L}_{n-2K}),(e_1,\ldots,e_K)} | P_{\mathcal{L}}^{\beta_1} \otimes \cdots \otimes P_{\mathcal{L}}^{\beta_n}) \, \mathrm{Sym}(P_{\mathcal{L}}^{\alpha_1} \otimes \cdots \otimes P_{\mathcal{L}}^{\alpha_n} | O_{\vec{z},\vec{a}}^{(J_1,\ldots,J_Y,L_1,\ldots,L_{n-2Y}),(c_1,\ldots,c_Y)} \rangle) \\
&\quad = (\langle O_{\vec{x},\vec{b}}^{(\tilde{J}_1,\ldots,\tilde{J}_K,\tilde{L}_1,\ldots,\tilde{L}_{n-2K}),(e_1,\ldots,e_K)} | P_{\mathcal{L}}^{\beta_1} \otimes \cdots \otimes P_{\mathcal{L}}^{\beta_n}) (P_{\mathcal{L}}^{\alpha_1} \otimes \cdots \otimes P_{\mathcal{L}}^{\alpha_n} | O_{\vec{z},\vec{a}}^{(J_1,\ldots,J_Y,L_1,\ldots,L_{n-2Y}),(c_1,\ldots,c_Y)} \rangle).
\end{aligned}$$

Thus each symmetrized state in the sum (A.17) is orthogonal to each symmetrized state in the sum (A.18).

To complete the proof, we show that

$$\Pi_0 |\phi\rangle$$

is a superposition of a *subset* of the states in the sum (A.17) and hence is orthogonal to $|\psi\rangle$. To see this, first note that $|\phi\rangle \in \mathcal{I}(G_1,n)$ by Lemma 5.4 since it is in the nullspace of $H(G_1,n)$ (by Lemma 8.5) and G_1 is an e_1-gate graph (by Lemma 8.2). Now comparing $\mathcal{I}(G_1,n)$ (defined in (5.15)) and $\mathcal{I}(G_1,G_X^{\mathrm{occ}},n)$ (defined in (5.21)), we see that

$$\Pi_0 |\Gamma\rangle = \Pi_0^{\mathrm{occ}} |\Gamma\rangle \text{ for all } |\Gamma\rangle \in \mathcal{I}(G_1,n)$$

where Π_0^{occ} projects onto the space

$$\operatorname{span}\{|\psi^{q_1}_{z_1,a_1}\rangle|\psi^{q_2}_{z_2,a_2}\rangle\ldots|\psi^{q_n}_{z_n,a_n}\rangle\colon z_i,a_i\in\{0,1\},\, q_i\in[R],\, \{q_i,q_j\}\notin E(G_X^{\text{occ}})\}\,. \tag{A.21}$$

In particular, $\Pi_0|\phi\rangle=\Pi_0^{\text{occ}}|\phi\rangle$. We claim that this quantity is a superposition of a subset of the states in the sum (A.17).

The diagram elements $q_1,\ldots,q_n$ appearing in (A.21) range over the set of all R diagram elements in the gate graph G_1; however, recall that $E(G_X^{\text{occ}})$ only contains edges between diagram elements in the subset $\mathcal{L}$ of these diagram elements. Since the $P_{\mathcal{L}}^{\alpha}$ either project onto this set of diagram elements or onto the complement, each state

$$\operatorname{Sym}(P_{\mathcal{L}}^{\alpha_1}\otimes\cdots\otimes P_{\mathcal{L}}^{\alpha_n}|O_{\vec{z},\vec{a}}^{(J_1,\ldots,J_Y,L_1,\ldots,L_{n-2Y}),(c_1,\ldots,c_Y)}\rangle)$$

is an eigenvector of Π_0^{occ}. Hence $\Pi_0|\phi\rangle$ is a superposition of the terms in (A.17) that are $+1$ eigenvectors of Π_0^{occ} (as the 0 eigenvectors are annihilated). It follows that $\langle\psi|\Pi_0|\phi\rangle=0$ since we established above that each such term is orthogonal to $|\psi\rangle$. □

A.3 Computation of matrix elements between states with legal configurations

In this section we compute the matrix elements of

$$H_1\big|_{S_1}, H_2\big|_{S_1}, H_{\text{in},i}\big|_{S_1}, H_{\text{out}}\big|_{S_1} \tag{A.22}$$

in the basis of S_1 consisting of the states

$$|j,\vec{d},\text{In}(\vec{z}),\vec{a}\rangle=\sum_{\vec{x}\in\{0,1\}^n}\big(\langle\vec{x}|\bar{U}_{j,d_1}(a_1)|\vec{z}\rangle\big)|j,\vec{d},\vec{x},\vec{a}\rangle \tag{A.23}$$

for $\vec{z},\vec{a}\in\{0,1\}$, $j\in[M]$, and

$$\vec{d}=(d_1,\ldots,d_n)\quad\text{with}\quad d_1=d_{s(j)}\in\{0,1,2\}\quad\text{and}\quad d_i\in\{0,1\}\ i\notin\{1,s(j)\}\,,$$

where

$$\bar{U}_{j,d_1}(a_1)=\begin{cases}U_{j-1}(a_1)U_{j-2}(a_1)\ldots U_1(a_1) & \text{if } d_1\in\{0,2\}\\ U_j(a_1)U_{j-1}(a_1)\ldots U_1(a_1) & \text{if } d_1=1.\end{cases} \tag{A.24}$$

Specifically, we prove the results stated in the four boxes in Section 8.4.

A.3.1 Matrix elements of H_1

We begin by computing the matrix elements of

$$H_1=\sum_{w=1}^{n}h_1^{(w)}$$

in the basis $\mathcal{B}_{\text{legal}}$; then we use them to compute the matrix elements of H_1 in the basis (A.23).

Note that since H_1 is symmetric under permutations of the n registers,

$$H_1|j,\vec{d},\vec{z},\vec{a}\rangle = \begin{cases} \mathrm{Sym}\left(H_1|\rho_{z_1,a_1}^{(1,j,d_1)}\rangle \bigotimes_{i=2}^{n} |\rho_{z_i,a_i}^{F(i,j,d_i)}\rangle\right) & d_1 = d_{s(j)} \in \{0,1\} \\ \mathrm{Sym}\left(H_1|T_{z_1,a_1,z_{s(j)},a_{s(j)}}^{j}\rangle \bigotimes_{\substack{i=2 \\ i\neq s(j)}}^{n} |\rho_{z_i,a_i}^{F(i,j,d_i)}\rangle\right) & d_1 = d_{s(j)} = 2 \end{cases} \tag{A.25}$$

and recall that

$$|T_{z_1,a_1,z_{s(j)},a_{s(j)}}^{j}\rangle = \frac{1}{\sqrt{2}}|\rho_{z_1,a_1}^{(1,j,0)}\rangle|\rho_{z_{s(j)},a_{s(j)}}^{(s(j),j,0)}\rangle + \frac{1}{\sqrt{2}}\sum_{x_1,x_2\in\{0,1\}} U_j(a_1)_{x_1x_2,z_1z_{s(j)}}|\rho_{x_1,a_1}^{(1,j,1)}\rangle|\rho_{x_2,a_{s(j)}}^{(s(j),j,1)}\rangle. \tag{A.26}$$

To compute $\langle k,\vec{c},\vec{x},\vec{b}|H_1|j,\vec{d},\vec{z},\vec{a}\rangle$, we first evaluate the matrix elements of h_1 between single-particle states of the form

$$|\rho_{z,a}^{(1,j,d)}\rangle,\ |\rho_{z,a}^{(s(j),j,d)}\rangle,\ |\rho_{z,a}^{F(i,j,d)}\rangle$$

(for $j\in[M]$, $i\in\{2,\ldots,n\}$, and $z,a,d\in\{0,1\}$) that appear in equation (A.25). To evaluate these matrix elements, we use the fact that h_1 is of the form (5.6), where $\mathcal{E}$ is the set of edges in rows $2,\ldots,n$ that are added to the gate diagram in step 3 of Section 7.2.

We have

$$\langle\rho_{x,b}^{F(i,j,0)}|h_1|\rho_{z,a}^{F(i,j,0)}\rangle = \frac{1}{8}\langle\psi_{x,b}^{F(i,j,0)}|h_1|\psi_{z,a}^{F(i,j,0)}\rangle = \frac{1}{64}\delta_{x,z}\delta_{a,b} \tag{A.27}$$

$$\langle\rho_{x,b}^{F(i,j,1)}|h_1|\rho_{z,a}^{F(i,j,1)}\rangle = \frac{1}{64}\delta_{x,z}\delta_{a,b} \tag{A.28}$$

for all $i\in\{2,\ldots,n\}$, $j\in[M]$, and $x,z,a,b\in\{0,1\}$. Similarly,

$$\langle\rho_{x,b}^{F(i,j,0)}|h_1|\rho_{z,a}^{F(i,j,1)}\rangle = \langle\rho_{x,b}^{F(i,j,1)}|h_1|\rho_{z,a}^{F(i,j,0)}\rangle = \frac{1}{64}\delta_{x,z}\delta_{a,b} \tag{A.29}$$

for all $i\in[n]\setminus\{1,s(j)\}$, $j\in[M]$, and $z,x,a,b\in\{0,1\}$. Furthermore,

$$h_1|\rho_{z,a}^{(1,j,d)}\rangle = 0 \tag{A.30}$$

for all $j\in[M]$ and $z,a,d\in\{0,1\}$, and

$$\langle\rho_{x,b}^{F(s(j),j,c)}|h_1|\rho_{z,a}^{(s(j),j,d)}\rangle = \frac{1}{64}\delta_{x,z}\delta_{a,b}\delta_{c,d} \tag{A.31}$$

$$\langle\rho_{x,b}^{(s(j),j,c)}|h_1|\rho_{z,a}^{(s(j),j,d)}\rangle = \frac{1}{64}\delta_{x,z}\delta_{a,b}\delta_{c,d} \tag{A.32}$$

for all $j\in[M]$ and $z,x,a,b,c,d\in\{0,1\}$.

Using equations (A.27), (A.28), (A.30), and (A.32), we compute the diagonal matrix elements of H_1:

$$\begin{aligned}\langle j,\vec{d},\vec{z},\vec{a}|H_1|j,\vec{d},\vec{z},\vec{a}\rangle &= \begin{cases} \sum_{i=2}^{n}\langle\rho_{z_i,a_i}^{F(i,j,d_i)}|h_1|\rho_{z_i,a_i}^{F(i,j,d_i)}\rangle & d_1\in\{0,1\} \\ \langle T_{z_1,a_1,z_{s(j)},a_{s(j)}}^{j}|1\otimes h_1|T_{z_1,a_1,z_{s(j)},a_{s(j)}}^{j}\rangle + \sum_{\substack{i=2 \\ i\neq s(j)}}^{n}\langle\rho_{z_i,a_i}^{F(i,j,d_i)}|h_1|\rho_{z_i,a_i}^{F(i,j,d_i)}\rangle & d_1 = 2 \end{cases} \\ &= \frac{n-1}{64}\end{aligned} \tag{A.33}$$

where in the last line we used equation (A.26) and the fact that $U_j(a_1)$ is unitary. We use equations (A.29) and (A.31) to compute the nonzero off-diagonal matrix elements of H_1 between states in $\mathcal{B}_{\text{legal}}$. We get

$$\langle k,\vec{c},\vec{x},\vec{b}|H_1|j,\vec{d},\vec{z},\vec{a}\rangle = \delta_{j,k}\delta_{\vec{a},\vec{b}}\cdot\begin{cases}\frac{1}{64}\delta_{\vec{x},\vec{z}}(n-1) & \vec{c}=\vec{d}\\ \frac{1}{64}\delta_{\vec{x},\vec{z}}\prod_{\substack{r=1\\r\neq i}}^{n}\delta_{c_r,d_r} & \exists i\in[n]\setminus\{1,s(j)\},c_i\neq d_i\\ \frac{1}{64\sqrt{2}}\delta_{\vec{x},\vec{z}}\prod_{\substack{r=2\\r\neq s(j)}}^{n}\delta_{c_r,d_r} & (c_1,d_1)\in\{(2,0),(0,2)\}\\ \frac{1}{64\sqrt{2}}U_j(a_1)^*_{z_1z_{s(j)},x_1x_{s(j)}}\prod_{\substack{r=2\\r\neq s(j)}}^{n}\delta_{c_r,d_r}\delta_{x_r,z_r} & (c_1,d_1)=(2,1)\\ \frac{1}{64\sqrt{2}}U_j(a_1)_{x_1x_{s(j)},z_1z_{s(j)}}\prod_{\substack{r=2\\r\neq s(j)}}^{n}\delta_{c_r,d_r}\delta_{x_r,z_r} & (c_1,d_1)=(1,2)\\ 0 & \text{otherwise.}\end{cases} \tag{A.34}$$

For the second case we used equation (A.29), for the third case we used equation (A.31) to get

$$\langle T^j_{x_1,b_1,x_{s(j)},b_{s(j)}}|1\otimes h_1|\rho^{(1,j,0)}_{z_1,a_1}\rangle|\rho^{F(s(j),j,0)}_{z_{s(j)}a_{s(j)}}\rangle = \delta_{x_1,z_1}\delta_{b_1,a_1}\delta_{x_{s(j)},z_{s(j)}}\delta_{b_{s(j)},a_{s(j)}}\frac{1}{64\sqrt{2}},$$

and for the fourth and fifth cases we used equation (A.31) to get

$$\langle T^j_{x_1,b_1,x_{s(j)},b_{s(j)}}|1\otimes h_1|\rho^{(1,j,1)}_{z_1,a_1}\rangle|\rho^{F(s(j),j,1)}_{z_{s(j)}a_{s(j)}}\rangle = \delta_{b_1,a_1}\delta_{b_{s(j)},a_{s(j)}}\frac{1}{64\sqrt{2}}U_j(a_1)^*_{z_1z_{s(j)},x_1x_{s(j)}}.$$

In the remaining case, $(c_1,d_1)\in\{(1,0),(0,1)\}$ and the matrix element is 0.

We now compute the matrix elements of H_1 in the basis (A.23). We have

$$\langle j,\vec{c},\mathrm{In}(\vec{x}),\vec{a}|H_1|j,\vec{d},\mathrm{In}(\vec{z}),\vec{a}\rangle = \sum_{\vec{x}',\vec{z}'\in\{0,1\}^n}\langle j,\vec{c},\vec{x}',\vec{a}|H_1|j,\vec{d},\vec{z}',\vec{a}\rangle\langle\vec{x}|\bar{U}_{j,d_1}(a_1)^\dagger|\vec{x}'\rangle\langle\vec{z}'|\bar{U}_{j,d_1}(a_1)|\vec{z}\rangle. \tag{A.35}$$

Using this with (A.34) gives

$$\langle k,\vec{c},\mathrm{In}(\vec{x}),\vec{b}|H_1|j,\vec{d},\mathrm{In}(\vec{z}),\vec{a}\rangle = \delta_{j,k}\delta_{\vec{a},\vec{b}}\delta_{\vec{x},\vec{z}}\cdot\begin{cases}\frac{n-1}{64} & \vec{c}=\vec{d}\\ \frac{1}{64}\prod_{\substack{r=1\\r\neq i}}^{n}\delta_{c_r,d_r} & \exists i\in[n]\setminus\{1,s(j)\},c_i\neq d_i\\ \frac{1}{64\sqrt{2}}\prod_{\substack{r=2\\r\neq s(j)}}^{n}\delta_{c_r,d_r} & (c_1,d_1)\in\{(2,0),(0,2),(2,1),(1,2)\}\\ 0 & \text{otherwise}\end{cases}$$

as claimed in equation (8.30). Note that in the basis $\mathcal{B}_{\text{legal}}$, H_1 has nonzero matrix elements between states with different values of $\vec{z}$; the basis (A.23) is convenient because H_1 only connects basis states with the same value of $\vec{z}$.

A.3.2 Matrix elements of H_2

Recall that

$$H_2 = \sum_{w=1}^{n} h_2^{(w)}$$

and note, just as in (A.25), that because H_2 is permutation invariant,

$$H_2|j,\vec{d},\vec{z},\vec{a}\rangle = \begin{cases} \mathrm{Sym}\left(H_2|\rho_{z_1,a_1}^{(1,j,d_1)}\rangle \bigotimes_{i=2}^{n} |\rho_{z_i,a_i}^{F(i,j,d_i)}\rangle\right) & d_1 = d_{s(j)} \in \{0,1\} \\ \mathrm{Sym}\left(H_2|T_{z_1,a_1,z_{s(j)},a_{s(j)}}^{j}\rangle \bigotimes_{\substack{i=2 \\ i\neq s(j)}}^{n} |\rho_{z_i,a_i}^{F(i,j,d_i)}\rangle\right) & d_1 = d_{s(j)} = 2. \end{cases} \tag{A.36}$$

Also recall that h_2 is of the form (5.6), where $\mathcal{E}$ is the set of edges in row 1 that are added in step 3 of Section 7.2.

To compute $\langle k,\vec{c},\vec{x},\vec{b}|H_2|j,\vec{d},\vec{z},\vec{a}\rangle$ we first evaluate the matrix elements of h_2 between the relevant single-particle states $|\rho_{z,a}^{L}\rangle$ with $L \in \mathcal{L}$ and $z,a \in \{0,1\}$. The only such matrix elements that are nonzero are

$$\begin{aligned} \langle\rho_{x,b}^{(1,j,0)}|h_2|\rho_{z,a}^{(1,j,0)}\rangle &= \begin{cases} 0 & j = 1 \\ \frac{1}{64}\delta_{z,x}\delta_{a,b} & j \in \{2,\ldots,M\} \end{cases} \\ \langle\rho_{x,b}^{(1,j,1)}|h_2|\rho_{z,a}^{(1,j,1)}\rangle &= \begin{cases} \frac{1}{64}\delta_{z,x}\delta_{a,b} & j \in \{1,\ldots,M-1\} \\ 0 & j = M \end{cases} \end{aligned} \tag{A.37}$$

for $z,a,x,b \in \{0,1\}$ and

$$\langle\rho_{x,b}^{(1,j-1,1)}|h_2|\rho_{z,a}^{(1,j,0)}\rangle = \langle\rho_{z,a}^{(1,j,0)}|h_2|\rho_{x,b}^{(1,j-1,1)}\rangle = \frac{1}{64}\delta_{z,x}\delta_{a,b} \tag{A.38}$$

for $j \in \{2,\ldots,M\}$ and $z,x,a,b \in \{0,1\}$.

Using equations (A.36) and (A.37), we compute the diagonal matrix elements of H_2 in the basis $\mathcal{B}_{\text{legal}}$:

$$\langle j,\vec{d},\vec{z},\vec{a}|H_2|j,\vec{d},\vec{z},\vec{a}\rangle = \begin{cases} 0 & d_1 = 0 \text{ and } j = 1, \text{ or } d_1 = 1 \text{ and } j = M \\ \frac{1}{128} & d_1 = 2 \text{ and } j \in \{1,M\} \\ \frac{1}{64} & \text{otherwise.} \end{cases} \tag{A.39}$$

Using equations (A.36) and (A.38), we compute the nonzero off-diagonal matrix elements, which are all of the form

$$\langle j-1,\vec{c},\vec{x},\vec{a}|H_2|j,\vec{d},\vec{z},\vec{a}\rangle \quad \text{or} \quad \langle j,\vec{d},\vec{z},\vec{a}|H_2|j-1,\vec{c},\vec{x},\vec{a}\rangle = \left(\langle j-1,\vec{c},\vec{x},\vec{a}|H_2|j,\vec{d},\vec{z},\vec{a}\rangle\right)^*$$

for $j \in \{2,\ldots,M\}$, $\vec{x},\vec{z},\vec{a} \in \{0,1\}^n$, and

$$\vec{d} = (d_1,\ldots,d_n) \quad \text{with} \quad d_1 = d_{s(j)} \in \{0,1,2\} \quad \text{and} \quad d_i \in \{0,1\} \text{ for all } i \notin \{1,s(j)\}.$$

We get

$$\begin{aligned}
&\langle j-1,\vec{c},\vec{x},\vec{a}|H_2|j,\vec{d},\vec{z},\vec{a}\rangle \\
&= \prod_{\substack{r=2\\ r\notin\{s(j),s(j-1)\}}}^{n} \delta_{d_r,c_r} \begin{cases}
\frac{1}{64}\delta_{\vec{x},\vec{z}} & (c_1,c_{s(j)},d_1,d_{s(j-1)}) = (1,0,0,1)\\
\frac{1}{64\sqrt{2}} U_{j-1}(a_1)^*_{z_1 z_{s(j-1)},x_1 x_{s(j-1)}} \prod_{\substack{r=2\\ r\neq s(j-1)}}^{n} \delta_{x_r,z_r} & (c_1,c_{s(j)},d_1,d_{s(j-1)}) = (2,0,0,0)\\
\frac{1}{128} U_{j-1}(a_1)^*_{z_1 z_{s(j-1)},x_1 x_{s(j-1)}} \prod_{\substack{r=2\\ r\neq s(j-1)}}^{n} \delta_{x_r,z_r} & (c_1,c_{s(j)},d_1,d_{s(j-1)}) = (2,1,2,0)\\
\frac{1}{64\sqrt{2}}\delta_{\vec{x},\vec{z}} & (c_1,c_{s(j)},d_1,d_{s(j-1)}) = (1,1,2,1).
\end{cases}
\end{aligned} \tag{A.40}$$

Now we compute the diagonal matrix elements of H_2 in the basis (A.23) using equations (A.35) and (A.39):

$$\langle j,\vec{d},\mathrm{In}(\vec{z}),\vec{a}|H_2|j,\vec{d},\mathrm{In}(\vec{z}),\vec{a}\rangle = \begin{cases} 0 & d_1 = 0 \text{ and } j = 1, \text{ or } d_1 = 1 \text{ and } j = M \\ \frac{1}{128} & d_1 = 2 \text{ and } j \in \{1,M\} \\ \frac{1}{64} & \text{otherwise.} \end{cases} \tag{A.41}$$

The nonzero off-diagonal matrix elements are (using equations (A.35) and (A.40))

$$\begin{aligned}
&\langle j-1,\vec{c},\mathrm{In}(\vec{x}),\vec{b}|H_2|j,\vec{d},\mathrm{In}(\vec{z}),\vec{a}\rangle = \langle j,\vec{d},\mathrm{In}(\vec{z}),\vec{a}|H_2|j-1,\vec{c},\mathrm{In}(\vec{x}),\vec{b}\rangle \\
&= \delta_{\vec{x},\vec{z}}\delta_{\vec{a},\vec{b}} \left(\prod_{\substack{r=2\\ r\notin\{s(j),s(j-1)\}}}^{n} \delta_{d_r,c_r} \right) \cdot \begin{cases}
\frac{1}{64} & (c_1,c_{s(j)},d_1,d_{s(j-1)}) = (1,0,0,1)\\
\frac{1}{64\sqrt{2}} & (c_1,c_{s(j)},d_1,d_{s(j-1)}) = (2,0,0,0)\\
\frac{1}{128} & (c_1,c_{s(j)},d_1,d_{s(j-1)}) = (2,1,2,0)\\
\frac{1}{64\sqrt{2}} & (c_1,c_{s(j)},d_1,d_{s(j-1)}) = (1,1,2,1).
\end{cases}
\end{aligned} \tag{A.42}$$

Combining equations (A.41) and (A.42) gives the result claimed in equations (8.31), (8.32), and (8.33).

A.3.3 Matrix elements of $H_{\mathrm{in},i}$

We now consider

$$H_{\mathrm{in},i} = \sum_{w=1}^{n} h_{\mathrm{in},i}^{(w)}$$

where i is from the set of indices of the ancilla qubits, i. e., $i \in \{n_{\mathrm{in}}+1,\ldots,n\}$. Using equation (8.3) we get

$$\langle \rho_{x,b}^{L_2}|h_{\mathrm{in},i}|\rho_{z,a}^{L_1}\rangle = \frac{1}{8}\langle \psi_{x,b}^{L_2}|h_{\mathrm{in},i}|\psi_{z,a}^{L_1}\rangle = \frac{1}{64}\delta_{x,1}\delta_{z,1}\delta_{a,b}\delta_{L_1,(i,0,1)}\delta_{L_2,(i,0,1)}$$

for $L_1,L_2 \in \mathcal{L}$ and $a,b,x,z \in \{0,1\}$. Thus $H_{\mathrm{in},i}$ is diagonal in the basis $\mathcal{B}_{\mathrm{legal}}$ with entries

$$\langle j,\vec{d},\vec{z},\vec{a}|H_{\mathrm{in},i}|j,\vec{d},\vec{z},\vec{a}\rangle = \begin{cases} \frac{1}{64} & d_i = 0,\ z_i = 1, \text{ and } F(i,j,0) = (i,0,1) \\ 0 & \text{otherwise.} \end{cases} \tag{A.43}$$

Note that $F(i,j,0) = (i,0,1)$ if and only if none of the gates $U_1, U_2, \ldots, U_{j-1}$ acts on the i-th qubit, i. e.,

$$j \leq j_{\min,i}$$

where

$$j_{\min,i} = \min\{j \in [M] : s(j) = i\}.$$

Now using this fact and equations (A.35) and (A.43), we get the following expression for the nonzero matrix elements of $H_{\text{in},i}$ in the basis (A.23):

$$\begin{aligned}
&\langle j, \vec{d}, \mathrm{In}(\vec{x}), \vec{a}|H_{\text{in},i}|j, \vec{d}, \mathrm{In}(\vec{z}), \vec{a}\rangle \\
&\quad = \sum_{\vec{w},\vec{y}\in\{0,1\}^n} \langle \vec{x}|\bar{U}^\dagger_{j,d_1}(a_1)|\vec{w}\rangle\langle \vec{y}|\bar{U}_{j,d_1}(a_1)|\vec{z}\rangle\langle j, \vec{d}, \vec{w}, \vec{a}|H_{\text{in},i}|j, \vec{d}, \vec{y}, \vec{a}\rangle \\
&\quad = \begin{cases} \sum_{\vec{y}\in\{0,1\}^n} \langle \vec{x}|\bar{U}^\dagger_{j,d_1}(a_1)|\vec{y}\rangle\langle \vec{y}|\bar{U}_{j,d_1}(a_1)|\vec{z}\rangle \frac{1}{64}\delta_{y_i,1} & j \leq j_{\min,i} \text{ and } d_i = 0 \\ 0 & \text{otherwise} \end{cases} \\
&\quad = \begin{cases} \langle \vec{x}|\bar{U}^\dagger_{j,d_1}(a_1)|1\rangle\langle 1|_i\bar{U}_{j,d_1}(a_1)|\vec{z}\rangle \frac{1}{64} & j \leq j_{\min,i} \text{ and } d_i = 0 \\ 0 & \text{otherwise} \end{cases} \\
&\quad = \begin{cases} \langle \vec{x}|U_1^\dagger(a_1)\ldots U_{j-1}^\dagger(a_1)|1\rangle\langle 1|_i U_{j-1}(a_1)\ldots U_1(a_1)|\vec{z}\rangle \frac{1}{64} & (j < j_{\min,i} \text{ and } d_i = 0 \text{ and } d_1 \in \{0,2\}) \\ & \text{or } (j = j_{\min,i} \text{ and } d_i = 0) \\ \langle \vec{x}|U_1^\dagger(a_1)\ldots U_j^\dagger(a_1)|1\rangle\langle 1|_i U_j(a_1)\ldots U_1(a_1)|\vec{z}\rangle \frac{1}{64} & j < j_{\min,i} \text{ and } d_i = 0 \text{ and } d_1 = 1 \\ 0 & \text{otherwise.} \end{cases}
\end{aligned}$$

In the last line we use the fact that $d_1 = d_i$ when $j = j_{\min,i}$ (since $s(j_{\min,i}) = i$). Since $[U_J(a_1), |1\rangle\langle 1|_i] = 0$ for $J < j_{\min,i}$, we have

$$\langle j, \vec{d}, \mathrm{In}(\vec{x}), \vec{a}|H_{\text{in},i}|j, \vec{d}, \mathrm{In}(\vec{z}), \vec{a}\rangle = \begin{cases} \frac{1}{64}\langle \vec{x}|\left(|1\rangle\langle 1|_i\right)|\vec{z}\rangle & j \leq j_{\min,i} \text{ and } d_i = 0 \\ 0 & \text{otherwise} \end{cases} \tag{A.44}$$

$$= \begin{cases} \frac{1}{64}\delta_{\vec{x},\vec{z}}\delta_{x_i,1} & j \leq j_{\min,i} \text{ and } d_i = 0 \\ 0 & \text{otherwise} \end{cases} \tag{A.45}$$

(with all other matrix elements equal to zero), which confirms the result stated in equation (8.34).

A.3.4 Matrix elements of H_{out}

Finally, consider

$$H_{\text{out}} = \sum_{w=1}^{n} h_{\text{out}}^{(w)}$$

where (from equation (8.3))

$$\langle \rho^{L_2}_{x,b}|h_{\text{out}}|\rho^{L_1}_{z,a}\rangle = \frac{1}{64}\delta_{a,b}\delta_{x,0}\delta_{z,0}\delta_{L_1,(2,M+1,0)}\delta_{L_2,(2,M+1,0)}$$

for $L_1, L_2 \in \mathcal{L}$ and $z, a, x, b \in \{0,1\}$. From this we see that H_{out} is diagonal in the basis $\mathcal{B}_{\text{legal}}$, with entries

$$\langle j, \vec{d}, \vec{z}, \vec{a} | H_{\text{out}} | j, \vec{d}, \vec{z}, \vec{a} \rangle = \begin{cases} \frac{1}{64} & d_2 = 1, F(2, j, 1) = (2, M+1, 0) \text{ and } z_2 = 0 \\ 0 & \text{otherwise.} \end{cases}$$

Note that $F(2, j, 1) = (2, M+1, 0)$ if and only if $j \geq j_{\max}$, where

$$j_{\max} = \max\{ j \in [M] : s(j) = 2 \}.$$

Using this fact we compute the nonzero matrix elements of H_{out} in the basis (A.23):

$$\begin{aligned}
&\langle j, \vec{d}, \text{In}(\vec{x}), \vec{a} | H_{\text{out}} | j, \vec{d}, \text{In}(\vec{z}), \vec{a} \rangle \\
&\quad = \sum_{\vec{w}, \vec{y} \in \{0,1\}^n} \langle \vec{x} | \bar{U}^\dagger_{j,d_1}(a_1) | \vec{w} \rangle \langle \vec{y} | \bar{U}_{j,d_1}(a_1) | \vec{z} \rangle \langle j, \vec{d}, \vec{w}, \vec{a} | H_{\text{out}} | j, \vec{d}, \vec{y}, \vec{a} \rangle \\
&\quad = \begin{cases} \langle \vec{x} | \bar{U}^\dagger_{j,d_1}(a_1) | 0 \rangle \langle 0 |_2 \bar{U}_{j,d_1}(a_1) | \vec{z} \rangle \frac{1}{64} & j \geq j_{\max} \text{ and } d_2 = 1 \\ 0 & \text{otherwise} \end{cases} \\
&\quad = \begin{cases} \langle \vec{x} | U_1^\dagger(a_1) \ldots U_j^\dagger(a_1) | 0 \rangle \langle 0 |_2 U_j(a_1) \ldots U_1(a_1) | \vec{z} \rangle \frac{1}{64} & j \geq j_{\max} \text{ and } d_1 = d_2 = 1 \\ \langle \vec{x} | U_1^\dagger(a_1) \ldots U_{j-1}^\dagger(a_1) | 0 \rangle \langle 0 |_2 U_{j-1}(a_1) \ldots U_1(a_1) | \vec{z} \rangle \frac{1}{64} & j > j_{\max} \text{ and } d_2 = 1 \text{ and } d_1 \in \{0,2\} \\ 0 & \text{otherwise} \end{cases} \\
&\quad = \begin{cases} \langle \vec{x} | U_1^\dagger(a_1) \ldots U_M^\dagger(a_1) | 0 \rangle \langle 0 |_2 U_M(a_1) \ldots U_1(a_1) | \vec{z} \rangle \frac{1}{64} & j \geq j_{\max} \text{ and } d_2 = 1 \\ 0 & \text{otherwise} \end{cases} \\
&\quad = \begin{cases} \langle \vec{x} | U^\dagger_{\mathcal{C}_X}(a_1) | 0 \rangle \langle 0 |_2 U_{\mathcal{C}_X}(a_1) | \vec{z} \rangle \frac{1}{64} & j \geq j_{\max} \text{ and } d_2 = 1 \\ 0 & \text{otherwise.} \end{cases}
\end{aligned}$$

In going from the second to the third equality we use the fact that $j = j_{\max}$ implies $d_1 = d_2$ (since $s(j_{\max}) = 2$). In the next-to-last line we use the fact that $[U_J(a_1), |0\rangle\langle 0|_2] = 0$ for $J > j_{\max}$. This confirms the result stated in equation (8.35).

References

[1] DORIT AHARONOV, DANIEL GOTTESMAN, SANDY IRANI, AND JULIA KEMPE: The power of quantum systems on a line. *Communications in Mathematical Physics*, 287(1):41–65, 2009. Preliminary version in FOCS'07. [doi:10.1007/s00220-008-0710-3, arXiv:0705.4077] 492

[2] DORIT AHARONOV AND AMNON TA-SHMA: Adiabatic quantum state generation and statistical zero knowledge. *SIAM J. Comput.*, 37(1):47–82, 2007. Preliminary version in STOC'03. [doi:10.1137/060648829, arXiv:quant-ph/0301023] 494, 506, 507, 514

[3] ADAM D. BOOKATZ: QMA-complete problems. *Quantum Inf. Comput.*, 14(5-6):361–383, 2014. ACM DL. [arXiv:1212.6312] 491

[4] SERGEY BRAVYI: Efficient algorithm for a quantum analogue of 2-SAT. *Contemporary Mathematics*, 536:33–48, 2011. [doi:10.1090/conm/536, arXiv:quant-ph/0602108] 492

[5] SERGEY BRAVYI, DAVID P. DIVINCENZO, ROBERTO I. OLIVEIRA, AND BARBARA M. TERHAL: The complexity of stoquastic local Hamiltonian problems. *Quantum Inf. Comput.*, 8(5):361–385, 2008. ACM DL. [arXiv:quant-ph/0606140] 492, 493, 496, 497

[6] SERGEY BRAVYI AND BARBARA TERHAL: Complexity of stoquastic frustration-free Hamiltonians. *SIAM J. Comput.*, 39(4):1462–1485, 2009. [doi:10.1137/08072689X, arXiv:0806.1746] 492

[7] NIKOLAS P. BREUCKMANN AND BARBARA M. TERHAL: Space-time circuit-to-Hamiltonian construction and its applications. *Journal of Physics A*, 47(19):195304, 2014. IOP Science. [arXiv:1311.6101] 496

[8] ANDREW M. CHILDS, DAVID GOSSET, AND ZAK WEBB: Universal computation by multiparticle quantum walk. *Science*, 339(6121):791–794, 2013. [doi:10.1126/science.1229957, arXiv:1205.3782] 493

[9] RICHARD CLEVE, ARTUR EKERT, CHIARA MACCHIAVELLO, AND MICHELE MOSCA: Quantum algorithms revisited. *Proceedings of the Royal Society of London, Series A*, 454(1969):339–354, 1998. [doi:10.1098/rspa.1998.0164, arXiv:quant-ph/9708016] 514

[10] TOBY S. CUBITT AND ASHLEY MONTANARO: Complexity classification of local Hamiltonian problems. Preprint, 2013-14. Extended abstract in FOCS'14. [arXiv:1311.3161] 492

[11] RICHARD P. FEYNMAN: Quantum mechanical computers. *Optics News*, 11(2):11–46, 1985. [doi:10.1364/ON.11.2.000011] 493, 494, 508

[12] MATTHEW P. A. FISHER, PETER B. WEICHMAN, G. GRINSTEIN, AND DANIEL S. FISHER: Boson localization and the superfluid-insulator transition. *Physical Review B*, 40(1):546–570, 1989. [doi:10.1103/PhysRevB.40.546] 492

[13] DAVID GOSSET AND DANIEL NAGAJ: Quantum 3-SAT is QMA_1-complete. Preprint, 2013. Extended abstract in FOCS'13. [arXiv:1302.0290] 492, 543

[14] DANIEL GOTTESMAN AND SANDY IRANI: The quantum and classical complexity of translationally invariant tiling and Hamiltonian problems. *Theory of Computing*, 9(2):31–116, 2013. Preliminary version in FOCS'09. [doi:10.4086/toc.2013.v009a002, arXiv:0905.2419] 492

[15] DOMINIK JANZING: Spin-1/2 particles moving on a two-dimensional lattice with nearest-neighbor interactions can realize an autonomous quantum computer. *Physical Review A*, 75(1):012307, 2007. [doi:10.1103/PhysRevA.75.012307, arXiv:quant-ph/0506270] 496

[16] DOMINIK JANZING AND PAWEL WOCJAN: BQP-complete problems concerning mixing properties of classical random walks on sparse graphs, 2006. [arXiv:quant-ph/0610235] 493, 494, 509

[17] STEPHEN P. JORDAN AND EDWARD FARHI: Perturbative gadgets at arbitrary orders. *Physical Review A*, 77(6):062329, 2008. [doi:10.1103/PhysRevA.77.062329, arXiv:0802.1874] 494, 543

[18] STEPHEN P. JORDAN, DAVID GOSSET, AND PETER J. LOVE: Quantum-Merlin-Arthur complete problems for stoquastic Hamiltonians and Markov matrices. *Physical Review A*, 81(3):032331, 2010. [doi:10.1103/PhysRevA.81.032331, arXiv:0905.4755] 509

[19] JULIA KEMPE, ALEXEI KITAEV, AND ODED REGEV: The complexity of the local Hamiltonian problem. *SIAM J. Comput.*, 35(5):1070–1097, 2006. Preliminary version in FSTTCS'04. [doi:10.1137/S0097539704445226, arXiv:quant-ph/0406180] 492, 494, 496, 543

[20] JULIA KEMPE AND ODED REGEV: 3-Local Hamiltonian is QMA-complete. *Quantum Inf. Comput.*, 3(3):258–264, 2003. ACM DL. [arXiv:quant-ph/0302079] 492, 496

[21] ALEXEI YU. KITAEV, ALEXANDER H. SHEN, AND MIKHAIL N. VYALYI: *Classical and Quantum Computation*. Amer. Math. Soc., 2002. ACM DL. 491, 492, 493, 500, 507, 508, 535, 564

[22] LEV D. LANDAU AND EVGENII M. LIFSHITZ: *Quantum Mechanics: Non-Relativistic Theory*. Pergamon Press, 1994. 502

[23] YI-KAI LIU, MATTHIAS CHRISTANDL, AND FRANK VERSTRAETE: Quantum computational complexity of the N-representability problem: QMA complete. *Physical Review Letters*, 98(11):110503, 2007. [doi:10.1103/PhysRevLett.98.110503, arXiv:quant-ph/0609125] 492

[24] CHRIS MARRIOTT AND JOHN WATROUS: Quantum Arthur-Merlin games. *Computational Complexity*, 14(2):122–152, 2005. Preliminary version in CCC'04. [doi:10.1007/s00037-005-0194-x, arXiv:cs/0506068] 500, 507, 535

[25] ARI MIZEL, DANIEL A. LIDAR, AND MORGAN MITCHELL: Simple proof of equivalence between adiabatic quantum computation and the circuit model. *Physical Review Letters*, 99(7):070502, 2007. [doi:10.1103/PhysRevLett.99.070502] 496, 542, 586

[26] BOJAN MOHAR: Eigenvalues, diameter, and mean distance in graphs. *Graphs and Combinatorics*, 7(1):53–64, 1991. [doi:10.1007/BF01789463] 576

[27] DANIEL NAGAJ AND SHAY MOZES: New construction for a QMA complete three-local Hamiltonian. *Journal of Mathematical Physics*, 48(7):072104, 2007. [doi:10.1063/1.2748377, arXiv:quant-ph/0612113] 498

[28] ROBERTO OLIVEIRA AND BARBARA M. TERHAL: The complexity of quantum spin systems on a two-dimensional square lattice. *Quantum Inf. Comput.*, 8(10):900–924, 2008. ACM DL. [arXiv:quant-ph/0504050] 492, 496

[29] NORBERT SCHUCH AND FRANK VERSTRAETE: Computational complexity of interacting electrons and fundamental limitations of density functional theory. *Nature Physics*, 5(10):732–735, 2009. [doi:10.1038/nphys1370, arXiv:0712.0483] 492, 496

[30] TZU-CHIEH WEI, MICHELE MOSCA, AND ASHWIN NAYAK: Interacting boson problems can be QMA hard. *Physical Review Letters*, 104(4):040501, 2010. [doi:10.1103/PhysRevLett.104.040501, arXiv:0905.3413] 492

AUTHORS

Andrew M. Childs
Department of Combinatorics and Optimization
and
Institute for Quantum Computing
University of Waterloo
amchilds@umd.edu
https://cs.umd.edu/~amchilds/

David Gosset
Department of Combinatorics and Optimization
and
Institute for Quantum Computing
University of Waterloo
dngosset@gmail.com
http://www.davidgosset.com

Zak Webb
Department of Physics & Astronomy
and
Institute for Quantum Computing
University of Waterloo
zakwwebb@gmail.com
http://zakwebb.me

ABOUT THE AUTHORS

ANDREW CHILDS received his Ph. D. in Physics from MIT in 2004, advised by Edward Farhi. His research focuses on quantum algorithms, including quantum walks on graphs, quantum simulation, quantum algorithms for algebraic problems, and quantum query complexity. From 2007 to 2014 he worked at the University of Waterloo, Department of Combinatorics and Optimization and the Institute for Quantum Computing. He is now at the University of Maryland, where he co-directs the Joint Center for Quantum Information and Computer Science.

DAVID GOSSET completed his Ph. D. in 2011, under the supervision of Edward Farhi at MIT. His research interests include quantum algorithms, quantum walks, Hamiltonian complexity, quantum circuit synthesis, and other areas in the theory of quantum computation. He is currently a postdoctoral fellow at the Institute for Quantum Information and Matter and the Burke Institute for Theoretical Physics at Caltech.

ZAK WEBB is a graduate student in physics at the Institute for Quantum Computing at the University of Waterloo, advised by Andrew Childs. His research interests include quantum walks on graphs and quantum Hamiltonian complexity.